Elastic Lateral Torsional Buckling of Beams Strengthened with Cover Plates while under Loading

by

Amin Iranpour

Supervised by

Dr. Magdi Mohareb

Thesis submitted to the University of Ottawa
in partial fulfillment of the requirements for the degree of
DOCTOR OF PHILOSOPHY
in Civil Engineering

Department of Civil Engineering
Faculty of Engineering
University of Ottawa

Abstract

The aging infrastructure worldwide and the typical increase in service loads relative to original design loads make it essential to develop effective techniques for strengthening and rehabilitating existing structures, to enhance their resistance. An effective method for strengthening existing steel I-beams is to weld either one or two cover plates to the flange(s). In many cases, it is not feasible to completely unload the beam before carrying out the strengthening procedure. In these conditions, operators resort to strengthen beams while under loading. In such scenarios, it becomes a challenging task to assess the lateral torsional buckling (LTB) capacity of the member under present steel design standards (e.g., CAN/CSA-S16 2019 and ANSI/AISC360 2022) which do not consider the effect of pre-strengthening loads on LTB resistance. Within this context, the present study investigates the effects of pre-strengthening loads on the critical moment capacity by developing a series of solutions, ranging from elaborate and accurate to simplified but approximate, to predict the elastic LTB capacity of beams strengthened with cover plate(s) while under load. In this respect, the study contributes to the existing body of knowledge through four aspects:

In the first contribution, a shell-based finite element (FE) study is developed to analyze the effect of various geometric and loading parameters on the LTB capacity of doubly symmetric beams strengthened symmetrically with two cover plates. The study carefully simulates the entire history, including the application of pre-existing loads, clamping forces to align the initially straight steel cover plates with the bent beam configuration, the rebound effect arising after clamping force removal, the contact at the interfaces between cover plates and flanges induced by welding, and the application of post-strengthening loads up to the point of elastic LTB initiation for the strengthened system, as determined by eigenvalue analysis. A simplified design equation is then proposed to quantify the post-strengthening critical moment capacity. The validity of the equation is assessed against FE results and its merits and limitations are discussed. The study shows that web distortional effects play a crucial role in reducing the elastic critical moment capacity. Practical recommendations are provided to mitigate such distortional effects and hence maximize the elastic critical moment capacity of the strengthened beams.

The second contribution formulates a variational principle for the LTB analysis of doubly symmetric beams strengthened symmetrically with identical steel cover plates. The formulation considers the full sequence of loading and strengthening and captures the effects of pre-strengthening loads and the beneficial effects of pre-buckling deformation (PBD). The study examines the effect of geometry, partial strengthening schemes, presence of different pre- and post-strengthening load patterns, and load height effects. The variational principle is subsequently used to develop a FE formulation, culminating in a quadratic eigenvalue problem. The validity of the FE formulation is assessed through comparisons with other numerical techniques predictions as well as experimental results by others, and subsequently used to conduct a parametric study to characterize the gain in elastic critical moment capacity attained by cover plate strengthening. For beams partly strengthened with cover plates along their spans, the study identifies the optimum locations for cover plates that maximize the critical moments.

The third contribution builds upon the variational principle developed by formulating a simple and approximate energy-based design-oriented solution to quantify the LTB resistance of simply supported I-beams strengthened with cover plates. The solution captures the detrimental effect of loads acting on the beam before strengthening and the beneficial effects resulting from PBD, pre- and post-strengthening load heights, as well as moment gradient effects. The potential use of the equations developed in practical applications involving beam strengthening is illustrated through design examples.

The fourth contribution expands the variational formulation to include beams with monosymmetric cross-sections and/or symmetric beams with unsymmetric cover plate geometries. The modified variational principle is used to develop a thin-walled beam FE formulation, which is subsequently employed to predict the non-distortional LTB capacity of monosymmetric strengthened beams. Comparative analyses with shell models confirm the validity of the proposed solutions, and practical design recommendations for suppressing web distortion are provided. The effects of various design parameters on the total elastic critical moment capacity are evaluated in a systematic parametric study. The study identifies the loading conditions under which the magnitude of pre-strengthening loads significantly influences the predicted total critical moments.

The solutions developed in the present study equip structural designers and analysts with novel techniques that reliably quantify the LTB strength of steel beams strengthened with cover plates, thus enabling them to optimize strengthening strategies for beams whose strengths are governed by LTB modes of failure.

Acknowledgment

I extend my heartfelt gratitude to the many individuals and institutions that have supported me on this remarkable journey of intellectual exploration and personal growth. First and foremost, I am deeply grateful to my esteemed advisor, Professor Magdi Mohareb, for his unwavering guidance, invaluable insights, and enduring encouragement throughout my research. His mentorship has been an inspiration that has significantly shaped both my academic and personal development.

I express my sincere gratitude to the members of my thesis examining committee: Professor Kaveh Arjomandi from the University of New Brunswick, Professor Heng-Aik Khoo from Carleton University, and Professor Beatriz Martin-Perez and Professor Martin Noël from the University of Ottawa. Their insightful feedback and attention to detail positively impacted the quality of the thesis content.

I wish to express my deepest appreciation to my beloved mother, whose presence envelops me in enduring calm, peace, and boundless love. Her unwavering encouragement and empathetic understanding have been the bedrock of my resilience. My gratitude also extends to my father, whose steadfast commitment to my success has illuminated my path. His tireless efforts in providing unwavering support and resources have empowered me to wholeheartedly immerse myself in this academic pursuit. Furthermore, I hold profound gratitude for my dear brother, who has transcended the role of a sibling to become a steadfast friend. His encouragement, sacrifices, and selflessness have afforded me the freedom to focus entirely on my studies. This achievement stands as a resounding testament to our exemplary teamwork.

I extend my sincere gratitude to my friends who have stood by me with their support, camaraderie, and encouragement throughout this journey. Your companionship and shared moments have added immeasurable joy to my academic pursuits. Thank you for being a source of inspiration and for being integral to my life.

Lastly, I would like to acknowledge the support of the University of Ottawa, which has provided me with a nurturing environment and resources that have fostered my academic growth.

To everyone who has played a role, no matter how significant, in shaping this thesis and my journey as a scholar, I offer my sincerest appreciation. Thank you for being an integral part of this significant milestone in my academic career.

Table of Contents

Chapter 6: Variational Principle and Finite Element Formulation for Strengthened Monosymmetric Beams

Chapter 7: Summary, Conclusions and Recommendations

List of Figures

List of tables

Chapter1: Introduction

1.1 General

Lateral torsional buckling (LTB) is a failure mode that usually governs the flexural strength of long-span members with open cross-sections bent about their strong axis when lacking sufficient lateral support. An example of such a beam is shown in Fig. 1.1a, where a beam is simply supported with respect to transverse deflection, lateral deflection, and twist at both ends, but is laterally unsupported along the span. As shown in Fig. 1.1b, under the reference loads Q, the reference axis of the member undergoes a transverse deflection V from the initially undeformed state (Configuration 1) to Equilibrium Configuration 2. The associated transverse displacements are anticipated to amplify as the reference loads increase, eventually leading the beam reaching Configuration 3, which marks the initiation of buckling and is characterized by the sought eigenvalue λ. As the member undergoes LTB, by shifting from Configuration 3 to Configuration 4 in Fig. 1.1b, the applied loads remain constant, but the reference axis of the beam undergoes lateral displacement U, accompanied by an angle of twist θ of the cross-section about its shear center.

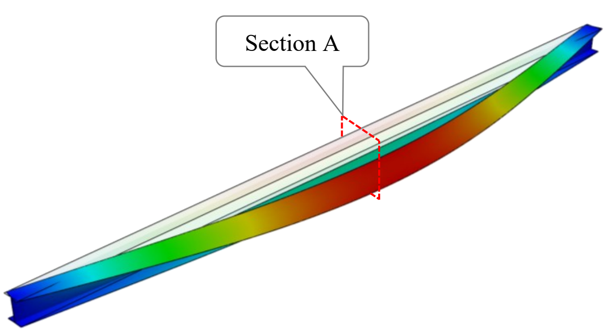

(a)

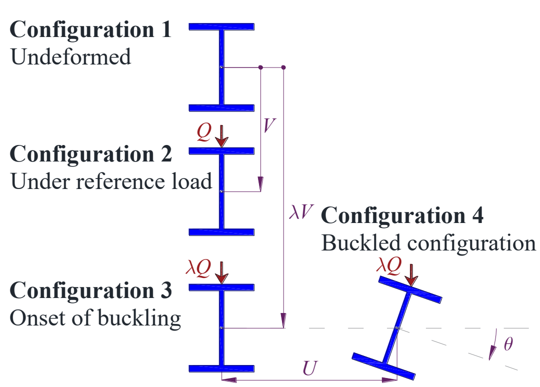

(b)

Fig. 1.1 (a) Buckled configuration; and (b) Stages of deformation at Section A

Steel design standards (e.g., CAN/CSA-S16 2019 and ANSI/AISC360 2022) recognize lateral torsional buckling (LTB) as a potential failure mode. The fundamental predictive equations they provide are initially formulated for simplified scenarios with idealized loading and boundary conditions. To encompass a wider range of loading configurations, standards introduce a moment gradient factor. The following section provides the flexural design guidelines presented by CAN/CSA-S16 (2019) and ANSI/AISC360 (2022).

1.2 Relevant Design Provisions in Structural Steel Standards

1.2.1 Canadian Standards

Quantifying the nominal flexural capacity for a laterally unbraced steel member with a doubly symmetric section bent about its major axis, according to CAN/CSA-S16 (2019), involves the following steps:

(1) Classifying the section to determine whether the member can attain its plastic resistance M_p prior to buckling locally (Class 1 and 2 sections) or whether it attains its yield moment resistance M_y prior to buckling locally, but buckles locally prior to attaining its plastic resistance M_p (Class 3 sections).

(2) Depending on the section class, calculating the cross-section flexural strength M_g of the member from

$$M_g = \begin{cases} M_p = Z_x F_y & \text{Class 1 and 2} \\ M_y = S_x F_y & \text{Class 3} \end{cases} \tag{1.1}$$

in which Z_x is the plastic section modulus, S_x is the elastic section modulus, and F_y is the yield strength of the steel.

(3) Calculating the elastic critical moment M_{cr-CA} from

$$M_{cr-CA} = C_{b-CA} M_{cr-u}$$
$$M_{cr-u} = \frac{\pi}{L_b}\sqrt{EI_y GJ + \left(\frac{\pi E}{L_b}\right)^2 I_y C_w}, \quad C_{b-CA} = \frac{4M_{\max}}{\sqrt{M_{\max}{}^2 + 4M_A{}^2 + 7M_B{}^2 + 4M_C{}^2}} \tag{1.2)a-c}$$

in which M_{cr-u} is the uniform critical moment for the hypothetical case where the beam is subjected to uniform moments, L_b is the unbraced length of the member, E is the modulus of elasticity, G is the shear modulus, I_y is the weak-axis moment of inertia, J is the Saint-Venant torsional constant, and C_w is the warping constant. The moment gradient factor C_{b-CA} accounts for non-uniform moment distribution within the unbraced length L_b of the member and is a function of the absolute values of four sampling points within the span: the quarter point moment M_A, the midspan moment M_B, the third-quarter point moment M_C and the peak moment $M_{\max}$.

(4) Given the cross-section flexural strength M_g and the elastic critical moment M_{cr-CA}, determining the nominal flexural resistance M_{n-CA} based on the piecewise definition

$$M_{n-CA} = \frac{M_{r-CA}}{\phi} = \begin{cases} M_g & M_{cr-CA}/M_g \geq 2.15 \\ 1.15M_g\left(1-0.28M_g/M_{cr-CA}\right) & 0.67 < M_{cr-CA}/M_g < 2.15 \\ M_{cr-CA} & M_{cr-CA}/M_g \leq 0.67 \end{cases} \tag{1.3)a-c}$$

Eq. (1.3)a relates to the cross-sectional strength based on yield considerations and will govern the flexural strength for beams with short span beams, whereas Eq. (1.3)c relates to elastic critical moment for the member and is applicable to long span beams. For beams with intermediate spans, where inelastic LTB occurs, the corresponding capacity can be estimated using Eq. (1.3)b. In Fig.

1.2, the black solid line depicts a schematic curve generated using Eq. (1.3), effectively illustrating the total nominal flexural resistance across the unbraced length and outlining three distinct regions for yielding, elastic LTB, and inelastic LTB.

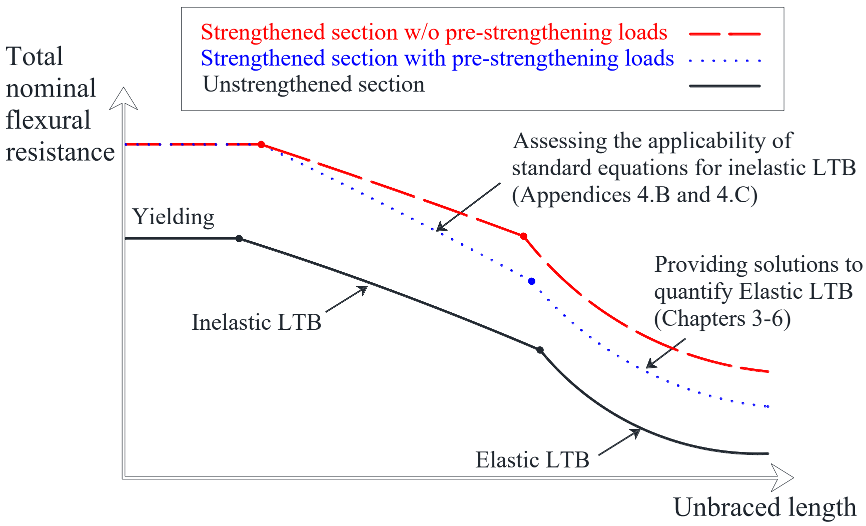

Fig. 1.2 Flexural resistance versus unbraced length - Effects of strengthening and pre-strengthening loads on flexural capacity

1.2.2 US Specifications

For doubly symmetric I-beams with compact webs and flanges, the nominal flexural capacity M_{n-US} according to ANSI/AISC360 (2022) is determined by

$$M_{n-US} = \begin{cases} M_p & L_b \le L_p \\ C_{b-US}\left[M_p - \left(M_p - 0.7F_y S_x\right)\left(L_b - L_f\right)/\left(L_r - L_f\right)\right] & L_p < L_b \le L_r \\ M_{cr-US} & L_p > L_r \end{cases} \quad (1.4)\text{a-c}$$

in which the elastic critical moment according to ANSI/AISC360 (2022) is given by

$$M_{cr-US} = C_{b-US} M_{cr-u} \quad (1.5)$$

and moment gradient factor C_{b-US} is given by

$$C_{b-US} = \frac{12.5M_{\max}}{2.5M_{\max} + 3M_A + 4M_B + 3M_C} \tag{1.6}$$

In Eq. (1.4), L_f is the fully braced length below which LTB does not occur, given in Clause F2-5 as

$$L_f = 1.76 r_y \sqrt{\frac{E}{F_y}} \tag{1.7}$$

in which r_y is the weak-axis radius of gyration of the cross-section. Also, in Eq. (1.4), L_r is the laterally unbraced length that delineates inelastic LTB from elastic LTB and is given by Clause F2-6 as

$$L_r = 1.95 \frac{E}{0.7F_y} \sqrt{\frac{\sqrt{I_{yy}C_w}}{S_x} \left[\frac{J}{S_x h} + \sqrt{\left(\frac{J}{S_x h} \right)^2 + 6.76 \left(\frac{0.7F_y}{E} \right)^2} \right]} \tag{1.8}$$

in which h is the distance between the flange centroids. Eqs. (1.3) and (1.4) can be used to generate a plot for the nominal flexural resistance of a beam in terms of the unbraced length L_b for a doubly symmetric laterally unbraced beam. Again, the black solid line in Fig. 1.2 schematically depicts such a relationship. Similar plots can be obtained by using relevant provisions for monosymmetric laterally unbraced beams.

1.3 Challenges in Resistance Assessment for Strengthened Members

The reuse of existing structures/members to carry additional loads is an integral part of achieving sustainable construction. Developing solutions for quantifying the resistance of strengthened members is thus becoming an important requirement to prolong the lifetime of existing structures expected to withstand increased operating loads. A common means to strengthen existing steel I-beams is to weld cover plates to a single or to both flanges. When feasible, it is recommended to fully unload the beam prior to strengthening it. In such cases, both the cross-sectional strength and the elastic LTB strength of the strengthened beam can be quantified by using Eqs. (1.3) and (1.4) and are expected to yield higher nominal flexural resistance, as schematically depicted by the red dashed line in Fig. 1.2. However, if practical considerations prevent a full removal of loads prior to strengthening, the beam would have to be strengthened while under the action of pre-strengthening loads, and the resulting nominal capacity of the member can be less effective, as schematically represented by the blue dotted line in Fig. 1.2. In this case, Eqs. (1.3) and (1.4) become inapplicable. Also, such equations do not account for the effects of load height and Pre-Buckling Deformation (PBD) when determining the capacity based on elastic and inelastic LTB. Determining the LTB capacity when the member is strengthened under loading becomes a challenging undertaking and is a motivation of the present study.

1.4 Objectives

The present study thus aims to develop a family of solutions that reliably quantify the elastic LTB resistance of beams strengthened under loading. The solution sought needs to account for the interaction between pre- and post-strengthening loads, moment gradient, load height, and PBD effects. The solutions sought will range from the elaborate/accurate to the simple/approximate and will provide practicing engineers with reliable predictions, thus empowering them to devise economic strengthening solutions that achieve the required level of structural safety when rehabilitating existing steel buildings and bridges.

Additionally, to investigate the applicability of the North American Standards equations [i.e., Eqs. (1.3)b and (1.4)b] in predicting the inelastic LTB capacity of beams strengthened while under loading, these equations are adopted in conjunction with the elastic critical moments predicted by proposed solutions and the predicted nominal inelastic moment resistances are compared to the rather limited experimental results found in the literature.

1.5 Thesis Outline

The present thesis consists of seven chapters. In present Chapter 1, an introduction has been presented along with an overview of the thesis objectives and scope. Chapter 2 provides a literature review pertinent to the various aspects of the study.

Chapter 3 (1) develops shell models for the LTB analysis of beams with doubly symmetric sections strengthened symmetrically with two cover plates and is subsequently used as a benchmark solution for the verification of the solutions in following Chapters 4-6, (2) proposes a simple intuitive design approach to estimate the post-strengthening critical moment, (3) quantifies the loss of capacity of the strengthened system due to possible web distortion resulting from adding cover plates to parts of the span, and (4) proposes practical recommendations to suppress web distortion.

To effectively quantify the LTB resistance of strengthened I-beams, Chapter 4 develops a thin-walled beam FE formulation for the problem which captures the effects of (1) pre-strengthening loads, (2) PBD, (3) partial strengthening schemes, (4) boundary conditions, and (5) different pre-strengthening and post-strengthening load distributions, and (6) pre-strengthening and post-strengthening load height effects.

Chapter 5 develops design-oriented simplified equations and procedures that reliably quantify the elastic LTB resistance of strengthened steel I-beams with doubly symmetric cross-sections.

As the contributions of Chapters 3-5 are limited to doubly symmetric cross-sections, Chapter 6 extends the solution to strengthened monosymmetric beams and/or doubly symmetric beams with unsymmetric cover plate schemes by developing a more general variational principle and a FE formulation.

Chapter 7 offers a summary and conclusion of the study and provides recommendations for future research.

1.6 References

ANSI/AISC360 (2022). "Specification for structural steel buildings (ANSI/AISC 360-22)." American Institute of Steel Construction, Chicago-Illinois.

CAN/CSA-S16 (2019). "CSA S16: 19, Design of Steel Structures, Canada." Canadian Standards Association.

Chapter 2: Literature Review

2.1 Introduction

The classical LTB theory (e.g., Vlasov 1961), which forms the basis of LTB provisions in steel design standards (e.g., CAN/CSA-S16 2019 and ANSI/AISC360 2022), comes with a number of limitations when applied to strengthened beams. From a kinematics viewpoint, the Vlasov theory omits shear deformation within the cross-section middle surface and cross-sectional distortion by assuming a beam cross-section to deform as rigid disk within its own plane. Other limitations arise from the inability of the theory to account for the effects of loads acting on the member prior to strengthening, pre- and post-strengthening loads being offset from the shear centre, and different distributions of pre- and post-strengthening loading. Also, the classical LTB theory based on the Vlasov theory neglects the effects of pre-buckling deformation (PBD). In this regard, Sections 2.2-2.5 of this chapter provide an overview of studies accounting for these effects.

From a cross-section geometry viewpoint, while doubly symmetric sections are most commonly used as bending members, the use of monosymmetric I-beams can offer practical and economic advantages in certain situations. Hence, the LTB strength of beams from both types of cross-sections will be investigated in present study. Studies specifically focused on monosymmetric I-beams will be reviewed in Section 2.6.

Numerous studies use Finite Element (FE) analysis to investigate the LTB behaviour of flexural members owing to its generality and amenability to handle general boundary conditions and loading conditions. While FE analysis is advantageous from an accuracy viewpoint and hence is an excellent research tool, it may be impractical for routine design. In this respect, energy-based solutions offer a more practical design approach. Thus, Section 2.7 provides a review on LTB energy-based approximate solutions.

The concluding section 2.8 of this chapter summarizes the objectives and the scope of the thesis and outlines its contributions within the existing body of knowledge.

2.2 LTB of strengthened beams

Within the vast literature on LTB, the number of studies related to strengthened beams is rather limited. Only a few studies investigated the elastic buckling strength of strengthened beams. This includes the study of MacCrimmon (2009) who provided a procedure to estimate the critical moments for built-up crane runway beams. Hsu et al. (2009 and 2012) investigated the torsional properties of I-beams strengthened with open-side down channels over the top flange to enable the evaluation of the LTB capacity of such beams. Pezeshky et al. (2020) developed a generalized thin-walled beam theory for the elastic LTB resistance of wide flange beams strengthened with any number of cross-sections to form a monosymmetric assembly. Based on a 3D shell-based Finite Element (FE) modelling, Reichenbach et al. (2020) conducted a parametric study to investigate the elastic LTB capacity of beams with stepped flanges strengthened with cover plates and proposed simplified procedures to estimate their effective properties. None of the above studies, however, investigated the detrimental effect of loads (pre-strengthening loads) that may be present on the member prior to the strengthening process.

2.3 Effect of pre-strengthening loads

Only a few studies investigated of the effect of pre-strengthening loads on the lateral torsional buckling of strengthened beams. Liu and Gannon (2009a-b) conducted nine tests and 93 FE simulations to investigate the behavior and capacity of I-beams strengthened while under load.

The authors reported that, while the pre-strengthening load level has a noticeable effect on the inelastic LTB capacity of the member, its effect is negligible on its yielding strength. None of the specimens tested failed in an elastic LTB mode of failure. Another experimental study on four specimens by Wang et al. (2015) confirmed the findings of Liu and Gannon (2009a), where it was found that pre-strengthening load levels adversely affect the inelastic LTB resistance of strengthened beams. Pham et al. (2017) conducted an analytical investigation on the effect of pre-strengthening loads on post-strengthening elastic response of flexural members. However, the study focused on the post-strengthening linearly elastic response and did not attempt to address the LTB mode of failure.

2.4 Effect of Pre-Buckling Deformation

The pre-buckling deformation (PBD) effect refers to the effect of in-plane transverse curvature of flexural members prior to buckling on the LTB resistance of the member. Conceptually, a simply supported beam under transverse gravity loads would assume a sagging arch configuration under loads and tends to be more resistant to LTB than a perfectly straight beam. As a simplification, classical solutions typically omit the sagging arch effect due to PBD, hence underestimating the LTB strength of the member. This simplification is justifiable when the difference in geometry between a beam that is transversely bent under load prior to buckling and the initial undeformed configuration of the beam is negligible.

The PBD effect was addressed in a limited number of specialized studies including the work of Trahair and Woolcock (1973) who studied the PBD effect on the elastic buckling of doubly symmetric beams. The study showed that the predicted critical moments for beams with wide flanges significantly increase when incorporating PBD effects. Similar results were reported by Vacharajittiphan et al. (1974) who showed that critical loads based on the classical treatment yield conservative predictions. Roberts and Azizian (1983) formulated a variational principle that accounts for PBD effects by retaining higher-order displacement derivatives. They reported that second-order terms related to twist in strain-displacement relations can significantly affect the LTB capacity of monosymmetric beams. Pi et al. (1992) developed a variational principle for the elastic LTB of doubly symmetric thin-walled beams which captures PBD effects and compared the resulting equation with the alternative formulation in (Gellin and Lee 1988). Discrepancies in the alternative study predictions with experimental results were attributed to the omission of some nonlinear terms in longitudinal displacements. Pi and Trahair (1992a) used the variational principle developed by Pi et al. (1992) to formulate the differential equations governing the LTB for I beam-columns and developed an FE formulation for the problem. In a companion paper, Pi and Trahair (1992b) compared numerical results against those based on the classical LTB solution. Andrade and Camotim (2004) derived the differential equations and boundary conditions governing the LTB of doubly symmetric tapered thin-walled beams with open cross-sections that capture PBD effects. Machado and Cortínez (2005) developed an energy-based solution that captures PBD and shear deformation effects for simply supported composite beams. It was shown that the buckling loads predicted by the linear theory, which omits PBD effects, are overly conservative. Mohri and Potier-Ferry (2006) derived analytical LTB solutions for channels and I-beams that capture PBD effects. By accounting for PBD and shear deformation effects, Erkmen and Attard (2011) developed an FE formulation for the LTB analysis of thin-walled beams. The study indicated that omitting PBDs can lead to very conservative predictions for sections with relatively large flanges. The effect of PBDs on the LTB behavior of monosymmetric beams was investigated by Mohri et al. (2012). Pezeshky and Mohareb (2018) developed an LTB formulation that captures the effects of web distortion, PBD and shear deformation on the elastic LTB analysis of doubly symmetric beam-columns. The formulation was used to investigate the effect of geometric parameters on predicted critical moments.

2.5 Effect of Cross-Sectional Distortion

The classical lateral torsional buckling treatment based on the Vlasov theory is based on the rigid disk assumption, whereby a beam-cross-section is assumed to deform as a rigid disc in its own plane, thus omitting any distortion that may occur in the web. More advanced studies have shown that the beam cross-sections might undergo distortion during LTB, leading to a reduction in the predicted LTB capacity of the beam. Such studies include the work of Rajasekaran and Murray (1973) who developed an FE solution that accounts for cross-sectional distortion. The solution integrated the Kirchhoff plate bending theory with the kinematics of the Vlasov thin-walled theory. Johnson and Will (1974) developed an FE methodology to compute critical buckling loads in three-dimensional structures employing two-dimensional shell elements. While this solution leads to accurate predictions, it involves a significant modelling and computational cost.

Bradford and Trahair (1982) developed an approximate FE solution to analyze the distortional buckling of beam-columns with a flexible web and rigid flange assemblies. The solution was used to investigate the effect of web distortion on the elastic buckling of lipped channel beams. The formulation was then extended to investigate the distortional buckling of monosymmetric I-beams (Bradford 1985). Other thin-walled beam formulations that capture distortional effects in monosymmetric beams include the work of Ma and Hughes (1996), Hughes and Ma (1996), and Bradford (1990). Towards investigating the distortional buckling of elastically restrained beam-columns, Bradford and Ronagh (1997) extended the work of Bradford and Trahair (1982). By incorporating PBD, Pezeshky and Mohareb (2018) formulated an FE solution for distortional bucking of doubly symmetric beam-columns. Shell FE models investigations of distortional buckling for monosymmetric beams include the work of Helwig et al. (1997), Samanta and Kumar (2006), and Kumar and Samanta (2006).

2.6 Effect of cross-section Monosymmetry

The classical differential equations governing the LTB capacity of monosymmetric I-shaped cross-sections were presented in Vlasov (1961), Trahair (1993), etc. Several researchers (e.g., Anderson and Trahair 1972), and Wang and Kitipornchai (1986a)] developed a direct solution of the governing differential equations for classical LTB. Other studies [e.g., Wang and Kitipornchai (1986a), Wang and Kitipornchai (1986b), Roberts and Benchiha (1987), Attard (1990), Mohri et al. (2003), Mohammadi et al. (2016)] developed energy-based approximate LTB solutions based on the Vlasov theory.

Krajcinovic (1969), Barsoum and Gallagher (1970) and Papangelis et al. (1998) adapted the LTB solution of Vlasov (1961) into an FE context to characterize the elastic LTB capacity of monosymmetric beams with monolithic cross-sections.

The effect of shear deformation on the LTB strength of beams with monosymmetric sections was investigated by Erkmen and Mohareb (2008), Attard and Kim (2010), Erkmen (2014) and Sahraei et al. (2015).

FE solutions that capture the PBD effect on the elastic LTB strength of monosymmetric cross-sections were developed by Attard (1986), and Pi and Trahair (1992a, 1992b).

2.7 Energy-based approximate solutions

The majority of LTB solutions presented are based on FE analysis, owing to its accuracy and amenability to handle various loading and boundary conditions. While FE analysis is an ideal research tool for LTB analysis, it may present a potential impracticality in routine design settings. To address this limitation, alternative energy-based approximate solutions have been proposed. Energy-based approximate solutions offer a more natural means of developing simplified design-oriented equations, albeit they may be restricted to special loading cases and/or boundary conditions. In this respect, past energy-based approximate solutions have resulted in expressions for moment gradient coefficients that account for non-uniform moment distribution along the span [e.g., Kitipornchai et al. (1986), Sahraei et al. (2018) and Bresser et al. (2020)], load height coefficients that account for the destabilizing effect induced by transverse loads that are offset from the shear centre [e.g., Mohri and Potier-Ferry (2006), Sahraei et al. (2018)], and PBD coefficients [e.g., Trahair and Woolcock (1973), Vacharajittiphan et al. (1974), Roberts and Azizian (1983), Andrade and Camotim (2004) and Machado and Cortínez (2005)].

2.8 Objectives and Scope

The present study aims to partially fill the gap within the existing literature concerning the LTB of strengthened members and involves the following aspects:

1. Investigate the effects of (a) pre-strengthening loading configuration and magnitude, (b) PBD, (c) moment gradient due to pre- and post-strengthening loads, and (d) pre- and post-strengthening load heights, on the post-strengthening elastic LTB capacity of a beam. For this purpose, several solutions are developed ranging from elaborate/accurate to simple/approximate (Table 2.1). Simplified solutions include developing design-oriented equations and procedures to predict the elastic critical moment of the strengthened system that reliably capture the effect of pre-strengthening loading.

2. Estimate the inelastic LTB resistance of members by integrating the elastic LTB solutions developed in the present study within the North American Standard provisions [i.e., Eqs. (1.3) b and (1.4)b or similar equations for monosymmetric beams].
3. Provide practical recommendations for strengthening steel members to increase their LTB strength (e.g., identify the most effective locations for transverse stiffeners and cover plates in partial strengthening scenarios).

Table 2.1 Features and limitations of developed solutions

#	1	2	3
Solution	Shell FEA modelling	Thin-walled beam FEA modelling	Energy-based approximate solution
Features	• Takes into account the cross-sectional distortion and shear deformations • Provides a basis to assess solutions 2 and 3	• Works for both prismatic and non-prismatic sections • Modelling process is less complex than that in solution 1 • Captures PBD effects	• Is the easiest solution among the proposed solutions • Captures PBD effects through a coefficient
Limitations	• Does not provide a direct way of capturing PBD effects	• Does not account for cross-sectional distortion and shear deformations	• Works only for prismatic doubly symmetric sections • Works only for simply supported BCs
Mapping to current research	Chapters 3, 4 and 6	Chapters 4 and 6	Chapter 5

2.9 References

Anderson, J. M. and N. S. Trahair (1972). "Stability of monosymmetric beams and cantilevers." Journal of the structural division **98**(1): 269-286.

Andrade, A. and D. Camotim (2004). "Lateral-torsional buckling of prismatic and tapered thin-walled open beams: assessing the influence of pre-buckling deflections." Steel and Composite Structures **4**(4): 281-301.

ANSI/AISC360 (2022). "Specification for structural steel buildings (ANSI/AISC 360-22)." American Institute of Steel Construction, Chicago-Illinois.

Arizou, R. and M. Mohareb (2021). "Design Considerations for Distortional Lateral Buckling." Journal of Structural Engineering **147**(12): 04021203.

Arizou, R. and M. Mohareb (2022). "Finite element formulation for distortional lateral buckling of I-beams." Engineering Structures **262**: 114265.

AS-4100 (2020). "Steel structures. Sydney, Australia."

Attard, M. M. (1986). "Lateral buckling analysis of beams by the FEM." Computers & structures **23**(2): 217-231.

Attard, M. M. (1990). "General non-dimensional equation for lateral buckling." Thin-Walled Structures **9**(1-4): 417-435.

Attard, M. M. and M.-Y. Kim (2010). "Lateral buckling of beams with shear deformations–A hyperelastic formulation." International Journal of Solids and Structures **47**(20): 2825-2840.

Barsoum, R. S. and R. H. Gallagher (1970). "Finite element analysis of torsional and torsional–flexural stability problems." International J. for Numerical Methods in Engineering **2**(3): 335-352.

Basaglia, C. and D. Camotim (2013). "Enhanced generalised beam theory buckling formulation to handle transverse load application effects." International Journal of Solids and Structures **50**(3-4): 531-547.

Bazant, Z. and L. Cedolin (2010). Stability of structures: elastic, inelastic, fracture and damage theories, World Scientific.

Bradford, M. A. (1985). "Distortional buckling of monosymmetric I-beams." Journal of Constructional Steel Research **5**(2): 123-136.

Bradford, M. A. (1990). "Stability of monosymmetric beam-columns with thin webs." Journal of Constructional Steel Research **15**(4): 323-339.

Bradford, M. A. and H. R. Ronagh (1997). "Generalized elastic buckling of restrained I-beams by FEM." Journal of Structural Engineering **123**(12): 1631-1637.

Bradford, M. A. and N. S. Trahair (1982). "Distortional buckling of thin-web beam-columns." Engineering Structures **4**(1): 2-10.

Bresser, D., G. Ravenshorst and P. Hoogenboom (2020). "General formulation of equivalent moment factor for elastic lateral torsional buckling of slender rectangular sections and I-sections." Engineering Structures **207**: 110230.

CAN/CSA-S6-19 (2019). "Canadian highway bridge design code." Canadian Standards Association.

CAN/CSA-S16 (2019). "CSA S16: 19, Design of Steel Structures, Canada." Canadian Standards Association.

Dinis, P. B., D. Camotim and N. Silvestre (2006). "GBT formulation to analyse the buckling behaviour of thin-walled members with arbitrarily ‘branched’open cross-sections." Thin-Walled Structures **44**(1): 20-38.

Erkmen, R. and M. Mohareb (2008). "Buckling analysis of thin-walled open members—a finite element formulation." Thin-walled structures **46**(6): 618-636.

Erkmen, R. E. (2014). "Shear deformable hybrid finite-element formulation for buckling analysis of thin-walled members." Finite Elements in Analysis and Design **82**: 32-45.

Erkmen, R. E. and M. M. Attard (2011). "Lateral–torsional buckling analysis of thin-walled beams including shear and pre-buckling deformation effects." International journal of mechanical sciences **53**(10): 918-925.

Gellin, S. and G. C. Lee (1988). "Finite elements available for the analysis of non-curved thin-walled structures." Finite element analysis of thin-walled structures(Elsevier Applied Science): 1-30.

Gjelsvik, A. (1981). The theory of thin-walled bars. New York, John Wiley & Sons publishing Inc.

Helwig, T. A., K. H. Frank and J. A. Yura (1997). "Lateral-torsional buckling of singly symmetric I-beams." Journal of Structural Engineering **123**(9): 1172-1179.

Hsu, W. T., D. M. Lue and Y. F. Chen (2012). "Design aid for moment strength of built-up crane runway girders." International Journal of Steel Structures **12**(3): 403-417.

Hsu, W. T., D. M. Lue and B. T. Hsiao (2009). "Numerical approach for torsion properties of built-up runway girders." Journal of Applied Science and Engineering **12**(4): 381-389.

Hughes, O. and M. Ma (1996). "Lateral distortional buckling of monosymmetric beams under point load." Journal of engineering mechanics **122**(10): 1022-1029.

Iranpour, A. and M. Mohareb (2022). Elastic Lateral Torsional Buckling Resistance for Continuous Beams Using Artificial Neural Networks. Canadian Society of Civil Engineering Annual Conference, Whistler, British Columbia, Canada, Springer.

Iranpour, A. and M. Mohareb (2022). Elastic Lateral Torsional Buckling Resistance of Beams Strengthened with Cover Plates under Pre-Existing Loads. Canadian Society of Civil Engineering Annual Conference, Whistler, British Columbia, Canada, Springer.

Iranpour, A. and M. Mohareb (2023a). "Elastic Lateral Torsional Buckling of I-Beams Strengthened While under Loading." Journal of Structural Engineering **149**(1): 04022206.

Iranpour, A. and M. Mohareb (2023b). "Design Expressions for Elastic Lateral Torsional Buckling Capacity of I-Beams Strengthened While under Loading." Journal of Structural Engineering **149**(7): 04023078.

Johnson, C. P. and K. M. Will (1974). "Beam buckling by finite element procedure." Journal of the Structural Division **100**(3): 669-685.

Kitipornchai, S., C. M. Wang and N. S. Trahair (1986). "Buckling of monosymmetric I-beams under moment gradient." Journal of Structural Engineering **112**(4): 781-799.

Krajcinovic, D. (1969). "A consistent discrete elements technique for thinwalled assemblages." International Journal of Solids and Structures **5**(7): 639-662.

Kumar, A. and A. Samanta (2006). "Distortional buckling in monosymmetric I-beams: Reverse-curvature bending." Thin-walled structures **44**(7): 721-725.

Liang, C., M. C. Reichenbach, T. A. Helwig, M. D. Engelhardt and J. A. Yura (2022). "Effects of Shear on the Elastic Lateral Torsional Buckling of Doubly Symmetric I-Beams." Journal of Structural Engineering **148**(3): 04021301.

Liu, Y. and L. Gannon (2009a). "Experimental behavior and strength of steel beams strengthened while under load." Journal of Constructional Steel Research **65**(6): 1346-1354.

Liu, Y. and L. Gannon (2009b). "Finite element study of steel beams reinforced while under load." Engineering Structures **31**(11): 2630-2642.

Ma, M. and O. Hughes (1996). "Lateral distortional buckling of monosymmetric I-beams under distributed vertical load." Thin-Walled Structures **26**(2): 123-145.

MacCrimmon, R. (2009). Guide for the Design of Crane-Supporting Steel Structures. Markham, ON, CA, Canadian Institute of Steel Construction.

Machado, S. P. and V. H. Cortínez (2005). "Lateral buckling of thin-walled composite bisymmetric beams with prebuckling and shear deformation." Engineering Structures **27**(8): 1185-1196.

Mohammadi, E., S. S. Hosseini and M. S. Rohanimanesh (2016). "Elastic lateral-torsional buckling strength and torsional bracing stiffness requirement for monosymmetric I-beams." Thin-Walled Structures **104**: 116-125.

Mohri, F., A. Brouki and J. Roth (2003). "Theoretical and numerical stability analyses of unrestrained, mono-symmetric thin-walled beams." Journal of Constructional Steel Research **59**(1): 63-90.

Mohri, F., N. Damil and M. Potier-Ferry (2012). "Pre-buckling deflection effects on stability of thin-walled beams with open sections." Steel & Composite Structures **13**(1): 71-89.

Mohri, F. and M. Potier-Ferry (2006). "Effects of load height application and pre-buckling deflections on lateral buckling of thin-walled beams." Steel and composite structures **6**(5): 401.

Papangelis, J., N. Trahair and G. Hancock (1998). "Elastic flexural–torsional buckling of structures by computer." Computers & structures **68**(1-3): 125-137.

Pezeshky, P. and M. Mohareb (2018). "Distortional lateral torsional buckling of beam-columns including pre-buckling deformation effects." Computers & Structures **209**: 93-116.

Pezeshky, P., A. Sahraei, F. Rong, S. Sasibut and M. Mohareb (2020). "Generalization of the Vlasov theory for lateral torsional buckling analysis of built-up monosymmetric assemblies." Engineering Structures **221**: 111055.

Pham, P. V., M. Mohareb and A. Fam (2017). "Elastic Analysis of Steel Beams Strengthened with GFRP Plates Including Preexisting Loading Effects." Journal of Structural Engineering **143**(12): 04017163.

Pi, Y. L. and N. Trahair (1992a). "Prebuckling deflections and lateral buckling. I: theory." Journal of structural engineering **118**(11): 2949-2966.

Pi, Y. L. and N. Trahair (1992b). "Prebuckling deflections and lateral buckling. II: applications." Journal of Structural Engineering **118**(11): 2967-2985.

Pi, Y. L., N. Trahair and S. Rajasekaran (1992). "Energy equation for beam lateral buckling." Journal of structural engineering **118**(6): 1462-1479.

Rajasekaran, S. and D. W. Murray (1973). "Coupled local buckling in wide-flange beam-columns." Journal of the Structural Division **99**(6): 1003-1023.

Reichenbach, M. C., Y. Liu, T. A. Helwig and M. D. Engelhardt (2020). "Lateral-Torsional Buckling of Singly Symmetric I-Girders with Stepped Flanges." Journal of Structural Engineering **146**(10): 04020203.

Roberts, T. and Z. Azizian (1983). "Instability of thin walled bars." Journal of Engineering Mechanics **109**(3): 781-794.

Roberts, T. and M. Benchiha (1987). "Lateral instability of monosymmetric beams with initial curvature." Thin-walled structures **5**(2): 111-123.

Sahraei, A., A. Iranpour and M. Mohareb (2020). User manual for LTB-UO V3.0 (LTB-UO is a computer program for Lateral Torsional Buckling analysis of beams/beam-columns, written at the University of Ottawa), University of Ottawa.

Sahraei, A., P. Pezeshky and M. Mohareb (2017). Lateral torsional buckling analysis and design of steel beams with continuous spans. Canadian Society for Civil Engineering (CSCE), Vancouver BC, Canada, Proceedings of the 6th international conference on engineering mechanics and materials.

Sahraei, A., P. Pezeshky, M. Mohareb and G. Doudak (2018). "Simplified expressions for elastic lateral torsional buckling of wooden beams." Engineering Structures **174**: 229-241.

Sahraei, A., L. Wu and M. Mohareb (2015). "Finite element formulation for lateral torsional buckling analysis of shear deformable mono-symmetric thin-walled members." Thin-Walled Structures **89**: 212-226.

Samanta, A. and A. Kumar (2006). "Distortional buckling in monosymmetric I-beams." Thin-walled structures **44**(1): 51-56.

Schardt, R. (1994). "Lateral torsional and distortional buckling of channel-and hat-sections." Journal of Constructional Steel Research **31**(2-3): 243-265.

SIMULIA (2020). Abaqus/CAE user's manual, Dassault Systemes.

Slein, R., R. J. Sherman and D. W. White (2022). "Manual Estimation of Elastic Lateral Torsional Buckling Resistance of I-Section Members with Cross-Section Transitions." Journal of Bridge Engineering **27**(10): 04022099.

Trahair, N. (1993). Flexural-torsional buckling of structures, CRC press.

Trahair, N. S. and S. T. Woolcock (1973). "Effect of major axis curvature on I-beam stability." Journal of the Engineering Mechanics Division **99**(1): 85-98.

Vacharajittiphan, P., S. Woolcock and N. S. Trahair (1974). "Effect of in-plane deformation on lateral buckling." Journal of Structural Mechanics **3**(1): 29-60.

Vlasov, V. (1961). Thin-Walled Elastic Beams. Jerusalem, Israel, Israel Program for Scientific Translations.

Wang, C. and S. Kitipornchai (1986a). "On stability of monosymmetric cantilevers." Engineering Structures **8**(3): 169-180.

Wang, C. M. and S. Kitipornchai (1986b). "Buckling capacities of monosymmetric I-beams." Journal of Structural Engineering **112**(11): 2373-2391.

Wang, Y.-q., L. Zong, R.-x. Zhu, X.-y. Liu and Y.-j. Shi (2015). "Behavior of I-section steel beam welding reinforced while under load." Journal of Constructional Steel Research **106**: 278-288.

Wu, L. and M. Mohareb (2011). "Buckling of shear deformable thin-walled members—I. Variational principle and analyticalsolutions." Thin-walled structures **49**(1): 197-207.

Chapter 3: Shell Finite Element Modelling of Strengthened Doubly Symmetric Beams[1]

Abstract

The present study investigates the elastic Lateral Torsional Buckling (LTB) behaviour of flexural steel members of W sections that are strengthened with steel cover plates while under loading. For this purpose, a finite element study is developed to investigate the effect of span, strengthening scenarios where only a portion of beam is strengthened, types and location of loading before and after strengthening, magnitude of pre-strengthening loads, boundary conditions and load height. Abaqus shell model is used to carefully simulate the full sequence of pre-existing loading application, application of clamping forces to bring into contact the initially straight steel cover plates with the bent configuration of the beam, the rebound arising during the removal of the clamping forces, welding at the interfaces between the cover plates and the flanges, the application of post-strengthening loads up to the point of onset of elastic LTB for the strengthened system as determined by eigenvalue analysis. It is shown that web distortional effects play an important role in reducing the elastic critical moment capacity. Practical recommendations are then provided to suppress distortional effects and maximize the elastic critical moment capacity of the strengthened beams. The study shows that cover plate strengthening is an effective means of increasing the LTB capacity of existing beams. A simplified design equation is then proposed to quantify the post-strengthening critical moment capacity of strengthened beams. The merits and limitations of the equation are identified and discussed.

[1] This chapter was published and presented in Canadian Society of Civil Engineering Annual Conference 2022 as: Iranpour A, Mohareb M. Elastic lateral torsional buckling resistance of beams strengthened with cover plates under pre-existing loads. Whistler, British Columbia, Canada. (pp. 547-564), Cham: Springer Nature Switzerland.

Keywords: Elastic lateral torsional buckling, Finite element analysis, Strengthening, Pre-existing loads.

3.1 Introduction and Literature Review

Existing steel structures need to be strengthened when required to withstand operating loads greater than those for which they were originally designed. Effective strengthening strategies need to be tailored to suit the failure modes expected under the expected increase in loads. Elastic lateral torsional buckling (LTB) is a failure mode that is likely to govern the capacity of wide flange beams with long unbraced lengths. Under such scenarios, the welding of steel cover plates to both flanges of the I-beam would be a practical method for strengthening existing steel beams. In most strengthening scenarios, entirely relieving members from loads before strengthening might maximize the effectiveness of strengthening. However, the full removal of existing loads is typically difficult and expensive to achieve. Hence, it is common to strengthen members while under at least partial loading. The classical LTB theory (e.g., Vlasov 1961), which forms the basis of LTB provisions in steel design standards (e.g., CAN/CSA-S16 2019 and ANSI/AISC360 2022[1]), does not account for the effect of the loads acting on the member prior to strengthening. Hence, applying it to strengthening applications of beams with pre-existing loads is questionable and is subject to the investigation of the present study.

Studies on the LTB of strengthened beams are scarce. MacCrimmon (2009) provided a procedure to estimate the critical moments for built-up crane runway beams. Hsu et al. (2009 and 2012) investigated the torsional properties of I-beams strengthened with open-side down channels over

[1] The original publication cited ANSI/AISC 360 (2016). Following the release of the updated version ANSI/AISC 360 (2022), a comparison was conducted between the two editions, revealing identical lateral torsional buckling provisions. As a result, the citation has been updated to reflect the latest edition.

the top flanges of wide flange beams in a bit to reliably evaluate the LTB capacity of the strengthened beams. Pezeshky et al. (2020) developed a generalized thin-walled beam theory for the elastic LTB analysis of wide flange sections strengthened with any number of cross-sections forming a monosymmetric assembly. Based on a 3D shell-based Finite Element (FE) modelling, Reichenbach et al. (2020) conducted a parametric study to investigate the elastic LTB capacity of beams with stepped flanges and proposed simplified procedures to estimate their effective properties. None of the above studies, however, investigated the effect of loads that may be acting on the member before the strengthening process.

Liu and Gannon (2009b) conducted experimental and numerical studies on nine tests and 93 FE runs to investigate the behaviour and capacity of I-beams strengthened while under load. The authors reported that, while the pre-strengthening load level has a noticeable effect on the inelastic LTB capacity of the member, its effect is negligible on its yielding strength. None of the experiments reported however failed in elastic LTB. Another experimental study on four specimens by Wang et al. (2015) confirmed the findings of Liu and Gannon (2009a), where it was found that pre-strengthening load levels adversely affect the inelastic LTB resistance of strengthened beams. Pham et al. (2017) conducted an analytical investigation on the effect of pre-strengthening loads on the post-strengthening elastic response of flexural members. The study did not address, however, the LTB mode of failure.

Within the above context, the present study aims to investigate the elastic LTB capacity of flexural members that are strengthened while under loads.

3.2 Statement of the Problem

An unloaded wide flange beam is depicted in Configuration 1 in Fig. 3.1. Under general transverse loads q_0, it undergoes a transverse deflection V_0 (Configuration 2). While under loading, the beam is to be strengthened using two initially straight plates. To enable the welding of the straight plates to the deflected beam, temporary loads q_t are applied to the plates to bring them into full contact with the flanges along the span. The plates are then clamped to the flanges (Configuration 4) and the temporary loads q_t are removed causing the system to rebound upwards while undergoing a deflection V_r to attain Configuration 5. Welding is then performed at Configuration 5 and additional operating external reference loads q_p are applied to the strengthened beam which brings the system to Configuration 6 by undergoing an additional displacement V_p. The applied reference loads q_p are then gradually increased to λq_p at which the strengthened system attains the state of onset of LTB (Configuration 7), in which λ is an unknown load multiplier to be determined from a buckling analysis. At this state, the system loses its lateral stiffness and has a tendency to buckle in a lateral torsional mode (Configuration 8) under no increase in loads.

It is required to determine the post-strengthening elastic critical moment M_{cr} of the system. For this purpose, the post-strengthening elastic critical moment M_{cr-FEA} is determined based on Finite Element Analysis (FEA) by using shell models in Abaqus (2020) to obtain the FE-predicted critical moments while modelling the full loading and strengthening sequence depicted in Fig. 3.1.

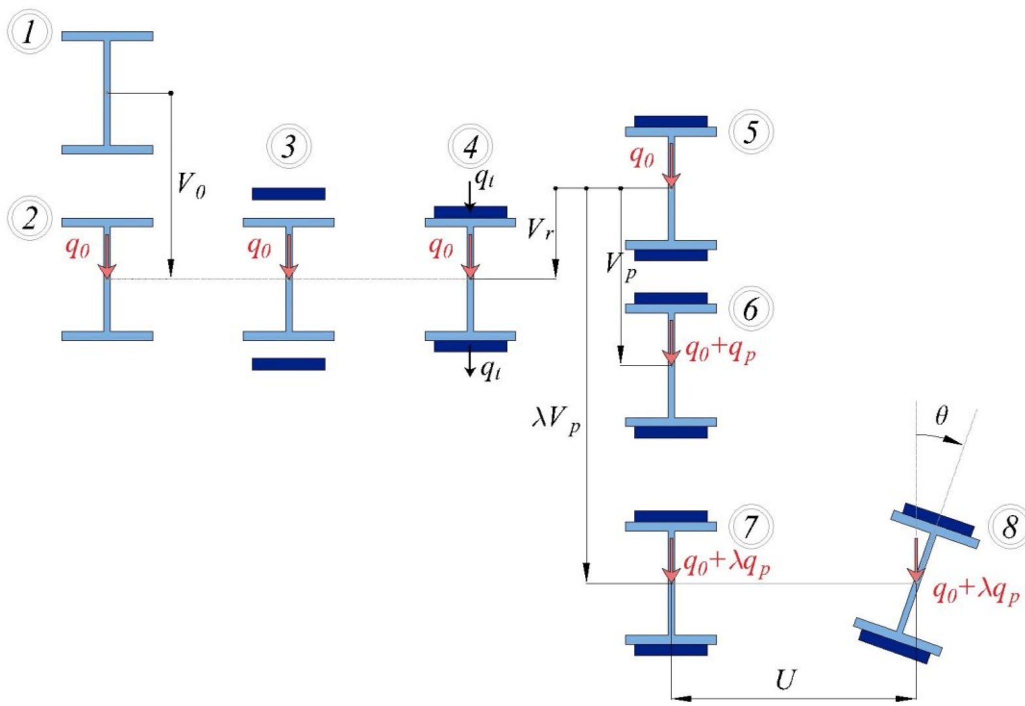

Fig. 3.1 Loading and strengthening sequence

3.3 Parametric Study

3.3.1 Reference Beam

A reference beam spanning 7m with a W310×52 cross-section is simply supported relative to transverse and lateral displacements and relative to twist at both ends. Prior to strengthening, the reference beam is subjected to two point loads (2PLs) at third span points (i.e., $L/3$ and $2L/3$) acting at the shear centre of the cross-section. The capacity of the beam prior to strengthening is governed by elastic LTB for yield strength $F_y = 350MPa$. The magnitude of the pre-strengthening loads applied to the reference beam is taken to correspond to a fraction $\Omega = 75\%$ of the critical moment M_{ua} of the unstrengthened beam as determined from

$$M_{ua} = \left(\omega_{2-CSA}\right)_a \frac{\pi}{L}\sqrt{EI_{ya}GJ_a + \left(\frac{\pi E}{L}\right)^2 I_{ya}C_{wa}} \tag{3.1}$$

in which E is the modulus of elasticity, G is shear modulus, L is the beam span, I_{ya} is the weak axis moment, J_a is the Saint-Venant torsional constant, C_{wa} is the warping constant and all subscripts a denote quantities pertaining to the unstrengthened beam. In Eq. (3.1), $\left(\omega_{2-CSA}\right)_a$ is the moment gradient factor according to (CAN/CSA-S6-19 2019) and is given by

$$\left(\omega_{2-CSA}\right)_i = \left(\frac{4M_{\max}}{\sqrt{M_{\max}^2 + 4M_A^2 + 7M_B^2 + 4M_C^2}}\right)_i \qquad i = a, b \tag{3.2}$$

in which $M_{\max}$, M_A, M_B and M_C are respectively the absolute values of the peak moment, the quarter-point, mid-span, and third-quarter point moments of the unbraced segments and subscript i takes the value $i = a$ to denote values pertaining to the pre-strengthening loads and $i = b$ to denote values pertaining to the post-strengthening loads. The critical moment for the unstrengthened beam as predicted by Eq. (3.1) is $M_{ua} = 131.6kNm$. Thus, the point loads corresponding to a fraction $\Omega = 75\%$ of the critical moment M_{ua} induce a peak moment of $0.75 \times 131.6kNm = 98.7kNm$.

The entire span of the reference beam is then strengthened by welding two cover plates $b_p \times t_p = 140mm \times 10mm$ and subsequently subjected to a post-strengthening loading scenario similar in distribution to the pre-strengthening load (i.e., 2PLs applied at third span points acting at the shear centre of the cross-section). It is required to obtain the post-strengthening critical moment for the strengthened section using the Abaqus shell model.

3.3.2 Finite Element Modeling

3.3.2.1 Shell Element Model

The S4R element in the Abaqus library Abaqus (2020) was used to mesh the model. The S4R is a four-node shell element with six degrees of freedom per node, with reduced integration, and hourglass control. A mesh study indicated that convergence is attained when an element size of nearly 15 mm is used throughout the beam. The interaction between the cover plates and beam flanges was modelled using the *CONTACT PAIR keyword in Abaqus, with the SMALL SLIDING, TYPE=SURFACE TO SURFACE features. These features enforce a small-sliding formulation between the two surfaces in contact by considering the sliding between the two surfaces as small/negligible relative to the deformations/motion of the structure (SIMULIA 2020). In order to prevent penetration between both surfaces, a HARD contact pressure over-closure relationship was defined.

The analysis in Abaqus is performed in three steps; (1) the unstrengthened section was first subjected to the pre-strengthening load while the cover plates were concurrently bent to match the configuration of the bent beam, (2) A ROUGH friction model was activated at the interfaces between the plates and the flanges by using the *FRICTION, ROUGH keyword while suppressing the separation between the two surfaces after contact has been established by using the *SURFACE BEHAVIOR, NO SEPARATION, PRESSURE-OVERCLOSURE=HARD keyword. The use of the above combination of features ensures surfaces to remain fully bonded together, with no separation nor tangential sliding, once they have been brought into contact, even when the contact pressure between them is tensile, and (3) The post-strengthening load is then applied and a linearized eigenvalue buckling analysis is performed, in order to obtain the residual critical moment for the strengthened beam.

3.3.2.2 Thin-Walled Beam Element Model

Given that the Abaqus shell models capture cross-sectional distortion, a thin-walled beam solution that suppresses web distortion is also used for comparison to determine the non-distortional LTB critical moment and provide a basis to quantify the effect of web distortion on the LTB capacity. For this purpose, the LTB-UO program (Sahraei et al. 2020) is used. This program is developed based on the formulation by Barsoum and Gallagher (1970) element and will be referred to subsequently as the BG element. The element omits the cross-sectional distortion and computes the elastic LTB capacity of beams under general transverse loading and general boundary conditions.

The FE formulation of the element is developed based on the total potential energy functional Π of a thin-walled beam during buckling. The simplest form of Π, omitting the effects of shear deformation, web distortion, pre-buckling deformation, and load height effects is

$$\Pi = \frac{1}{2}\int_L \left(EI_y U''^2 + EC_w \theta''^2 + GJ\theta'^2 + 2\lambda M \theta U'' \right) dx \tag{3.3}$$

in which E is the modulus of elasticity, G is shear modulus, I_y is the weak axis moment of inertia, J is the Saint-Venant torsional constant, C_w is the warping constant, $U = U(x)$ is the lateral displacement, $\theta = \theta(x)$ is the angle of twist, λ is a buckling load multiplier to be determined from an eigenvalue analysis, $M = M(x)$ is the moment distribution under the applied transverse loads. Within the finite element, it is obtained by adopting linear interpolation over the element length L_e, i.e.,

$$M(x) = -M_1 \left(1 - x/L_e\right) + M_2 \left(x/L_e\right) \tag{3.4}$$

in which, M_1 and M_2 are bending moment values at element ends and are obtained from the pre-buckling analysis. The BG element is a two-node thin-walled beam element with four buckling degrees of freedom per node: the lateral displacement U, the rotation about the weak axis U', the angle of twist θ and the warping deformation θ' (Fig. 3.2).

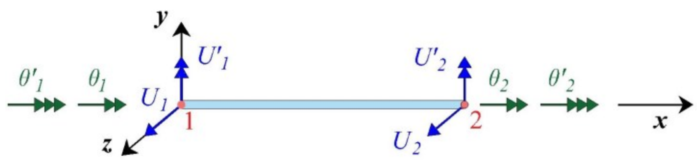

Fig. 3.2 Degrees of freedom of the BG element employed in the LTB-UO program

The lateral displacement $U(x)$ and angle twist $\theta(x)$ within the element are related to the vector of degrees of freedom $\mathbf{d}^{\mathbf{T}} = \langle U_1 \quad U_1' \quad U_2 \quad U_2' \quad \theta_1 \quad \theta_1' \quad \theta_2 \quad \theta_2' \rangle$ through

$$U(x) = \mathbf{H_U}^{\mathbf{T}}\mathbf{d},\ \theta(x) = \mathbf{H_\theta}^{\mathbf{T}}\mathbf{d} \qquad (3.5)\text{a-b}$$

in which the vectors of shape functions are defined by

$$\begin{aligned}
&\mathbf{H_U}^{\mathbf{T}} = \mathbf{H_U}^{\mathbf{T}}(x) = \langle H_1 \quad -H_2 \quad H_3 \quad -H_4 \quad 0 \quad 0 \quad 0 \quad 0 \rangle \\
&\mathbf{H_\theta}^{\mathbf{T}} = \mathbf{H_\theta}^{\mathbf{T}}(x) = \langle 0 \quad 0 \quad 0 \quad 0 \quad H_1 \quad H_2 \quad H_3 \quad H_4 \rangle \\
&\langle H_1,\ H_2,\ H_3,\ H_4 \rangle = \left\langle 1 - 3\zeta^2 + 2\zeta^3,\ L_e\zeta(1-\zeta)^2,\ 3\zeta^2 - 2\zeta^3,\ L_e\zeta^2(\zeta - 1) \right\rangle,\ \zeta = x/L_e
\end{aligned} \qquad (3.6)\text{a-d}$$

From Eqs. (3.5)a-b, by substituting into the variational principle in Eq. (3.3) and evoking the stationarity conditions $(\partial\Pi/\partial\mathbf{d})\delta\mathbf{d} = 0$, one obtains the linearized eigenvalue problem that yields the load multiplier λ corresponding to the state of onset of buckling, i.e.,

$$(\mathbf{k_E} - \lambda\mathbf{k_G})_{8\times8}\,\mathbf{d}_{8\times1} = \mathbf{0}_{8\times1} \qquad (3.7)$$

in which $\mathbf{k_E}$ is the elastic stiffness matrix and $\mathbf{k_G}$ is the geometric matrix.

It is noted that the total potential energy expression in Eq. (3.3) forms the basis of the critical moment equation in design standards (e.g., CAN/CSA-S16 2019 and ANSI/AISC360 2022). For example, for a simply supported beam relative to twist and lateral displacement subjected to uniform moment, by assuming the displacement functions $U(x) = A\sin(\pi x/L)$ and $\theta(x) = B\sin(\pi x/L)$), substituting into Eq. (3.3), taking, evoking the stationary condition (i.e., $\partial\Pi/\partial A = \partial\Pi/\partial B = 0$), expressing the result in a matrix form, and setting to zero the determinant of the matrix of coefficient, one obtains the critical moment equation

$$\lambda M = \pm\frac{\pi}{L}\sqrt{EI_y GJ + \left(\frac{\pi E}{L}\right)^2 I_y C_w} \tag{3.8}$$

Since the potential energy expression in Eq. (3.3) omits the cross-sectional distortion, Eq. (3.8) does not account for distortional effects.

3.3.3 Design of Parametric Study

An additional 22 cases were investigated by varying the beam span, the strengthening configuration (Fig. 3.3a), the loading configurations and locations before and after strengthening of the beam (Fig. 3.3b and Fig. 3.4), the magnitude of the pre-strengthening load, the boundary conditions (Fig. 3.3c) and the load height. Table 3.1 provides the input parameters for each case. By varying the span from 7 to 11 and 14m (Column 2 in Table 3.1), three values of span to depth ratio L/d are investigated (Column 3).

As shown in Fig. 3.3a, in addition to the unstrengthened beam, three strengthening schemes are investigated (Column 4 in Table 3.1): (1) Full Strengthening of the entire beam, (2) End Strengthening through plates located at beam ends, and (3) Midspan Strengthening through plates located at midspan. Seven loading configurations are investigated (Fig. 3.3b and Fig. 3.4): (1) 1PL:

Point load applied at the beam midspan, (2) 2PLs: Two point loads applied at third points, (3) 3PLs: Three point loads applied at quarter points, (4) 4PLs: Four point loads applied at fifth points, (5) UDL: Uniformly distributed load, (6) PL-L/4: Point load applied at L/4, and (7) PL-3L/4: Point load applied at 3L/4. The distributions of pre- and post-strengthening loads are different in some cases as presented in Columns 5 and 7. The magnitude of pre-strengthening loads is taken as a fraction Ω (Column 6) of the critical moment of the unstrengthened beam. As shown in Fig. 3.3c, three sets of boundary conditions are investigated (Column 8). Column 9 reports the load height of each run. Three scenarios are investigated: (1) SC: Loads are acting at the Shear Centre, (2) TF: Loads are acting at the Top Flange, and (3) BF: Loads are acting at the Bottom Flange.

3.3.4 Suppressing Web Distortion

Past studies reported that web distortion can significantly affect the LTB capacity of beams with slender webs and stocky flanges in beams with short spans (Pezeshky and Mohareb 2018, Liang et al. 2022). According to Arizou and Mohareb (2021), simply supported unstrengthened beams undergoing LTB exhibit maximum distortion at beam ends and midspan. Using transverse stiffeners to suppress web distortion at these locations was shown to increase the distortional LTB capacity and help approaching the non-distortional LTB capacity. One of the objectives of the present study is to extend the investigation for strengthened beams. Towards this objective, web distortion is suppressed at different locations of shell models by employing kinematic constraints that suppress web distortion between both flanges while coupling the angles of twist of both flanges and the web to emulate the action of a transverse stiffener at the stiffened section while enabling the section to warp freely.

For Run 1 in Table 3.1, the critical moment is 118.7kNm (Column 10 in Table 3.1) when no stiffeners are provided, i.e., web distortion is enabled (Fig. 3.5b). By suppressing the distortion at the beam ends, cross-sectional distortion decreases (Fig. 3.5c) and, subsequently, the critical moment increases to 126.2kNm (Column 11), a 6.3% increase. This value compares to 127.2kNm based on the non-distortional critical moment obtained using the BG element. Cross-sectional distortion is subsequently suppressed at midspan. The further increase in critical moment observed is a mere 0.10%. It is concluded that suppressing only the beam ends in Run 1 suffices to attain its non-distortional critical LTB moment capacity. This conclusion is also confirmed by observing the web distortion along the beam span as discussed in the following section.

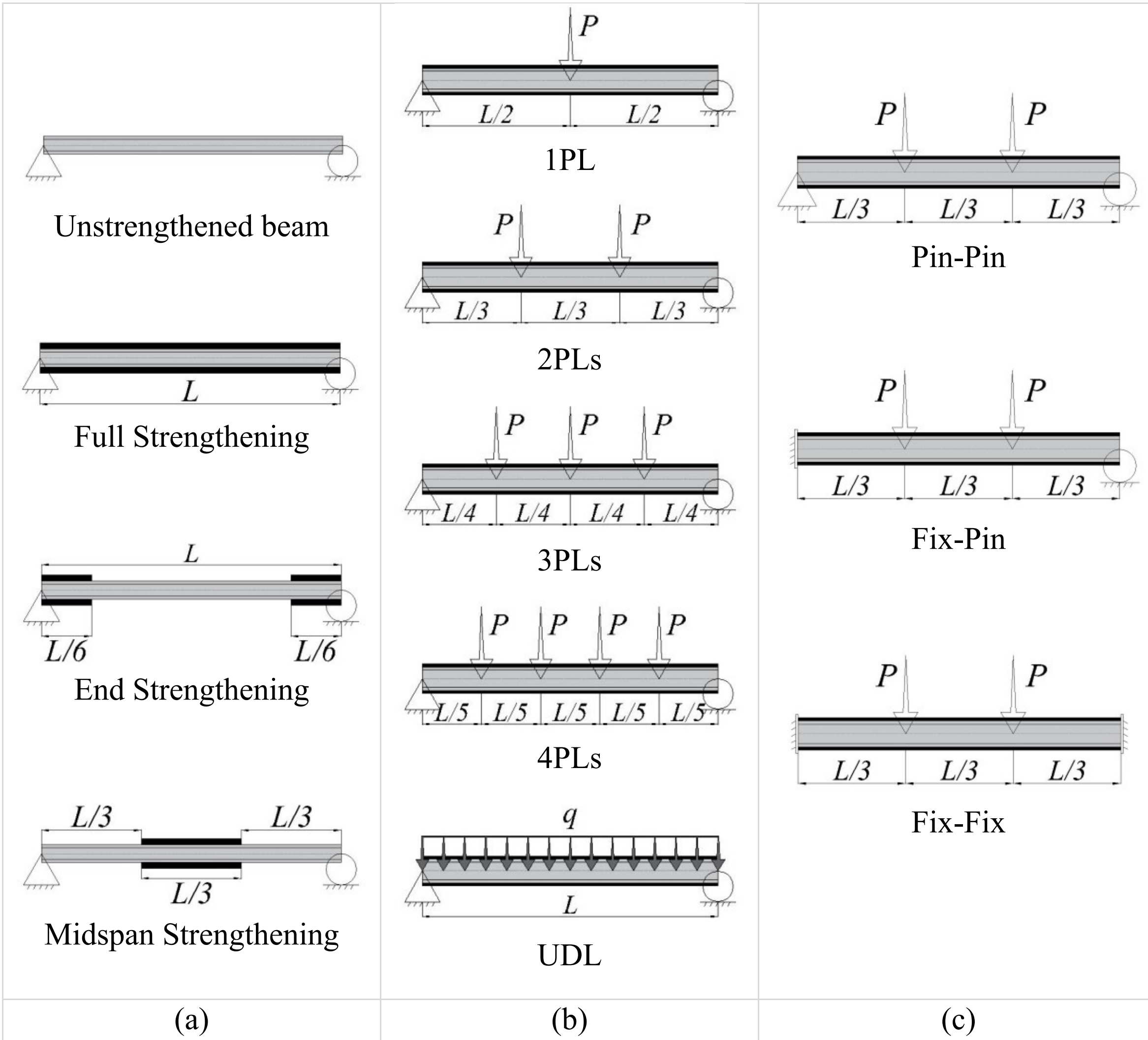

Fig. 3.3 Variables investigated (a) Strengthening configurations (Runs R, 4, 5 and 6), (b) Loading configurations (Runs R, 7-14) and (c) Boundary conditions (Runs R, 18 and 19)

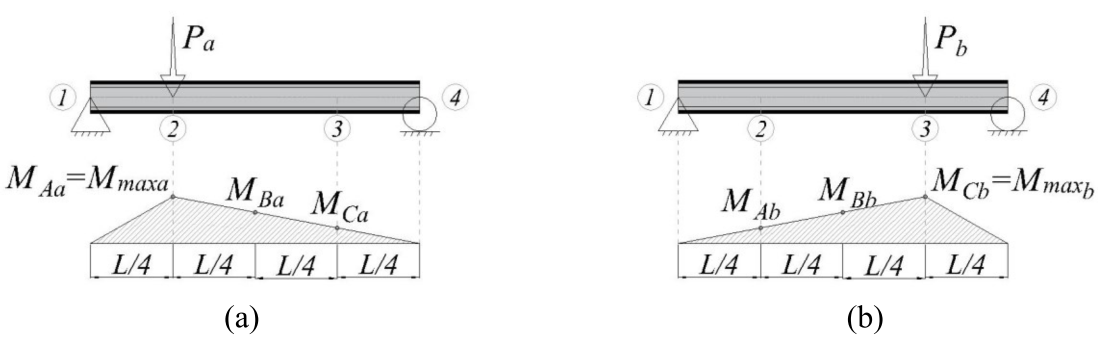

Fig. 3.4 Location of applied loads and corresponding bending moments for Run 22 (a) prior to strengthening, and (b) after strengthening

Table 3.1 Table of runs (effect of stiffeners on critical moment increase)

				Loading and boundary conditions					Critical moments (kNm)			Percentage change	
Run Number	Span *L* (m)	Span to depth ratio *L*/*d*	Strengthening scheme	Pre-strengthening load configuration	Pre-strengthening moment fraction Ω	Post-strengthening load configuration	Boundary conditions	Load height	Unstiffened web	End stiffeners	Ends and midspan stiffeners	(11-10)/(10)×100	(12-10)/(10)×100
(1)	(2)	(3)	(4)	(5)	(6)	(7)	(8)	(9)	(10)	(11)	(12)	(13)	(14)
1	7	22.0	US[a]	2PLs	0.00	2PLs	Pin-Pin	SC	118.7	126.2	126.3	6.3%	6.4%
R	**7**	**22.0**	Full[b]	2PLs[e]	0.75	2PLs	Pin-Pin	SC[l]	137.0	175.7	178.1	28.3%	30.0%
2	**11**	**34.6**	Full	2PLs	0.75	2PLs	Pin-Pin	SC	95.9	112.8	113.2	17.6%	18.1%
3	**14**	**44.0**	Full	2PLs	0.75	2PLs	Pin-Pin	SC	78.1	88.8	89.0	13.6%	13.9%
R	7	22.0	**Full**	2PLs	0.75	2PLs	Pin-Pin	SC	137.0	175.7	178.1	28.3%	30.0%
4	7	22.0	**US**	2PLs	0.75	2PLs	Pin-Pin	SC	20.0	27.5	27.6	37.5%	37.9%
5	7	22.0	**End**[c]	2PLs	0.75	2PLs	Pin-Pin	SC	46.6		See Table 3.2		
6	7	22.0	**Mid**[d]	2PLs	0.75	2PLs	Pin-Pin	SC	44.3	53.6	54.5	21.1%	23.2%
7	7	22.0	Full	**1PL**[f]	0.75	2PLs	Pin-Pin	SC	148.2	186.3	188.9	25.7%	27.4%
R	7	22.0	Full	**2PLs**	0.75	2PLs	Pin-Pin	SC	137.0	175.7	178.1	28.3%	30.0%
8	7	22.0	Full	**3PLs**[g]	0.75	2PLs	Pin-Pin	SC	144.8	183.5	185.9	26.8%	28.5%
9	7	22.0	Full	**4PLs**[h]	0.75	2PLs	Pin-Pin	SC	139.2	178.0	180.4	27.9%	29.6%
10	7	22.0	Full	**UDL**[i]	0.75	2PLs	Pin-Pin	SC	140.2	179.4	181.8	28.0%	29.7%
11	7	22.0	Full	2PLs	0.75	**1PL**	Pin-Pin	SC	172.3	219.4	222.8	27.3%	29.3%
R	7	22.0	Full	2PLs	0.75	**2PLs**	Pin-Pin	SC	137.0	175.7	178.1	28.3%	30.0%
12	7	22.0	Full	2PLs	0.75	**3PLs**	Pin-Pin	SC	148.4	190.4	193.1	28.3%	30.1%
13	7	22.0	Full	2PLs	0.75	**4PLs**	Pin-Pin	SC	139.9	179.7	182.1	28.4%	30.2%
14	7	22.0	Full	2PLs	0.75	**UDL**	Pin-Pin	SC	141.3	182.0	184.5	28.8%	30.5%
15	7	22.0	Full	2PLs	**0.00**	2PLs	Pin-Pin	SC	237.4	275.9	278.2	16.2%	17.2%
16	7	22.0	Full	2PLs	**0.25**	2PLs	Pin-Pin	SC	203.9	242.5	244.8	18.9%	20.1%
17	7	22.0	Full	2PLs	**0.50**	2PLs	Pin-Pin	SC	170.5	209.1	211.5	22.7%	24.1%
R	7	22.0	Full	2PLs	**0.75**	2PLs	Pin-Pin	SC	137.0	175.7	178.1	28.3%	30.0%
R	7	22.0	Full	2PLs	0.75	2PLs	**Pin-Pin**	SC	137.0	175.7	178.1	28.3%	30.0%
18	7	22.0	Full	2PLs	0.75	2PLs	**Fix-Pin**	SC	398.5		See Table 3.3		
19	7	22.0	Full	2PLs	0.75	2PLs	**Fix-Fix**	SC	643.0		See Table 3.4		
20	7	22.0	Full	2PLs	0.75	2PLs	Pin-Pin	**TF**[m]	91.9	130.3	132.3	41.8%	44.0%
R	7	22.0	Full	2PLs	0.75	2PLs	Pin-Pin	**SC**	137.0	175.7	178.1	28.3%	30.0%
21	7	22.0	Full	2PLs	0.75	2PLs	Pin-Pin	**BF**[n]	192.0	229.1	232.0	19.4%	20.9%
22	7	22.0	Full	PL-L/4[j]	0.75	PL-3L/4[k]	Pin-Pin	SC	212.6	267.6	270.4	25.9%	27.2%

[a] US: Unstrengthening beam
[b] Full: Full strengthening scheme
[c] End: End strengthening scheme
[d] Mid: Midspan strengthening scheme
[e] 2PLs: 2 point loads applied at L/3 and 2L/3
[f] 1PL: Point load applied at the beam midspan
[g] 3PLs: 3 point loads applied at L/4, L/2 and 3L/4
[h] 4PLs: 4 point loads applied at L/5, 2L/5, 3L/5 and 4L/5
[i] UDL: Uniformly distributed load
[j] PL-L/4: Point load applied at L/4
[k] PL-3L/4: Point load applied at 3L/4
[l] SC: Shear centre loading
[m] TF: Top flange loading
[n] BF: Bottom flange loading
[o] NA: Not applicable

Table 3.2 Effect of stiffeners on critical moment increase in Run 5

Transverse Stiffener Location		M_{cr-FEA} (kNm)	Percentage change
Unstiffened		46.6	-
End stiffeners		70.6	51.4%
Ends + locations of section change		81.6	75.0%
Ends + locations of section change + midspan		81.8	75.4%

Table 3.3 Effect of stiffeners on critical moment increase in Fixed-Pinned Beam (Run 18)

Transverse Stiffener Location		M_{cr-FEA} (kNm)	Percentage change
Unstiffened	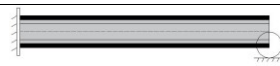	399	-
Pinned end	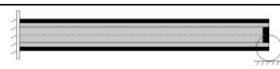	453	13.7%
Pinned end + 1m from fixed end	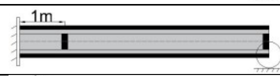	459	15.1%
Pinned end + 1m from fixed end + midspan	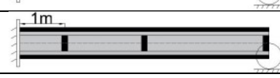	465	16.6%

Table 3.4 Effect of stiffeners on critical moment increase in Fixed-Fixed Beam (Run 19)

Transverse Stiffener Location		M_{cr-FEA} (kNm)	Percentage change
Unstiffened	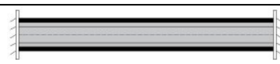	643	-
1m from both fixed ends		675	4.9%
1m from both fixed ends + midspan		686	6.7%

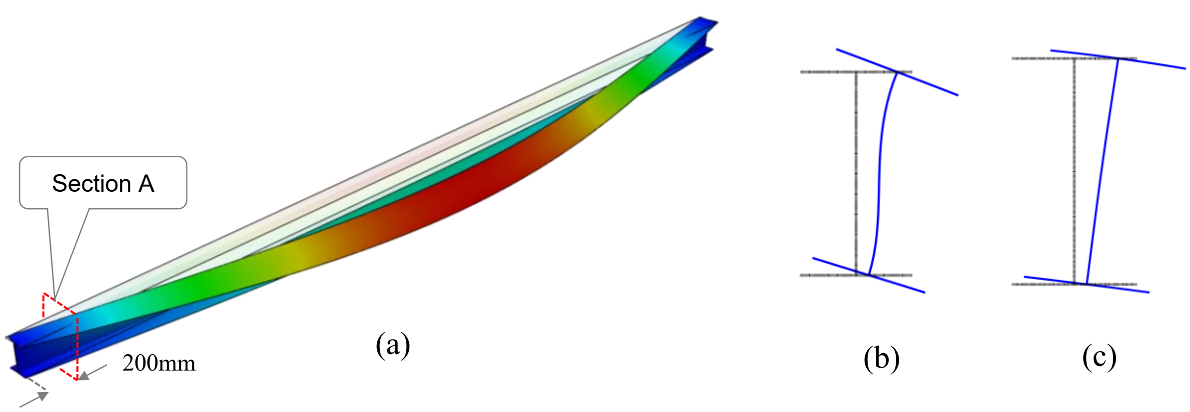

Fig. 3.5 Run 1 (a) Buckled Configuration, (b) No transverse stiffener provided at beam ends: Distortion takes place at Section A, and (c) Transverse stiffener provided at beam ends: Distortion roughly suppressed at Section A

Fig. 3.6 compares the buckled configurations of the top and bottom flanges for Run 1 based on three models: (1) the shell FEA which captures the web distortion along the entire span, (2) the shell FEA with suppressed distortion at both ends, and (3) the non-distortional solution based on the BG element. In all three cases, the buckling modes were normalized with respect to the peak lateral displacement at the top flange. For this reason, the lateral displacements of the top flange in all three models are nearly identical. At the bottom flange, however, the lateral displacement predicted by the shell model which captures web distortion slightly differs from that based on the non-distortional BG model. The difference is attributed to web distortion in the former model. When the cross-sectional distortion is suppressed in the shell model at beam ends, the buckled configuration of the shell model approaches/coincides with that of the non-distortional BG element. Hence, the web distortion in Run 1 can effectively be suppressed by providing end stiffeners. For this reason, the critical moment of Run 1 based on the shell model with end stiffeners, which is 126.2kNm (Column 11 in Table 3.1), is very close to that based on the non-distortional solution, which is 127.2kNm.

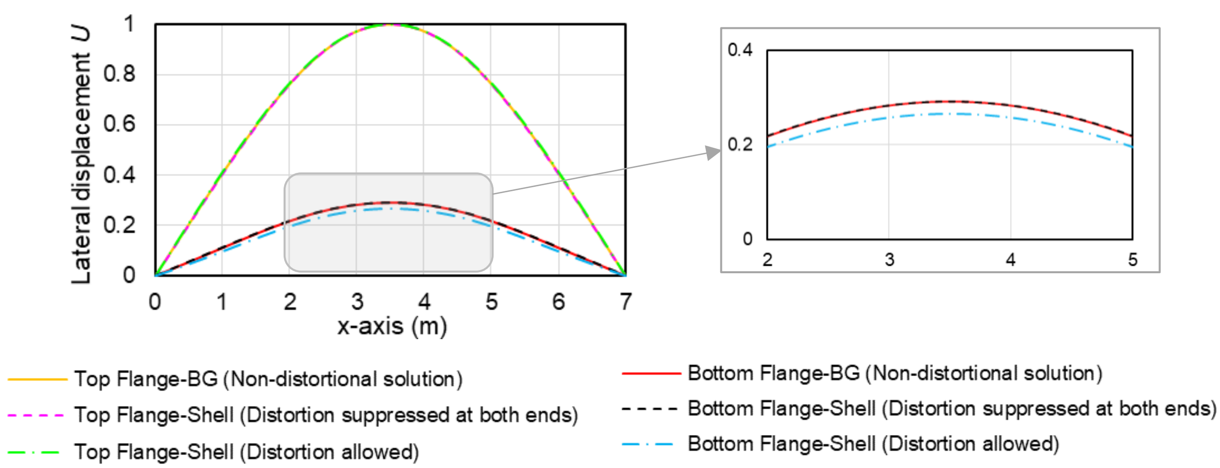

Fig. 3.6 Comparison of buckled shapes of the top and bottom flanges in Run 1

Table 3.1-Table 3.4 summarize the effect of suppressing the cross-sectional distortion at different locations for all models investigated. In all cases, suppressing distortion at midspan was found to have a negligible effect on the critical moment (around 2%).

When the strengthening cover plates are provided at end portions of the beam (e.g., Run 5 and Table 3.2), the web was found to distort at the location of section change in addition to the beam ends. Suppressing the distortion by providing transverse stiffeners at these locations was found to significantly increase the elastic critical moment capacity (by 75%). Conversely, when the strengthening cover plate is provided in the middle portion of the beam (e.g., Run 6 in Table 3.1), cross-sectional distortion at the location of section change was found to be negligible.

For beams with fixed end supports (i.e., Runs 18 and 19), maximum distortion was found to take place in the vicinity of the fixed support. As a result, suppressing cross-sectional distortion at these regions was found to increase the LTB capacity of the beam (Tables 3 and 4).

To exclude the effects of cross-sectional distortion on LTB capacity, and hence maximize the elastic LTB capacity attained, cross-sectional distortion is suppressed at proper locations in all models (beam ends, one meter away from the fixed support, locations of the section change and midspan).

3.3.5 Effect of Cover Plate Strengthening on the Critical Moment

3.3.5.1 General

For the reference beam, the post-strengthening critical moment as predicted by the Abaqus shell model is $M_{cr-FEA} = 178.1 kNm$ (Column 12 in Table 3.5). Towards devising a simplified methodology to estimate the post-strengthening critical moments, the following expression is proposed to quantify the additional post-strengthening critical moment M_{cr-m}

$$M_{cr-m} = (\omega_2)_b \frac{\pi}{L}\sqrt{EI_{yb}GJ_b + \left(\frac{\pi E}{L}\right)^2 I_y C_{wb}} - M_0 \qquad (3.9)$$

in which the cross-sectional properties of the strengthened beam are the weak axis moment of inertia I_{yb}, the Saint-Venant torsional constant J_b, the warping constant C_{wb}. In Eq. (3.9), M_0 denotes the pre-strengthening bending moment value (e.g., $M_0 = M_{Ca} = M_{\max a}/3$ in Fig. 3.4a) corresponding to the location of the peak post-strengthening moment (e.g., Point 3 in Fig. 3.4b) and $(\omega_2)_b$ is the moment gradient factor corresponding to the post-strengthening loads which can be obtained in two ways: (1) Setting $i = b$ in Eq. (3.2), and (2) Using FEA results.

For the reference beam, $(\omega_{2-CSA})_b$ as predicted by Eq. (3.2) is 1.13 (Column 15 in Table 3.5). This value is slightly greater than the moment gradient factor obtained from FEA $(\omega_{2-FEA})_b$, which is 1.10 (Column 16). FEA predicted values for the moment gradient factor $(\omega_{2-FEA})_b$ are obtained in three steps: (1) Omitting pre-strengthening loads and analyzing the beam under the post-strengthening loads, (2) Analyzing the same model under the uniform moment, and (3) dividing the critical moment of step 1 by that of step 2, to obtain a more accurate moment gradient factor $(\omega_{2-FEA})_b$ than that based on the standard.

For the reference beam, the critical moment of the unstrengthened beam due to pre-strengthening loads M_{ua} as predicted by Eq. (3.1) is 131.6kNm (Column 11 in Table 3.5). As discussed, the applied pre-strengthening loads induce a peak moment ΩM_{ua}, which gives $0.75 \times 131.6 = 98.7 kNm$ for the reference beam. The peak moments corresponding to pre- and post-strengthening loads occur at the same location since the pre- and post-strengthening loads have the same distribution, so $M_0 = 98.7 kNm$ (Column 10). The predicted value of the post-strengthening critical moment using Eq. (3.9) with $(\omega_{2-FEA})_b$ is found to be $M_{cr-m} = 186.2 kNm$ (Column 13).

The ratio M_{cr-m}/M_{cr-FEA} is used to assess the accuracy of the predictions of Eq. (3.9). When pre-strengthening loads are set to zero, M_{cr-m}/M_{cr-FEA} is very close to unity. However, when the beam is under load prior to strengthening, the accuracy of Eq. (3.9) will vary. For the reference beam, one has $M_{cr-m}/M_{cr-FEA} = 1.05$ (Column 14), indicating that Eq. (3.9) overpredicts the post-strengthening critical moment by 4.6%. Similar results are obtained for all runs and reported in Table 3.5.

The ratio of total flexural capacity of the strengthened beam to that of the unstrengthened beam is a possible indicator of the efficiency of strengthening. For the reference beam, the total flexural capacity of the strengthened beam can be obtained by adding the applied pre-strengthening moment to the FEA predicted post-strengthening critical moment (i.e., $M_0 + M_{cr-FEA} = 98.7 + 178.1 = 276.8 kNm$). Thus, the strengthening efficiency attained for the reference beam is defined as $\left(M_0 + M_{cr-FEA}\right)/M_{ua} = 2.1$ (Column 17 in Table 3.5), suggesting that the addition of the cover plates is an effective means of increasing the elastic LTB resistance for the beam. Column 17 of Table 3.5 provides the strengthening effectiveness ratio $\left(M_0 + M_{cr-FEA}\right)/M_{ua}$ for the cases investigated.

Table 3.5 Effect of pre-existing loads on post-strengthening critical moments

				Loading and boundary conditions						Critical moments (kNm)				ω_2 for post-strengthening loads		
Run Number	Span L (m)	Span to depth ratio L/d	Strengthening scheme	Pre-strengthening load configuration	Pre-strengthening moment fraction Ω	Post-strengthening load configuration	Boundary conditions	Load height	Pre-existing moment at location of peak post-strengthening moment M_0	For unstrengthened beam M_{ua}	Post-strengthening predicted by FEA M_{cr-FEA}	Post-strengthening predicted by Eq. (3.9) M_{cr-m}	M_{cr-m}/M_{cr-FEA}	Predicted by Eq. (3.2) $(\omega_{2-CSA})_b$	Predicted by FEA $(\omega_{2-FEA})_b$	Strengthening effectiveness [(10)+(12)]/(11)
(1)	(2)	(3)	(4)	(5)	(6)	(7)	(8)	(9)	(10)	(11)	(12)	(13)	(14)	(15)	(16)	(17)
R	**7**	**22**	Full	2PLs	0.75	2PLs	PP	SC	98.7	131.6	178.1	186.2	1.05	1.13	1.10	2.10
2	**11**	**35**	Full	2PLs	0.75	2PLs	PP	SC	57.1	76.1	113.2	117.0	1.03	1.13	1.11	2.24
3	**14**	**44**	Full	2PLs	0.75	2PLs	PP	SC	43.6	58.1	89.0	91.5	1.03	1.13	1.11	2.28
R	7	22	**Full**	2PLs	0.75	2PLs	PP	SC	98.7	131.6	178.1	186.2	1.05	1.13	1.10	2.10
4	7	22	**US**	2PLs	0.75	2PLs	PP	SC	98.7	131.6	27.6	28.1	1.02	1.13	1.09	-
5	7	22	**End**	2PLs	0.75	2PLs	PP	SC	98.7	131.6	81.8	NA	-	1.13	1.07	1.37
6	7	22	**Mid**	2PLs	0.75	2PLs	PP	SC	98.7	131.6	54.5	NA	-	1.13	1.13	1.16
7	7	22	Full	**1PL**	0.75	2PLs	PP	SC	110.4	147.1	188.9	174.6	0.92	1.13	1.10	2.03
R	7	22	Full	**2PLs**	0.75	2PLs	PP	SC	98.7	131.6	178.1	186.2	1.05	1.13	1.10	2.10
8	7	22	Full	**3PLs**	0.75	2PLs	PP	SC	98.7	131.6	185.9	186.5	1.00	1.13	1.11	2.16
9	7	22	Full	**4PLs**	0.75	2PLs	PP	SC	98.7	131.6	180.4	186.7	1.03	1.13	1.11	2.12
10	7	22	Full	**UDL**	0.75	2PLs	PP	SC	98.7	131.6	181.8	186.2	1.02	1.13	1.10	2.13
11	7	22	Full	2PLs	0.75	**1PL**	PP	SC	98.7	131.6	222.8	256.5	1.15	1.26	1.38	2.44
R	7	22	Full	2PLs	0.75	**2PLs**	PP	SC	98.7	131.6	178.1	186.2	1.05	1.13	1.10	2.10
12	7	22	Full	2PLs	0.75	**3PLs**	PP	SC	98.7	131.6	193.1	210.2	1.09	1.13	1.20	2.22
13	7	22	Full	2PLs	0.75	**4PLs**	PP	SC	98.7	131.6	182.1	192.9	1.06	1.13	1.13	2.13
14	7	22	Full	2PLs	0.75	**UDL**	PP	SC	98.7	131.6	184.5	196.0	1.06	1.13	1.14	2.15
15	7	22	Full	2PLs	**0.00**	2PLs	PP	SC	0.0	131.6	278.2	282.7	1.02	1.13	1.10	2.11
16	7	22	Full	2PLs	**0.25**	2PLs	PP	SC	32.9	131.6	244.8	252.0	1.03	1.13	1.10	2.11
17	7	22	Full	2PLs	**0.50**	2PLs	PP	SC	65.8	131.6	211.5	219.1	1.04	1.13	1.10	2.11
R	7	22	Full	2PLs	**0.75**	2PLs	PP	SC	98.7	131.6	178.1	186.2	1.05	1.13	1.10	2.10
R	7	22	Full	2PLs	0.75	2PLs	**PP**	SC	98.7	131.6	178.1	186.2	1.05	1.13	1.10	2.10
18	7	22	Full	2PLs	0.75	2PLs	**FP**[b]	SC	180.2	240.3	464.6	257.3	0.55	2.07	1.70	2.68
19	7	22	Full	2PLs	0.75	2PLs	**FF**[c]	SC	205.8	274.4	685.8	184.1	0.27	2.36	1.51	3.25
20	7	22	Full	2PLs	0.75	2PLs	PP	**TF**	98.7	131.6	132.3	NA	-	1.13	1.10	1.76
R	7	22	Full	2PLs	0.75	2PLs	PP	**SC**	98.7	131.6	178.1	186.2	1.05	1.13	1.10	2.10
21	7	22	Full	2PLs	0.75	2PLs	PP	**BF**	98.7	131.6	232.0	NA	-	1.13	1.10	2.51
22	7	22	Full	PL-L/4	0.75	PL-3L/4	PP	SC	39.8	159.1	270.4	341.2	1.26	1.37	1.48	1.95

[a] PP: Pin-Pin boundary condition (BC) [b] FP: Fix-Pin BC [c] FF: Fix-Fix BC

3.3.5.2 Effect of Strengthening Scheme (Runs R and 4-6)

Eq. (3.9) is not applicable to partial strengthening schemes (i.e., End and Midspan strengthening schemes). Thus, the post-strengthening critical moments for these scenarios are obtained only by FEA. These values are then normalized by the corresponding value for the unstrengthened beam $M_{cr-FEA-US}$ to quantify the efficiency of partial strengthening schemes. As Fig. 3.7 indicates, the

End Strengthening scheme is 50% more effective than the Midspan strengthening scheme. By normalizing the mode shapes relative to the peak lateral displacement, it is shown that the fully strengthened beam shows the least twist at beam end (Fig. 3.8b), followed by the End strengthening scheme, while the largest angles of twist correspond to the Midspan strengthening scheme. The rate of variation in the angle of twist represents the warping deformation, and as Fig. 3.8b indicates, the warping deformation at the ends of the beam with the End strengthening scheme is close to that of the fully strengthened beam. It is concluded that strengthening the ends of the beam can effectively restrain the warping deformation at these locations and provide an effective and economic means of increasing the critical moment.

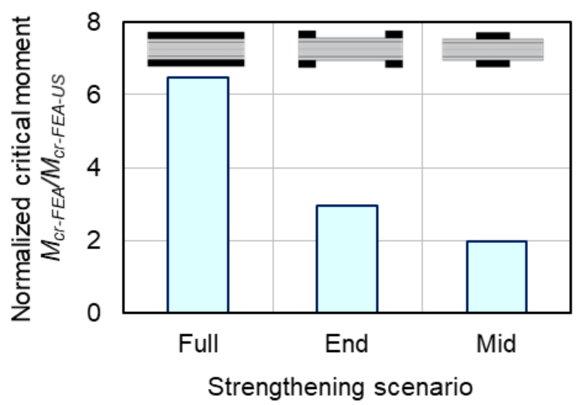

Fig. 3.7 Effect of strengthening schemes on the post-strengthening critical moments normalized relative to the critical moment of the unstrengthened beam

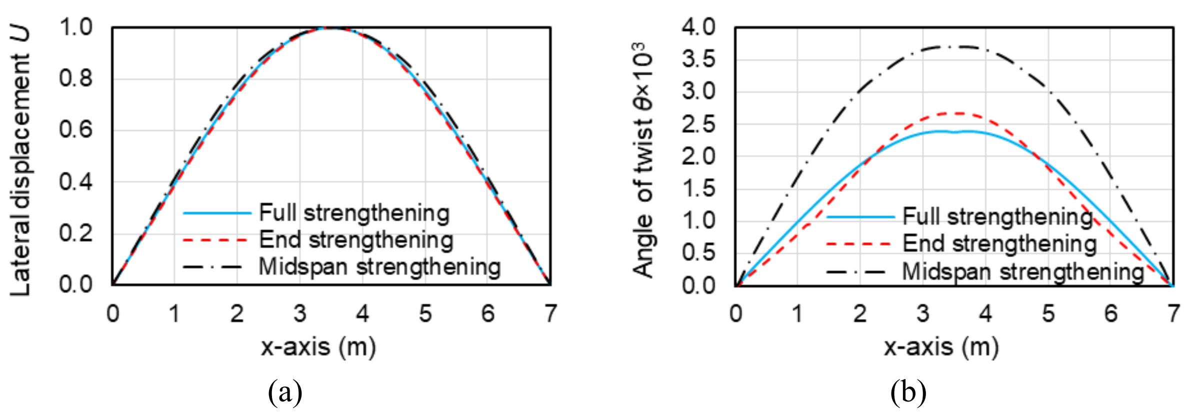

Fig. 3.8 Normalized mode shapes for Runs R and 4-6 (a) Lateral displacement, and (b) Angle of twist

3.3.5.3 Effects of Span to Depth Ratio (Runs R, 2 and 3), Pre-Strengthening Moment Fraction (Runs R and 15-17) and Loading Configurations and Locations (Runs R, 7-14 and 22)

Values of M_{cr-m}/M_{cr-FEA} for Runs R, 2, 3, and 15-17 in Table 3.5 show that L/d and Ω lead to a critical moment ratio that is slightly larger than unity, i.e., Eq. (3.9) overpredicts the post-strengthening critical moment. Conversely, results for Runs R, 7-14 indicate that the loading distribution before and after strengthening influence the accuracy of the predictions of Eq. (3.9). When the beam is subjected to a midspan point load prior to strengthening and two point loads at third span points after strengthening (Run 7), Eq. (3.9) is shown to underpredict the critical moment by 8.0%. Conversely, Eq. (3.9) overpredicts the result by 15% for Run 11. Another parameter that can significantly alter the inaccuracy of Eq. (3.9) predictions, is the load distribution before and after strengthening. The results for Run 22 (Table 3.5) in which the pre-strengthening point load is applied at $L/4$, and post-strengthening point load is applied at $3L/4$ (Fig. 3.4), show that Eq. (3.9) overpredicts the critical moment by 26%.

3.3.5.4 Effect of Boundary Conditions (Runs R, 18 and 19)

As discussed in Section 3.3.2.2, predictive equations for LTB capacity (e.g., Eqs. (3.1) and (3.8)) presented in steel design standards (e.g., CAN/CSA-S6-19 2019, ANSI/AISC360 2022) are derived based on the basic case of a simply supported beam in which weak axis rotation and warping deformation are free at both ends. As a result, these equations are expected to underpredict the critical moment of beams with fixed supports (e.g., Runs 18 and 19 in Table 3.5). Values of M_{cr-m}/M_{cr-FEA} for Runs R, 18 and 19 (Table 3.5) show that Eq. (3.9) accurately predicts the critical moments when both beam ends are free to warp and rotate about weak axis (i.e., Pin-Pin boundary condition relative to twist and weak axis rotation). However, by fixing one end of the beam and restraining warping and weak axis rotation at that point, Eq. (3.9) underpredicts the post-strengthening critical moment by 45%. Furthermore, by fixing both ends of the beam, Eq. (3.9) underpredicts the critical moment by 73%, due to the fact that the moment gradient coefficient ω_{2-CSA} in Eq. (3.9) is not intended for such boundary conditions.

3.3.5.5 Effect of Load Height (Runs R, 20 and 21)

Eq. (3.9) does not account for the load height effect. In this regard, three cases are considered (Runs R, 20 and 21) and their FEA predicted critical moments are normalized to the critical moment of the reference case $M_{cr-FEA-SC}$, in which the load is applied at the shear centre. As results indicate, placing downward transverse load on the top flange decreases the critical moment by 26% while placing the load on the bottom flange increases the capacity by 30%.

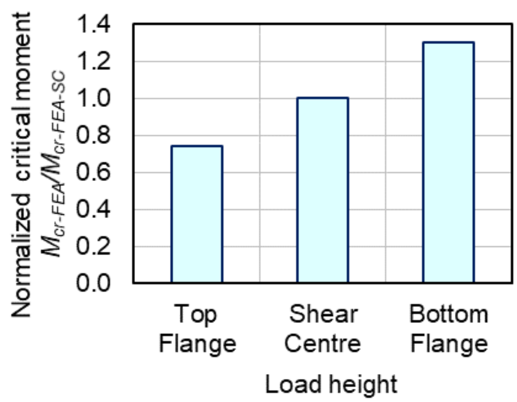

Fig. 3.9 Load height effect on normalized critical moments

3.4 Summary and Conclusions

The present study investigates the elastic lateral torsional buckling behaviour of flexural steel members that are strengthened with steel cover plates while under loading. For this purpose, a finite element study is developed to investigate the effect of span, strengthening scenarios where only a portion of beam is strengthened, types and location of loading before and after strengthening, magnitude of pre-strengthening loads, boundary conditions and load height. The following conclusions can be drawn from the present study:

1. Providing cover plates is an effective means of increasing the LTB resistance of existing steel beams.
2. End strengthening can be an effective and economic means of strengthening existing steel beams.
3. While distortional effects tend to have a small/moderate effect on the elastic LTB resistance of most unstrengthened beams, their effect becomes more pronounced in beams strengthened with cover plates. It is thus important to minimize web distortion in strengthened beams by providing transverse stiffeners.
4. Effective locations for transverse stiffeners include beam ends. Cover plate ends are also shown to be very effective in end strengthening scenarios.

A simplified equation is proposed to estimate the post-strengthening critical moment when distortional effects are suppressed through transverse stiffeners at key locations. The predictions of the equation are in reasonable agreement with finite element results for cases where pre-strengthening and post-strengthening loads have similar distributions. In its present form, the proposed equation is limited to cases of full-strengthening, shear centre loading, and beams that are simply supported relative to weak axis rotation and twist.

3.5 References

Abaqus (2020). Abaqus/CAE user's manual, Dassault Systemes.

ANSI/AISC360 (2016). "Specification for structural steel buildings (ANSI/AISC 360-16)." American Institute of Steel Construction, Chicago-Illinois.

ANSI/AISC360 (2022). "Specification for structural steel buildings (ANSI/AISC 360-22)." American Institute of Steel Construction, Chicago-Illinois.

Arizou, R. and M. Mohareb (2021). "Design Considerations for Distortional Lateral Buckling." Journal of Structural Engineering **147**(12): 04021203.

Barsoum, R. S. and R. H. Gallagher (1970). "Finite element analysis of torsional and torsional–flexural stability problems." International J. for Numerical Methods in Engineering **2**(3): 335-352.

CAN/CSA-S6-19 (2019). "Canadian highway bridge design code." Canadian Standards Association.

CAN/CSA-S16-19 (2019). "CSA S16: 19, Design of Steel Structures, Toronto, Canada." Canadian Standards Association.

Hsu, W. T., D. M. Lue and Y. F. Chen (2012). "Design aid for moment strength of built-up crane runway girders." International Journal of Steel Structures **12**(3): 403-417.

Hsu, W. T., D. M. Lue and B. T. Hsiao (2009). "Numerical approach for torsion properties of built-up runway girders." Journal of Applied Science and Engineering **12**(4): 381-389.

Liang, C., M. C. Reichenbach, T. A. Helwig, M. D. Engelhardt and J. A. Yura (2022). "Effects of Shear on the Elastic Lateral Torsional Buckling of Doubly Symmetric I-Beams." Journal of Structural Engineering **148**(3): 04021301.

Liu, Y. and L. Gannon (2009). "Experimental behavior and strength of steel beams strengthened while under load." Journal of Constructional Steel Research **65**(6): 1346-1354.

Liu, Y. and L. Gannon (2009). "Finite element study of steel beams reinforced while under load." Engineering Structures **31**(11): 2630-2642.

MacCrimmon, R. (2009). Guide for the Design of Crane-Supporting Steel Structures, Markham, ON, CA.

Pezeshky, P. and M. Mohareb (2018). "Distortional lateral torsional buckling of beam-columns including pre-buckling deformation effects." Computers & Structures **209**: 93-116.

Pezeshky, P., A. Sahraei, F. Rong, S. Sasibut and M. Mohareb (2020). "Generalization of the Vlasov theory for lateral torsional buckling analysis of built-up monosymmetric assemblies." Engineering Structures **221**: 111055.

Pham, P. V., M. Mohareb and A. Fam (2017). "Elastic Analysis of Steel Beams Strengthened with GFRP Plates Including Preexisting Loading Effects." Journal of Structural Engineering **143**(12): 04017163.

Reichenbach, M. C., Y. Liu, T. A. Helwig and M. D. Engelhardt (2020). "Lateral-Torsional Buckling of Singly Symmetric I-Girders with Stepped Flanges." Journal of Structural Engineering **146**(10): 04020203.

Sahraei, A., A. Iranpour and M. Mohareb (2020). User manual for LTB-UO V3.0 (LTB-UO is a computer program for Lateral Torsional Buckling analysis of beams/beam-columns, written at the University of Ottawa), University of Ottawa.

Vlasov, V. (1961). Thin-Walled Elastic Beams. Jerusalem, Israel, Israel Program for Scientific Translations.

Wang, Y.-q., L. Zong, R.-x. Zhu, X.-y. Liu and Y.-j. Shi (2015). "Behavior of I-section steel beam welding reinforced while under load." Journal of Constructional Steel Research 106: 278-288.

Chapter 4: Variational Principle and Finite Element Formulation for Strengthened Doubly Symmetric Beams[1]

Abstract

The present study investigates the elastic lateral torsional buckling resistance for steel I-beams that are strengthened with steel cover plates while being subjected to loading. A variational principle is developed for the problem by accounting for the full sequence of pre-strengthening load application, strengthening process, post-strengthening load application, up to the buckling response. The variational principle is then used to develop a finite element formulation for the problem leading to a quadratic eigenvalue problem. The formulation successfully captures the effects of pre-strengthening loads, the beneficial effects due to pre-buckling deformation, and the interactions between both effects. The study documents the benefit of providing transverse stiffeners to maximize the critical moment capacity attained when cover plates are used for strengthening. The study determines the locations of cover plates that would maximize the gain in critical moments in strengthening scenarios where only part of the beam span is to be strengthened. A systematic parametric study is developed to characterize the gain in elastic critical moment strength attained by cover-plate strengthening, and associated pre-buckling deformation effects, in terms of dimensionless parameters that characterize the effects of pre-strengthening load magnitude, beam span, cross-sectional geometry, length of cover plates, and cover plate cross-section. Other parameters investigated include the distributions of pre-strengthening and post-strengthening loading.

[1] This chapter has been published as: Iranpour, A. and M. Mohareb (2023). "Elastic Lateral Torsional Buckling of I-Beams Strengthened While under Loading." Journal of Structural Engineering, **149**(1): 04022206.

Keywords: Elastic lateral torsional buckling, thin-walled beam, finite element, strengthening, cover plates, pre-strengthening loads, pre-buckling deformation.

4.1 Introduction

The aging infrastructure worldwide, along with the typical increase in service loads relative to past load levels, requires developing techniques to strengthen and rehabilitate existing structures to increase their resistance. A viable technique for strengthening existing steel beams is to weld steel plates to both flanges. For the strengthening process to be effective, steel members would ideally need to be unloaded prior to strengthening, an impractical undertaking in most practical situations. When dealing with long-span beams that are prone to lateral torsional buckling (LTB), structural engineers are faced with the challenge of determining the LTB resistance for the strengthened member in the presence of pre-strengthening loads. Within this context, the present study develops a variational principle and finite element (FE) formulation that reliably quantifies the elastic LTB load-carrying capacity of strengthened steel wide flange beams, and accounts for the effects of pre-strengthening loads, pre-buckling deformation (PBD) and the interactions between both effects.

4.2 Literature Review

The classical LTB solution (e.g., Vlasov 1961) forming the basis of LTB provisions in steel design standards (e.g., ANSI/AISC360 2022[1] and CAN/CSA-S16 2019) does not account for the effect of pre-strengthening loads on the LTB strength of flexural members. In fact, the literature on LTB of strengthened beams is rather scarce. Only a few studies investigated the elastic buckling strength

[1] The original publication cited ANSI/AISC 360 (2016). Following the release of the updated version ANSI/AISC 360 (2022), a comparison was conducted between the two editions, revealing identical lateral torsional buckling provisions. As a result, the citation has been updated to reflect the latest edition.

of strengthened beams. This includes the study of MacCrimmon (2009) who provided a procedure to estimate the critical moments for built-up crane runway beams. Hsu et al. (2009 and 2012) investigated the torsional properties of I-beams strengthened with open-side down channels over the top flange to help engineers evaluate the LTB capacity of such beams more accurately. Pezeshky et al. (2020) developed a generalized thin-walled beam theory for the elastic LTB of wide flange sections strengthened with any number of cross-sections to form monosymmetric assemblies. Based on a 3D shell-based finite element modelling, Reichenbach et al. (2020) conducted a parametric study to investigate the elastic LTB capacity of beams with stepped flanges and proposed simplified procedures to estimate their effective properties.

None of the above studies, however, investigated the effect of loads that may be acting on the member during the strengthening process. Liu and Gannon (2009a-b) conducted experimental and numerical studies on nine tests and 93 FE runs to investigate the behavior and capacity of I-beams strengthened while under load. The authors reported that, while the pre-strengthening load level has a noticeable effect on the inelastic LTB capacity of the member, its effect is negligible on its yielding strength. None of the experiments reported failed in elastic LTB. Another experimental study on four specimens by Wang et al. (2015) confirmed the findings of Liu and Gannon (2009a), where it was found that pre-strengthening load levels adversely affect the inelastic LTB resistance of strengthened beams. Pham et al. (2017) conducted an analytical investigation on the effect of pre-strengthening loads on post-strengthening elastic response of flexural members. The study did not address, however, the LTB mode of failure.

Within the above context, the present study aims to develop an elastic LTB solution for flexural members that are strengthened while under loads. Unlike the classical LTB treatment which omits PBD effects, the solution sought herein captures the PBD effects, and their interactions with and pre-strengthening load effects when characterizing the elastic LTB strength of the strengthened member.

Past studies that captured the PBD effect include the work of Trahair and Woolcock (1973) who studied the PBD effect on the elastic buckling of doubly symmetric beams. The study showed that the predicted critical moments for beams with wide flanges significantly increase when incorporating PBD effects. Similar results were obtained by Vacharajittiphan et al. (1974) who showed that critical loads based on the classical treatment yield conservative predictions. Roberts and Azizian (1983) formulated a variational principle that accounts for PBD effects by retaining higher-order displacement derivatives. They reported that second order terms related to twist in strain-displacement relations can significantly affect the LTB capacity of monosymmetric beams. Pi et al. (1992) developed a variational principle for the elastic LTB of doubly symmetric thin-walled beams which captures PBD effects and compared the resulting equation with the alternative formulation in (Gellin and Lee 1988). Discrepancies of the alternative study predictions with experimental results were attributed to the omission of some nonlinear terms in longitudinal displacements. Pi and Trahair (1992a) used the variational principle developed in Pi et al. (1992) to formulate the differential equations governing the LTB for I beam-columns and developed an FE formulation for the problem. In a companion paper, Pi and Trahair (1992b) compared numerical results against those based on the classical LTB solution.

Andrade and Camotim (2004) derived the differential equations and boundary conditions governing the LTB of doubly symmetric tapered thin-walled beams with open cross-sections that capture PBD effects. Machado and Cortínez (2005) developed an energy-based solution that captures pre-buckling and shear deformation effects for simply supported composite beams. It was shown that the buckling loads predicted by the linear theory, which omits PBD effects, are overly conservative. Mohri and Potier-Ferry (2006) derived analytical LTB solutions for channels and I-beams that capture PBD effects. By accounting for PBD and shear deformation effects, Erkmen and Attard (2011) developed an FE formulation for the LTB analysis of thin-walled beams. The study indicated that omitting PBDs can lead to very conservative predictions for sections with relatively large flanges. The effect of PBDs on the LTB behaviour of monosymmetric beams was investigated by Mohri et al. (2012). Pezeshky and Mohareb (2018) developed an LTB formulation that captures the effects of web distortion, pre-buckling and pre-buckling shear deformation on the elastic LTB analysis of doubly symmetric beam-columns. The formulation was used to investigate the effect of various geometric parameters on critical moments.

4.3 Statement of the Problem

A wide flange section is subjected to general transverse loads. While under loading, the beam is strengthened with two identical plates welded to both flanges. It is required to develop a FE formulation to determine the elastic critical moment of the strengthened system.

4.4 Assumptions

The main assumptions of the formulation are:

(a) Beams are prismatic with doubly symmetric open cross-sections and are strengthened with two identical plates welded to the flanges. As a result, the composite system is also doubly symmetric, and its shear centre (SC) coincides with that of the unstrengthened beam section,

(b) Weld-induced deformations are considered negligible. This condition would be approached when the technique adopted to weld both plates to the respective flanges is identical and the welding-induced deformations are minimized (e.g., by adopting an alternate welding sequence that is carefully planned to minimize weld distortions, and/or minimizing the weld volumes).

(c) Strains are small, and rotations are moderate,

(d) The kinematics of the beam, strengthening plates and the resulting strengthened system follow those of the Gjelsvik beam (Gjelsvik 1981), i.e.,

(d1) Cross-sectional distortions are omitted (Vlasov 1961),

(d2) Shear strains at the middle surface vanish (Vlasov 1961), and

(d3) A line normal to the middle surface remains normal after deformation in a manner consistent with the Kirchhoff plate theory,

(e) Shear deformation due to bending and warping are negligible,

(f) Nonlinear effects throughout PBD are negligible, i.e., the pre-buckling response is linear,

(g) Materials are linearly elastic isotropic,

(h) The member is subjected to transverse loads. Hence, the system is subjected to strong axis bending moments with no axial loading,

(i) Throughout buckling, the loads remain constant so the beam curvature in the *yz*-plane remains unchanged, i.e., the member buckles in an inextensional mode (e.g., Trahair 1993),

(j) Before welding, the strengthening plates are assumed to slide relative to the beam flanges in a frictionless manner, and

(k) After welding, no relative slip occurs between the plates and the flanges, i.e., full shear transfer takes place at the plate-flange interface, resulting in a monolithic strengthened section.

4.5 Description of the Sequence of Strengthening and Loading

Fig. 4.1 depicts the sequence of strengthening/loading/deformation for a steel I-beam. The process involves six steps relating eight configurations. The loads and displacements corresponding to each step are summarized in Table 4.1. The centroidal axis undergoes only a transverse displacement V along the y axis, a lateral displacement U along the x axis and the section undergoes an angle of twist θ about the longitudinal z axis.

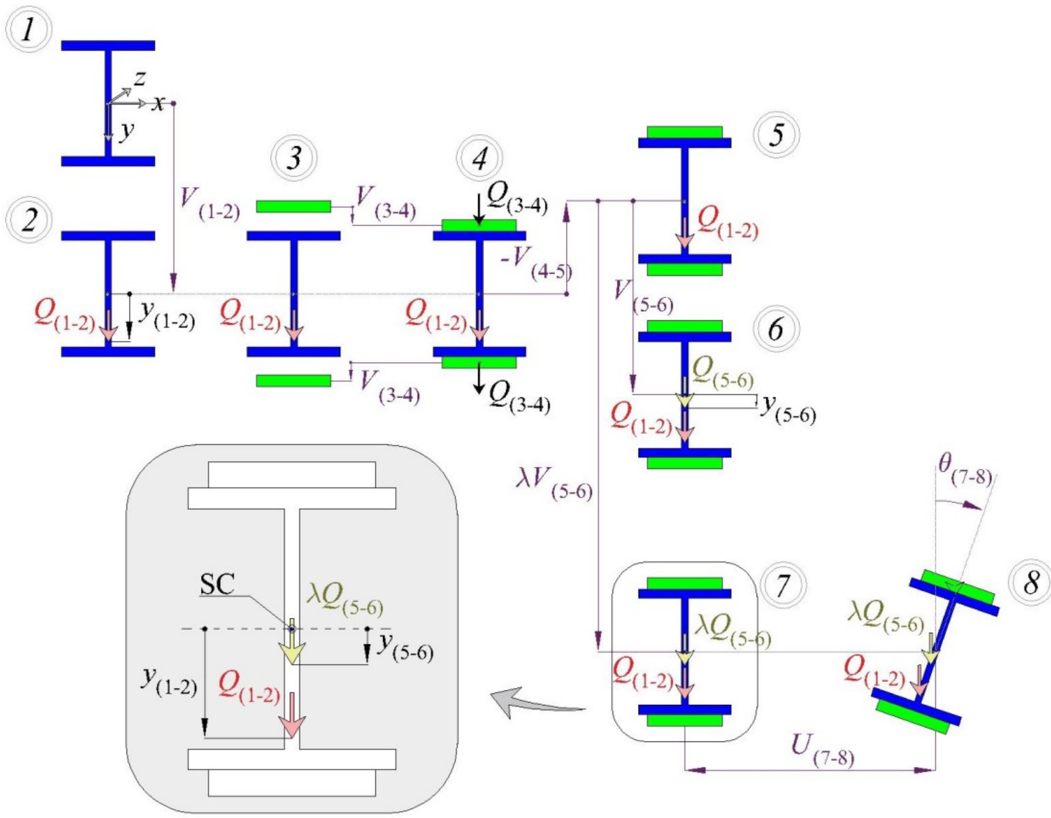

Fig. 4.1 Configurations of strengthening and loading history

Table 4.1 Loads and displacements for each component corresponding to each step

Description	Step	Element	New loads	Total Loads at the end of the step	$U(z)$	$V(z)$	$\theta(z)$
Pre-Buckling Steps (Before Strengthening)	1-2	Beam	$Q_{(1-2)}$	$Q_{(1-2)}$	0	$V_{(1-2)}$	0
	3-4	Upper Plate	$Q_{(3-4)}$	$Q_{(3-4)}$	0	$V_{(3-4)}$	0
		Beam	0	$Q_{(1-2)}$	0	0	0
		Lower Plate	$Q_{(3-4)}$	$Q_{(3-4)}$	0	$V_{(3-4)}$	0
Pre-Buckling Steps (After Strengthening)	4-5	Non-composite system	$-2Q_{(3-4)}$	$Q_{(1-2)}$	0	$V_{(4-5)}$	0
	5-6	Composite system	$Q_{(5-6)}$	$Q_{(1-2)}+Q_{(5-6)}$	0	$V_{(5-6)}$	0
	5-7	Composite system	$\lambda Q_{(5-6)}$	$Q_{(1-2)}+\lambda Q_{(5-6)}$	0	$\lambda V_{(5-6)}$	0
Buckling Step	7-8	Composite system	0	$Q_{(1-2)}+\lambda Q_{(5-6)}$	$U_{(7-8)}$	0	$\theta_{(7-8)}$

4.5.1 Pre-Buckling Steps

Throughout Step 1-2 (i.e., in going from Configurations 1 to 2), the beam, subsequently denoted by subscript B, is subjected to a load from zero to $Q_{(1-2)}(z)$ applied at distance $y_{(1-2)}(z)$ from the shear centre (taken as positive when the point of application of the load is below the shear centre), where z is the longitudinal coordinate. Under the applied loading, the beam undergoes a transverse deflection $V_{(1-2)}(z)$ and attains equilibrium at Configuration 2. At Configuration 3, two initially straight plates, denoted by subscript P, are provided to strengthen the beam. To enable the welding of the straight plates to the curved beam flanges, the plates are brought into full contact with the flanges along the span, i.e., the gaps between the straight plates and the bent beam $V_{(3-4)}$ (Configuration 3) need to be eliminated by applying additional temporary loads $Q_{(3-4)}$ throughout Step 3-4. After plates have been brought into full contact with the beam flanges, they are clamped to the flanges (Configuration 4). Loads $Q_{(3-4)}$ in Configuration 4 are then removed causing the frictionless composite system (Assumption (j)) to rebound upwards by undergoing an upward deflection $V_{(4-5)}$ and attain equilibrium at Configuration 5. Welding is then performed at Configuration 5. After weld solidification, the system acts as a monolithic composite entity. Additional operating external reference loads $Q_{(5-6)}$ are applied at distance $y_{(5-6)}$ from the shear centre (taken as positive when the point of application of the load is below the shear centre) in Step 5-6. Under these loads, the composite beam attains a new equilibrium at Configuration 6 by undergoing an additional displacement $V_{(5-6)}$. During Step 6-7, the applied reference transverse loads $Q_{(5-6)}$ are assumed to increase to reach $\lambda Q_{(5-6)}$ where the system attains the state of onset of LTB (Configuration 7), in which λ is an unknown load multiplier to be determined from a buckling analysis. Assuming a linear pre-buckling response (Assumption (f)), the transverse displacement proportionally increases to $\lambda V_{(5-6)}(z)$. Thus, at the onset of buckling (Configuration 7), the total loads are $Q_{(1-2)} + \lambda Q_{(5-6)}$ and the corresponding transverse displacement of the system is $V_{(1-2)}(z) + V_{(4-5)}(z) + \lambda V_{(5-6)}(z)$.

4.5.2 Buckling Step

In Step 7-8, the strengthened system undergoes LTB. Throughout buckling, the applied loads $Q_{(1-2)} + \lambda Q_{(5-6)}$ remain unchanged, and the shear centre axis of the strengthened system undergoes a lateral displacement $U_{(7-8)}(z)$ along the *x*-direction and an angle of twist $\theta_{(7-8)}(z)$, and a cross-section originally normal to the z axis undergoes a rotation $U'_{(7-8)}(z)$ about the *y* axis and a warping deformation $\theta'_{(7-8)}(z)$.

4.6 Displacement Fields

Fig. 4.2 depicts the coordinate systems (x, y_B, z) for the beam, (x, y_U, z) and (x, y_L, z) for the upper and lower strengthening plates, and (x, y, z) for the whole composite system (Fig. 4.2c). Given that the strengthening plates are identical (Assumption (a)), we have $y_U = y_L = y_P$.

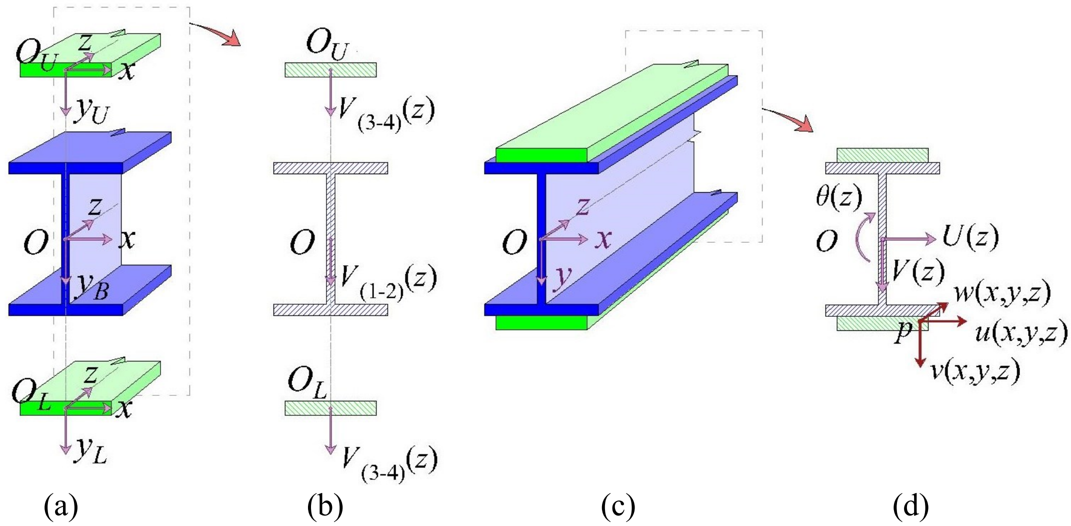

Fig. 4.2 (a) Coordinates of the individual components (beam B, and strengthening plates P) prior to strengthening, (b) Displacements before strengthening, (c) Coordinates of the composite system and (d) Displacements of the strengthened system

Displacements u, v and w for a point $p\left(x,y,z\right)$ of the strengthened section are expressed in terms of displacements $U\left(z\right)$ and $V\left(z\right)$ of the shear centre axis and the angle of twist $\theta\left(z\right)$ for the cross-section as the sum of linear and nonlinear components (e.g., Pi et al. 1992, Pi and Trahair 1992a), i.e.,

$$\begin{Bmatrix} u \\ v \\ w \end{Bmatrix} = \begin{Bmatrix} U - y\theta \\ V + x\theta \\ -xU' - yV' - \omega\theta' \end{Bmatrix} + \begin{Bmatrix} -\frac{1}{2}x\theta^2 + \left[-\frac{1}{2}x\left(U'^2 + U'V'\theta\right) - \frac{1}{2}y\left(U'V' + U'^2\theta\right) - \omega U'K_z\right] \\ -\frac{1}{2}y\theta^2 + \left[-\frac{1}{2}x\left(U'V' + V'^2\theta\right) - \frac{1}{2}y\left(V'^2 - U'V'\theta\right) - \omega V'K_z\right] \\ y\left(U'\theta + \frac{1}{2}V'\theta^2\right) - x\left(V'\theta - \frac{1}{2}U'\theta^2\right) - \omega\left[K_z - \theta' - \frac{1}{2}K_z\left(V'^2 + U'^2\right)\right] \end{Bmatrix}$$

(4.1)a-c

in which ω is the sectorial coordinate (e.g., Vlasov 1961), and all primes denote differentiation with respect to z. In Eq. (4.1)c, the longitudinal displacement at the centroid is taken to vanish (Assumption (h)), and the twist curvature K_z of the cross-section is expressed by

$$K_z = \theta' + \frac{1}{2}\left(U''V' - U'V''\right) \tag{4.2}$$

It is common (e.g., Pi et al. 1992) to approximate Eq. (4.2) as $K_z \approx \theta'$ and to ignore the nonlinear terms $xU'\theta^2/2$, $yV'\theta^2/2$ arising in the right-hand side of Eq. (4.1)c and the nonlinear terms appearing in Eqs. (4.1)a-b (e.g., Trahair 1993, Wu and Mohareb 2011). In contrast, the present study retains the four nonlinear terms involving θ^2 in Eq. (4.1)a-c (Assumption (c)). The terms in the square brackets are omitted since present numerical investigations revealed that their effects are negligible.

4.7 Strain-Displacement and Stress-Strain Relations

The non-vanishing strain components are the shear strain γ due to uniform torsion and the longitudinal normal strain ε. The shear strain γ (Vlasov 1961) is given by

$$\gamma = -2n\theta' \tag{4.3}$$

where n is the distance normal to section contour. The strain-displacement relation for the longitudinal strain is

$$\varepsilon = w' + \frac{1}{2}\left(u'^2 + v'^2 + w'^2\right) \approx w' + \frac{1}{2}\left(u'^2 + v'^2\right) \tag{4.4}$$

where the term $1/2\left(w'^2\right)$ has been neglected relative to w'. From Eq. (4.1)a-c, by substituting into Eq. (4.4), one obtains

$$\varepsilon = \left(-xU'' - yV'' - \omega\theta''\right) + \frac{1}{2}\left[U'^2 + V'^2 + \left(x^2 + y^2\right)\left(\theta'^2 + \theta^2\theta'^2\right) - x\left(2V''\theta - U''\theta^2\right) + y\left(2U''\theta + V''\theta^2\right)\right] \tag{4.5}$$

Finally, we note that Eqs. (4.3) and (4.5) are generic and are hence applicable for any of the deformed configurations in Fig. 4.1 as will be discussed in the following section.

In pre-buckling steps 1-7, the section undergoes only a vertical deflection V and $U=\theta=0$. Hence, by assuming linearly elastic isotropic material response (Assumption (g)), the longitudinal normal strains $\varepsilon_{i,(m-n)}$ and corresponding stress $\sigma_{i,(m-n)}$, for a pre-buckling step from configuration *m* to configuration *n*, are obtained by omitting U and θ in Eq. (4.5), yielding

$$\varepsilon_{i,(m-n)}=-y_i V''_{(m-n)}+\frac{1}{2}V_i'^2\approx -y_i V''_{(m-n)}, \qquad \sigma_{i,(m-n)}\approx -Ey_i V''_{(m-n)} \qquad \text{(4.6)a-b}$$

where subscript *i* denotes the component of interest ($i=B$ for beam, $i=P$ for either plate and no subscript i denotes the strengthened system) and y_i is the *y*-coordinate taken from the centroid of component i (Fig. 4.2). The expressions for normal and shear strains for all steps are summarized in Table 4.2. During pre-buckling, $\theta=0$ implies vanishing shear strains and stresses (i.e., $\gamma_{i,(m-n)}=\tau_{i,(m-n)}=0$).

In Step 3-4, the deflected shapes of the plates must match that of the beam i.e., $V''_{(1-2)}=V''_{(3-4)}$. In all pre-buckling steps, the curvature in the *y-z* plane for all components $V''_{(m-n)}$ is obtained from Eq. (4.6)b by substituting into Eq. (4.7)b yielding

$$V''_{(m-n)}(z)=\frac{-M_{(m-n)}(z)}{EI_{xx-i}}, \qquad M_{(m-n)}(z)=\int_{A_i} y_i\sigma_{i,(m-n)}(z)\,dA_i, \qquad I_{xx-i}=\int_{A_i} y_i^2\,dA_i \qquad \text{(4.7)a-c}$$

in which $M_{(m-n)}(z)$ is the bending moment, I_{xx-i} is the moment of inertia about the x axis and A_i is the area for the component *i*. By equating the curvatures of the plates and the beam, one obtains the temporary bending moment $M_{(3-4)}$ that must be applied to each plate prior to welding as

$$M_{(3-4)}(z) = \frac{I_{xx-P}}{I_{xx-B}} M_{(1-2)}(z) \tag{4.8}$$

Table 4.2 Expressions for normal and shear strains of each component in each step

Type	Step	Component	Normal Strain	Shear Strain
Pre-Buckling Steps (Before Strengthening)	1-2	Beam	$\varepsilon_{B,(1-2)} = -y_B V''_{(1-2)}$	0
	3-4	Upper Plate	$\varepsilon_{P,(3-4)} = -y_P V''_{(1-2)}$	0
		Beam	0	0
		Lower Plate	$\varepsilon_{P,(3-4)} = -y_P V''_{(1-2)}$	0
Pre-Buckling Steps (After Strengthening)	4-5	Upper Plate	$\varepsilon_{P,(4-5)} = -y_P V''_{(4-5)}$	0
		Beam	$\varepsilon_{B,(4-5)} = -y_B V''_{(4-5)}$	
		Lower Plate	$\varepsilon_{P,(4-5)} = -y_P V''_{(4-5)}$	0
	5-6	Composite system	$\varepsilon_{(5-6)} = -y V''_{(5-6)}$	0
	5-7	Composite system	$\lambda \varepsilon_{(5-6)}$	0
Buckling Step	7-8	Composite system	Eq. (4.13)	$\gamma_{(7-8)} = -2n\theta'_{(7-8)}$

In Step 4-5, the temporary loads applied to the plates in the previous step are removed and the non-composite assembly undergoes an upward rebound deflection $V_{(4-5)}(z)$. The corresponding rebound curvature $V''_{(4-5)}$ is obtained by applying $-2M_{(3-4)}(z)$ to the system. As $V''_{(1-2)} = V''_{(3-4)}$, one obtains

$$V''_{(4-5)} = \frac{-2I_{xx-p}}{I_{xx-B} + 2I_{xx-P}} V''_{(1-2)} \tag{4.9}$$

From Eq. (4.6)b, and noting that the stresses corresponding to Step 4-5 are $\sigma_{P,(4-5)} = -Ey_P V''_{(4-5)}$ for the plates and $\sigma_{B,(4-5)} = -Ey_B V''_{(4-5)}$ for the beam, adding the stresses $\sigma_{B,(1-2)} = -Ey_B V''_{(1-2)}$ of Step 1-2, and $\sigma_{P,(3-4)} = -Ey_P V''_{(1-2)}$ for Step 3-4, and noting that $V''_{(1-2)} = -M_{(1-2)}(z)/EI_{xx-B}$, the total stress at Configuration 5 $\sigma_{(1-5)}$ is given by

$$\sigma_{(1-5)}(z)=\begin{cases}\dfrac{M_{(1-2)}(z)}{I_{xx-B}}\alpha\left(y+y_{C-P}\right) & -\left(\dfrac{d}{2}+t_p\right)\le y\le -\dfrac{d}{2}\\ \dfrac{M_{(1-2)}(z)}{I_{xx-B}}\alpha y & -\dfrac{d}{2}\le y\le \dfrac{d}{2}\\ \dfrac{M_{(1-2)}(z)}{I_{xx-B}}\alpha\left(y-y_{C-P}\right) & \dfrac{d}{2}\le y\le\left(\dfrac{d}{2}+t_p\right)\end{cases} \tag{4.10)a-c}$$

in which $y_{C-P}=\left(d+t_p\right)/2$, t_p is the plate thickness and d is the overall depth of the I-beam. The distances from the centroid of the composite section to that of the upper plate is $-y_{C-P}$, to the lower plate is y_{C-P} to the I-beam centroid is 0.0. Thus, we have $y_P=y+y_{C-P}$ for the upper plate, $y_P=y-y_{C-P}$ for the lower plate, and $y_B=y$ for the I-beam, and parameter α is given by

$$\alpha=1-\frac{2I_{xx-P}}{I_{xx-B}+2I_{xx-P}} \tag{4.11}$$

Using Eqs. (4.6)b and (4.7)a, the stresses induced in Step 5-6 can be expressed by

$$\sigma_{(5-6)}(z)=-EyV''_{(5-6)}(z)=\frac{M_{(5-6)}(z)}{I_{xx}}y \tag{4.12}$$

Noting that throughout Step 5-7, the curvature increases linearly with the applied loads to $\lambda V''_{(5-6)}$ (Assumption (f)), the corresponding stress is $\lambda\sigma_{(5-6)}=\lambda M_{(5-6)}(z)\,y/I_{xx}$.

The additional strain $\varepsilon_{(7-8)}$ induced throughout buckling Step 7-8 is obtained by deducting the total strain at the onset of buckling $\varepsilon_{(1-7)}$ from the total strain at the buckled configuration $\varepsilon_{(1-8)}$ yielding

$$\begin{aligned}\varepsilon_{(7-8)} = &\left[-xU''_{(7-8)} - \omega\theta''_{(7-8)}\right] + \left[\frac{1}{2}U'^{2}_{(7-8)} + \frac{1}{2}\left(x^2+y^2\right)\left(\theta'^{2}_{(7-8)} + \theta^{2}_{(7-8)}\theta'^{2}_{(7-8)}\right)\right.\\ &\left. + x\left(-V''_{(1-7)}\,\theta_{(7-8)} + \frac{1}{2}U''_{(7-8)}\theta^{2}_{(7-8)}\right) + y\left(U''_{(7-8)}\theta_{(7-8)} + \frac{1}{2}V''_{(1-7)}\,\theta^{2}_{(7-8)}\right)\right]\end{aligned} \tag{4.13}$$

Also, the shear strain throughout buckling is

$$\gamma_{(7-8)} = -2n\theta'_{(7-8)} \tag{4.14}$$

4.8 Variational Principle

The total potential energy $\Pi_{i,(m-n)}$ for component $i = B, P$ subjected to a load $q_{(m-n)}(z)$ in going from configuration m to configuration n is given by

$$\Pi_{i,(m-n)} = \frac{1}{2}\int_L\int_{A_i}\sigma_{i,(m-n)}\,\varepsilon_{i,(m-n)}dA_i\,dz - \int_L q_{(m-n)}(z)V_{(m-n)}(z)dz \tag{4.15}$$

For the buckling step, the total potential energy Π is given by

$$\begin{aligned}\Pi_{(7-8)} = &\frac{1}{2}\int_L\int_A\left[E\varepsilon^{2}_{(7-8)} + G\gamma^{2}_{(7-8)}\right]dAdz + \int_L\int_A\left[\left(\sigma_{(1-5)} + \lambda\sigma_{(5-6)}\right)\varepsilon_{(7-8)}\right]dAdz\\ &+ \frac{1}{2}\int_L\left[\left(q_{(1-2)}y_{(1-2)} + \lambda q_{(5-6)}y_{(5-6)}\right)\theta_{(7-8)}(z)^2\right]dz\end{aligned} \tag{4.16}$$

At the neutral stability state (Configuration 7 in Fig. 4.1), the second variation of the total potential energy $\overline{\overline{\Pi}}_{(7-8)}$ throughout buckling must vanish. From the expressions for $\sigma_{(1-5)}$, $\sigma_{(5-6)}$, $\varepsilon_{(7-8)}$ and $\gamma_{(7-8)}$ in Eqs. (4.10)-(4.14), by substituting into Eq. (4.16), $\Pi_{(7-8)}$ is expressed in terms of the buckling displacements $U'_{(7-8)}, U''_{(7-8)}, \theta_{(7-8)}, \theta'_{(7-8)}$ and $\theta''_{(7-8)}$ and pre-buckling curvature $V''_{(1-7)}$. Performing the area integrals, and noting the relationships

$$\begin{aligned}&\int_A ydA = \int_A \omega xdA = \int_A y(x^2+y^2)dA = \int_A y_{C-i}\,dA = \int_A y_{C-i}\left(x^2+y^2\right)dA = 0\\ &I_{xx} = \int_A y^2dA,\quad I_{yy} = \int_A x^2dA,\quad C_w = \int_A \omega^2dA,\quad J = \int_A 4n^2dA,\quad \int_A y_{C-i}\,ydA = 2A_p y_{C-P}^{\;2}\end{aligned} \tag{4.17)a-f}$$

the expression for $\overline{\overline{\Pi}}_{(7-8)}$ is found to take the form (additional details regarding the second variation of total potential energy can be found in Appendix 4.A)

$$\begin{aligned}
\overline{\overline{\Pi}}_{(7-8)} =& \frac{1}{2}\int_L \left[EI_{yy}\overline{U''}_{(7-8)}\left(z\right)^2 + EC_w\overline{\theta''}_{(7-8)}\left(z\right)^2 + GJ\overline{\theta'}_{(7-8)}\left(z\right)^2 \right] dz + \\
&+\int_L \left[EI_{yy}V''_{(1-7)}\left(\lambda,z\right) + M_{(1-2)}\left(z\right) + \lambda M_{(5-6)}\left(z\right)\right]\overline{\theta}_{(7-8)}\left(z\right)\overline{U''}_{(7-8)}\left(z\right) dz \\
&+\frac{1}{2}\int_L \left[EI_{yy}V''_{(1-7)}\left(\lambda,z\right) + M_{(1-2)}\left(z\right) + \lambda M_{(5-6)}\left(z\right)\right]V''_{(1-7)}\left(\lambda,z\right)\overline{\theta}_{(7-8)}\left(z\right)^2 dz \\
&+\frac{1}{2}\int_L \left(q_{(1-2)}y_{(1-2)} + \lambda q_{(5-6)}y_{(5-6)}\right)\overline{\theta}_{(7-8)}\left(z\right)^2 dz
\end{aligned} \tag{4.18}$$

in which pre-buckling curvature $V''_{(1-7)}$ is given by

$$V''_{(1-7)}\left(\lambda,z\right) = V''_{(1-2)}\left(z\right) + V''_{(4-5)}\left(z\right) + \lambda V''_{(5-6)}\left(z\right) = -\left(\frac{\alpha M_{(1-2)}\left(z\right)}{EI_{xx-B}} + \frac{\lambda M_{(5-6)}\left(z\right)}{EI_{xx}}\right) \tag{4.19}$$

and $\overline{(\ )}$ and $\overline{\overline{(\ )}}$ respectively denote the first and second variations of the argument functions. The first bracketed term in Eq. (4.18) represents the additional internal strain energy stored during buckling, the expressions including $M_{(1-2)}\left(z\right)$ and $M_{(5-6)}\left(z\right)$ represent the work done by the loads and the expressions including $y_{(1-2)}$ and $y_{(5-6)}$ denote the contribution of load heights. For the special case of a point load f acting at a height relative to the shear centre and at a location $z = z_0$ along the span, one has $q = f \times Dirac\left(z - z_0\right)$, in which $Dirac\left(z - z_0\right)$ is the Dirac delta function. By omitting the terms involving $M_{(1-2)}$ related to the effects of pre-strengthening loads, all loads in Steps 1-2 and 4-5 vanish and omitting warping effects, the variational principle reduces to that of LTB of rectangular beams considering PBD effects, reported in (Sahraei et al. 2018). Furthermore, by excluding the effects of PBD (i.e., by setting $V''_{(1-7)} \approx 0$) and load heights (i.e., by setting $y_{(1-2)} = y_{(5-6)} = 0$) while retaining the warping term, the resulting equation reverts to the classical LTB variational principle (e.g., Barsoum and Gallagher 1970).

4.9 Finite Element Formulation

4.9.1 Pre-Buckling Analyses

The two pre-buckling bending moments $M_{(1-2)}(z)$, $M_{(5-6)}(z)$ appearing in Eq. (4.18) are determined from separate pre-buckling analyses based on the conventional two-node Euler Bernoulli element. Moments $M_{(1-2)}(z)$ correspond to the pre-strengthening loads $q_{(1-2)}$ acting on the unstrengthened beam with moment of inertia I_{xx-B} while moments $M_{(5-6)}(z)$ correspond to the post-strengthening/pre-buckling loads $q_{(5-6)}$ acting on the strengthened beam with moment of inertia I_{xx}. Each analysis yields end bending moments $M_{1(m-n)}$ and $M_{2(m-n)}$. Linear interpolation is then adopted over the element L_e to recover the moment $M(z) = -M_{1(m-n)}(1 - z/L_e) + M_{2(m-n)}(z/L_e)$ at section z.

4.9.2 Buckling Analysis

A two-node beam element with four buckling degrees of freedom per node Fig. 4.3 is developed based on the variational principle in Eq. (4.18).

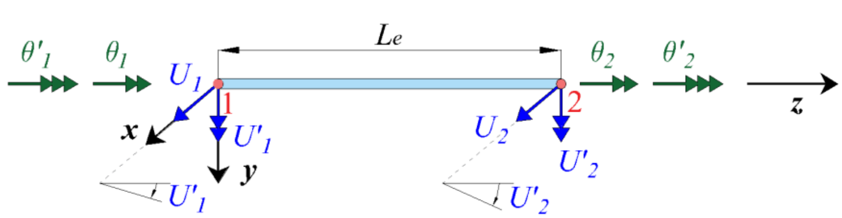

Fig. 4.3 Degrees of freedom of the buckling element

The first variation $\bar{U}(z)$ and $\bar{\theta}(z)$ of displacement functions are related to the vector of nodal degrees of freedom $\mathbf{d}^{\mathbf{T}} = \langle U_1 \quad U_1' \quad U_2 \quad U_2' \quad \theta_1 \quad \theta_1' \quad \theta_2 \quad \theta_2' \rangle$ through

$$\bar{U}(z) = \mathbf{H_U}^{\mathbf{T}}\bar{\mathbf{d}},\ \bar{\theta}(z) = \mathbf{H_\theta}^{\mathbf{T}}\bar{\mathbf{d}} \tag{4.20)a-b}$$

in which the vectors of shape functions are defined by

$$\begin{aligned}
&\mathbf{H_U}^{\mathbf{T}} = \mathbf{H_U}^{\mathbf{T}}(z) = \langle H_1 \quad H_2 \quad H_3 \quad H_4 \quad 0 \quad 0 \quad 0 \quad 0 \rangle \\
&\mathbf{H_\theta}^{\mathbf{T}} = \mathbf{H_\theta}^{\mathbf{T}}(z) = \langle 0 \quad 0 \quad 0 \quad 0 \quad H_1 \quad H_2 \quad H_3 \quad H_4 \rangle \\
&\langle H_1, H_2, H_3, H_4 \rangle = \left\langle 1 - 3\zeta^2 + 2\zeta^3,\ L_e\zeta(1-\zeta)^2,\ 3\zeta^2 - 2\zeta^3,\ L_e\zeta^2(\zeta - 1) \right\rangle,\ \zeta = z/L_e
\end{aligned} \tag{4.21)a-d}$$

From Eqs. (4.20)a-b, by substituting into the variational principle in Eq. (4.18) and evoking the stationarity conditions $\left(\partial\bar{\bar{\Pi}}/\partial\bar{\mathbf{d}}\right)\delta\bar{\mathbf{d}} = 0$, one obtains the quadratic eigenvalue problem

$$\left(\mathbf{k_E} + \lambda\mathbf{k_{G1}} + \lambda^2\mathbf{k_{G2}}\right)_{8\times8}\bar{\mathbf{d}}_{8\times1} = \mathbf{0}_{8\times1} \tag{4.22}$$

in which the elastic matrix $\mathbf{k_E} = \mathbf{k_{E\text{-}a}} + \mathbf{k_{E\text{-}b}} + \mathbf{k_{E\text{-}c}}$ consists of the conventional elastic matrix $\mathbf{k_{E\text{-}a}}$

$$\mathbf{k_{E\text{-}a}} = \int_{L_e}\left[EI_{yy}\mathbf{H_U''}\mathbf{H_U''}^{\mathbf{T}} + EC_w\mathbf{H_\theta''}\mathbf{H_\theta''}^{\mathbf{T}} + GJ\mathbf{H_\theta'}\mathbf{H_\theta'}^{\mathbf{T}} + q_{(1-2)}y_{(1-2)}\mathbf{H_\theta}\mathbf{H_\theta}^{\mathbf{T}}\right]dz \tag{4.23}$$

and $\mathbf{k_{E\text{-}b}}$ reflects the combined effects of pre-strengthening loads and their PBD effects, and is defined by

$$\mathbf{k_{E\text{-}b}} = \int_{L_e}\left[\frac{\alpha M_{(1-2)}(z)^2}{EI_{xx-B}}\left(\frac{\alpha I_{yy}}{I_{xx-B}} - 1\right)\mathbf{H_\theta}\mathbf{H_\theta}^{\mathbf{T}} - M_{(1-2)}(z)\frac{\alpha I_{yy}}{I_{xx-B}}\left(\mathbf{H_\theta}\mathbf{H_U''}^{\mathbf{T}} + \mathbf{H_U''}\mathbf{H_\theta}^{\mathbf{T}}\right)\right]dz \tag{4.24}$$

and $\mathbf{k_{E\text{-}c}}$ represents the effect of pre-strengthening loads and is given by

$$\mathbf{k_{E\text{-}c}} = \int_{L_e} M_{(1-2)}(z)\left(\mathbf{H_\theta}\mathbf{H_U''}^{\mathbf{T}} + \mathbf{H_U''}\mathbf{H_\theta}^{\mathbf{T}}\right)dz \tag{4.25}$$

Also, in Eq. (4.22), the geometric stiffness matrix $\mathbf{k_{G1}} = \mathbf{k_{G1\text{-}a}} + \mathbf{k_{G1\text{-}b}} + \mathbf{k_{G1\text{-}c}}$ consists of a destabilizing matrix due to the post-strengthening pre-buckling loads (akin to the conventional LTB destabilizing matrix)

$$\mathbf{k_{G1\text{-}a}} = \int_{L_e} \left[M_{(5-6)}(z)\left(\mathbf{H_\theta}\mathbf{H}_\mathbf{U}''^{\mathbf{T}} + \mathbf{H}_\mathbf{U}''\mathbf{H_\theta}^{\mathbf{T}}\right) + q_{(5-6)}y_{(5-6)}\mathbf{H_\theta}\mathbf{H_\theta}^{\mathbf{T}} \right] dz \tag{4.26}$$

and $\mathbf{k_{G1\text{-}b}}$ represents the PBD effects related to the post-strengthening loads and is given by

$$\mathbf{k_{G1\text{-}b}} = -\int_{L_e} \frac{I_{yy}}{I_{xx}} M_{(5-6)}(z)\left(\mathbf{H_\theta}\mathbf{H}_\mathbf{U}''^{\mathbf{T}} + \mathbf{H}_\mathbf{U}''\mathbf{H_\theta}^{\mathbf{T}}\right) dz \tag{4.27}$$

and $\mathbf{k_{G1\text{-}c}}$ is an additional matrix that captures the interaction between the pre-strengthening loads and PBD effects associated with the pre-and post-strengthening loads, defined by

$$\mathbf{k_{G1\text{-}c}} = \int_{L_e} \frac{M_{(1-2)}(z)M_{(5-6)}(z)}{EI_{xx-B}}\left(\frac{2\alpha I_{yy}}{I_{xx}} - \alpha - \frac{I_{xx-B}}{I_{xx}}\right)\mathbf{H_\theta}\mathbf{H_\theta}^{\mathbf{T}}\, dz \tag{4.28}$$

In Eq. (4.22), $\mathbf{k_{G2}}$ accounts for the effect of PBD due to post-strengthening loads and is defined by

$$\mathbf{k_{G2}} = -\int_{L_e} \frac{M_{(5-6)}(z)^2}{EI_{xx}}\left(1 - \frac{I_{yy}}{I_{xx}}\right)\mathbf{H_\theta}\mathbf{H_\theta}^{\mathbf{T}} dz \tag{4.29}$$

4.10 Verification

A beam with a W310×39 cross-section is simply supported relative to transverse and lateral displacements and relative to twist. As a reference case, a 6m span is considered. Young modulus is taken as $E = 200{,}000MPa$ and the shear modulus is taken as $G = 77{,}000MPa$. Prior to strengthening, the reference beam is subjected to uniformly distributed transverse load (UDL) applied at the shear centre that induces a peak moment corresponding to a specified fraction

$\Omega = 80\%$ of the critical moment M_{uB} of the unstrengthened beam due to pre-strengthening loads as determined from the ANSI/AISC360 (2022) provisions:

$$M_{uB} = C_a \frac{\pi}{L}\sqrt{EI_{yy-B}GJ_B + \left(\frac{\pi E}{L}\right)^2 I_{yy-B}C_{w-B}}, \; C_a = \frac{12.5M_{\max}}{2.5M_{\max} + 3M_A + 4M_B + 3M_C} \tag{4.30a-b}$$

in which C_a is the moment gradient factor corresponding to the pre-strengthening loads and $M_{\max}$, M_A, M_B and M_C are the absolute values of peak moment, the quarter point, midspan, and third-quarter point moments of the unbraced length corresponding to the pre-strengthening loads. The cross-section is then symmetrically strengthened by welding two cover plates $b_p \times t_p = 100mm \times 10mm$ and subsequently subjected to a post-strengthening midspan point load at the shear centre.

4.10.1 Description of Present Model

A mesh sensitivity analysis indicated that convergence is attained in the present model when 12 elements are taken along the beam span. The Saint-Venant torsional constant J and the warping constant C_w are obtained by assuming full shear transfer at the plate-flange interface (in a manner consistent with the Abaqus models as described subsequently), i.e., the strengthened section was considered to act as a monolithic entity. In this case, constant J is given by $J = J_B - (2/3)B_C t_f^{\,3} + (2/3)B_C\left(t_p + t_f\right)^3 + (2/3)B_E t_p^{\,3}$ in which J_B is the Saint-Venant torsional constant of the unstrengthened beam, $B_C = \min\left(b_f, b_p\right)$, $B_E = \max\left(b_p - b_f, 0\right)$, b_f and t_f are the flange width and thickness of the unstrengthened beam, and b_p and t_p are the width and thickness of each cover plate, respectively. The warping constant $C_w = \int_A \omega^2 dA = C_{wL} + C_{wG}$ is the sum of the global warping constant C_{wG} and the sum of local warping constants C_{wL} given by

$$C_{wL} = \begin{cases} \dfrac{1}{144}\left[h^3 t_w^{\ 3} + 2b_p^{\ 3}\left(t_p + t_f\right)^3 + 2\left(b_f - b_p\right)^3 t_f^{\ 3}\right] & b_p \le b_f \\ \dfrac{1}{144}\left[h^3 t_w^{\ 3} + 2b_f^{\ 3}\left(t_p + t_f\right)^3 + 2\left(b_p - b_f\right)^3 t_p^{\ 3}\right] & b_p > b_f \end{cases}$$

$$C_{wG} = 2\left(I_{yyS} e_S^{\ 2} + I_{yyE} e_E^{\ 2}\right)$$

$$I_{yyS} = \frac{1}{12}\left(t_p + t_f\right) b_S^{\ 3}, \quad b_S = \min\left(b_f, b_p\right) \tag{4.31)a-j}$$

$$e_S = \frac{1}{2}\left(h + t_p\right), \qquad e_E = \begin{cases} h/2 & b_p \le b_f \\ \left(h + t_f + t_p\right)/2 & b_p > b_f \end{cases}$$

$$I_{yyE} = \begin{cases} \dfrac{t_f}{12}\left[\left(b_f + t_p b_p / e_E\right)^3 - \left(b_p + t_p b_p / e_E\right)^3\right] & b_p \le b_f \\ \dfrac{t_p}{12}\left[\left(b_p - t_f b_f / e_E\right)^3 - \left(b_f - t_f b_f / e_E\right)^3\right] & b_p > b_f \end{cases}$$

4.10.2 Description of Abaqus Model

The S4R shell element was used to mesh the 3D shell model in Abaqus. The S4R is a four-node element with six degrees of freedom per node, with reduced integration, and hourglass control. A mesh study indicated that convergence is attained when an element size of nearly 15mm is used throughout. The interaction between the plates and beam flanges was modelled using the *CONTACT PAIR keyword in Abaqus, with the SMALL SLIDING, TYPE=SURFACE TO SURFACE features. These features treat the sliding between the two surfaces in contact as small/negligible relative to the deformations/motion of the structure (SIMULIA 2020). In order to prevent penetration between both surfaces, a HARD contact pressure over-closure relationship was defined. The Abaqus analysis involves three loading steps; (1) the unstrengthened beam was first subjected to pre-strengthening loads while the cover plates were concurrently bent to match the configuration of the bent beam, (2) A ROUGH friction model was activated at the interfaces between the plates and the flanges by using the *FRICTION, ROUGH keyword while suppressing the separation between the two surfaces after contact has been established by using the

*SURFACE BEHAVIOR, NO SEPARATION, PRESSURE-OVERCLOSURE=HARD keyword. The use of the above combination of features ensures surfaces to remain fully bonded together, with no separation nor tangential sliding, once they have been in contact, even when the contact pressure between them is tensile, and (3) The post-strengthening point load is then applied and a linearized eigenvalue buckling analysis is performed, to obtain the post-strengthening critical moment that would induce buckling of the strengthened beam. Fig. 4.4 depicts the deformed mesh in the buckled configuration for the reference beam.

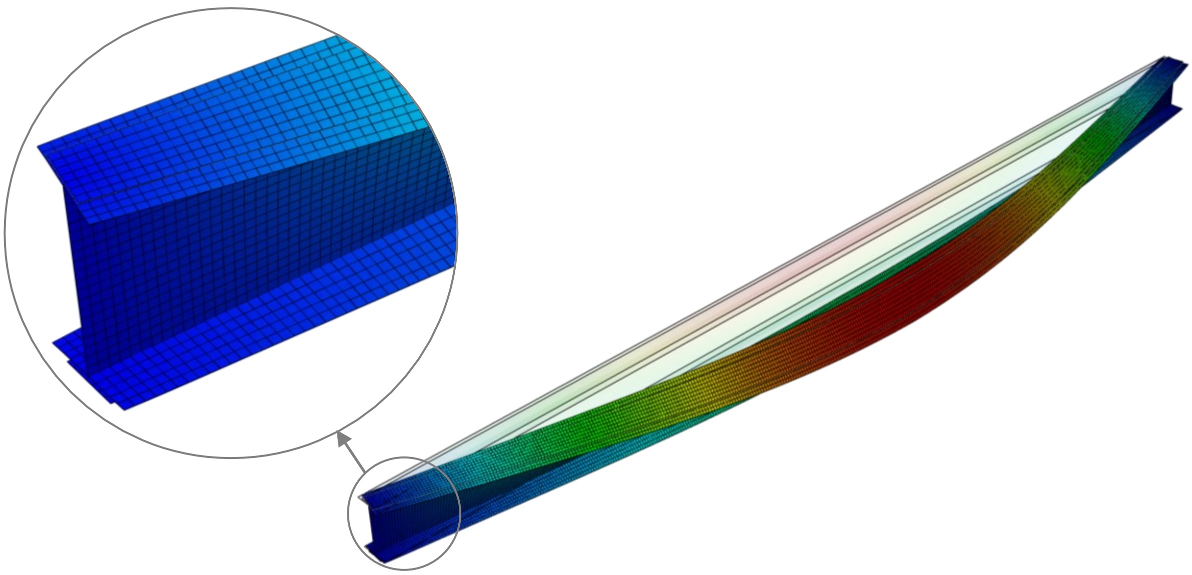

Fig. 4.4 Deformed mesh in the buckled configuration for the reference beam

4.10.3 Outline of Verification Study

The verification is done in two steps: a verification against shell FEA results and an experimental verification. In the former verification, the predictions of the present formulation are compared against those based on Abaqus shell model. The effect of PBD on the critical moments cannot be directly captured within the linearized eigenvalue buckling analysis solver in Abaqus. Hence the FEA verification is done in two parts; (1) suppressing PBD effects in the present formulation to match the Abaqus solution, and (2) including PBD effects in the present formulation and comparing the results against Abaqus predictions based on a special iterative process devised within the Abaqus model to account for pre-buckling effects.

4.10.3.1 Verification against 3D FE analysis-Part 1

The PBD effects were suppressed from the present model by omitting matrices $\mathbf{k}_{\mathbf{E\text{-}b}}$, $\mathbf{k}_{\mathbf{G1\text{-}b}}$, $\mathbf{k}_{\mathbf{G1\text{-}c}}$ and $\mathbf{k}_{\mathbf{G2}}$ in order to enable a direct comparison with shell model predictions. Two series of analyses were then conducted using the shell model; (1) without attempting to prevent web distortion and (2) while providing transverse stiffeners at beam ends and at midspan to suppress web distortion at these locations. A recent study (Arizou and Mohareb 2021) showed that web distortion is most pronounced at these three locations. The effect of the stiffeners was modelled in Abaqus by enforcing kinematic constraints that suppress web distortion while coupling the angles of twist of both flanges and the web. In this manner, the stiffened section is restrained from distorting but is kept free to warp.

For the reference beam, the critical moment due to uniformly distributed load before strengthening as predicted by Eq. (4.30) is $96.8kNm$ (Column 8 in Table 4.3). A uniformly distributed pre-strengthening load that induces a peak moment of $0.8\times 96.8kNm = 77.4kNm$ is applied. After strengthening, a Point Load is applied at beam midspan, and the additional post-strengthening critical moment as predicted by the present model is $132.6kNm$ (Column 9) while that based on the shell model is $108.8kNm$ (Column 10). The difference is attributed to web distortion, which is omitted in the present model (Assumption (d)) but captured in the shell model. In fact, when suppressing distortional effects in the shell model at midspan and end sections, the post-strengthening critical moments predicted by the shell model were found to increase to $128.4kNm$ (Column 11), i.e., the ratio of post-strengthening critical moments predicted by the shell model without stiffeners to those based on the present model increased from 0.82 (Column 12) to 0.97 (Column 13). In this case, the provision of stiffeners has increased the critical moment gained by strengthening by 18% (Column 14).

Table 4.3 Comparison of critical moments obtained from 3D FEA (Abaqus) and present FEA, when pre-buckling deformation effects are omitted

	Dimensions			Loading information			Critical moments (kNm)				Comparison		
# (1)	L (m) (2)	b_p (mm) (3)	t_p (mm) (4)	Pre-strengthening load (5)	Ω (6)	Post-strengthening load (7)	M_{uB} (8)	Present study (9)	Shell (distortion allowed) (10)	Shell (distortion suppressed [a]) (11)	(10)/(9) (12)	(11)/(9) (13)	(11)/(10) (14)
R1	6	100	10	UDL[b]	0.8	PL[d]	96.8	132.6	108.8	128.4	0.82	0.97	1.18
2	8	100	10	UDL	0.8	PL	64.3	99.1	86.2	97.5	0.87	0.98	1.13
3	10	100	10	UDL	0.8	PL	48.1	79.2	71.3	78.6	0.90	0.99	1.10
4	6	150	10	UDL	0.8	PL	96.8	227.7	183.1	218.0	0.80	0.96	1.19
5	6	200	10	UDL	0.8	PL	96.8	353.3	295.3	345.4	0.84	0.98	1.17
6	6	100	8	UDL	0.8	PL	96.8	104.6	88.2	101.8	0.84	0.97	1.15
7	6	100	12	UDL	0.8	PL	96.8	163.6	130.0	157.2	0.80	0.96	1.21
8	6	100	14	UDL	0.8	PL	96.8	197.3	151.4	191.6	0.77	0.97	1.27
9	6	100	10	UDL	0.2	PL	96.8	201.8	179.4	198.6	0.89	0.98	1.11
10	6	100	10	UDL	0.4	PL	96.8	178.8	156.0	175.3	0.87	0.98	1.12
11	6	100	10	UDL	0.6	PL	96.8	155.7	132.4	151.9	0.85	0.98	1.15
12	6	100	10	UDL	0.8	UDL	96.8	110.4	89.6	105.9	0.81	0.96	1.18
13	6	100	10	UDL	0.8	2PL[e]	96.8	106.3	88.4	104.2	0.83	0.98	1.18
14	6	100	10	UM[c]	0.8	PL	85.2	134.6	111.6	131.2	0.83	0.98	1.18
15	6	100	10	PL	0.8	PL	112.1	135.1	111.6	130.9	0.83	0.97	1.17
								Average:			0.84	0.97	1.17
								Standard deviation:			0.035	0.0094	0.040

[a] Cross-sectional distortion is suppressed at midspan and both ends
[b] UDL: Uniformly distributed load
[c] UM: Uniform moment applied at both ends
[d] PL: Point load applied at the beam midspan
[e] 2PL: Two point loads applied at third span points

An additional 14 cases were investigated by varying the beam span, the dimensions of cover plates, the types of loading before and after strengthening of the beam and the magnitude of the pre-strengthening moment. Table 4.3 provides the input parameters of each case and the post-strengthening critical moments predicted by the present and shell models. The ratios of post-strengthening critical moments predicted by the shell model without stiffeners to those based on the present model (Column 12) average 0.84 with a standard deviation of 0.035. In contrast, the ratio of post-strengthening critical moments predicted by shell model with stiffeners to those based on the present model (Column 13) average 0.97 with a standard deviation of 0.0094, confirming that (a) suppressing distortional effects by providing stiffeners increases the post-strengthening critical moment capacity by 17% on average and hence is a desirable/recommended strengthening practice, and (b) the present model provides very close predictions of the post-strengthening critical moments for strengthened beams with web stiffeners.

A comparison of the entries in Column 14 of Table 4.3 for runs 1, 12-15, indicates that the type of loading before and after strengthening has a negligible effect on web distortion. Results of runs 1, 9-11 show that web distortion increases with the magnitude of pre-strengthening moments. Therefore, when strengthening beams subjected to relatively heavy pre-strengthening loads, it becomes more critical to supply transverse stiffeners.

Fig. 4.5a-d depict the additional post-strengthening critical moment versus beam span, plate width, plate thickness and the ratio of pre-strengthening moment to pre-strengthening critical moment (denoted by pre-strengthening moment fraction Ω). As can be seen, web distortion becomes more pronounced as the beam span decreases (Fig. 4.5a), as the cover plate width and thickness increase (Fig. 4.5b-c) or as Ω increases (Fig. 4.5d). In all cases, the present model is able to closely predict the additional post-strengthening critical moment when web distortion is suppressed by stiffeners.

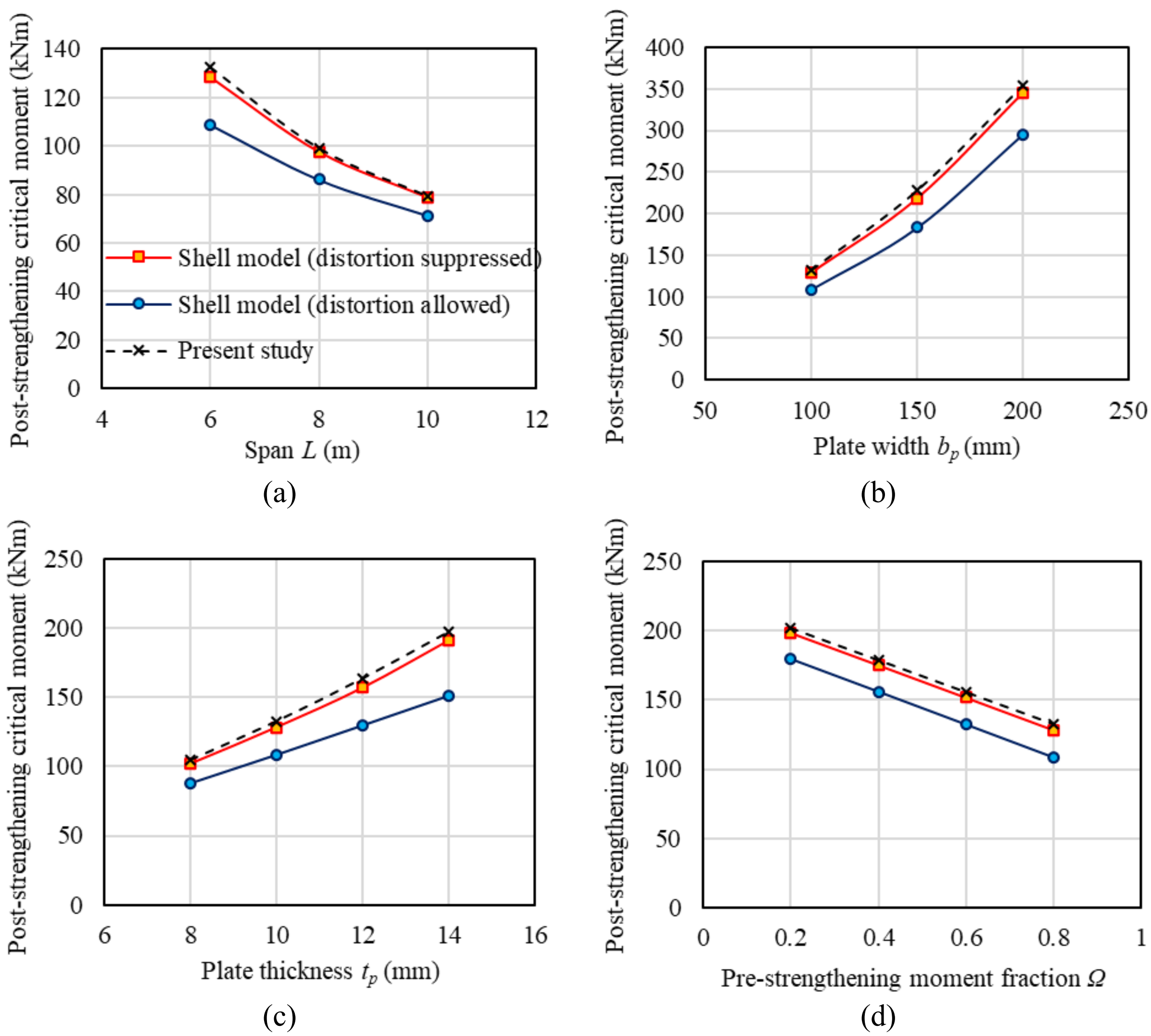

Fig. 4.5 Post-strengthening critical moments versus (a) span, (b) width of the cover plates, (c) thickness of the cover plates and (d) pre-strengthening moment fraction

4.10.3.2 Verification against 3D FE analysis-Part 2

As the linearized eigenvalue buckling analysis in Abaqus cannot directly account for PBD effects on the critical moment, the iterative procedure in (Pezeshky and Mohareb 2018) was employed to determine the elastic critical moment, including pre-buckling effect, in multiple steps using Abaqus. In this procedure, (1) a linearized eigenvalue analysis is first conducted to obtain the critical load. The linearized buckling analysis omits the pre-buckling curvature of the beam i.e., it assumes the beam at the onset of buckling to be perfectly straight as an approximation, (2) a static analysis is conducted under the critical load obtained in the previous step to obtain the pre-buckling deflected shape of the beam, (3) a new buckling model is built for the curved beam configuration as obtained in Step (2) and a new linearized eigenvalue analysis is conducted to account for the sagging beam configuration. Steps (2) and (3) are repeated until convergence is achieved.

Seven of the 15 runs described in Table 4.3 were investigated: 1, 3, 5, 8, 9, 12 and 15 using the iterative procedure. Cross-sectional distortion was suppressed by providing stiffeners. Table 4.4 summarizes the values of post-strengthening critical moments based on the present model (Column 9) and those obtained from the iterative shell model (Column 10). The ratios (Column 13) of both solutions averaged 0.97 with a standard deviation of 0.014, suggesting the accuracy of the present model in capturing PBD effects. Table 4.4 also summarizes the values of post-strengthening critical moments with and without PBD effects (Columns 11 and 12), web distortion having been suppressed. On average, both the present model and the iterative Abaqus procedure show that PBD effects increase the post-strengthening critical moments by 7.0 %.

Table 4.4 Comparison of critical moments obtained from 3D FEA (Abaqus) and present FEA, when distortion is suppressed

	Dimensions			Loading information			Critical moments (kNm)					Comparison		
#	L (m)	b_p (mm)	t_p (mm)	Pre-strengthening load	Ω	Post-strengthening load	M_{uB}	Present study (PBD included)	Shell (PBD included)	Present study (PBD omitted)	Shell (PBD omitted)	(10)/(9)	(9)/(11)	(10)/(12)
(1)	(2)	(3)	(4)	(5)	(6)	(7)	(8)	(9)	(10)	(11)	(12)	(13)	(14)	(15)
R1	6	100	10	UDL	0.8	PL	96.8	142.4	138.0	132.6	128.4	0.97	1.07	1.08
3	10	100	10	UDL	0.8	PL	48.1	84.5	84.2	79.2	78.6	1.00	1.07	1.07
5	6	200	10	UDL	0.8	PL	96.8	388.8	375.5	353.3	345.4	0.97	1.10	1.09
8	6	100	14	UDL	0.8	PL	96.8	209.0	199.8	197.3	191.6	0.96	1.06	1.04
9	6	100	10	UDL	0.2	PL	96.8	210.1	207.4	201.8	198.6	0.99	1.04	1.04
12	6	100	10	UDL	0.8	UDL	96.8	118.7	113.5	110.4	105.9	0.96	1.07	1.07
15	6	100	10	PL	0.8	PL	112.1	145.3	141.0	135.1	130.9	0.97	1.07	1.08
									Average:			0.97	1.07	1.07
									Standard deviation:			0.014	0.017	0.016

4.10.3.3 Experimental Verification

The present study developed an elastic LTB solution for beams strengthened under loading. Within the scarce literature on LTB on beams strengthened under loading, the authors were unable to find any experimental results reported for beams strengthened under loading failing in an elastic LTB mode. Nevertheless, among the specimens tested by Wang et al. (2015), a single specimen with a doubly symmetric section was strengthened under loading with cover plates (Specimen BI-S2) and was reported to fail by inelastic LTB. This specimen is hence used subsequently to indirectly verify the validity of the present FE formulation by combining the critical moments as predicted by the present formulation (which accounts for the effect of pre-strengthening loads, PBD, boundary conditions representative of those of the test, and load height effect -all of which are outside of the scope of North American Standards equations) in conjunction with existing inelastic LTB procedures available in ANSI/AISC360 (2022) and CAN/CSA-S16 (2019) which empirically account for inelastic effects.

Fig. 4.6a depicts a schematic of the test setup for specimen BI-S2 by Wang et al. (2015). In addition to lateral displacement and twist restrains at both ends as per the classical solution, additional clamp supports were provided at both ends to provide weak axis rotational restrains. The load was applied as opposed to shear centre loading as implied in present standard provisions.

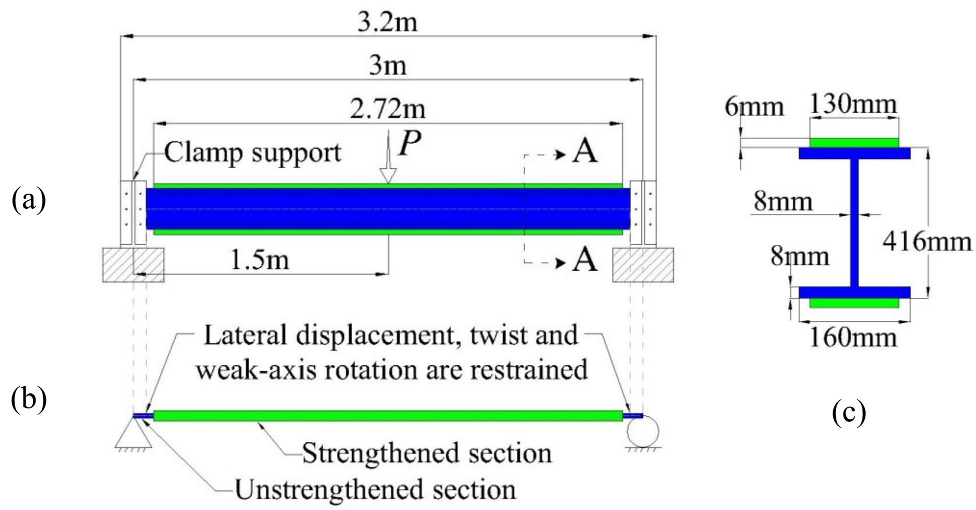

Fig. 4.6 Specimen BI-S2 (adapted from Wang et al. 2015) (a) Test details, (b) Idealized model, and (c) Cross-sectional geometry (Section A-A)

The sequence of loading and strengthening was done in the following seven steps:

(1) The cover plates were clamped to the beam flanges,

(2) A midspan point load was applied to the top flange prior to strengthening, and was increased gradually up to $120kN$,

(3) The pre-strengthening load was kept unchanged while the cover plates were fixed at their locations by spot welds to the beam flanges,

(4) The lower cover plate was welded to the bottom flange using several segments of welds, starting from the beam end and progressing towards midspan, resulting in two continuous lines of welds,

(5) The upper plate was subsequently welded to the top flange using the same welding sequence,

(6) The specimen was left at room temperature to cool down, and

(7) The midspan point load was then increased up until inelastic LTB failure is attained.

The experimentally recorded inelastic LTB failure load including pre-strengthening and post-strengthening loads is $P_{u-\exp} = 496.3kN$. This value compares to $P_{n-AISC} = 504.2kN$ (Appendix 4.B) as predicted by combining the elastic critical moment predicted by the present model with the ANSI/AISC360 (2022) inelastic LTB provisions, corresponding to a load ratio $P_{n-AISC} / P_{u-\exp} = 1.02$. When combining the elastic critical moment predicted by the present study with the CAN/CSA-S16 (2019) inelastic LTB provision, one obtains $P_{n-CSA} = 522.8kN$ (Appendix 4.C) which corresponds to a load ratio $P_{n-CSA} / P_{u-\exp} = 1.05$.

4.11 Parametric Study

The reference case defined in the verification section is re-considered in the present parametric study. One recalls that, for the reference case, the entire span is strengthened, pre-strengthening load is UDL applied at the shear centre, post-strengthening load is PL applied at the shear centre, the pre-strengthening moment fraction $\Omega = 0.8$, the span to height ratio is $L/h = 20.0$, web slenderness is $h/t_w = 51.8$, height to flange width ratio is $h/b_f = 1.82$, flange slenderness is $b_f / t_f = 17.0$, normalized plate width is $b_p / b_f = 0.606$ and the normalized plate thickness is $t_p / t_f = 1.03$.

All numeric results of the parametric study are presented in Appendix 4.D.

4.11.1 Effect of Cover Plate Location

In cases where only a portion L_p of the entire span L is to be strengthened, it would be of interest to identify the location for the strengthening plates along the span that would maximize the critical moment capacity. Towards this goal, we investigate the case where the reference beam is to be strengthened by two plates of length $L_p = L/6$. Three partial strengthening scenarios are considered: (1) Plates are located at the ends of the beam span (End Strengthening, E), (2) Plates are located between the ends and midspan locations (Intermediate Strengthening, I), and (3) Plates are located at midspan (Midspan Strengthening, M) (Fig. 4.7a). The reference Scenario corresponding to the case where the entire span is strengthened (Full Strengthening, F) is provided as a benchmark. For all four cases, the post-strengthening critical moments M_i are determined by omitting PBD effects as well as the post-strengthening critical moment $M_{i,p}$ while accounting for pre-buckling effects. Fig. 4.7b depicts the total elastic critical moment capacity (sum of pre-strengthening moments and post-strengthening critical moments) for the cases of the unstrengthened beam (B), in addition to partially and fully strengthened beams.

The percentage gain $G_p = \left(M_{i,p} - M_u\right) / \left(M_s - M_u\right)$ in critical moments $M_{i,p}$ (in which subscript p denotes that PBD effects are retained) corresponding to partial strengthening scenarios $i = E, I, M$ relative to the gain achieved under Full Strengthening were determined. Parameters M_u and M_s denote post-strengthening critical moments when excluding PBD effects for the unstrengthened beam and for the Full Strengthening Scenario, respectively. The percentage gain G_p shows that the End Strengthening Scenario is the most effective as it provides 50% of the gain attained by Full Strengthening. This compares to 39% for Intermediate Strengthening and 25% for the Midspan Strengthening Scenarios. The percentage gains $G_{np} = \left(M_i - M_u\right) / \left(M_s - M_u\right)$ excluding PBD effects are 43%, 33% and 19% for End, Intermediate and Midspan Strengthening Scenarios, respectively.

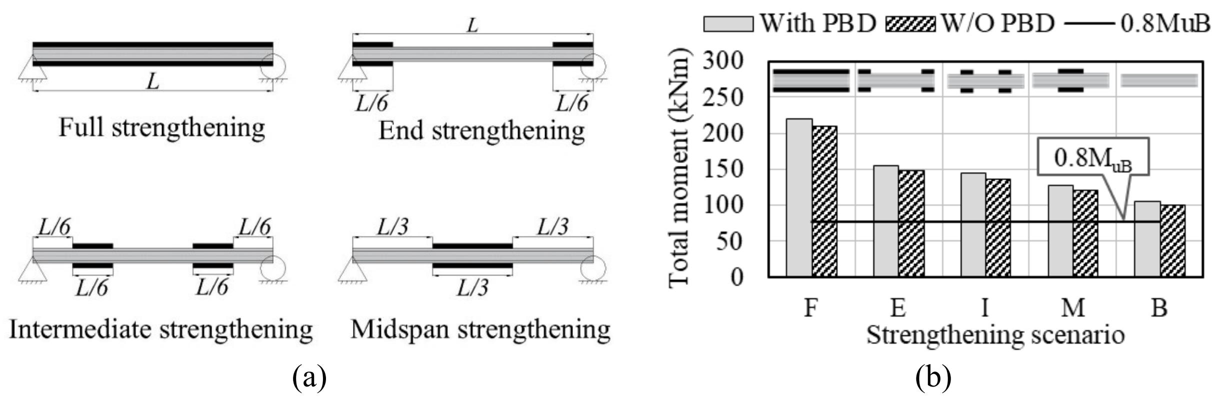

Fig. 4.7 (a) Selected scenarios for the location of strengthening cover plates, (b) effect of strengthening scenario on the gain in post-strengthening LTB capacity (total moment is the summation of the applied pre-strengthening moment and the post-strengthening critical moment)

The effectiveness of the End Strengthening Scenario is attributed to the fact that the strengthening plates at beam ends are more effective in reducing the large warping deformations that take place near the beam ends (Fig. 4.8d) when compared to Intermediate or Midspan Strengthening Scenarios. In fact, by normalizing the mode shapes relative to the peak lateral displacement, it is shown that the fully strengthened beam exhibits the least twist (Fig. 4.8c), followed by the End Strengthening Scenario, and then by the Intermediate Strengthening Scenario, while the largest angles of twist correspond to the Midspan Strengthening Scenario.

The ratio $C_p = M_{i,p} / M_i$ is indicative of the gain in capacity achieved by accounting for PBD effects. The value of this parameter for Scenarios F, E, I, and M are 1.07, 1.11, 1.12 and 1.15, respectively, indicating that the PBD effect is most pronounced for Midspan Strengthening. In this case, omitting PBD effects underestimates the post-strengthening critical moment by 15%. In comparison, for the reference case of Full Strengthening, the omission of PBD effects underestimates the post-strengthening critical moment only by 7.4%.

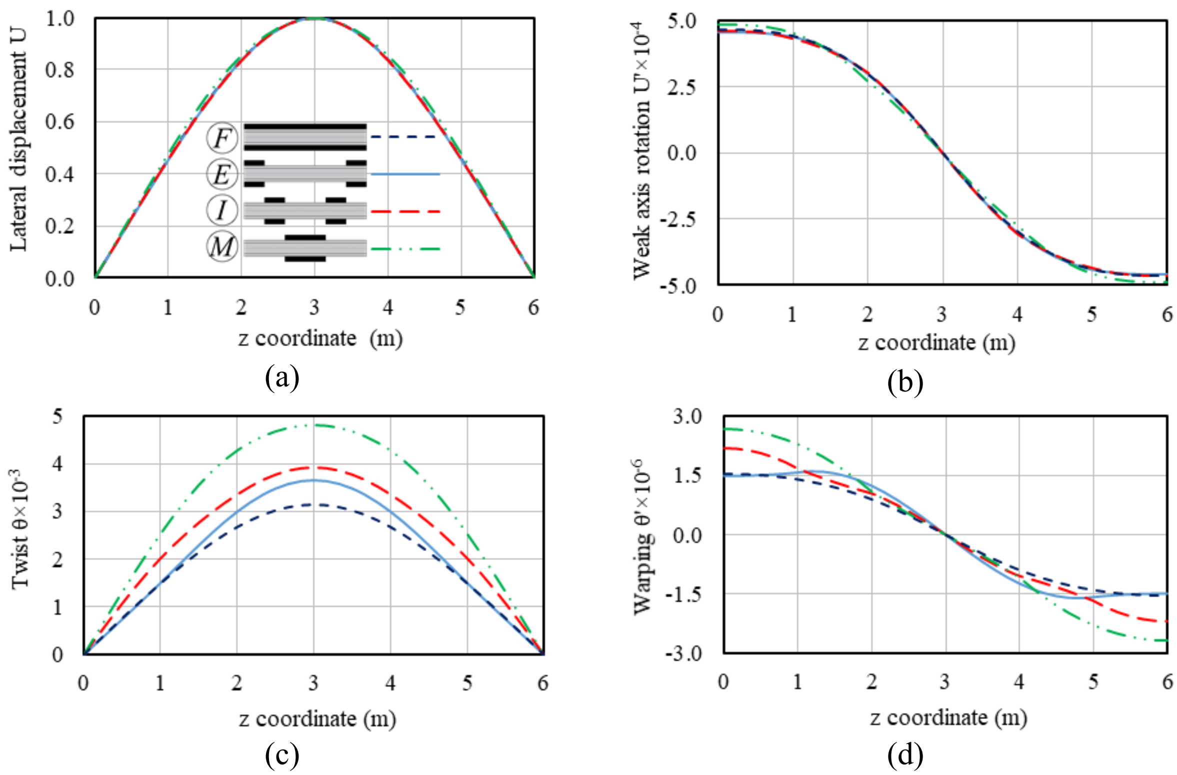

Fig. 4.8 Normalized mode shapes for strengthening scenarios including PBD (a) lateral displacement, (b) weak axis rotation, (c) twist, and (d) warping – All mode shapes have been normalized relative to the peak lateral displacement U

4.11.2 Effect of Cover Plate Length

To investigate the effect of plate length L_p on the critical moment, L_p was varied from 0.5 to 3m (i.e., Full Strengthening) within the End Strengthening Scenario. As expected, the gain in post-strengthening critical moment achieved increases with the plate length (Fig. 4.9a). The effect of PBD is observed to reduce as the plate length increases. By increasing the ratio L_p/L from 0.08 to 0.5, the pre-buckling coefficient C_p decreases from 1.13 to 1.07.

4.11.3 Effect of Plate Geometry

The cover plate width is varied from 100 to 250mm and the thickness is varied from 8 to 14mm, leading to 28 combinations involving partial and full strengthening scenarios. By increasing the plate width, Fig. 4.9b shows that the effectiveness of the End and Intermediate Strengthening Scenarios decreases. In cases where the cover plate width is less than that of the flange, End

Strengthening Scenario is found to be the most effective. Conversely, for cases where the strengthening plates are wider than the flanges, the Midspan Strengthening Scenario can be more effective. Fig. 4.9c shows that the efficiency of partial strengthening scenarios reduces with the increase in plate thickness. Since the 100mm width of the reference plate is less than the flange width, the End Strengthening Scenario is most effective in all cases shown in Fig. 4.9c.

For full strengthening, Fig. 4.10a shows that the pre-buckling coefficient C_p increases with the plate width. This observation does not always hold true for partial strengthening. Fig. 4.10b shows that the PBD effects reduce with the plate thickness. In the ranges of plate dimensions investigated, the effect of PBD was found to be most pronounced for the case of Midspan Strengthening.

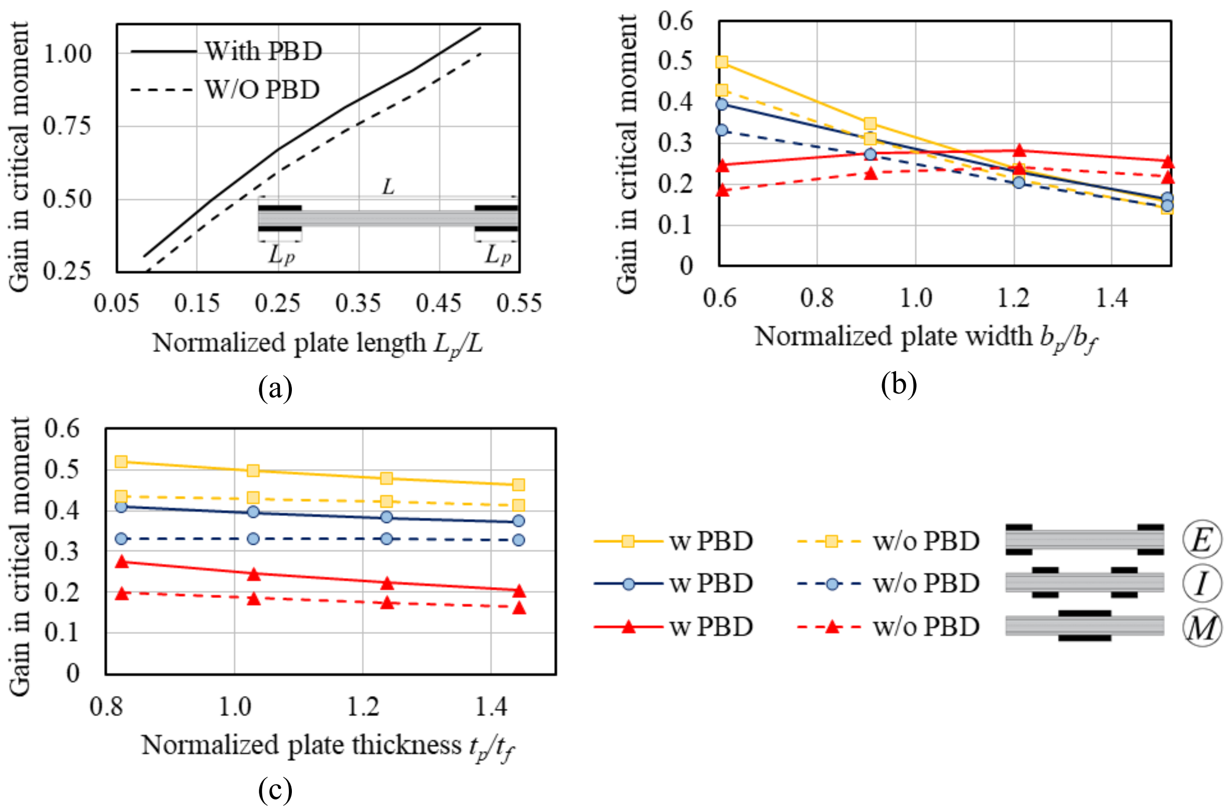

Fig. 4.9 Gain in post-strengthening LTB capacity versus (a) normalized plate length in End Strengthening Scenario, (b) normalized plate width, and (c) normalized plate thickness (Gain including PBD $\left(M_{i,p}-M_u\right)/\left(M_s-M_u\right)$ and excluding PBD $\left(M_i-M_u\right)/\left(M_s-M_u\right)$)

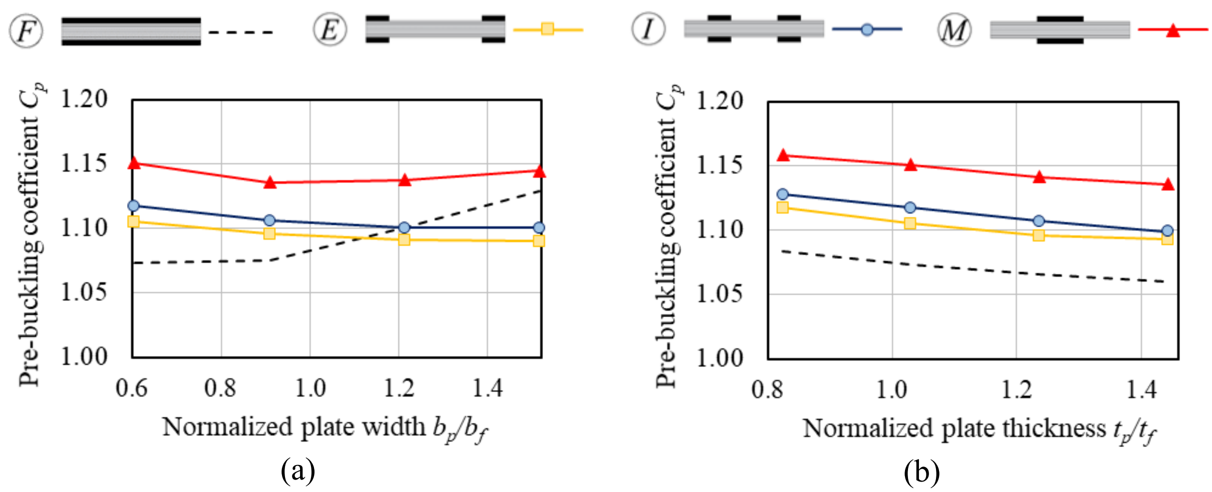

Fig. 4.10 Pre-buckling coefficient versus (a) normalized plate width, and (b) normalized plate thickness

4.11.4 Effect of Beam Geometric Parameters

The gain in critical moment attained is investigated for different pre-strengthening moment fraction Ω for the End Strengthening Scenario. The parameters $L_p/L = 0.167$, $b_p/b_f = 0.606$ and $t_p/t_f = 1.03$ are taken as reference values. In addition, the effects of the geometric parameters L/h, h/t_w, h/b_f and b_f/t_f were varied one parameter at a time.

Beam span was varied from 4 to 8m leading to 20 combinations (Fig. 4.11a). Web thickness was varied from 5.8 to 10mm leading to 25 combinations (Fig. 4.11b). The section aspect ratio h/b_f was varied from 1.33 to 2.42 leading to 20 combinations (Fig. 4.11c). Also, the flange slenderness b_f/t_f was varied from 8.25 to 20.6 leading to 25 combinations (Fig. 4.11d). In all cases, Fig. 4.11a-d show that the gain in post-strengthening critical moment very mildly increases with Ω. Fig. 4.11a-b indicate that the gain in post-strengthening critical moment is nearly independent of the normalized span L/h and the web slenderness h/t_w. Conversely, the section aspect ratio h/b_f is observed to significantly affect the gain in post-strengthening critical moment (Fig. 4.11c). By increasing h/b_f from 1.33 to 2.42, the gain in post-strengthening critical moment reduces by 21%

on average. Fig. 4.11d shows that, for thinner flanges with $b_f/t_f \geq 13.8$, the effect of flange slenderness b_f/t_f can be considered negligible.

Fig. 4.12 shows that the effect of PBD on the critical moment as characterized by the pre-buckling coefficient C_p becomes more pronounced when pre-strengthening moment fraction Ω increases for shallower sections with low aspect ratio h/b_f (Fig. 4.12c). The peak value of pre-buckling coefficient attained is 1.22 and takes place at ($h/b_f = 1.33$, $\Omega = 0.8$). The plots indicate that C_p is most sensitive to h/b_f and Ω, but is insensitive to L/h, h/t_w and b_f/t_f. The findings are consistent with the results reported by Pezeshky and Mohareb (2018) for non-strengthened sections.

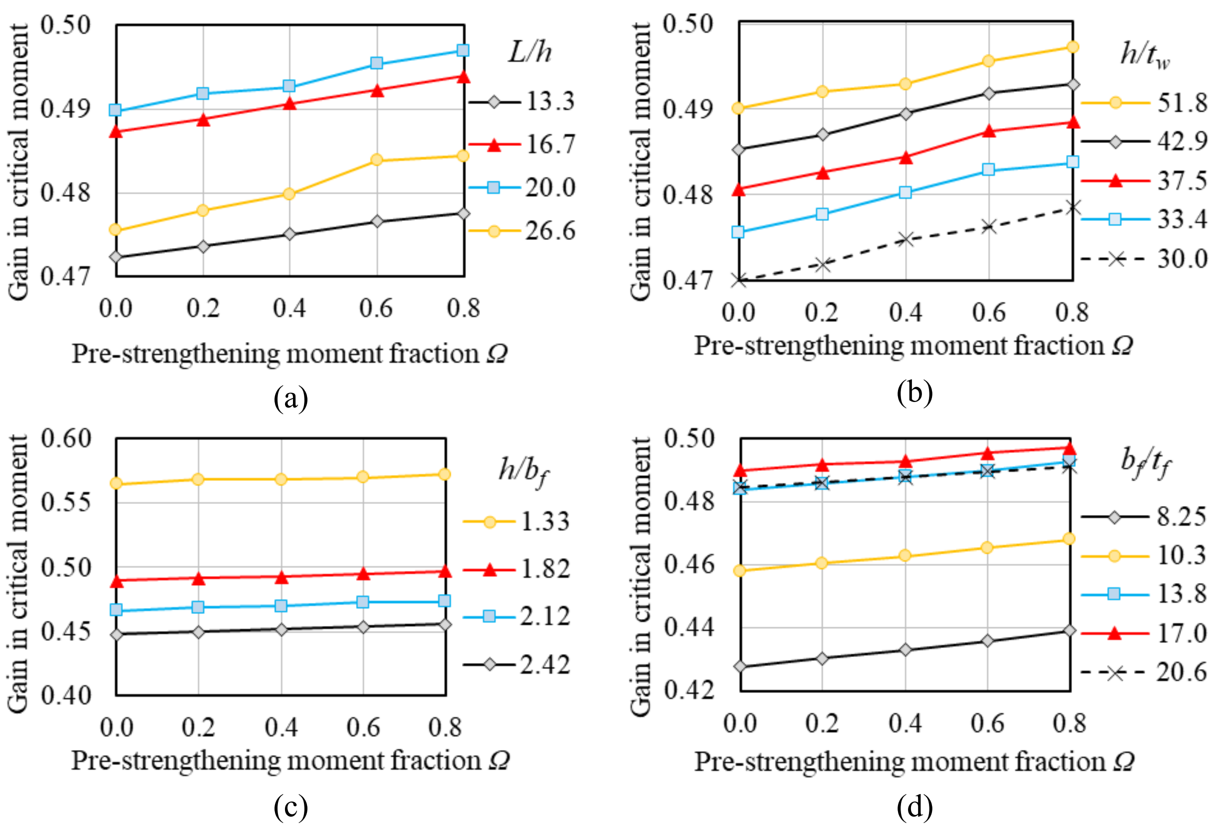

Fig. 4.11 Gain in post-strengthening LTB capacity including PBD effects versus pre-strengthening moment fraction (a) effect of span to depth ratio, (b) effect of web slenderness (c) effect of beam depth to flange width ratio, and (d) effect of flange slenderness

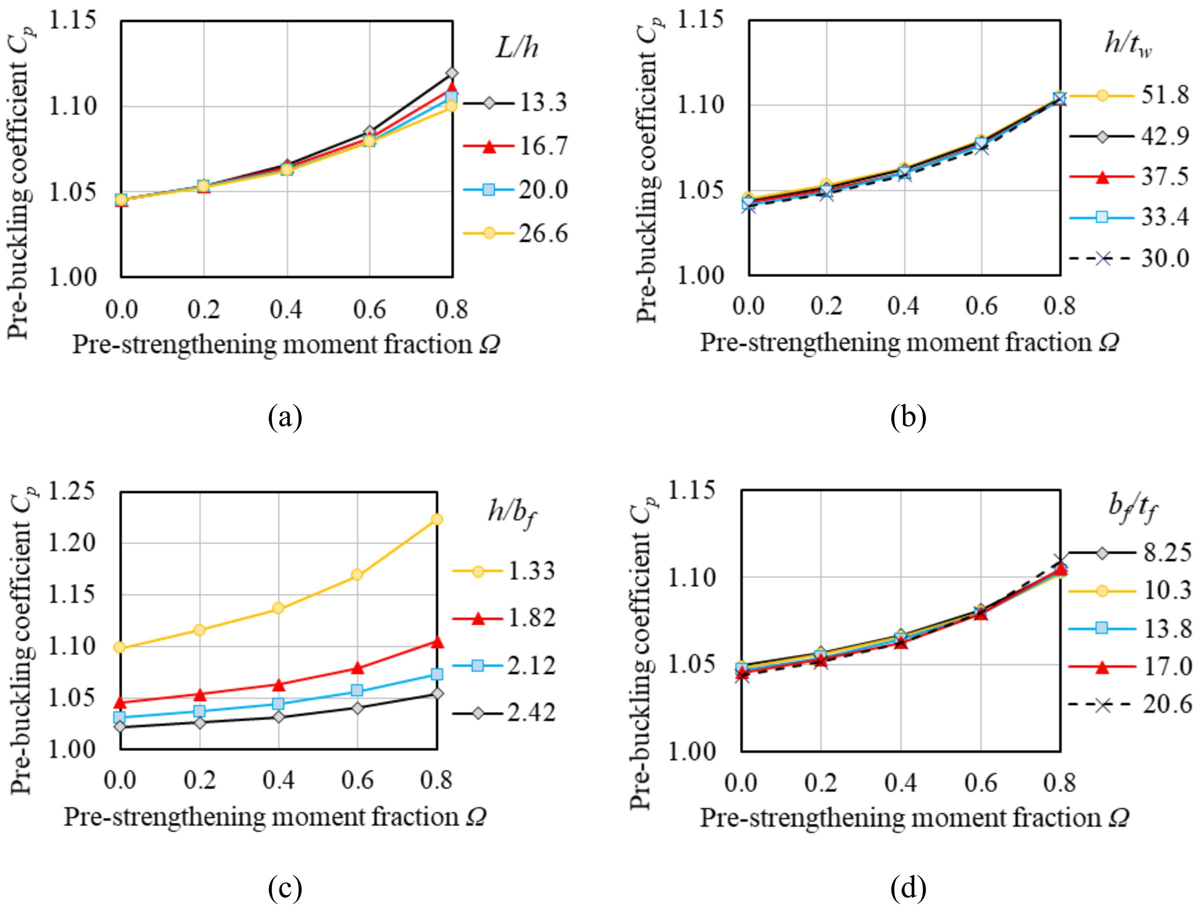

Fig. 4.12 Pre-buckling coefficient versus pre-strengthening moment fraction (a) effect of span to depth ratio, (b) effect of web slenderness (c) effect of beam depth to flange width ratio, and (d) effect of flange slenderness

4.11.5 Effect of Loading Type before and after Strengthening

Four combinations are examined (Fig. 4.13) by varying the loading types before and after strengthening for End Strengthening Scenario, with a pre-strengthening moment fraction $\Omega = 0.8$. Fig. 4.13 suggests that type of loading before and after strengthening has a negligible effect on the gain in critical moment, as the difference between the larger and smaller gains attained among all four cases considered is less than 3%. The pre-buckling coefficient C_p for the four loading combinations investigated is approximately constant at 1.1.

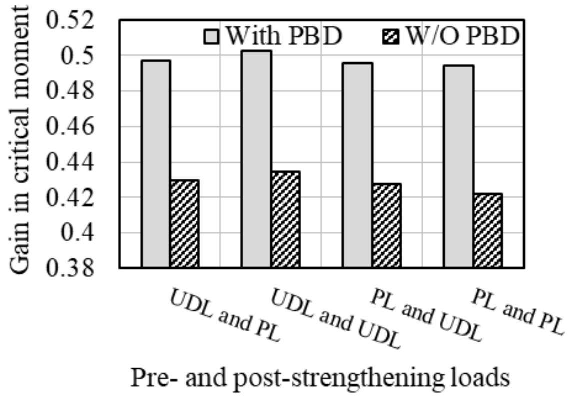

Fig. 4.13 Effect of pre- and post-strengthening loadings on gain in post-strengthening critical moment

4.12 Summary and Conclusions

The presented study developed a variational principle and finite element formulation to quantify the elastic lateral torsional buckling load-carrying capacity of steel I-beams that are partially/fully strengthened using cover plates welded to both flanges. The formulation incorporates the effects of pre-strengthening loads and pre-buckling deformation (PBD). Comparisons with shell models showed that the present model closely predicts the post-strengthening critical moment when web distortion is suppressed by stiffeners. Further comparisons against experimental results of Wang et al. (2015) suggest the validity of the results when combined with present American and Canadian specifications for inelastic lateral torsional buckling. Using the present FE model, a parametric study was conducted to quantify the gain in post-strengthening critical moment and PBD effects. The study investigated the effects of beam and plate geometry, the location of strengthening plates in cases where only part of the beam span is strengthened, the types of loading before and after strengthening and the magnitude of the pre-strengthening moment.

The following observations are made based on the parametric runs conducted in the present study:

- Suppressing distortional effects at beam ends and midspan of a simply supported beam using stiffeners increases the post-strengthening critical moment capacity by 17% on average and hence is a desirable/recommended strengthening practice when cover plates are provided.
- For cases where the cover plate width is less than that of the flange, the End Strengthening Scenario examined in the present study is found to be the most effective. Conversely, for cases where the strengthening plates are wider than flanges, the Midspan Strengthening Scenario can be more effective.
- The PBD effect is most pronounced for Midspan Strengthening. In this case, omitting PBD effect underestimates the post-strengthening critical moment by 15%. In comparison, for Full Strengthening, the omission of PBD effect underestimates the post-strengthening critical moment only by 7.4%.
- The gain in post-strengthening critical moment achieved is nearly independent of the flange slenderness b_f/t_f (when $b_f/t_f \geq 13.8$), the normalized span L/h, the web slenderness h/t_w, the pre-strengthening moment fraction Ω and the loading type before and after strengthening.
- The gain in post-strengthening critical moment is most sensitive to L_p/L, b_p/b_f, the location of strengthening plates (in partial strengthening scenarios) and to the section aspect ratio h/b_f
- Conversely, the gain in post-strengthening critical moment achieved increases with the normalized plate length L_p/L, and decreases with the normalized plate width b_p/b_f (for the End and Intermediate Strengthening Scenarios), the normalized plate thickness t_p/t_f (for partial strengthening scenarios) and with the section aspect ratio h/b_f.
- The effect of PBD is observed to be most sensitive to h/b_f and Ω but insensitive to L/h, h/t_w, b_f/t_f and the loading types before and after strengthening.

- The PBD reduces with b_p/b_f (for the End and Intermediate Strengthening Scenarios), t_p/t_f, L_p/L and h/b_f, but increases with b_p/b_f (for the Full Strengthening Scenario) and pre-strengthening moment fraction Ω.

4.13 Appendix 4.A: Second variation of Total Potential Energy

The second variation of $\Pi_{(7-8)}$ with respect to buckling displacements $U'_{(7-8)}, U''_{(7-8)}, \theta_{(7-8)}, \theta'_{(7-8)}$ and $\theta''_{(7-8)}$ is expressed by (e.g., Bazant and Cedolin 2010)

$$\overline{\overline{\Pi}}_{(7-8)} = \frac{1}{2}\sum_{j=1}^{5}\sum_{k=1}^{5}\frac{\partial^2 \Pi_{(7-8)}}{\partial q_j \partial q_k}\delta q_j \delta q_k, \qquad \{q_1, q_2, q_2, q_4, q_5\} = \left\{U'_{(7-8)}, U''_{(7-8)}, \theta_{(7-8)}, \theta'_{(7-8)}, \theta''_{(7-8)}\right\} \tag{4.32}$$

The obtained expression $\overline{\overline{\Pi}}_{(7-8)}$ would be a functional of buckling displacements and their first variations ($\overline{U''}_{(7-8)}$, $\overline{\theta}_{(7-8)}$, $\overline{\theta'}_{(7-8)}$ and $\overline{\theta''}_{(7-8)}$) in which symbols $\overline{(\ )}$ and $\overline{\overline{(\ )}}$ respectively denote the first and second variations of the argument functions. Since $\overline{\overline{\Pi}}_{(7-8)}$ is determined in an infinitely small neighborhood of the equilibrium state at Configuration 7 (Fig. 4.1), all buckling displacements must vanish, while their first variations are arbitrary non-zero functions.

4.14 Appendix 4.B: Resistance of Beam BI-S2 in Wang et al. (2015) according to American Specifications

It can be shown that the section meets the compactness requirements of AISC 360 (2022). For flexural members with compact sections, inelastic LTB governs the resistance when the unbraced length L_b satisfies the condition $L_f \le L_b \le L_r$ where L_f is the fully braced length below which LTB does not occur, given by Clause F2-5 as

$$L_f = 1.76 r_y \sqrt{\frac{E}{F_y}} \tag{4.33}$$

in which r_y is the radius of gyration of the cross-section about y axis and F_y is the yield stress. The length L_r is the laterally unbraced length that delineates inelastic LTB from elastic LTB as given by Clause F2-6 as

$$L_r = 1.95 \frac{E}{0.7F_y} \sqrt{\frac{\sqrt{I_{yy} C_w}}{S_x} \left[\frac{J}{S_x h} + \sqrt{\left(\frac{J}{S_x h} \right)^2 + 6.76 \left(\frac{0.7F_y}{E} \right)^2} \right]} \tag{4.34}$$

in which S_x is the elastic section modulus, and h is the distance between the flange centroids. When $L_f \le L_b \le L_r$, the nominal flexural capacity based on LTB M_{n-AISC} as given by Clause F2-2 is expressed by

$$M_{n-AISC} = C_b \left[M_p - \left(M_p - 0.7F_y S_x \right) \frac{\left(L_b - L_f \right)}{\left(L_r - L_f \right)} \right] \tag{4.35}$$

in which M_p is the section plastic moment and C_b is the moment gradient factor which accounts for the variation of moments along the unbraced segment. Conceptually, the moment gradient factor C_b for a given case is obtained by dividing the elastic critical moment M_{cr-FEA} for the loading case of interest by the uniform elastic critical moment M_{cr-u} for an identical beam segment with full lateral and torsional restraints (Sahraei et al. 2017, Iranpour and Mohareb 2022, Arizou and Mohareb 2021, Arizou and Mohareb 2022) and no weak axis rotation nor warping restraints at both ends subject to uniform moment, i.e.,

$$C_b = \frac{M_{cr-FEA}}{M_{cr-u}}, \; M_{cr-u} = \frac{\pi}{L_b} \sqrt{E I_{yy} G J + \left(\frac{\pi E}{L_b} \right)^2 I_{yy} C_w} \tag{4.36)a-b}$$

An estimate of the moment gradient factor C_b is provided in Clause F1-1 of AISC 360 (2022) as a function of four sampling moment values within the unbraced length L_b: The absolute values of the quarter point moment M_A, the midspan moment M_B, the third-quarter point moment M_C and the peak moment $M_{\max}$ within the unbraced length

$$C_b = \frac{12.5M_{\max}}{2.5M_{\max} + 3M_A + 4M_B + 3M_C} \tag{4.37}$$

Eq. (4.35) has the following limitations:

(1) It is intended for the basic case of unbraced beam segments with full lateral and torsional restraints and no weak axis rotation nor warping restraints at both ends. This condition does not reflect the test boundary condition where both ends had full lateral, torsional, and weak axis rotational restraints, but free warping restrains.

(2) It is intended for loads acting at the shear centre of the section, a condition also differing from the test by Wang et al. (2015) in which the load was applied to the top flange.

(3) It does not account for PBD effects nor for pre-strengthening load effects.

The unstrengthened cross-sectional properties for specimen BI-S2 (Fig. 4.6c) by (Wang et al. 2015) beam are $I_{xx-B} = 1.52\times10^8 mm^4$, $I_{yy-B} = 5.48\times10^6 mm^4$, $J_B = 1.24\times10^5 mm^4$ and $C_{w-B} = 2.28\times10^{11} mm^6$. For the strengthened section, one has $S_x = 1.03\times10^6 mm^3$, $I_{xx} = 2.21\times10^8 mm^4$, $I_{yy} = 7.68\times10^6 mm^4$, $J = 3.18\times10^5 mm^4$, $C_w = 3.31\times10^{11} mm^6$, $r_y = 32.4mm$, $E = 2.1\times10^5 MPa$, $G = E/2.6$ and h is taken as $414mm$. Coupon test results by Wang et al. (2015) on the 8mm thick plates forming the built-up I-beam (Fig. 4.6c) provided a yield strength $F_{yb} = 380MPa$. Also, for the 6mm thick strengthening plates, the yield strength was found to be

$F_{yp} = 399MPa$. The corresponding plastic moment is $M_p = 451.4kNm$. Assuming a linear strain distribution in which the outermost fiber of the flange is at the onset of yielding, $F_{yb} = 380MPa$, the stress at the outermost fiber of the cover plate is found to reach $391MPa$. As a result, when calculating the yield moment resistance $M_y = S_x F_y$ appearing in Eqs. (4.34) and (4.35), the yield stress $F_y = 391MPa$ is adopted. However, when determining slenderness limits for the web, flange and cover plate, a yield stress $F_{yb} = 380MPa$ was used for the web and flanges, and $F_{yp} = 399MPa$ for the cover plates. The section is found to meet the compactness requirements of AISC360 (2022).

By using Eqs. (4.33) and (4.34), one obtains $L_f = 1321mm$ and $L_r = 3812mm$. Since the unbraced length of the member falls within $L_f < L_b = 2800mm < L_r$, AISC360 (2022) predicts inelastic LTB to occur, which is consistent with the findings reported in the test. In this case, the nominal resistance of the beam is estimated by Eq. (4.35).

Owing to the fact that the test of Wang et al. (2015) falls outside the limitations (1-3), it becomes necessary to develop an alternative coefficient C_{b-Test} that reflects the boundary conditions of the test, top flange loading, PBD effects, and pre-strengthening loading effects, in addition to the moment gradient effect. This is accomplished by determining the elastic critical moment for the tested specimen from the present finite element solution M_{cr-FEA} which appropriately accounts for the factors missed under limitations (1-3) and leads to the critical moment $M_{cr-FEA} = 516.5kNm$. The uniform elastic critical moment M_{cr-u} for an identical beam segment with standard boundary conditions as given by Eq. (4.36)b is $M_{cr-u} = 479.2kNm$ which closely matches the uniform critical moment $M_{cr-u-FEA} = 480.1kNm$ as predicted by the present model for the uniform elastic critical moment of the beam. By substituting into Eq. (4.36)a, one obtains the sought moment gradient factor $C_{b-Test} = 1.08$.

In summary, from the values $L_f = 1321mm$, $L_b = 2800mm$, $L_r = 3812mm$, $C_{b-Test} = 1.08$, $M_p = 451.4kNm$, $S_x = 1.03 \times 10^6 mm^3$ and $F_y = 391MPa$, by substituting into Eq. (4.35), one obtains $M_{n-AISC} = 378.2kNm$. Given that the distance between transverse supports is $L_v = 3000mm$, the midspan point load that corresponds to M_{n-AISC} is $P_{n-AISC} = 4M_{n-AISC}/L_v = 504.2kN$ which closely matches the experimental value reported by Wang et al. (2015) $P_{u-\exp} = 496.3kN$.

4.15 Appendix 4.C: Resistance of Beam BI-S2 in Wang et al. (2015) according to Canadian Standards

According to CAN/CSA-S16 (2019), the elastic critical moment M_{cr} is determined from

$$M_{cr} = C_{b-CSA} \frac{\pi}{L_b} \sqrt{EI_{yy}GJ + \left(\frac{\pi E}{L_b}\right)^2 I_{yy}C_w}, \qquad C_{b-CSA} = \frac{4M_{\max}}{\sqrt{M_{\max}^{\;2} + 4M_a^{\;2} + 7M_b^{\;2} + 4M_c^{\;2}}} \qquad \text{(4.38)a-b}$$

in which the moment gradient factor C_{b-CSA} accounts for non-uniform moment effects within the unbraced length. Eq. (4.38) has the same limitations as those of the American Standard (i.e., limitations 1-3 in Appendix 4.B) and its application does not reflect the specific conditions of the test of Wang et al. (2015). Instead, the elastic critical moment M_{cr} is computed from the present FE solution, i.e., $M_{cr} = M_{cr-FEA}$ to account for the moment gradient effect, restrained weak axis rotation at supports, load height effect, PBD and pre-strengthening load effects. The section of Specimen BI-S2 in Wang et al. (2015) was verified to satisfy Class 2 requirements. For flexural members meeting Class 2 requirements for which $0.67 < M_{cr}/M_p < 2.15$, CAN/CSA-S16 (2019) stipulates that inelastic LTB governs the capacity. The corresponding nominal flexural inelastic LTB resistance equation is

$$M_{n-CSA} = 1.15 M_p \left(1 - \frac{0.28 M_p}{M_{cr}} \right) \tag{4.39}$$

The elastic critical moment obtained by FEA is $M_{cr-FEA} = 516.5 kNm$. Given that the moment ratio satisfies the condition $0.67 < M_{cr-FEA} / M_p < 2.15$, inelastic LTB governs the resistance and the nominal flexural capacity as predicted by Eq. (4.39) is $M_{n-CSA} = 392.1 kNm$. The corresponding midspan point load is $P_{n-CSA} = 4 M_{n-CSA} / L_v = 522.8 kN$ which closely matches the experimental value of $P_{u-CSA} = 496.3 kN$ reported by Wang et al. (2015).

4.16 Appendix 4.D: Numeric Results of Parametric Study

Table 4.5 Catalog of parametric study

Section title	Parameter under investigation	Figure Number	Relevant Run Numbers
Effect of cover plate location		4.7(b)	1-4
Effect of cover plate length	L_p / L	4.9(a)	1-2, 5-8
Effect of plate geometry	b_p / b_f	4.9(b) and 4.10(a)	1-4, 9-20
	t_p / t_f	4.9(c) and 4.10(b)	1-4, 21-32
Effect of beam geometric parameters	L / h	4.11(a) and 4.12(a)	2, 33-51
	h / t_w	4.11(b) and 4.12(b)	2, 52-75
	h / b_f	4.11(c) and 4.12(c)	2, 76-94
	b_f / t_f	4.11(d) and 4.12(d)	2, 95-118
Effect of loading type before and after strengthening		4.13	2, 119-121

Table 4.6 Results of parametric study

		Geometric Parameters								Dimensionless parameters							Loading			Critical moments (kNm)							
Run number	Configuration	L (m)	b_p (mm)	t_p (mm)	L_p (m)	b_f (mm)	t_f (mm)	h (mm)	t_w (mm)	L/h	h/t_w	h/b_f	b_f/t_f	L_p/L	b_p/b_f	t_p/t_f	Pre-strengthening	Ω	Post-strengthening	M_{uB}	M_{ip}	M_i	M_u	M_s	G_p	G_{np}	C_p
(1)	(2)	(3)	(4)	(5)	(6)	(7)	(8)	(9)	(10)	(11)	(12)	(13)	(14)	(15)	(16)	(17)	(18)	(19)	(20)	(21)	(22)	(23)	(24)	(25)	(26)	(27)	(28)
1	**F** [a]	6.0	100	10.0	3.00	165	9.7	300	5.80	20.0	51.8	1.82	17.0	0.500	0.606	1.03	UDL	0.8	PL	96.8	142.4	132.6	23.4	132.6	1.09	1.00	1.07
2	**E** [b]	6.0	100	10.0	1.00	165	9.7	300	5.80	20.0	51.8	1.82	17.0	0.167	0.606	1.03	UDL	0.8	PL	96.8	77.7	70.3	23.4	132.6	0.50	0.43	1.11
3	**I** [c]	6.0	100	10.0	1.00	165	9.7	300	5.80	20.0	51.8	1.82	17.0	0.167	0.606	1.03	UDL	0.8	PL	96.8	66.5	59.5	23.4	132.6	0.39	0.33	1.12
4	**M** [d]	6.0	100	10.0	1.00	165	9.7	300	5.80	20.0	51.8	1.82	17.0	0.167	0.606	1.03	UDL	0.8	PL	96.8	50.3	43.7	23.4	132.6	0.25	0.19	1.15
5	E	6.0	100	10.0	0.50	165	9.7	300	5.80	20.0	51.8	1.82	17.0	**0.083**	0.606	1.03	UDL	0.8	PL	96.8	56.4	49.9	23.4	132.6	0.30	0.24	1.13
6	E	6.0	100	10.0	1.50	165	9.7	300	5.80	20.0	51.8	1.82	17.0	**0.250**	0.606	1.03	UDL	0.8	PL	96.8	96.6	88.3	23.4	132.6	0.67	0.59	1.09
7	E	6.0	100	10.0	2.00	165	9.7	300	5.80	20.0	51.8	1.82	17.0	**0.333**	0.606	1.03	UDL	0.8	PL	96.8	112.5	103.6	23.4	132.6	0.82	0.73	1.09
8	E	6.0	100	10.0	2.50	165	9.7	300	5.80	20.0	51.8	1.82	17.0	**0.417**	0.606	1.03	UDL	0.8	PL	96.8	126.6	117.2	23.4	132.6	0.94	0.86	1.08
9	**F**	6.0	150	10.0	3.00	165	9.7	300	5.80	20.0	51.8	1.82	17.0	0.500	**0.909**	1.03	UDL	0.8	PL	96.8	244.8	227.7	23.4	227.7	1.08	1.00	1.08
10	**F**	6.0	200	10.0	3.00	165	9.7	300	5.80	20.0	51.8	1.82	17.0	0.500	**1.212**	1.03	UDL	0.8	PL	96.8	388.8	353.3	23.4	353.3	1.11	1.00	1.10
11	**F**	6.0	250	10.0	3.00	165	9.7	300	5.80	20.0	51.8	1.82	17.0	0.500	**1.515**	1.03	UDL	0.8	PL	96.8	596.5	528.5	23.4	528.5	1.13	1.00	1.13
12	**E**	6.0	150	10.0	1.00	165	9.7	300	5.80	20.0	51.8	1.82	17.0	0.167	**0.909**	1.03	UDL	0.8	PL	96.8	94.5	86.3	23.4	227.7	0.35	0.31	1.10
13	**E**	6.0	200	10.0	1.00	165	9.7	300	5.80	20.0	51.8	1.82	17.0	0.167	**1.212**	1.03	UDL	0.8	PL	96.8	100.7	92.3	23.4	353.3	0.23	0.21	1.09
14	**E**	6.0	250	10.0	1.00	165	9.7	300	5.80	20.0	51.8	1.82	17.0	0.167	**1.515**	1.03	UDL	0.8	PL	96.8	103.1	94.6	23.4	528.5	0.16	0.14	1.09
15	**I**	6.0	150	10.0	1.00	165	9.7	300	5.80	20.0	51.8	1.82	17.0	0.167	**0.909**	1.03	UDL	0.8	PL	96.8	87.0	78.6	23.4	227.7	0.31	0.27	1.11
16	**I**	6.0	200	10.0	1.00	165	9.7	300	5.80	20.0	51.8	1.82	17.0	0.167	**1.212**	1.03	UDL	0.8	PL	96.8	98.9	89.9	23.4	353.3	0.23	0.20	1.10
17	**I**	6.0	250	10.0	1.00	165	9.7	300	5.80	20.0	51.8	1.82	17.0	0.167	**1.515**	1.03	UDL	0.8	PL	96.8	106.0	96.3	23.4	528.5	0.16	0.14	1.10
18	**M**	6.0	150	10.0	1.00	165	9.7	300	5.80	20.0	51.8	1.82	17.0	0.167	**0.909**	1.03	UDL	0.8	PL	96.8	79.7	70.2	23.4	227.7	0.28	0.23	1.14
19	**M**	6.0	200	10.0	1.00	165	9.7	300	5.80	20.0	51.8	1.82	17.0	0.167	**1.212**	1.03	UDL	0.8	PL	96.8	116.8	102.7	23.4	353.3	0.28	0.24	1.14
20	**M**	6.0	250	10.0	1.00	165	9.7	300	5.80	20.0	51.8	1.82	17.0	0.167	**1.515**	1.03	UDL	0.8	PL	96.8	153.1	133.8	23.4	528.5	0.26	0.22	1.14

Table 4.6 Results of parametric study (Continued)

		Geometric Parameters								Dimensionless parameters							Loading			Critical moments (kNm)							
Run number	Configuration	L (m)	b_p (mm)	t_p (mm)	L_p (m)	b_f (mm)	t_f (mm)	h (mm)	t_w (mm)	L/h	h/t_w	h/b_f	b_f/t_f	L_p/L	b_p/b_f	t_p/t_f	Pre-strengthening	Ω	Post-strengthening	M_{uB}	M_{ip}	M_i	M_u	M_s	G_p	G_{np}	C_p
(1)	(2)	(3)	(4)	(5)	(6)	(7)	(8)	(9)	(10)	(11)	(12)	(13)	(14)	(15)	(16)	(17)	(18)	(19)	(20)	(21)	(22)	(23)	(24)	(25)	(26)	(27)	(28)
21	F	6.0	100	8.0	3.00	165	9.7	300	5.80	20.0	51.8	1.82	17.0	0.500	0.606	**0.82**	UDL	0.8	PL	96.8	113.3	104.6	23.4	104.6	1.11	1.00	1.08
22	F	6.0	100	12.0	3.00	165	9.7	300	5.80	20.0	51.8	1.82	17.0	0.500	0.606	**1.24**	UDL	0.8	PL	96.8	174.3	163.6	23.4	163.6	1.08	1.00	1.07
23	F	6.0	100	14.0	3.00	165	9.7	300	5.80	20.0	51.8	1.82	17.0	0.500	0.606	**1.44**	UDL	0.8	PL	96.8	209.0	197.3	23.4	197.3	1.07	1.00	1.06
24	E	6.0	100	8.0	1.00	165	9.7	300	5.80	20.0	51.8	1.82	17.0	0.167	0.606	**0.82**	UDL	0.8	PL	96.8	65.5	58.6	23.4	104.6	0.52	0.43	1.12
25	E	6.0	100	12.0	1.00	165	9.7	300	5.80	20.0	51.8	1.82	17.0	0.167	0.606	**1.24**	UDL	0.8	PL	96.8	90.5	82.6	23.4	163.6	0.48	0.42	1.10
26	E	6.0	100	14.0	1.00	165	9.7	300	5.80	20.0	51.8	1.82	17.0	0.167	0.606	**1.44**	UDL	0.8	PL	96.8	103.8	95.0	23.4	197.3	0.46	0.41	1.09
27	I	6.0	100	8.0	1.00	165	9.7	300	5.80	20.0	51.8	1.82	17.0	0.167	0.606	**0.82**	UDL	0.8	PL	96.8	56.6	50.2	23.4	104.6	0.41	0.33	1.13
28	I	6.0	100	12.0	1.00	165	9.7	300	5.80	20.0	51.8	1.82	17.0	0.167	0.606	**1.24**	UDL	0.8	PL	96.8	77.1	69.6	23.4	163.6	0.38	0.33	1.11
29	I	6.0	100	14.0	1.00	165	9.7	300	5.80	20.0	51.8	1.82	17.0	0.167	0.606	**1.44**	UDL	0.8	PL	96.8	88.2	80.3	23.4	197.3	0.37	0.33	1.10
30	M	6.0	100	8.0	1.00	165	9.7	300	5.80	20.0	51.8	1.82	17.0	0.167	0.606	**0.82**	UDL	0.8	PL	96.8	45.8	39.6	23.4	104.6	0.28	0.20	1.16
31	M	6.0	100	12.0	1.00	165	9.7	300	5.80	20.0	51.8	1.82	17.0	0.167	0.606	**1.24**	UDL	0.8	PL	96.8	54.7	47.9	23.4	163.6	0.22	0.17	1.14
32	M	6.0	100	14.0	1.00	165	9.7	300	5.80	20.0	51.8	1.82	17.0	0.167	0.606	**1.44**	UDL	0.8	PL	96.8	59.1	52.1	23.4	197.3	0.21	0.16	1.14
33	E	4.0	100	10.0	0.67	165	9.7	300	5.80	**13.3**	51.8	1.82	17.0	0.167	0.606	1.03	UDL	**0.0**	PL	184.6	296.6	283.7	221.5	380.5	0.47	0.39	1.05
34	E	4.0	100	10.0	0.67	165	9.7	300	5.80	**13.3**	51.8	1.82	17.0	0.167	0.606	1.03	UDL	**0.2**	PL	184.6	252.9	240.0	177.5	336.6	0.47	0.39	1.05
35	E	4.0	100	10.0	0.67	165	9.7	300	5.80	**13.3**	51.8	1.82	17.0	0.167	0.606	1.03	UDL	**0.4**	PL	184.6	209.1	196.1	133.4	292.6	0.48	0.39	1.07
36	E	4.0	100	10.0	0.67	165	9.7	300	5.80	**13.3**	51.8	1.82	17.0	0.167	0.606	1.03	UDL	**0.6**	PL	184.6	165.1	152.2	89.2	248.6	0.48	0.40	1.09
37	E	4.0	100	10.0	0.67	165	9.7	300	5.80	**13.3**	51.8	1.82	17.0	0.167	0.606	1.03	UDL	**0.8**	PL	184.6	121.0	108.1	44.8	204.4	0.48	0.40	1.12

Table 4.6 Results of parametric study (Continued)

		Geometric Parameters								Dimensionless parameters							Loading			Critical moments (kNm)							
Run number	Configuration	L (m)	b_p (mm)	t_p (mm)	L_p (m)	b_f (mm)	t_f (mm)	h (mm)	t_w (mm)	L/h	h/t_w	h/b_f	b_f/t_f	L_p/L	b_p/b_f	t_p/t_f	Pre-strengthening	Ω	Post-strengthening	M_{uB}	M_{ip}	M_i	M_u	M_s	G_p	G_{np}	C_p
(1)	(2)	(3)	(4)	(5)	(6)	(7)	(8)	(9)	(10)	(11)	(12)	(13)	(14)	(15)	(16)	(17)	(18)	(19)	(20)	(21)	(22)	(23)	(24)	(25)	(26)	(27)	(28)
38	E	5.0	100	10.0	0.83	165	9.7	300	5.80	**16.7**	51.8	1.82	17.0	0.167	0.606	1.03	UDL	**0.0**	PL	128.2	216.5	207.1	153.7	282.5	0.49	0.41	1.05
39	E	5.0	100	10.0	0.83	165	9.7	300	5.80	**16.7**	51.8	1.82	17.0	0.167	0.606	1.03	UDL	**0.2**	PL	128.2	186.2	176.8	123.2	252.0	0.49	0.42	1.05
40	E	5.0	100	10.0	0.83	165	9.7	300	5.80	**16.7**	51.8	1.82	17.0	0.167	0.606	1.03	UDL	**0.4**	PL	128.2	155.9	146.4	92.6	221.5	0.49	0.42	1.06
41	E	5.0	100	10.0	0.83	165	9.7	300	5.80	**16.7**	51.8	1.82	17.0	0.167	0.606	1.03	UDL	**0.6**	PL	128.2	125.4	116.0	61.9	191.0	0.49	0.42	1.08
42	E	5.0	100	10.0	0.83	165	9.7	300	5.80	**16.7**	51.8	1.82	17.0	0.167	0.606	1.03	UDL	**0.8**	PL	128.2	94.9	85.5	31.1	160.4	0.49	0.42	1.11
43	E	6.0	100	10.0	1.00	165	9.7	300	5.80	**20.0**	51.8	1.82	17.0	0.167	0.606	1.03	UDL	**0.0**	PL	96.8	169.3	162.0	116.1	224.8	0.49	0.42	1.05
44	E	6.0	100	10.0	1.00	165	9.7	300	5.80	**20.0**	51.8	1.82	17.0	0.167	0.606	1.03	UDL	**0.2**	PL	96.8	146.5	139.1	93.0	201.8	0.49	0.42	1.05
45	E	6.0	100	10.0	1.00	165	9.7	300	5.80	**20.0**	51.8	1.82	17.0	0.167	0.606	1.03	UDL	**0.4**	PL	96.8	123.6	116.2	69.9	178.8	0.49	0.43	1.06
46	E	6.0	100	10.0	1.00	165	9.7	300	5.80	**20.0**	51.8	1.82	17.0	0.167	0.606	1.03	UDL	**0.6**	PL	96.8	100.7	93.3	46.7	155.7	0.50	0.43	1.08
47	E	8.0	100	10.0	1.33	165	9.7	300	5.80	**26.6**	51.8	1.82	17.0	0.167	0.606	1.03	UDL	**0.0**	PL	64.3	116.6	111.5	77.0	160.2	0.48	0.41	1.05
48	E	8.0	100	10.0	1.33	165	9.7	300	5.80	**26.6**	51.8	1.82	17.0	0.167	0.606	1.03	UDL	**0.2**	PL	64.3	101.5	96.4	61.7	145.0	0.48	0.42	1.05
49	E	8.0	100	10.0	1.33	165	9.7	300	5.80	**26.6**	51.8	1.82	17.0	0.167	0.606	1.03	UDL	**0.4**	PL	64.3	86.4	81.3	46.4	129.7	0.48	0.42	1.06
50	E	8.0	100	10.0	1.33	165	9.7	300	5.80	**26.6**	51.8	1.82	17.0	0.167	0.606	1.03	UDL	**0.6**	PL	64.3	71.3	66.1	31.0	114.4	0.48	0.42	1.08
51	E	8.0	100	10.0	1.33	165	9.7	300	5.80	**26.6**	51.8	1.82	17.0	0.167	0.606	1.03	UDL	**0.8**	PL	64.3	56.0	50.9	15.5	99.1	0.48	0.42	1.10
52	E	6.0	100	10.0	1.00	165	9.7	300	10.0	20.0	**30.0**	1.82	17.0	0.167	0.606	1.03	UDL	**0.0**	PL	112.3	182.7	175.6	134.5	237.2	0.47	0.40	1.04
53	E	6.0	100	10.0	1.00	165	9.7	300	10.0	20.0	**30.0**	1.82	17.0	0.167	0.606	1.03	UDL	**0.2**	PL	112.3	156.3	149.1	107.8	210.5	0.47	0.40	1.05
54	E	6.0	100	10.0	1.00	165	9.7	300	10.0	20.0	**30.0**	1.82	17.0	0.167	0.606	1.03	UDL	**0.4**	PL	112.3	129.8	122.6	81.0	183.8	0.47	0.40	1.06
55	E	6.0	100	10.0	1.00	165	9.7	300	10.0	20.0	**30.0**	1.82	17.0	0.167	0.606	1.03	UDL	**0.6**	PL	112.3	103.1	95.9	54.1	157.1	0.48	0.41	1.07
56	E	6.0	100	10.0	1.00	165	9.7	300	10.0	20.0	**30.0**	1.82	17.0	0.167	0.606	1.03	UDL	**0.8**	PL	112.3	76.5	69.3	27.1	130.2	0.48	0.41	1.10

Table 4.6 Results of parametric study (Continued)

		Geometric Parameters								Dimensionless parameters							Loading			Critical moments (kNm)							
(1) Run number	(2) Configuration	(3) L (m)	(4) b_p (mm)	(5) t_p (mm)	(6) L_p (m)	(7) b_f (mm)	(8) t_f (mm)	(9) h (mm)	(10) t_w (mm)	(11) L/h	(12) h/t_w	(13) h/b_f	(14) b_f/t_f	(15) L_p/L	(16) b_p/b_f	(17) t_p/t_f	(18) Pre-strengthening	(19) Ω	(20) Post-strengthening	(21) M_{uB}	(22) M_{ip}	(23) M_i	(24) M_u	(25) M_s	(26) G_p	(27) G_{np}	(28) C_p
57	E	6.0	100	10.0	1.00	165	9.7	300	9.00	20.0	**33.4**	1.82	17.0	0.167	0.606	1.03	UDL	**0.0**	PL	107.3	178.3	171.1	128.6	233.1	0.48	0.41	1.04
58	E	6.0	100	10.0	1.00	165	9.7	300	9.00	20.0	**33.4**	1.82	17.0	0.167	0.606	1.03	UDL	**0.2**	PL	107.3	153.0	145.8	103.1	207.6	0.48	0.41	1.05
59	E	6.0	100	10.0	1.00	165	9.7	300	9.00	20.0	**33.4**	1.82	17.0	0.167	0.606	1.03	UDL	**0.4**	PL	107.3	127.7	120.4	77.4	182.1	0.48	0.41	1.06
60	E	6.0	100	10.0	1.00	165	9.7	300	9.00	20.0	**33.4**	1.82	17.0	0.167	0.606	1.03	UDL	**0.6**	PL	107.3	102.3	95.0	51.7	156.5	0.48	0.41	1.08
61	E	6.0	100	10.0	1.00	165	9.7	300	9.00	20.0	**33.4**	1.82	17.0	0.167	0.606	1.03	UDL	**0.8**	PL	107.3	76.7	69.5	26.0	130.9	0.48	0.42	1.10
62	E	6.0	100	10.0	1.00	165	9.7	300	8.00	20.0	**37.5**	1.82	17.0	0.167	0.606	1.03	UDL	**0.0**	PL	103.2	174.6	167.5	123.7	229.8	0.48	0.41	1.04
63	E	6.0	100	10.0	1.00	165	9.7	300	8.00	20.0	**37.5**	1.82	17.0	0.167	0.606	1.03	UDL	**0.2**	PL	103.2	150.3	143.1	99.1	205.3	0.48	0.41	1.05
64	E	6.0	100	10.0	1.00	165	9.7	300	8.00	20.0	**37.5**	1.82	17.0	0.167	0.606	1.03	UDL	**0.4**	PL	103.2	125.9	118.7	74.5	180.7	0.48	0.42	1.06
65	E	6.0	100	10.0	1.00	165	9.7	300	8.00	20.0	**37.5**	1.82	17.0	0.167	0.606	1.03	UDL	**0.6**	PL	103.2	101.6	94.3	49.8	156.1	0.49	0.42	1.08
66	E	6.0	100	10.0	1.00	165	9.7	300	8.00	20.0	**37.5**	1.82	17.0	0.167	0.606	1.03	UDL	**0.8**	PL	103.2	77.0	69.8	25.0	131.5	0.49	0.42	1.10
67	E	6.0	100	10.0	1.00	165	9.7	300	7.00	20.0	**42.9**	1.82	17.0	0.167	0.606	1.03	UDL	**0.0**	PL	99.8	171.8	164.5	119.7	227.1	0.49	0.42	1.04
68	E	6.0	100	10.0	1.00	165	9.7	300	7.00	20.0	**42.9**	1.82	17.0	0.167	0.606	1.03	UDL	**0.2**	PL	99.8	148.2	141.0	95.9	203.4	0.49	0.42	1.05
69	E	6.0	100	10.0	1.00	165	9.7	300	7.00	20.0	**42.9**	1.82	17.0	0.167	0.606	1.03	UDL	**0.4**	PL	99.8	124.7	117.4	72.1	179.7	0.49	0.42	1.06
70	E	6.0	100	10.0	1.00	165	9.7	300	7.00	20.0	**42.9**	1.82	17.0	0.167	0.606	1.03	UDL	**0.6**	PL	99.8	101.1	93.7	48.2	155.9	0.49	0.42	1.08
71	E	6.0	100	10.0	1.00	165	9.7	300	7.00	20.0	**42.9**	1.82	17.0	0.167	0.606	1.03	UDL	**0.8**	PL	99.8	77.3	70.0	24.2	132.1	0.49	0.43	1.10
72	E	6.0	100	10.0	1.00	165	9.7	300	5.80	20.0	**51.8**	1.82	17.0	0.167	0.606	1.03	UDL	**0.0**	PL	96.8	169.3	162.0	116.1	224.8	0.49	0.42	1.05
73	E	6.0	100	10.0	1.00	165	9.7	300	5.80	20.0	**51.8**	1.82	17.0	0.167	0.606	1.03	UDL	**0.2**	PL	96.8	146.5	139.1	93.0	201.8	0.49	0.42	1.05
74	E	6.0	100	10.0	1.00	165	9.7	300	5.80	20.0	**51.8**	1.82	17.0	0.167	0.606	1.03	UDL	**0.4**	PL	96.8	123.6	116.2	69.9	178.8	0.49	0.43	1.06
75	E	6.0	100	10.0	1.00	165	9.7	300	5.80	20.0	**51.8**	1.82	17.0	0.167	0.606	1.03	UDL	**0.6**	PL	96.8	100.7	93.3	46.7	155.7	0.50	0.43	1.08

Table 4.6 Results of parametric study (Continued)

		Geometric Parameters								Dimensionless parameters							Loading			Critical moments (kNm)							
Run number	Configuration	L (m)	b_p (mm)	t_p (mm)	L_p (m)	b_f (mm)	t_f (mm)	h (mm)	t_w (mm)	L/h	h/t_w	h/b_f	b_f/t_f	L_p/L	b_p/b_f	t_p/t_f	Pre-strengthening	Ω	Post-strengthening	M_{uB}	M_{ip}	M_i	M_u	M_s	G_p	G_{np}	C_p
(1)	(2)	(3)	(4)	(5)	(6)	(7)	(8)	(9)	(10)	(11)	(12)	(13)	(14)	(15)	(16)	(17)	(18)	(19)	(20)	(21)	(22)	(23)	(24)	(25)	(26)	(27)	(28)
76	E	4.4	100	10.0	0.73	165	9.7	220	4.25	20.0	51.8	**1.33**	17.0	0.167	0.606	1.03	UDL	**0.0**	PL	128.2	239.1	217.7	153.7	304.9	0.56	0.42	1.10
77	E	4.4	100	10.0	0.73	165	9.7	220	4.25	20.0	51.8	**1.33**	17.0	0.167	0.606	1.03	UDL	**0.2**	PL	128.2	209.1	187.5	123.2	274.5	0.57	0.43	1.12
78	E	4.4	100	10.0	0.73	165	9.7	220	4.25	20.0	51.8	**1.33**	17.0	0.167	0.606	1.03	UDL	**0.4**	PL	128.2	178.6	157.2	92.6	244.0	0.57	0.43	1.14
79	E	4.4	100	10.0	0.73	165	9.7	220	4.25	20.0	51.8	**1.33**	17.0	0.167	0.606	1.03	UDL	**0.6**	PL	128.2	148.2	126.8	61.9	213.4	0.57	0.43	1.17
80	E	4.4	100	10.0	0.73	165	9.7	220	4.25	20.0	51.8	**1.33**	17.0	0.167	0.606	1.03	UDL	**0.8**	PL	128.2	117.9	96.4	31.0	182.8	0.57	0.43	1.22
81	E	6.0	100	10.0	1.00	165	9.7	300	5.80	20.0	51.8	**1.82**	17.0	0.167	0.606	1.03	UDL	**0.0**	PL	96.8	169.3	162.0	116.1	224.8	0.49	0.42	1.05
82	E	6.0	100	10.0	1.00	165	9.7	300	5.80	20.0	51.8	**1.82**	17.0	0.167	0.606	1.03	UDL	**0.2**	PL	96.8	146.5	139.1	93.0	201.8	0.49	0.42	1.05
83	E	6.0	100	10.0	1.00	165	9.7	300	5.80	20.0	51.8	**1.82**	17.0	0.167	0.606	1.03	UDL	**0.4**	PL	96.8	123.6	116.2	69.9	178.8	0.49	0.43	1.06
84	E	6.0	100	10.0	1.00	165	9.7	300	5.80	20.0	51.8	**1.82**	17.0	0.167	0.606	1.03	UDL	**0.6**	PL	96.8	100.7	93.3	46.7	155.7	0.50	0.43	1.08
85	E	7.0	100	10.0	1.17	165	9.7	350	6.76	20.0	51.8	**2.12**	17.0	0.167	0.606	1.03	UDL	**0.0**	PL	85.9	145.8	141.4	103.0	194.9	0.47	0.42	1.03
86	E	7.0	100	10.0	1.17	165	9.7	350	6.76	20.0	51.8	**2.12**	17.0	0.167	0.606	1.03	UDL	**0.2**	PL	85.9	125.6	121.2	82.6	174.5	0.47	0.42	1.04
87	E	7.0	100	10.0	1.17	165	9.7	350	6.76	20.0	51.8	**2.12**	17.0	0.167	0.606	1.03	UDL	**0.4**	PL	85.9	105.2	100.8	62.1	154.0	0.47	0.42	1.04
88	E	7.0	100	10.0	1.17	165	9.7	350	6.76	20.0	51.8	**2.12**	17.0	0.167	0.606	1.03	UDL	**0.6**	PL	85.9	85.0	80.5	41.5	133.5	0.47	0.42	1.06
89	E	7.0	100	10.0	1.17	165	9.7	350	6.76	20.0	51.8	**2.12**	17.0	0.167	0.606	1.03	UDL	**0.8**	PL	85.9	64.4	60.1	20.8	113.0	0.47	0.43	1.07
90	E	8.0	100	10.0	1.33	165	9.7	400	7.73	20.0	51.8	**2.42**	17.0	0.167	0.606	1.03	UDL	**0.0**	PL	78.9	129.8	127.0	94.6	173.3	0.45	0.41	1.02
91	E	8.0	100	10.0	1.33	165	9.7	400	7.73	20.0	51.8	**2.42**	17.0	0.167	0.606	1.03	UDL	**0.2**	PL	78.9	111.2	108.4	75.8	154.6	0.45	0.41	1.03
92	E	8.0	100	10.0	1.33	165	9.7	400	7.73	20.0	51.8	**2.42**	17.0	0.167	0.606	1.03	UDL	**0.4**	PL	78.9	92.6	89.7	57.0	135.8	0.45	0.42	1.03
93	E	8.0	100	10.0	1.33	165	9.7	400	7.73	20.0	51.8	**2.42**	17.0	0.167	0.606	1.03	UDL	**0.6**	PL	78.9	73.9	71.0	38.1	117.0	0.45	0.42	1.04
94	E	8.0	100	10.0	1.33	165	9.7	400	7.73	20.0	51.8	**2.42**	17.0	0.167	0.606	1.03	UDL	**0.8**	PL	78.9	55.1	52.3	19.1	98.1	0.46	0.42	1.05

Table 4.6 Results of parametric study (Continued)

		Geometric Parameters								Dimensionless parameters							Loading			Critical moments (kNm)							
Run number	Configuration	L (m)	b_p (mm)	t_p (mm)	L_p (m)	b_f (mm)	t_f (mm)	h (mm)	t_w (mm)	L/h	h/t_w	h/b_f	b_f/t_f	L_p/L	b_p/b_f	t_p/t_f	Pre-strengthening	Ω	Post-strengthening	M_{uB}	M_{ip}	M_i	M_u	M_s	G_p	G_{np}	C_p
(1)	(2)	(3)	(4)	(5)	(6)	(7)	(8)	(9)	(10)	(11)	(12)	(13)	(14)	(15)	(16)	(17)	(18)	(19)	(20)	(21)	(22)	(23)	(24)	(25)	(26)	(27)	(28)
95	E	6.0	100	20.6	1.00	165	20	300	5.80	20.0	51.8	1.82	**8.3**	0.167	0.606	1.03	UDL	**0.0**	PL	305.2	576.7	549.5	365.1	860.0	0.43	0.37	1.05
96	E	6.0	100	20.6	1.00	165	20	300	5.80	20.0	51.8	1.82	**8.3**	0.167	0.606	1.03	UDL	**0.2**	PL	305.2	505.7	478.4	292.5	787.8	0.43	0.38	1.06
97	E	6.0	100	20.6	1.00	165	20	300	5.80	20.0	51.8	1.82	**8.3**	0.167	0.606	1.03	UDL	**0.4**	PL	305.2	434.4	407.1	219.8	715.4	0.43	0.38	1.07
98	E	6.0	100	20.6	1.00	165	20	300	5.80	20.0	51.8	1.82	**8.3**	0.167	0.606	1.03	UDL	**0.6**	PL	305.2	363.0	335.7	146.8	642.9	0.44	0.38	1.08
99	E	6.0	100	20.6	1.00	165	20	300	5.80	20.0	51.8	1.82	**8.3**	0.167	0.606	1.03	UDL	**0.8**	PL	305.2	291.6	264.2	73.5	570.3	0.44	0.38	1.10
100	E	6.0	100	16.5	1.00	165	16	300	5.80	20.0	51.8	1.82	**10.3**	0.167	0.606	1.03	UDL	**0.0**	PL	208.1	392.2	374.0	249.2	561.5	0.46	0.40	1.05
101	E	6.0	100	16.5	1.00	165	16	300	5.80	20.0	51.8	1.82	**10.3**	0.167	0.606	1.03	UDL	**0.2**	PL	208.1	343.6	325.3	199.7	512.2	0.46	0.40	1.06
102	E	6.0	100	16.5	1.00	165	16	300	5.80	20.0	51.8	1.82	**10.3**	0.167	0.606	1.03	UDL	**0.4**	PL	208.1	294.8	276.6	150.0	462.8	0.46	0.40	1.07
103	E	6.0	100	16.5	1.00	165	16	300	5.80	20.0	51.8	1.82	**10.3**	0.167	0.606	1.03	UDL	**0.6**	PL	208.1	245.9	227.7	100.2	413.4	0.47	0.41	1.08
104	E	6.0	100	16.5	1.00	165	16	300	5.80	20.0	51.8	1.82	**10.3**	0.167	0.606	1.03	UDL	**0.8**	PL	208.1	197.0	178.7	50.2	363.8	0.47	0.41	1.10
105	E	6.0	100	12.4	1.00	165	12	300	5.80	20.0	51.8	1.82	**13.8**	0.167	0.606	1.03	UDL	**0.0**	PL	131.7	240.6	229.8	157.8	328.9	0.48	0.42	1.05
106	E	6.0	100	12.4	1.00	165	12	300	5.80	20.0	51.8	1.82	**13.8**	0.167	0.606	1.03	UDL	**0.2**	PL	131.7	209.6	198.8	126.5	297.6	0.49	0.42	1.05
107	E	6.0	100	12.4	1.00	165	12	300	5.80	20.0	51.8	1.82	**13.8**	0.167	0.606	1.03	UDL	**0.4**	PL	131.7	178.6	167.8	95.1	266.3	0.49	0.42	1.06
108	E	6.0	100	12.4	1.00	165	12	300	5.80	20.0	51.8	1.82	**13.8**	0.167	0.606	1.03	UDL	**0.6**	PL	131.7	147.5	136.7	63.5	234.9	0.49	0.43	1.08
109	E	6.0	100	12.4	1.00	165	12	300	5.80	20.0	51.8	1.82	**13.8**	0.167	0.606	1.03	UDL	**0.8**	PL	131.7	116.4	105.5	31.9	203.5	0.49	0.43	1.10
110	E	6.0	100	10.0	1.00	165	9.7	300	5.80	20.0	51.8	1.82	**17.0**	0.167	0.606	1.03	UDL	**0.0**	PL	96.8	169.3	162.0	116.1	224.8	0.49	0.42	1.05
111	E	6.0	100	10.0	1.00	165	9.7	300	5.80	20.0	51.8	1.82	**17.0**	0.167	0.606	1.03	UDL	**0.2**	PL	96.8	146.5	139.1	93.0	201.8	0.49	0.42	1.05
112	E	6.0	100	10.0	1.00	165	9.7	300	5.80	20.0	51.8	1.82	**17.0**	0.167	0.606	1.03	UDL	**0.4**	PL	96.8	123.6	116.2	69.9	178.8	0.49	0.43	1.06
113	E	6.0	100	10.0	1.00	165	9.7	300	5.80	20.0	51.8	1.82	**17.0**	0.167	0.606	1.03	UDL	**0.6**	PL	96.8	100.7	93.3	46.7	155.7	0.50	0.43	1.08

Table 4.6 Results of parametric study (Continued)

		Geometric Parameters								Dimensionless parameters							Loading			Critical moments (kNm)							
Run number	Configuration	L (m)	b_p (mm)	t_p (mm)	L_p (m)	b_f (mm)	t_f (mm)	h (mm)	t_w (mm)	L/h	h/t_w	h/b_f	b_f/t_f	L_p/L	b_p/b_f	t_p/t_f	Pre-strengthening	Ω	Post-strengthening	M_{uB}	M_{ip}	M_i	M_u	M_s	G_p	G_{np}	C_p
(1)	(2)	(3)	(4)	(5)	(6)	(7)	(8)	(9)	(10)	(11)	(12)	(13)	(14)	(15)	(16)	(17)	(18)	(19)	(20)	(21)	(22)	(23)	(24)	(25)	(26)	(27)	(28)
114	E	6.0	100	8.25	1.00	165	8.0	300	5.80	20.0	51.8	1.82	**20.6**	0.167	0.606	1.03	UDL	**0.0**	PL	75.0	124.8	119.5	89.9	161.8	0.48	0.41	1.04
115	E	6.0	100	8.25	1.00	165	8.0	300	5.80	20.0	51.8	1.82	**20.6**	0.167	0.606	1.03	UDL	**0.2**	PL	75.0	107.0	101.8	72.1	144.0	0.49	0.41	1.05
116	E	6.0	100	8.25	1.00	165	8.0	300	5.80	20.0	51.8	1.82	**20.6**	0.167	0.606	1.03	UDL	**0.4**	PL	75.0	89.3	84.0	54.2	126.1	0.49	0.41	1.06
117	E	6.0	100	8.25	1.00	165	8.0	300	5.80	20.0	51.8	1.82	**20.6**	0.167	0.606	1.03	UDL	**0.6**	PL	75.0	71.5	66.2	36.2	108.2	0.49	0.42	1.08
118	E	6.0	100	8.25	1.00	165	8.0	300	5.80	20.0	51.8	1.82	**20.6**	0.167	0.606	1.03	UDL	**0.8**	PL	75.0	53.6	48.3	18.2	90.3	0.49	0.42	1.11
119	E	6.0	100	10.0	1.00	165	9.7	300	5.80	20.0	51.8	1.82	17.0	0.167	0.606	1.03	**UDL**	0.8	**UDL**	96.8	65.2	58.9	19.4	110.4	0.50	0.43	1.11
120	E	6.0	100	10.0	1.00	165	9.7	300	5.80	20.0	51.8	1.82	17.0	0.167	0.606	1.03	**PL**	0.8	**UDL**	112.1	67.4	61.1	22.2	113.3	0.50	0.43	1.10
121	E	6.0	100	10.0	1.00	165	9.7	300	5.80	20.0	51.8	1.82	17.0	0.167	0.606	1.03	**PL**	0.8	**PL**	112.1	80.1	72.3	26.4	135.1	0.49	0.42	1.11

[a] F: Full strengthening

[b] E: End strengthening

[c] I: Intermediate strengthening

[d] M: Midspan strengthening

4.17 References

Abaqus (2020). Abaqus/CAE user's manual, Dassault Systemes.

Andrade, A. and D. Camotim (2004). "Lateral-torsional buckling of prismatic and tapered thin-walled open beams: assessing the influence of pre-buckling deflections." Steel and Composite Structures **4**(4): 281-301.

ANSI/AISC360 (2016). "Specification for structural steel buildings (ANSI/AISC 360-16)." American Institute of Steel Construction, Chicago-Illinois.

ANSI/AISC360 (2022). "Specification for structural steel buildings (ANSI/AISC 360-22)." American Institute of Steel Construction, Chicago-Illinois.

Arizou, R. and M. Mohareb (2021). "Design Considerations for Distortional Lateral Buckling." Journal of Structural Engineering **147**(12): 04021203.

Arizou, R. and M. Mohareb (2022). "Finite element formulation for distortional lateral buckling of I-beams." Engineering Structures **In press**.

Barsoum, R. S. and R. H. Gallagher (1970). "Finite element analysis of torsional and torsional–flexural stability problems." International J. for Numerical Methods in Engineering **2**(3): 335-352.

CAN/CSA-S16 (2019). "CSA S16: 19, Design of Steel Structures, Toronto, Canada." Canadian Standards Association.

Erkmen, R. E. and M. M. Attard (2011). "Lateral–torsional buckling analysis of thin-walled beams including shear and pre-buckling deformation effects." International journal of mechanical sciences **53**(10): 918-925.

Gellin, S. and G. C. Lee (1988). "Finite elements available for the analysis of non-curved thin-walled structures." Finite element analysis of thin-walled structures: 1-30.

Gjelsvik, A. (1981). The theory of thin-walled bars. New York, John Wiley & Sons publishing Inc.

Hsu, W. T., D. M. Lue and Y. F. Chen (2012). "Design aid for moment strength of built-up crane runway girders." International Journal of Steel Structures **12**(3): 403-417.

Hsu, W. T., D. M. Lue and B. T. Hsiao (2009). "Numerical approach for torsion properties of built-up runway girders." Journal of Applied Science and Engineering **12**(4): 381-389.

Iranpour, A. and M. Mohareb (2022). Elastic Lateral Torsional Buckling Resistance for Continuous Beams Using Artificial Neural Networks. CSCE 2022 Annual Conference, Whistler, British Columbia, Canada.

Liu, Y. and L. Gannon (2009a). "Experimental behavior and strength of steel beams strengthened while under load." Journal of Constructional Steel Research **65**(6): 1346-1354.

Liu, Y. and L. Gannon (2009b). "Finite element study of steel beams reinforced while under load." Engineering Structures **31**(11): 2630-2642.

MacCrimmon, R. (2009). Guide for the Design of Crane-Supporting Steel Structures, Markham, ON, CA.

Machado, S. P. and V. H. Cortínez (2005). "Lateral buckling of thin-walled composite bisymmetric beams with prebuckling and shear deformation." Engineering Structures **27**(8): 1185-1196.

Mohri, F., N. Damil and M. Potier-Ferry (2012). "Pre-buckling deflection effects on stability of thin-walled beams with open sections." Steel & Composite Structures **13**(1): 71-89.

Mohri, F. and M. Potier-Ferry (2006). "Effects of load height application and pre-buckling deflections on lateral buckling of thin-walled beams." Steel and composite structures **6**(5): 401.

Pezeshky, P. and M. Mohareb (2018). "Distortional lateral torsional buckling of beam-columns including pre-buckling deformation effects." Computers & Structures **209**: 93-116.

Pezeshky, P., A. Sahraei, F. Rong, S. Sasibut and M. Mohareb (2020). "Generalization of the Vlasov theory for lateral torsional buckling analysis of built-up monosymmetric assemblies." Engineering Structures **221**: 111055.

Pham, P. V., M. Mohareb and A. Fam (2017). "Elastic Analysis of Steel Beams Strengthened with GFRP Plates Including Preexisting Loading Effects." Journal of Structural Engineering **143**(12): 04017163.

Pi, Y. L. and N. Trahair (1992a). "Prebuckling deflections and lateral buckling. I: theory." Journal of structural engineering **118**(11): 2949-2966.

Pi, Y. L. and N. Trahair (1992b). "Prebuckling deflections and lateral buckling. II: applications." Journal of Structural Engineering **118**(11): 2967-2985.

Pi, Y. L., N. Trahair and S. Rajasekaran (1992). "Energy equation for beam lateral buckling." Journal of structural engineering **118**(6): 1462-1479.

Reichenbach, M. C., Y. Liu, T. A. Helwig and M. D. Engelhardt (2020). "Lateral-Torsional Buckling of Singly Symmetric I-Girders with Stepped Flanges." Journal of Structural Engineering **146**(10): 04020203.

Roberts, T. M. and Z. G. Azizian (1983). "Instability of thin walled bars." Journal of Engineering Mechanics **109**(3): 781-794.

Sahraei, A., P. Pezeshky and M. Mohareb (2017). Lateral torsional buckling analysis and design of steel beams with continuous spans. Canadian Society for Civil Engineering (CSCE), Vancouver BC, Canada, Proceedings of the 6th international conference on engineering mechanics and materials.

Sahraei, A., P. Pezeshky, M. Mohareb and G. Doudak (2018). "Simplified expressions for elastic lateral torsional buckling of wooden beams." Engineering Structures **174**: 229-241.

Trahair, N. (1993). Flexural-torsional buckling of structures, CRC press.

Trahair, N. S. and S. T. Woolcock (1973). "Effect of major axis curvature on I-beam stability." Journal of the Engineering Mechanics Division **99**(1): 85-98.

Vacharajittiphan, P., S. Woolcock and N. S. Trahair (1974). "Effect of in-plane deformation on lateral buckling." Journal of Structural Mechanics **3**(1): 29-60.

Vlasov, V. (1961). Thin-Walled Elastic Beams. Jerusalem, Israel, Israel Program for Scientific Translations.

Wang, Y.-q., L. Zong, R.-x. Zhu, X.-y. Liu and Y.-j. Shi (2015). "Behavior of I-section steel beam welding reinforced while under load." Journal of Constructional Steel Research **106**: 278-288.

Wu, L. and M. Mohareb (2011). "Buckling of shear deformable thin-walled members—I. Variational principle and analyticalsolutions." Thin-walled structures **49**(1): 197-207.

Chapter 5: Simplified Design Approach for Strengthened Doubly Symmetric Beams[1]

Abstract

Starting from a recently developed variational principle for the lateral torsional buckling analysis of steel I-beams strengthened with cover plates, the present study formulates an energy-based solution that quantifies the lateral torsional buckling resistance of simply supported strengthened I-beams. The solution captures the detrimental effect of loads that may act on the beam prior to strengthening through an interaction relation combining the pre-strengthening and post-strengthening peak moments. Additionally, it captures the effects of moment gradient and load height for pre- and post-strengthening loads, as well as pre-buckling deformation effects through a series of design-oriented coefficients. A systematic comparison of the solution to finite element analysis (FEA) predictions demonstrates its accuracy for a wide range of cross-sections, strengthening plate geometries, spans, pre- and post-strengthening load distributions and load heights. The use of the proposed solution in typical strengthening design scenarios is illustrated through two examples. The simplicity of the solution compared to the FEA, the universality implied by its dimensionless format, and its predictive accuracy make it attractive in a design environment.

Keywords: Lateral torsional buckling, Strengthened beams, I-beams, Cover plates, Design procedure, Moment gradient, Load height, Pre-buckling deformation, Pre-strengthening loads

[1] This chapter has been publication as: Iranpour, A. and M. Mohareb (2023). "Design Expressions for Elastic Lateral Torsional Buckling Capacity of I-Beams Strengthened While under Loading." Journal of Structural Engineering, **149**(7): 04023078.

5.1 Introduction

The reuse of existing structures to carry additional loads is an integral part of achieving sustainable construction. Strengthening techniques are thus becoming an important requirement to prolong the lifetime of existing structures expected to withstand increasing operating loads. A common means to strengthen existing steel I-beams is to weld cover plates to both flanges. In many cases, the beam cannot be fully unloaded before strengthening, forcing the operators to strengthen beams while under loading. Determining the lateral torsional buckling (LTB) capacity in such situations, becomes a challenging undertaking requiring careful finite element (FE) modelling of the entire sequence of pre-strengthening load application, strengthening process, post-strengthening load application, up to the attainment of the point of onset of buckling for the strengthened system. Within this context, the present study develops design-oriented equations and procedures that reliably quantify the LTB resistance of strengthened steel I-beams while accounting for the interaction between pre-strengthening and post-strengthening loads, moment gradient, load height, and Pre-Buckling Deformation (PBD) effects.

5.2 Literature review

Studies on the LTB of strengthened beams include the work of MacCrimmon (2009) who investigated the LTB of built-up crane runway beams. Hsu et al. (2009 and 2012) focused on I-beams strengthened with open-side down channels over the top flange. Pezeshky et al. (2020) developed an LTB solution for I-sections strengthened with other cross-sections to form monosymmetric assemblies. Reichenbach et al. (2020) and Slein et al. (2022) investigated the elastic LTB capacity of beams with stepped flanges. The preceding studies did not account for the effect of loads that may act on the member prior to strengthening. Also, steel design standards (e.g., ANSI/AISC360 2022[1], CAN/CSA-S16 2019 and AS-4100 2020) are not intended for beams that are strengthened while under load. In this respect, Pham et al. (2017) analytically investigated the effect of pre-strengthening loads on the elastic response of flexural members. However, the study did not investigate the LTB mode of failure. Liu and Gannon (2009b) and Wang et al. (2015) experimentally and numerically investigated the LTB capacity of I-beams strengthened while under load. Iranpour and Mohareb (2022) proposed a simple approach to estimate the LTB resistance of I-beams strengthened with cover plates that accounts for the effect of pre-strengthening loads acting on the beams. The solution is limited for cases where pre- and post-strengthening loads have similar distributions and does not capture the PBD and load height effects. To overcome these limitations, Iranpour and Mohareb (2023a) formulated a variational principle and FE formulation for the LTB analysis of beams strengthened while under loads. Although the FEA solution was shown to be accurate, it may be impractical to use in a design environment. To overcome this limitation, starting with the variational principle in Iranpour and Mohareb (2023a), the present study aims to develop energy-based design-oriented solutions to characterize the LTB strength of beams that are strengthened under loads. The solution captures the interaction between pre-strengthening and post-strengthening loads, moment gradient, load height, and PBD effects.

Past energy-based approximate solutions have resulted in expressions for moment gradient coefficients that account for non-uniform moment distribution along the span [e.g., Kitipornchai et al. 1986, Sahraei et al. 2018 and Bresser et al. 2020], load height coefficients that account for the destabilizing effect induced by transverse loads that are offset from the shear centre [e.g., Mohri

[1] The original publication cited ANSI/AISC 360 (2016). Following the release of the updated version ANSI/AISC 360 (2022), a comparison was conducted between the two editions, revealing identical lateral torsional buckling provisions. As a result, the citation has been updated to reflect the latest edition.

and Potier-Ferry 2006, Sahraei et al. 2018], and PBD coefficients that capture the effect of in-plane transverse curvature of flexural members prior to buckling. Energy-based coefficients that capture the PBD effects include the work of Trahair and Woolcock (1973), Vacharajittiphan et al. (1974), Roberts and Azizian (1983), Pi and Trahair (1992b), Andrade and Camotim (2004) and Machado and Cortínez (2005) while comprehensive reviews of other numerical investigations related to the PBD effect are provided in Pezeshky and Mohareb (2018) and Iranpour and Mohareb (2023a).

5.3 Statement of the problem

A prismatic beam of span L with an I-section is simply supported relative to the transverse and lateral displacements and twist. The beam is subjected to transverse loads $q_a(z)$ (subsequently denoted by pre-strengthening loads) under which it undergoes a transverse displacement $V_a(z)$ (Step a in Fig. 5.1). While under loading, the beam is to be strengthened with two identical plates welded to both flanges. The gap $V_g(z)$ between the straight plates and the sagging beam requires both surfaces to be brought into perfect contact prior to welding. This is achieved by clamping the plates to the beam through multiple clamps along the span. As the clamps are tightened, they close the gap between the strengthening plates and the beam (e.g., the top plate moves downwards while the top of the beam moves slightly upwards) until the gap $V_g(z)$ is completely eliminated. Welding is then performed and the clamps are removed subsequently. As a simplification, the variational principle developed in (Iranpour and Mohareb 2023a) simulated the process in three steps: (1) applying temporary loads $q_t(z)$ on the plates until they come into contact with the flanges along the span, (2) holding the strengthening plates and the beam flanges together along the normal direction but enabling them to slide along the tangential direction, and (3) removing the temporary loads, thus enabling the system to rebound while undergoing displacement $V_r(z)$. The latter sequence is expected to yield the same rebound displacement as that of the original scenario. Additional loads $q_b(z)$ (subsequently denoted by post-strengthening loads) are then applied to the strengthened system under which the beam undergoes an additional transverse displacement $V_b(z)$ (Step b). The post-strengthening loads are increased to $\lambda q_b(z)$ at which the beam attains the state of onset of buckling. Under the post-strengthening load $\lambda q_b(z)$, the beam undergoes a transverse displacement $\lambda V_b(z)$. At the onset of buckling, the beam has a tendency to buckle in a lateral torsional mode characterized by lateral displacement $U(z)$ and an angle of twist $\theta(z)$ without an increase in the load $q_a(z)+\lambda q_b(z)$. It is required to develop solutions to predict the elastic critical moment of the strengthened system which reliably capture the effect of pre-strengthening loading.

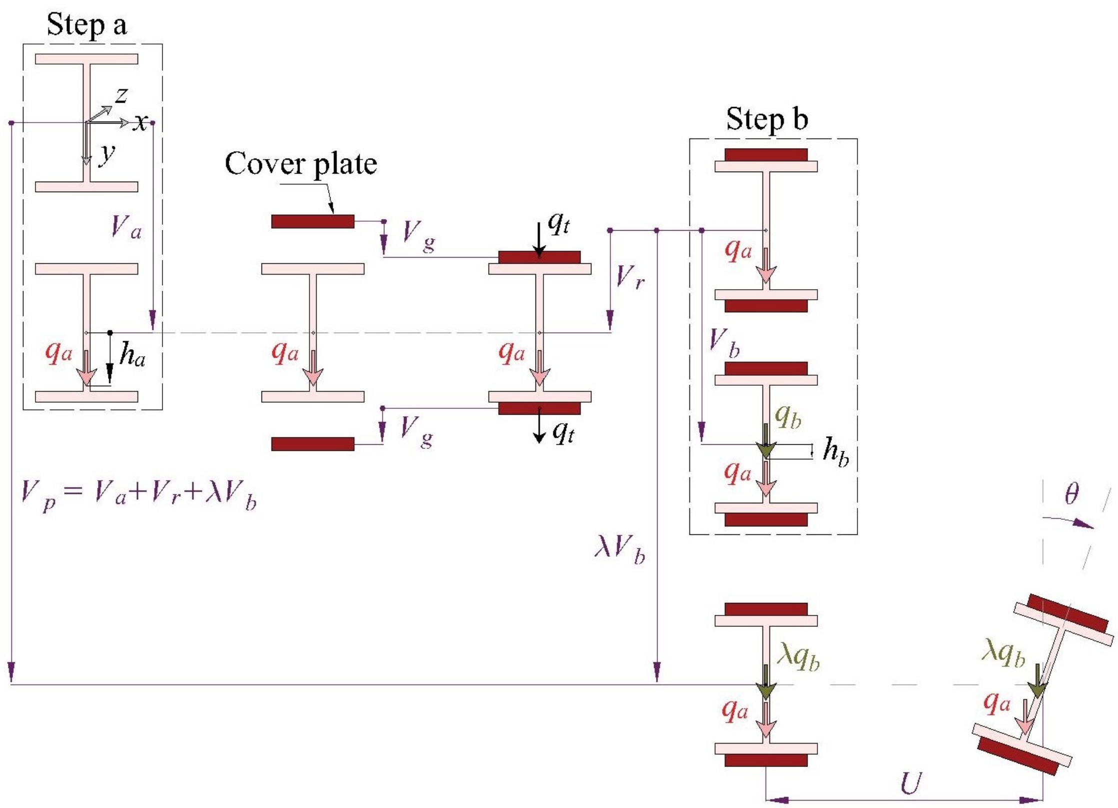

Fig. 5.1 Loading and strengthening history

5.4 Motivation

In general, the load distribution before strengthening may differ from the load distribution after strengthening. An illustrative example in an existing industrial plant is depicted in (Fig. 5.2a). The system consists of grating supported by secondary beams, which are supported by two girders of span L. Girders are connected to column webs through shear connections (i.e., with negligible end moments). As the secondary beams are connected to the girder webs at $L/3$ and $2L/3$ through simple shear connections, they provide no twist restraints at these locations. Also, since both girders have the same stiffness and are subject to identical loads, the secondary beams spanning both girders provide no relative lateral restraints when both beams buckle laterally. Also, steel grating offers negligible stiffness in its own plane. During operating conditions prior to strengthening, the girders are subjected to (1) two point loads at $L/3$ and $2L/3$ due to occupancy loads on the grating, in addition to (2) a concentrated load at $L/3$ due to a suspended pipe (Fig. 5.2a). Contemplated new operating conditions of the plant necessitate the addition of a new pipe to be suspended at $2L/3$ (Fig. 5.2b) and hence the supporting girders are to be strengthened.

Before strengthening, the occupancy loads are removed (self-weight is assumed negligible). However, operating conditions within the plant prevent the removal of the pipe. First, the secondary beam at $2L/3$ is replaced by a heavier beam to withstand the additional loads induced by the anticipated new pipe. Then, the girders are strengthened by welding cover plates to both flanges (Fig. 5.2b). Under the new operating conditions, the strengthened girder then supports the load induced by the newly added pipe and the occupancy loads in addition to the pre-strengthening load induced by the existing pipe. Fig. 5.2c-f depict the sequence of bending moment distributions in the girders during initial operating conditions, after removal of occupancy loads right prior to strengthening, under additional loads applied after strengthening, and the total loads under the new operating conditions.

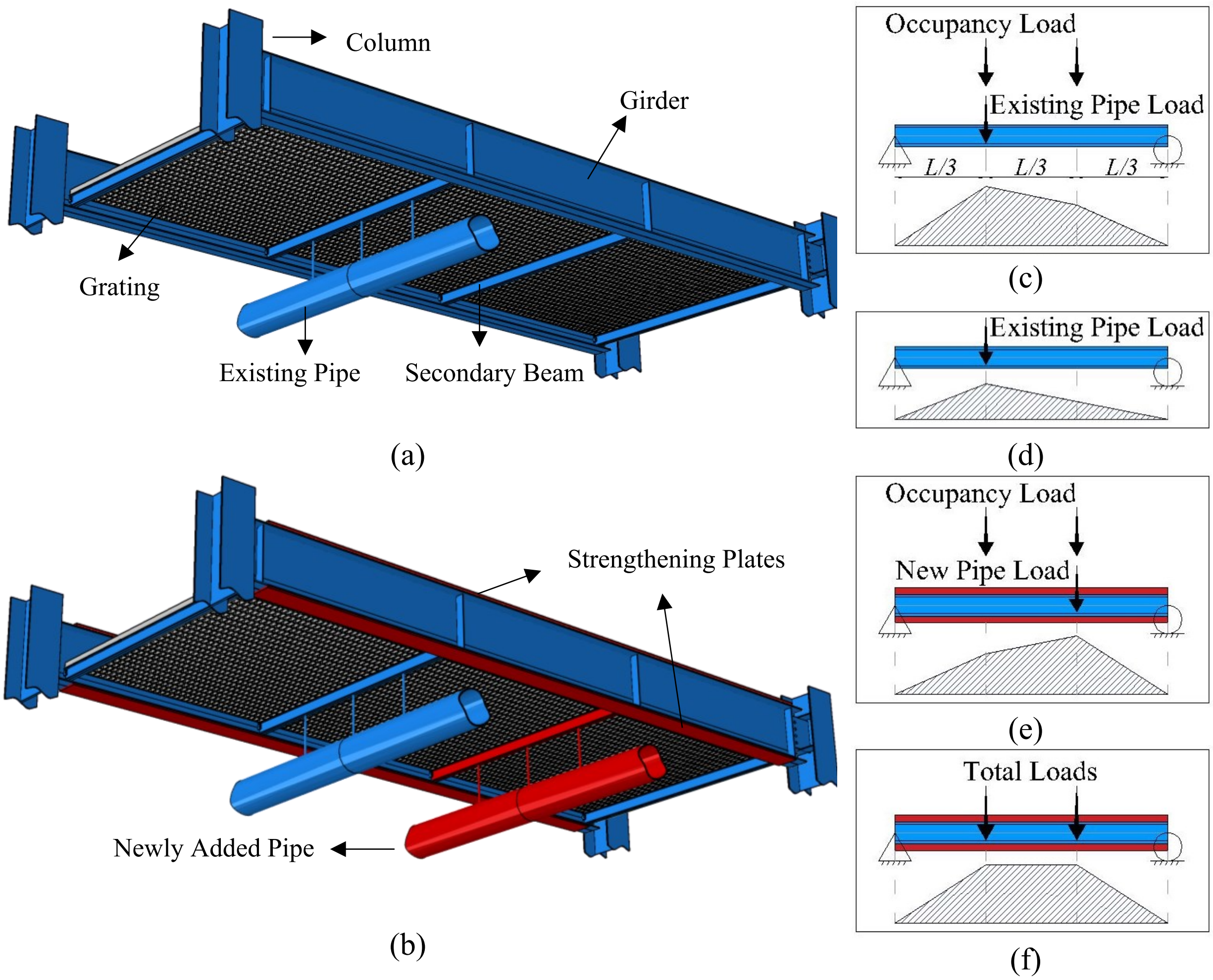

Fig. 5.2 Overall view of a structure in an industrial plant (a) Prior to strengthening (b) After strengthening. Loads and bending moments (c) During operating condition before strengthening, (d) After removal of occupancy loads right prior to strengthening, (e) Additional loads after strengthening, and (f) Total loads during operating condition after strengthening (d+e)

5.5 Variational principle

The formulation is based on the variational principle in Iranpour and Mohareb (2023a). As a simplification, the formulation omitted (a) weld-induced deformations, (b) cross-sectional distortion, (c) mid-surface shear strains, (d) shear deformations due to bending and warping, and (e) through thickness transverse shear strains. Additionally, the pre-buckling response was assumed linear and the material response was assumed to be linearly elastic isotropic. Beams are assumed to be prismatic with doubly symmetric I-sections and are strengthened with two identical plates welded to the flanges. As a result, the composite system is also doubly symmetric. Finally, before welding, the strengthening plates were assumed to slide relative to the beam flanges in a frictionless manner, while after welding full shear transfer was assumed to take place at the plate-flange interface, resulting in a monolithic strengthened section. Under the above assumptions/simplification, the second variation of total potential energy throughout buckling $\bar{\bar{\Pi}}$ was shown to take the form

$$\bar{\bar{\Pi}} = \bar{\bar{\Pi}}_U + \bar{\bar{\Pi}}_P + \bar{\bar{\Pi}}_V + \bar{\bar{\Pi}}_L \tag{5.1}$$

in which $\overline{\overline{(\ )}}$ denotes the second variation of the argument functional, Π_U represents the internal strain energy contribution stored during buckling, Π_P is an additional term accounting for PBD effects, Π_V represents the destabilizing contribution of the work done by the loads throughout buckling, and Π_L represents the effect of the pre- and post-strengthening loads being offset from the shear centre (e.g., in cases where the load is applied to the top or bottom flange). The terms $\bar{\bar{\Pi}}_U$, $\bar{\bar{\Pi}}_P$, $\bar{\bar{\Pi}}_V$ and $\bar{\bar{\Pi}}_L$ are given by:

$$\begin{aligned}
\bar{\bar{\Pi}}_U &= \frac{1}{2}\int_L \left[EI_{y,b}\bar{U}''(z)^2 + EC_{w,b}\bar{\theta}''(z)^2 + GJ_b\bar{\theta}'(z)^2 \right] dz \\
\bar{\bar{\Pi}}_P &= \frac{1}{2}\int_L \left\{ 2EI_{y,b}\bar{U}''(z) + \left[EI_{y,b}V_p''(\lambda,z) + \tilde{M}_a(z) + \lambda\tilde{M}_b(z) \right]\bar{\theta}(z) \right\} V_p''(\lambda,z)\bar{\theta}(z)\, dz \\
\bar{\bar{\Pi}}_V &= \int_L \left[\tilde{M}_a(z) + \lambda\tilde{M}_b(z) \right]\bar{\theta}(z)\bar{U}''(z)\, dz \\
\bar{\bar{\Pi}}_L &= \frac{1}{2}\int_L \left[q_a(z)h_a + \lambda q_b(z)h_b \right]\bar{\theta}(z)^2\, dz
\end{aligned} \tag{5.2)a-d$$

in which h_a is the load height of the pre-strengthening load q_a, and is taken as positive when the point of application of load is below the shear centre, h_b is the load height of the post-strengthening load q_b, and $V_p''(\lambda,z)$ is the pre-buckling curvature and as given by Iranpour and Mohareb (2023a),

$$V_p''(\lambda, z) = -\left(\frac{\alpha \tilde{M}_a(z)}{EI_{x,a}} + \frac{\lambda \tilde{M}_b(z)}{EI_{x,b}}\right), \quad \alpha = 1 - \frac{2I_{xP}}{I_{x,a} + 2I_{xP}} \tag{5.3}$$

in which E is the modulus of elasticity, $I_{x,a}$ is the x-axis moment of inertia for the unstrengthened beam, $I_{x,b}$ is the x-axis moment of inertia for the strengthened beam, I_{xP} is the x-axis moment of inertia for each strengthening plate, $\tilde{M}_a(z)$ is the moment distribution under the applied pre-strengthening loads q_a, $\tilde{M}_b(z)$ is the moment distribution under the post-strengthening load q_b and λ is an unknown load multiplier to be determined from a buckling analysis. When the member is in a neutral stability state (i.e., at the onset of buckling), the variation of $\overline{\overline{\Pi}}$ throughout the buckling step must vanish (e.g., Bazant and Cedolin 2010) for an arbitrary set of buckling deformations (i.e., $\delta\overline{\overline{\Pi}} = 0$). In Eq. (5.2), G is the shear modulus, $I_{y,b}$ is the weak axis moment of inertia of the strengthened section, J_b is the Saint-Venant torsional constant of the strengthened section, $C_{w,b}$ is the warping constant of the strengthened section, $U(z)$ is the lateral displacement and $\theta(z)$ is the angle of twist.

5.6 General Framework

Starting with the variational expression defined in Eq. (5.1), a general interaction equation is developed to relate the post-strengthening critical moment of the strengthened system to the magnitude of the peak pre-strengthening moment. The solution provides a series of approximate coefficients that capture effects of moment gradient, load height and PBD on the critical moment of the strengthened system. Two cases are considered separately: (1) the peak moments due to pre- and post-strengthening loads occur at the same location along the span, and (2) the peak moments take place at different locations.

5.7 Case 1: Pre- and Post-Strengthening loads with coinciding bending moment peaks

This section is concerned with loading patterns for which the bending moments induced by the pre- and post-strengthening loads peak at the same location (e.g., a pre-strengthening midspan point load followed by post-strengthening uniformly distributed load, both induced by gravity loads).

5.7.1 Formulation

Consider a beam simply supported relative to lateral displacements and twist (i.e., $\bar{U}=\bar{U}''=\bar{\theta}=\bar{\theta}''=0$) at both ends. For the boundary conditions defined, the first variation of lateral displacement $\bar{U}(z)$ and angle of twist $\bar{\theta}(z)$ are postulated to take the form

$$\bar{U}(z)=\bar{A}\sin(\pi z/L),\quad \bar{\theta}(z)=\bar{B}\sin(\pi z/L) \tag{5.4)a-b}$$

The assumed displacement functions in Eqs. (5.4)a-b are symmetric and, strictly speaking, do not accurately represent the buckling mode shapes under unsymmetric loading. The effect of this approximation will be assessed subsequently. The pre- and post-strengthening bending moment distributions are cast into the form

$$\tilde{M}_a(z)=M_a m_a(z),\quad \tilde{M}_b(z)=M_b m_b(z) \tag{5.5)a-b}$$

where M_a and M_b are the peak bending moments and $m_a(z)$ and $m_b(z)$ are distribution functions of the bending moments that depend on the pre- and post-strengthening loading patterns, respectively. For the reference beam under uniform moment, one has $m_a=m_b=1.0$.

From Eqs. (5.4)a-b and (5.5)a-b, by substituting into the variational expression defined in Eq. (5.1) , performing the integrations, evoking the stationary conditions $\delta\bar{\bar{\Pi}}=\left(\partial\bar{\bar{\Pi}}/\partial\bar{A}\right)\delta\bar{A}+\left(\partial\bar{\bar{\Pi}}/\partial\bar{B}\right)\delta\bar{B}=0$, placing the resulting equations in a matrix form, and setting to zero the determinant of the resulting matrix of coefficients (Appendix 5.A), one obtains the interaction equation

$$\frac{1}{C_{p1}^{\ 2}}\left(m_{cr}+C_{p3}m_{an}\right)^2-2\left(C_{h,a}m_{an}+C_{h,b}m_{cr}\right)-C_{p2}m_{an}^{\ 2}=1 \tag{5.6}$$

which relates the normalized pre-strengthening moment ratio $m_{an}=M_a\big/\left(C_aM_{u,b}\right)$ to the normalized post-strengthening critical moment ratio $m_{cr}=M_{cr}\big/\left(C_bM_{u,b}\right)$, in which $C_aM_{u.b}$ is the critical moment capacity of the strengthened beam under the pre-strengthening load pattern, in the absence of the load height and post-strengthening loads effects. Coefficient C_a is the moment gradient factor corresponding to the pre-strengthening loads, and $M_{u,b}$ is the critical moment of the strengthened beam under uniform moments, i.e.,

$$M_{u,b}=\frac{\pi}{L}\sqrt{EI_{y,b}GJ_b+\left(\frac{\pi E}{L}\right)^2 I_{y,b}C_{w,b}} \tag{5.7}$$

Similarly, $M_{cr}=\lambda M_b$ is the sought post-strengthening critical moment that can be safely applied to the beam, $C_bM_{u,b}$ is the critical moment capacity of the strengthened beam under the post-strengthening loading pattern, in the absence of the load height and pre-strengthening loads effects, C_b is the moment gradient factor corresponding to the post-strengthening loads. Approximate moment gradient factors C_{a-E} and C_{b-E} based on the present energy-based solution in conjunction with the displacement functions assumed in Eqs. (5.4)a-b take the form

$$C_{a,E}=\frac{L}{2\int_L m_a\left(z\right)\sin^2(\pi z/L)dz},\qquad C_{b,E}=\frac{L}{2\int_L m_b\left(z\right)\sin^2(\pi z/L)dz} \tag{5.8)a-b}$$

Since the lateral displacement and angle of twist at the buckled configuration (i.e., Eqs. (5.4)a-b) were assumed to be sinusoidal, Eqs. (5.8)a-b are approximate. The effect of this approximation will be subsequently assessed, and improved moment gradient factors will be proposed.

In Eq. (5.6), pre- and post-strengthening load height coefficients $C_{h,a}$ and $C_{h,b}$ arise from the $\bar{\bar{\Pi}}_L$ term in Eq. (5.1), i.e., by omitting $\bar{\bar{\Pi}}_L$, load height coefficients vanish. According to the variational principle described, these coefficients are defined by

$$\left(C_{h,a}, C_{h,b}\right) = \frac{EI_{y,b}}{M_{u,b}L^2}\left(\alpha_{L,a} C_a h_a, \alpha_{L,b} C_b h_b\right) \tag{5.9a-b}$$

in which the coefficients $\alpha_{L,a}$ and $\alpha_{L,b}$ depend on the pre-strengthening and post-strengthening loading patterns. The expressions for $\alpha_{L,a}$ and $\alpha_{L,b}$ for common loading cases are

$$\alpha_{L,i} = \begin{cases} 4.0 & \text{uniformly distributed load} \\ \sin^2\left(\pi\tilde{z}\right) / \left[\tilde{z}\left(1-\tilde{z}\right)\right] & \text{point load applied at } z_0 \\ 2\sin^2\left(\pi\tilde{z}\right)/\tilde{z} & \text{two equal point loads each applied at } z_0 \text{ from nearest support} \end{cases} \tag{5.10}$$

in which $\tilde{z} = z_0/L$, and $i = a$ for pre-strengthening loads and $i = b$ for post-strengthening loads. Both $C_{h,a}$ and $C_{h,b}$ are dimensionless factors that are positive when gravity loads are applied below the shear centre, i.e., when $h_a, h_b > 0$. To derive Eq. (5.10) for the special case of a point load P_a, P_b acting at location $z = z_0$ along the span, one has $\left(q_a, q_b\right) = \left(P_a, P_b\right)\mathrm{Dirac}\left(z - z_0\right)$, in which $\mathrm{Dirac}\left(z - z_0\right)$ is the Dirac delta function. For the special case where the loads are applied at the shear centre, one has $h_a = h_b = 0$ and Eq. (5.9) leads to $C_{h,a} = C_{h,a} = 0$.

In Eq. (5.6), coefficients C_{p1} - C_{p3} characterize the PBD effect and are given by

$$C_{p1} = \frac{1}{\sqrt{\left(1-n\right)\left[1+\left(2C_b^{\,2}K_2 - 1\right)n\right]}}, \quad C_{p2} = \frac{\left(\alpha n - m\right)}{m^2}\left(2\alpha K_1 n C_a^2 - \alpha n + m\right) + \left(\frac{C_{p3}}{C_{p1}}\right)^2$$
$$C_{p3} = \frac{C_{p1}^{\;2}}{m}\left[\left(m - \alpha n\right)\left(1-n\right) - K_3 n C_a C_b\left(2\alpha n - \alpha - m\right)\right] \tag{5.11a-c}$$

in which

$$n=\frac{I_{y,b}}{I_{x,b}},\qquad m=\frac{I_{x,a}}{I_{x,b}},\qquad K_1=\frac{1}{L}\int_L m_a(z)^2\sin^2\left(\frac{\pi z}{L}\right)dz,$$
$$K_2=\frac{1}{L}\int_L m_b(z)^2\sin^2\left(\frac{\pi z}{L}\right)dz, K_3=\frac{1}{L}\int_L m_a(z)m_b(z)\sin^2\left(\frac{\pi z}{L}\right)dz \qquad (5.12)\text{a-e}$$

It is noted that C_{p1} is identical to the PBD coefficient reported by Sahraei et al. (2018) for non-strengthened beams. While C_{p1} depends only upon the post-strengthening moment distribution, coefficients C_{p2} and C_{p3} depend on pre- and post-strengthening moment distributions. Table 5.1 provides the numeric values for K_1 - K_3 as computed by Eq. (5.12)c-e for common loading cases defined in Table 5.2. For example, for a beam subjected to UDL-2PLs (i.e., a UDL prior to strengthening and 2PLs after strengthening), Table 5.1 gives $K_1=0.390$, $K_2=0.417$ and $K_3=0.403$.

Table 5.1 Constants K_1, K_2 and K_3 as computed from Eq. (5.12)c-e

Pre-or post-strengthening Load		UM	2PLs	UDL	PLM	PLQ	PL3Q	LM	RM
K_1 or K_2		0.500	0.417	0.390	0.268	0.224	0.224	0.141	0.141
K_3		Pre-strengthening load							
		UM	2PLs	UDL	PLM	PLQ	PL3Q	LM	RM
Post-strengthening load	UM	0.500	0.447	0.435	0.351	0.318	0.318	0.250	0.250
	2PLs	0.447	0.417	0.403	0.331	0.291	0.291	0.224	0.224
	UDL	0.435	0.403	0.390	0.321	0.282	0.282	0.217	0.217
	PLM	0.351	0.331	0.321	0.268	0.230	0.230	0.176	0.176
	PLQ	0.318	0.291	0.282	0.230	0.224	0.187	0.175	0.143
	PL3Q	0.318	0.291	0.282	0.230	0.187	0.224	0.143	0.175
	LM	0.250	0.224	0.217	0.176	0.175	0.143	0.141	0.109
	RM	0.250	0.224	0.217	0.176	0.143	0.175	0.109	0.141

Table 5.2 Common load cases investigated

Acronym	Definition
UDL	Uniformly Distributed Load
PLM	Point Load applied at the Midspan
PLQ	Point Load applied at the Quarter span
PL3Q	Point Load applied at three Quarter span
2PLs	Two Point Loads at third span (i.e., $L/3$ and $2L/3$)
UM	Uniform Moment
LM	Left Moment (i.e., linear bending moment distribution where only the left end of the beam is subjected to a moment)
RM	Right Moment (i.e., linear bending moment distribution where only the right end of the beam is subjected to a moment)

Solving the interaction relation defined in Eq. (5.6) for m_{cr} yields a positive and a negative value. The positive value corresponds to the case when both pre- and post-strengthening loads are acting downwards (as may be the case when both pre- and post-strengthening loads acting on a horizontal beam are induced by gravity) while the negative value corresponds to the case where the pre-strengthening load is acting downwards while the post-strengthening load is acting upwards (e.g., gravity induced pre-strengthening loads followed by wind uplift post-strengthening loads).

5.7.2 Verification

The accuracy of expressions derived in the previous section is assessed by comparing their predicted results against those of the FE formulation developed in (Iranpour and Mohareb 2023a). The element, a two-node thin-walled beam element with four degrees of freedom per node, is developed based on the variational principle in Eq. (5.1). The FE formulation leads to a quadratic eigenvalue problem which yields the buckling load multipliers and the corresponding mode shapes. Using the FE formulation, a reference case is defined and examined. Subsequently, the geometric and loading parameters are altered one at a time to assess the ability of the proposed solution to cover a wide range of parameters.

5.7.2.1 Reference Case

A W310×45 cross-section spanning $5m$ is selected as a reference beam. Young modulus is $E=2\times10^5 MPa$ and the shear modulus is $G=77\times10^3 MPa$. The beam is simply supported relative to transverse and lateral displacements and relative to twist at both ends. Prior to strengthening, the beam is subjected to a uniform moment. The capacity of the beam prior to strengthening is governed by elastic LTB strength (for a yield strength of $F_y = 350MPa$). The magnitude of the pre-strengthening loads applied is taken to correspond to a fraction $\Omega = 75\%$ of the critical moment $M_{cr,a}$ of the unstrengthened beam as quantified from the ANSI/AISC360 (2022) provisions, i.e.,

$$M_{cr,a} = C_a M_{u,a},\ M_{u,a} = \frac{\pi}{L}\sqrt{EI_{y,a}GJ_a + \left(\frac{\pi E}{L}\right)^2 I_{y,a}C_{w,a}},\ C_a = \frac{12.5M_{\max,a}}{2.5M_{\max,a} + 3M_{1,a} + 4M_{2,a} + 3M_{3,a}} \tag{5.13a-c}$$

in which C_a is the moment gradient factor corresponding to the pre-strengthening loads and $M_{\max,a}$, $M_{1,a}$, $M_{2,a}$ and $M_{3,a}$ are the absolute values of peak moment, the quarter point, midspan, and third-quarter point moments of the unbraced length. The beam cross-section is then strengthened by welding two cover plates $b_p \times t_p = 100mm \times 8mm$ and subsequently subjected to additional post-strengthening uniform moments.

5.7.2.2 Uniform critical moment for reference case

The elastic critical moment for the reference case is obtained by setting $m_a(z) = m_b(z) = 1.0$ leading to $C_a = C_b = 1.0$, while omitting load height effects (by setting $h_a = h_b = 0.0$ which would lead to $C_{h,a} = C_{h,b} = 0.0$) and PBD effects (by setting $V_p'' = 0.0$ or omitting the term $\bar{\bar{\Pi}}_P$ in Eq.

(5.1) which would lead to the values $C_{p1} = C_{p3} = 1.0$ and $C_{p2} = 0.0$ in Eq. (5.6)). In this situation, Eq. (5.6) reduces to a simple form and by solving it for the critical moment M_{cr}, one obtains

$$\lambda M_b = M_{cr} = \frac{\pi}{L}\sqrt{EI_{y,b}GJ_b + \left(\frac{\pi E}{L}\right)^2 I_{y,b}C_{w,b}} - M_a \tag{5.14}$$

5.7.2.3 Uniform critical moments for other cases

Ten additional runs are conducted by varying the span from 5 to 9m, the cover plate width from 50 to 200mm, the cover plate thickness from 6 to 12 and the pre-strengthening moment fraction from 0.25 to 0.75. The critical moments as predicted from Eq. (5.14) (Column 8 in Table 5.3) are compared to those from the FE formulation in (Iranpour and Mohareb 2023a) (Column 9). The perfect agreement of the results (Column 10) is indicative of the fact that Eq. (5.14) accurately predicts the critical moments for the basic case of a beam under uniform moments. This is a natural outcome of the fact that the assumed displacement functions [Eqs. (5.4)a-b] happen to exactly coincide with the buckled shape for a simply supported beam under uniform moment.

Table 5.3 Comparison of critical moments determined from Eq. (5.14) with those obtained from FEA for the basic case of a beam under uniform moment

	Dimensions				Critical moments (kNm)				
Run number (1)	L (m) (2)	b_p (mm) (3)	t_p (mm) (4)	Pre-strengthening moment fraction Ω (5)	For Unstrengthened beam $M_{cr,a}$ (6)	For strengthened beam $M_{u,b}$ (7)	Predicted by Eq. (5.14) (8)	Predicted by FEA (9)	(8)/(9) (10)
R1	**5**	100	8	0.75	141.2	220.5	114.6	114.6	1.00
2	**7**	100	8	0.75	87.1	145.3	79.9	79.9	1.00
3	**9**	100	8	0.75	62.8	108.8	61.7	61.7	1.00
4	5	**50**	8	0.75	141.2	176.2	70.3	70.3	1.00
5	5	**150**	8	0.75	141.2	292.1	186.1	186.1	1.00
6	5	**200**	8	0.75	141.2	388.2	282.3	282.3	1.00
7	5	100	**6**	0.75	141.2	196.4	90.5	90.5	1.00
8	5	100	**10**	0.75	141.2	247.4	141.4	141.4	1.00
9	5	100	**12**	0.75	141.2	276.9	170.9	171.0	1.00
10	5	100	8	**0.25**	141.2	220.5	185.2	185.2	1.00
11	5	100	8	**0.50**	141.2	220.5	149.9	149.9	1.00

5.7.2.4 Moment gradient factors

By omitting the load height and PBD effects in Eq. (5.6), one obtains the interaction equation $\left(m_{cr}+m_{an}\right)^2=1$. By then solving for the positive post-strengthening critical moment, one obtains

$$M_{cr}=C_b M_{u,b}\left(1-m_{an}\right)=C_b\left(\frac{\pi}{L}\sqrt{EI_{y,b}GJ_b+\left(\frac{\pi E}{L}\right)^2 I_{y,b}C_{w,b}}-\frac{1}{C_a}M_a\right) \tag{5.15}$$

It is noted that Eq. (5.15) is similar to a design equation intuitively proposed by Iranpour and Mohareb (2022). We recall that owing to the approximation made in Eq. (5.4), the moment gradient factors introduced in Eqs. (5.8)a-b are approximate. Alternatively, one can adopt expressions for the moment gradient coefficients provided in steel design standards. The moment gradient coefficients C_{i-US} provided in ANSI/AISC360 (2022), C_{i-CA} provided in CAN/CSA-S16 (2019) and C_{i-AS} provided in AS-4100 (2020) are

$$C_{i-US} = \frac{12.5M_{\max,i}}{2.5M_{\max,i} + 3M_{1,i} + 4M_{2,i} + 3M_{3,i}}, \qquad C_{i-CA} = \frac{4M_{\max,i}}{\sqrt{M_{\max,i}^2 + 4M_{1,i}^2 + 7M_{2,i}^2 + 4M_{3,i}^2}}$$
$$C_{i-AS} = \frac{1.7M_{\max,i}}{\sqrt{M_{1,i}^2 + M_{2,i}^2 + M_{3,i}^2}} \tag{5.16)a-c}$$

in which $i = a$ for pre-strengthening loads and $i = b$ for post-strengthening loads.

5.7.2.4.1 Moment gradient factors in the absence of pre-strengthening loads

Table 5.4 compares the moment gradient factors predicted by Eq. (5.8)b (Column 5 in Table 5.4) and those predicted by the standards [Eqs. (5.16)a-c] (Columns 6-8), with the predictions by the finite element results (Column 4) for common loading cases defined previously. The FEA analysis is conducted by omitting the PBD, load height and pre-strengthening load effects (i.e., by setting V_p'', h_a, h_b and M_a to zero), leading to the critical moments $M_{cr-FEA-np}$ (Column 3 in Table 5.4) and the corresponding moment gradient factor (Column 4) is

$$C_{b-FEA} = M_{cr-FEA-np} / M_{u,b} \tag{5.17}$$

which serves as a benchmark to assess the accuracy of other moment gradient expressions/solutions. As Column 9 indicates, the moment gradient expression of Eq. (5.8)b overpredicts the moment gradient factors by 4% on average with the largest discrepancies observed for unsymmetric loading cases. This is a natural outcome of the approximate nature of the displacement functions postulated in Eqs. (5.4)a-b. In this respect, it is more appropriate from a design perspective to adopt the standard-based moment gradient equations given their more conservative nature. In fact, for the loading cases considered, Columns (10) to (12) show that, when compared to FEA predictions, the ratio of moment gradient factors predicted by ANSI/AISC360 and CAN/CSA-S16 averages 0.974 i.e., both standards slightly err, on average, on the conservative side. Comparatively, the average ratio for the Australian standard is 1.01, i.e., on average, it nearly matches the FEA predictions.

Table 5.4 Moment gradient coefficients for reference beam with no pre-strengthening load with various loading cases after strengthening

			Moment gradient coefficient C_b					Ratio (relative to FEA)			
Run number	Post-strengthening load	Critical moments predicted by FEA (kNm)	Finite Element [Eq. (5.17)]	Energy Solution Eq. (5.8)b]	US Standard [Eq. (5.16) a]	Canadian Standard [Eq. (5.16)b]	Australian Standard Eq. (5.16)c]	Energy solution (5)/(4)	US Standard (6)/(4)	Canadian Standard (7)/(4)	Australian Standard (8)/(4)
(1)	(2)	(3)	(4)	(5)	(6)	(7)	(8)	(9)	(10)	(11)	(12)
1	UM	220.5	1.00	1.00	1.00	1.00	1.00	1.00	1.00	1.00	1.00
2	2PLs	241.2	1.09	1.12	1.14	1.13	1.17	1.02	1.04	1.03	1.07
3	UDL	250.7	1.14	1.15	1.14	1.13	1.17	1.01	1.00	1.00	1.03
4	PLM	300.1	1.36	1.42	1.32	1.26	1.39	1.05	0.967	0.929	1.02
5	PLQ or PL3Q	323.6	1.47	1.57	1.36	1.37	1.36	1.07	0.929	0.932	0.929
6	LM or RM	403.0	1.83	2.00	1.67	1.75	1.82	1.09	0.912	0.955	0.995
					Average:			1.04	0.974	0.974	1.01
					Standard deviation:			0.0336	0.0437	0.0385	0.0415

5.7.2.4.2 Critical moments in the presence of pre-strengthening loads

An additional 21 cases were analyzed for the reference beam while changing the type of pre- and post-strengthening loads. To conform with the limitations of Case 1, the pre- and post-strengthening load distributions in all cases were selected to have their peak moments occurring at the same location along the span. The critical moments for all runs as determined from Eq. (5.15) are provided in Column 7 of Table 5.5 and those based on the FEA are provided in Column 8. To exclude any errors attributable to the approximate nature of the moment gradient equation in Eq. (5.8)a-b, the FEA predicted moment gradient values (i.e., Column 4 in Table 5.4) are adopted in the computations. As shown in Column 9 of Table 5.5, the critical moment ratio of both methods is found to average 0.989 with a standard deviation of 1.25%, suggesting that Eq. (5.15) is able to accurately predict FEA results.

Table 5.5 Critical moments under different pre- and post-strengthening loads - Case 1: Peak moments occurring at the same location

Run number	Pre-strengthening load	Post-strengthening load	Moment gradient coefficient: For pre-strengthening loads C_a	Moment gradient coefficient: For post-strengthening loads C_b	Peak pre-strengthening moment M_a *(kNm)*	Critical Moments (kNm): Predicted by Eq. (5.15) M_{cr}	Critical Moments (kNm): Predicted by FEA $M_{cr\text{-}FEA}$	$M_{cr}/M_{cr\text{-}FEA}$
(1)	(2)	(3)	(4)	(5)	(6)	(7)	(8)	(9)
1	UM	UM	1.00	1.00	105.9	114.6	114.6	1.00
2	UM	2PLs	1.00	1.09	105.9	125.4	126.6	0.990
3	UM	UDL	1.00	1.14	105.9	130.3	131.3	0.992
4	UM	PLM	1.00	1.36	105.9	156.0	159.2	0.979
5	UM	PLQ	1.00	1.47	105.9	168.2	173.5	0.969
6	UM	LM	1.00	1.83	105.9	209.4	218.0	0.961
7	2PLs	UM	1.09	1.00	120.4	110.5	111.7	0.990
8	2PLs	2PLs	1.09	1.09	120.4	120.9	120.9	1.00
9	2PLs	UDL	1.09	1.14	120.4	125.6	125.6	1.00
10	2PLs	PLM	1.09	1.36	120.4	150.4	151.1	0.995
11	UDL	UM	1.14	1.00	120.4	114.6	115.6	0.992
12	UDL	2PLs	1.14	1.09	120.4	125.4	125.5	1.00
13	UDL	UDL	1.14	1.14	120.4	130.3	130.3	1.00
14	UDL	PLM	1.14	1.36	120.4	156.0	156.6	1.00
15	PLM	UM	1.36	1.00	139.4	118.1	120.5	0.980
16	PLM	2PLs	1.36	1.09	139.4	129.2	129.8	1.00
17	PLM	UDL	1.36	1.14	139.4	134.3	134.8	1.00
18	PLM	PLM	1.36	1.36	139.4	160.7	160.7	1.00
19	PLQ	UM	1.47	1.00	144.4	122.1	125.7	0.971
20	PLQ	PLQ	1.47	1.47	144.4	179.2	179.2	1.00
21	LM	UM	1.83	1.00	176.5	123.9	128.6	0.964
22	LM	LM	1.83	1.83	176.5	226.4	226.4	1.00
					Minimum:			0.961
					Maximum:			1.00
					Average:			0.989
					Standard deviation:			0.0125

5.7.2.5 Load height factor

The validity of the energy-based load height expression of Eq. (5.9) is assessed in the absence of the PBD effects (by setting $C_{p1} = C_{p3} = 1.0$ and $C_{p2} = 0.0$). The resulting interaction equation is then solved for the post-strengthening critical moment M_{cr} leading to

$$M_{cr} = C_b M_{u,b} \left(C_{h,b} - m_{an} + \sqrt{C_{h,b}^{\ 2} + 2m_{an} \left(C_{h,a} - C_{h,b} \right) + 1} \right) \tag{5.18}$$

All 22 runs defined in the previous section were considered with four different pre- and post-strengthening load height combinations (Table 5.6). An identifier of the form L_1-L_2 is assigned to each run, where L_1 represents the load height for the pre-strengthening loads and L_2 denotes the load height for the post-strengthening loads. For example, B-T denotes that pre-strengthening loads are applied at the Bottom flange while post-strengthening loads are applied at the Top flange. The ratios of post-strengthening critical moments (Columns 12-15 in **Table 5.6**) predicted by Eq. (5.18) to those obtained from FEA are indicating the predictive accuracy of the proposed equation. For all load height scenarios considered T-T, B-B, T-B and B-T, the ratio of predicted critical moments averages nearly 100% with a standard deviation ranging from 1.3% for B-T to 2.9% for T-T. The maximum difference between both solutions of 11.7% corresponds to the case where both pre- and post-strengthening loads are PLQ applied at the top flange. This is attributed to the fact that the buckled configuration postulated in Eq. (5.4) to derive the load height coefficient departs from the buckled configuration predicted by FEA. In fact, for PLQ, one has $z_0 = L/4$ and based on the present approximate solution for point load applied at $z_0 = L/4$, Eq. (5.10) yields $\alpha_{L,i} = 2.67$, which, based on the present solution, would be applicable both for top and bottom flange loading. More accurate values for $\alpha_{L,i}$ can be obtained from FEA. For this purpose, the critical moments M_{cr} are first determined from FEA for PLQ top and bottom flange loading cases, and the corresponding normalized critical moments $m_{cr} = M_{cr} \big/ \left(C_b M_{u,b} \right)$ are computed. From both values of m_{cr}, by substituting into Eq. (5.6) after omitting PBD effects (by setting $C_{p1} = C_{p3} = 1.0$, $C_{p2} = 0.0$) and pre-strengthening load effects (by setting $m_{an} = 0$), and solving for $C_{h,b}$, one obtains $C_{h,b} = 0.5\left(m_{cr} - 1/m_{cr}\right)$. By substituting into Eq. (5.9) and solving for $\alpha_{L,b}$, one obtains $\alpha_{L,b} = 3.27$ for top flange loading which happens to differ from $\alpha_{L,b} = 2.84$ for bottom flange loading. Interestingly, adopting $\alpha_{L,a} = \alpha_{L,b} = 3.27$ instead of $\alpha_{L,a} = \alpha_{L,b} = 2.67$ as predicted by the approximate relation in Eq. (5.10), the 11.7% deviation from FEA originally observed is found to reduce to a mere -0.091% difference.

Table 5.6 Comparison of critical moments determined from Eq. (5.18) with those obtained from FEA for various load combinations and load heights before and after strengthening where pre- and post-strengthening peak moments occur at the same location

Run number	Pre-strengthening load	Post-strengthening load	Critical moments (kNm)								Comparison			
			Predicted by Eq. (5.18) M_{cr}				Predicted by FEA $M_{cr\text{-}FEA}$				$M_{cr}/M_{cr\text{-}FEA}$			
			T-T[a]	B-B[b]	T-B[c]	B-T[d]	T-T	B-B	T-B	B-T	T-T	B-B	T-B	B-T
(1)	(2)	(3)	(4)	(5)	(6)	(7)	(8)	(9)	(10)	(11)	(12)	(13)	(14)	(15)
1	UM	UM	114.6	114.6	114.6	114.6	114.6	114.6	114.6	114.6	1.00	1.00	1.00	1.00
2	UM	2PLs	96.9	168.0	168.0	96.9	97.7	169.7	169.7	97.7	0.99	0.99	0.99	0.99
3	UM	UDL	102.6	170.5	170.5	102.6	103.3	172.0	172.0	103.3	0.99	0.99	0.99	0.99
4	UM	PLM	117.6	215.9	215.9	117.6	119.1	221.6	221.6	119.1	0.99	0.97	0.97	0.99
5	UM	PLQ	136.7	211.7	211.7	136.7	136.7	221.2	221.2	136.7	1.00	0.96	0.96	1.00
6	UM	LM	209.4	209.4	209.4	209.4	218.0	218.0	218.0	218.0	0.96	0.96	0.96	0.96
7	2PLs	UM	77.7	139.0	77.7	139.0	78.6	140.3	78.6	140.3	0.99	0.99	0.99	0.99
8	2PLs	2PLs	63.3	196.5	121.0	120.7	63.2	195.7	121.0	120.7	1.00	1.00	1.00	1.00
9	2PLs	UDL	67.1	200.1	122.2	127.6	67.2	199.7	122.2	127.6	1.00	1.00	1.00	1.00
10	2PLs	PLM	76.6	251.5	156.8	146.8	76.7	253.9	158.6	146.0	1.00	0.99	0.99	1.01
11	UDL	UM	85.7	140.2	85.7	140.2	86.6	141.2	86.6	141.2	0.99	0.99	0.99	0.99
12	UDL	2PLs	70.2	198.7	132.3	121.4	70.3	198.2	132.2	121.4	1.00	1.00	1.00	1.00
13	UDL	UDL	74.4	202.3	133.7	128.3	74.5	201.9	133.7	128.3	1.00	1.00	1.00	1.00
14	UDL	PLM	84.9	254.3	171.1	147.6	84.9	256.4	173.0	146.8	1.00	0.99	0.99	1.01
15	PLM	UM	84.2	147.4	84.2	147.4	85.4	150.2	85.4	150.2	0.99	0.98	0.99	0.98
16	PLM	2PLs	68.4	208.0	131.2	128.0	68.1	209.2	130.0	128.8	1.01	0.99	1.01	0.99
17	PLM	UDL	72.6	211.8	132.5	135.3	72.1	213.0	131.5	136.1	1.01	0.99	1.01	0.99
18	PLM	PLM	82.8	266.1	169.9	155.7	80.7	267.6	170.2	155.6	1.03	0.99	1.00	1.00
19	PLQ	UM	99.3	142.7	99.3	142.7	99.0	147.2	99.0	147.2	1.00	0.97	1.00	0.97
20	PLQ	PLQ	115.9	257.9	188.8	172.9	103.7	263.6	190.7	172.0	1.12	0.98	0.99	1.00
21	LM	UM	123.9	123.9	123.9	123.9	128.6	128.6	128.6	128.6	0.96	0.96	0.96	0.96
22	LM	LM	226.4	226.4	226.4	226.4	226.4	226.4	226.4	226.4	1.00	1.00	1.00	1.00
								Minimum:			0.96	0.96	0.96	0.96
								Maximum:			1.12	1.00	1.01	1.01
								Average:			1.00	0.99	0.99	0.99
								Standard deviation:			0.029	0.014	0.014	0.013

[a] T-T: Both pre- and post-strengthening loads are applied at the top flange (i.e., $h_a=h_b=-d/2=-156.5$mm)
[b] B-B: Both pre- and post-strengthening loads are applied at the bottom flange (i.e., $h_a=h_b=d/2=156.5$mm)
[c] T-B: $h_a=-156.5$mm and $h_b=156.5$mm
[d] B-T: $h_a=156.5$mm and $h_b=-156.5$mm

5.7.2.6 Pre-buckling deformation factors

The reference beam is re-considered under different load configurations. Prior to strengthening, the beam is subjected to a midspan point load. The corresponding moment gradient factor as predicted by FEA is $C_a = 1.36$. For a yield strength of $F_y = 350MPa$, the capacity of the beam prior to strengthening is governed by its elastic LTB resistance according to ANSI/AISC360 (2022). The elastic critical moment is $M_{cr,a} = C_a \, \pi/L \sqrt{EI_{y,a}GJ_a + (\pi E/L)^2 I_{y,a}C_{w,a}} = 192.2kNm$. Thus, the peak pre-strengthening moment M_a can be increased by up to $\phi_b M_{cr,a} = 0.9M_{cr,a} = 173.0kNm$, in which ϕ_b denotes the resistance factor for flexure.

After strengthening through two cover plates $b_p \times t_p = 100mm \times 8mm$, the beam is subjected to an additional midspan point load, i.e., $C_b = 1.36$. The uniform critical moment for the strengthened beam is $M_{u,b} = \pi/L \sqrt{EI_{y,b}GJ_b + (\pi E/L)^2 I_{y,b}C_{w,b}} = 220.5kNm$ and the upper bound for the normalized pre-strengthening moment ratio is $m_{an} = 173/(1.36 \times 220.5) \approx 0.60$.

Assuming the load is applied to the bottom/top flange, one has $h_a = h_b = \pm d/2 = \pm 156.5mm$ and $C_{h,a} = C_{h,b} = \pm 0.305$. Pre-buckling deformation coefficients are $C_{p1} = 1.04$, $C_{p2} = 0.000221$ and $C_{p3} = 0.984$. By substituting into the interaction equation in Eq. (5.6), varying m_{an} from 0 to 0.6 and solving for m_{cr}, interaction plots relating m_{cr} and m_{an} are obtained (Fig. 5.3a and Fig. 5.4a).

In addition to the present load combination PLM-PLM (PLM pre-strengthening load followed by PLM post-strengthening load) other loading combinations are examined: PLM-2PLs, PLM-UDL and UDL-PLM. The interaction plots corresponding to each load combination are provided on Fig. 5.3a-d and Fig. 5.4a-d. The results obtained from FEA are overlaid on the figures for comparison. An identifier L_1-L_2-L_3-L_4 is assigned to each run, where L_1 represents the load height of the pre-strengthening load and takes the values B for bottom flange, S for shear centre and T for top flange, L_2 denotes the load height of post-strengthening load (L_2=B, S or T), L_3 determines whether PBD effects are omitted (L_3=nP) or included (L_3=P), and L_4 denotes the type of solution (L_4=EQ when Eq. (5.6) is used, and L_4=FEA for FEA results). For example, T-B-nP-FEA denotes top flange pre-strengthening load followed by bottom flange post-strengthening load, while omitting the PBD effects, based on FEA predictions. Fig. 5.3 and Fig. 5.4 indicate critical moment predictions of the interaction equation [Eq. (5.6)] are consistently in close agreement with FEA results with ratios of both solutions averaging 1.00 with a standard deviation of 0.87%.

The strengthened cross-section investigated in this section has $n = I_{y,b}/I_{x,b} = 0.070$. Also, it can be numerically verified that C_{p1} is insensitive to post-strengthening load patterns with a nearly constant value $C_{p1} \approx 1.04$. As will be discussed in the following section, one has $C_{p2} \approx 0$ and $C_{p3} \approx 1.0$ in general. Thus, when omitting the effect of pre-strengthening loads in Eq. (5.6), the ratio R_p, defined as the critical moment while accounting for PBD to that based on omitting PBD effects, is about 1.04 on average. In all cases, ratio R_p is found to increase with the magnitude of pre-strengthening moment ratio m_{an} as a result of the increase of pre-strengthening deflections (and hence the beneficial effect of PBD). On average, ratio R_p is 1.07 with a maximum ratio of 1.22 occurring for the PLM-PLM load combination with T-B load height combination and $m_{an} = 0.6$.

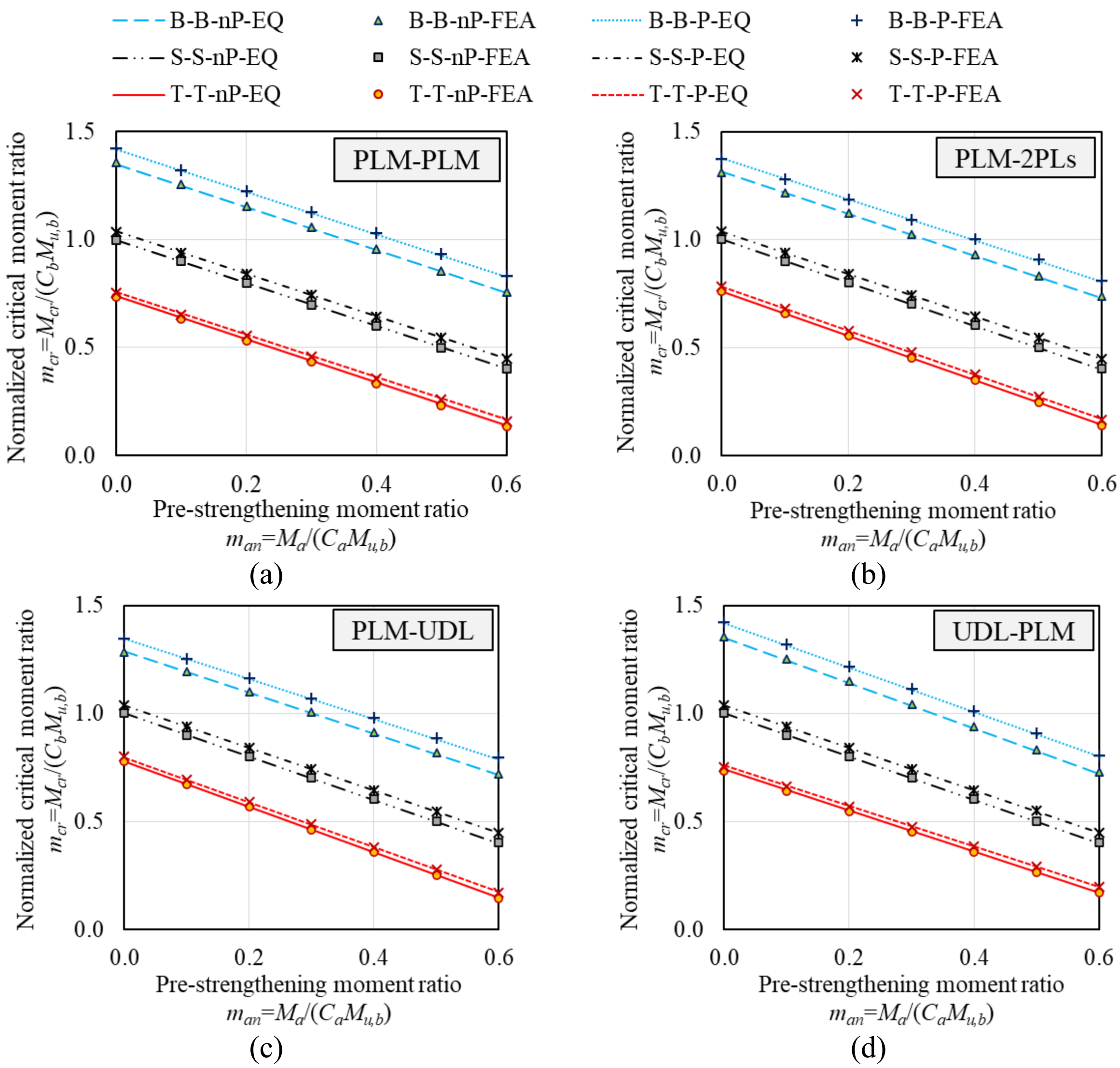

Fig. 5.3 Normalized critical moment ratio versus pre-strengthening moment ratio for the cases when pre- and post-strengthening load heights are identical while pre- and post-strengthening load configurations are different – For acronyms PLM, 2PLs and UDL refer to Table 5.2

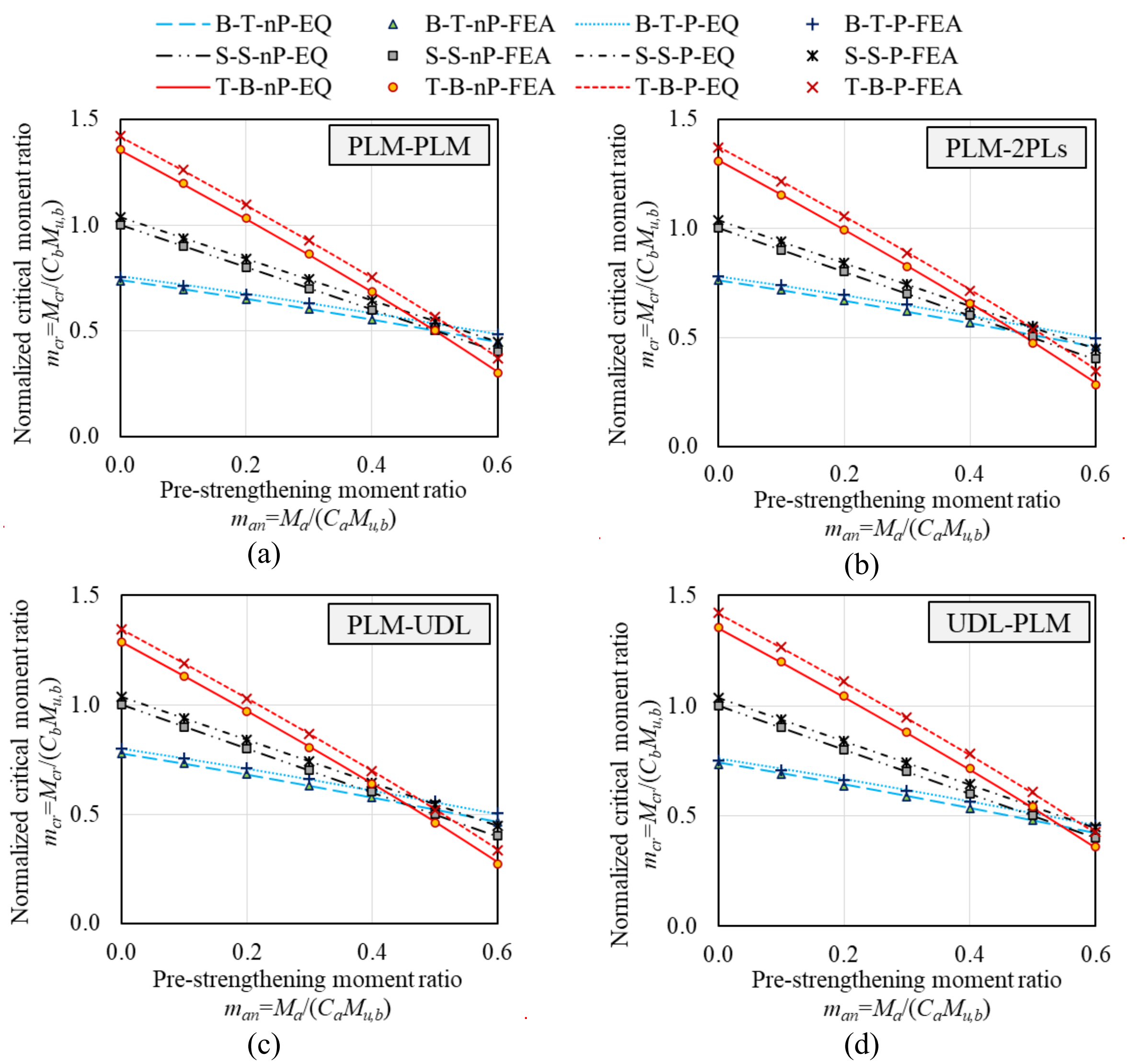

Fig. 5.4 Normalized critical moment ratio versus pre-strengthening moment ratio for the cases with different pre- and post-strengthening load heights and load configurations – For acronyms PLM, 2PLs and UDL refer to Table 5.2

5.7.2.7 Simplifying Approximation

In Eq. (5.6), C_{p2} and C_{p3} capture the interaction between the PBD effect and the presence of pre-strengthening loading. Numeric experimentation with a wide range of practical beam dimensions has shown that $C_{p2} \approx 0$ and $C_{p3} \approx 1.0$. Adopting these approximations into Eq. (5.6) yields

$$\frac{1}{C_{p1}^{\ 2}}\left(m_{cr}+m_{an}\right)^2-2\left(C_{h,a}m_{an}+C_{h,b}m_{cr}\right)\approx 1 \tag{5.19}$$

To assess the influence of the above simplification, the reference case under PLM-PLM is selected and the ratio R_s of critical moment predicted by Eq. (5.19) to that predicted by Eq. (5.6) is examined by varying one at a time the strengthening plate and beam cross-section geometric parameters, (Fig. 5.5a-c), normalized span, pre-strengthening load level (Fig. 5.5c), and load configuration before and after strengthening (Fig. 5.5d). Fig. 4a-d show that the effect of the above approximation is minor in all cases as the ratio R_s is observed to range from 0.952 to 1.00, i.e., Eq. (5.19) always errs on the conservative side. In all examples provided in Fig. 5.5, loads are applied at the shear centre. A further investigation of the influence of load height effect on the predicted moment ratio R_s for the reference case revealed that $R_s = 0.980$ for top flange loading, $R_s = 0.986$ for shear centre loading, and $R_s = 0.989$ for bottom flange loading.

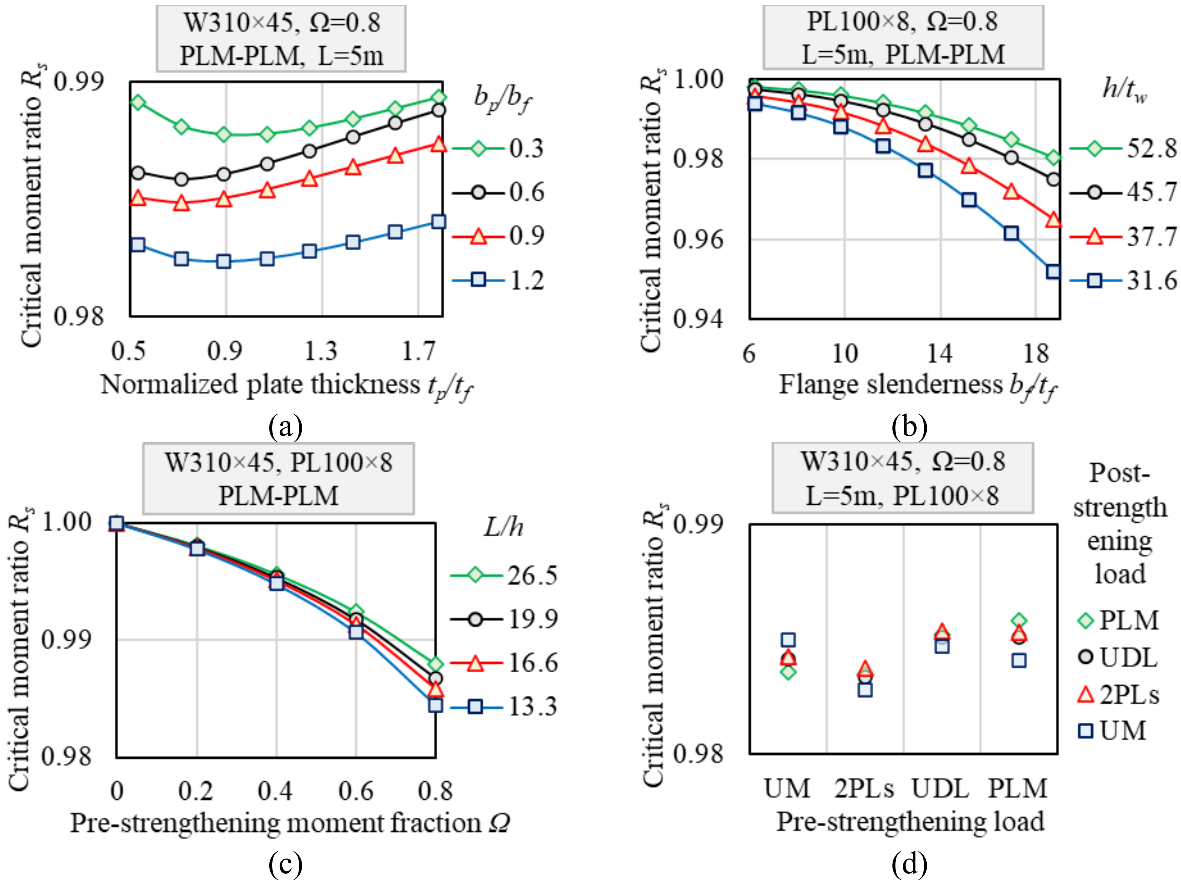

Fig. 5.5 Critical moment ratio versus (a) normalized plate thickness and width (b) normalized flange width and section height; (c) pre-strengthening moment fraction and span-to-height ratio; and (d) pre- and post-strengthening loads

5.7.2.8 Summary

In summary, the above sections show that Eq. (5.6) and its simplified form in Eq. (5.19) accurately predict the critical moments for beams strengthened with cover plates when the peaks of the pre- and post-strengthening moments coincide. The more general case where both peaks are offset is tackled separately in the following section.

5.8 Case 2: Pre- and Post-Strengthening loads with offset bending moment peaks

5.8.1 Formulation

When the peak moments due to pre- and post-strengthening loads occur at different locations, Eq. (5.6) does not, in general, accurately predict critical moments. A procedure is developed in this section to tackle the more general case where both peak moments are offset. However, the procedure is limited to the case where both pre- and post-strengthening loads are induced by gravity. By defining the total moments as $M_T\left(z,\lambda\right)=\tilde{M}_a\left(z\right)+\lambda\tilde{M}_b\left(z\right)=M_a m_a\left(z\right)+M_{cr}\left(\lambda\right)m_b\left(z\right)$ while omitting PBD and load height effects, one can re-write Eqs. (5.1) and (5.2) as

$$\bar{\bar{\Pi}}=\frac{1}{2}\int_L\left[EI_{y,b}\bar{U}''\left(z\right)^2+EC_{w,b}\bar{\theta}''\left(z\right)^2+GJ_b\bar{\theta}'\left(z\right)^2\right]dz+\int_L M_T\left(z,\lambda\right)\bar{\theta}\left(z\right)\bar{U}''\left(z\right)dz \tag{5.20}$$

From Eqs. (5.4)a-b, by substituting into Eq. (5.20), performing integrations, evoking the stationary conditions $\partial\bar{\bar{\Pi}}/\partial\bar{A}=\partial\bar{\bar{\Pi}}/\partial\bar{B}=0$, placing the resulting equations in a matrix form, and setting to zero the determinant of the resulting matrix of coefficients (Appendix 5.B), one obtains the positive root

$$\begin{aligned}&M_{\max}\left(\lambda\right)=C_{b,T}\left(\lambda\right)M_{u,b}\\&C_{b,T}\left(\lambda\right)=L\Big/\left\{2\int_L\left[M_T\left(z,\lambda\right)/M_{\max}\left(\lambda\right)\right]\sin^2(\pi z/L)dz\right\}\\&M_{\max}\left(\lambda\right)=\max\left[M_T\left(z,\lambda\right)\right]\end{aligned} \tag{5.21a-c}$$

in which $C_{b,T}\left(\lambda\right)$ is the moment gradient factor due to the total bending moments $M_T\left(z,\lambda\right)$. Coefficient $C_{b,T}\left(\lambda\right)$ can also be computed from moment gradient equations in steel design standards or, alternatively, from the FEA solution in Iranpour and Mohareb (2023a). Under all three solutions, the dependence of $C_{b,T} = C_{b,T}(\lambda)$ on λ implies the need for an iterative procedure. By defining the normalized total moment $m_T(\lambda)$ as

$$m_T(\lambda) = M_{\max}(\lambda) / \left[C_{b,T}(\lambda) M_{u,b} \right] \tag{5.22}$$

It can be shown that Eq. (5.21)a can be rewritten as $m_T(\lambda) = 1$. This expression is analogous to that found from Eq. (5.6) for Case 1, after omitting the load height and PBD effects, leading to $m_{cr} + m_{an} = 1$. The relation $m_T(\lambda) = m_{cr} + m_{an}$ thus enables extending the use of Eq. (5.19) originally derived for Case 1 to Case 2 so as to incorporate the load height and PBD effects. By setting $m_{cr} + m_{an} = m_T(\lambda)$ in Eq. (5.19) and solving for $m_T(\lambda)$, one obtains

$$m_T(\lambda) \approx C_{p1} \sqrt{1 + 2\left[C_{h,a} m_{an} + C_{h,b} m_{cr}(\lambda) \right]} \tag{5.23}$$

5.8.2 Proposed Iterative Procedure for gravity loads

In order to obtain the critical moment using Eq. (5.23), the following steps can be implemented:

(1) For the first iteration ($j = 1$), given m_{an}, C_{p1}, $C_{h,a}$ and $C_{h,b}$, solve Eq. (5.19) for the normalized critical moment $m_{cr}(\lambda_1) = C_{p1}{}^2 C_{h,b} - m_{an} + C_{p1}\sqrt{2\left(C_{h,a} - C_{h,b}\right) m_{an} + C_{h,b}{}^2 C_{p1}{}^2 + 1}$ and compute the corresponding post-strengthening critical moment $\lambda_1 M_b = M_{cr}(\lambda_1) = m_{cr}(\lambda_1) C_b M_{u,b}$.

For iterations $j = 1$ to the maximum number of iterations $j_{\max}$, perform Steps 2-7:

(2) Given $M_a m_a(z)$ and $M_{cr}(\lambda_j) m_b(z)$, determine the total moment $M_T(z, \lambda_j) = M_a m_a(z) + M_{cr}(\lambda_j) m_b(z)$ at the onset of buckling.

(3) Given the total moments $M_T(z, \lambda_j)$, compute the moment gradient $C_{b,T}(\lambda_j)$ from the moment equation given in the standards.

(4) Identify the location $z_{\max}\left(\lambda_j\right)$ of the peak total moment $M_{\max}\left(\lambda_j\right)=\max\left[M_T\left(z,\lambda_j\right)\right]$ and express the moment at peak location as a linear combination of the pre-strengthening peak moment M_a and the post-strengthening critical moment $M_{cr}\left(\lambda_j\right)$, i.e.,

$$M_{\max}\left(\lambda_j\right)=m_a\left[z_{\max}\left(\lambda_j\right)\right]M_a+m_b\left[z_{\max}\left(\lambda_j\right)\right]M_{cr}\left(\lambda_j\right) \tag{5.24}$$

When both pre- and post-strengthening moment peaks coincide, one has $m_a\left[z_{\max}\left(\lambda_j\right)\right]=m_b\left[z_{\max}\left(\lambda_j\right)\right]=1.0$ and, as discussed at the end of this section, the present algorithm reverts to the solution for Case 1. When the moment peaks due to gravity loads occur at different locations, the peak total moment will lie between the peak locations of M_a and M_{cr}, and one has either ($m_a\left[z_{\max}\left(\lambda_j\right)\right]\leq 1$ and $m_b\left[z_{\max}\left(\lambda_j\right)\right]<1$) or ($m_a\left[z_{\max}\left(\lambda_j\right)\right]<1$ and $m_b\left[z_{\max}\left(\lambda_j\right)\right]\leq 1$).

(5) From m_{an}, $m_{cr}\left(\lambda_j\right)$, substitute into Eq. (5.23) to obtain the normalized peak total moment value $m_T\left(\lambda_j\right)=C_{p1}\sqrt{1+2\left[C_{h,a}m_{an}+C_{h,b}m_{cr}\left(\lambda_j\right)\right]}$

(6) Using the moment gradient factor $C_{b,T}\left(\lambda_j\right)$ in Step 3 and $m_T\left(\lambda_j\right)$ in Step 5, determine the peak total moment $M_{\max}\left(\lambda_j\right)=m_T\left(\lambda_j\right)C_{b,T}\left(\lambda_j\right)M_{u,b}$

(7) Given the peak total moment $M_{\max}\left(\lambda_j\right)$ computed in Step 6, and $m_a\left[z_{\max}\left(\lambda_j\right)\right]$ and $m_b\left[z_{\max}\left(\lambda_j\right)\right]$ computed in Step 4, obtain an improved value for the post-strengthening critical moment through an updated form of Eq. (5.24) yielding

$M_{cr}\left(\lambda_{j+1}\right)=\left\{M_{\max}\left(\lambda_j\right)-m_a\left[z_{\max}\left(\lambda_j\right)\right]M_a\right\}/m_b\left[z_{\max}\left(\lambda_j\right)\right]$ and compute the corresponding normalized critical moment $m_{cr}\left(\lambda_{j+1}\right)=M_{cr}\left(\lambda_{j+1}\right)/\left(C_b M_{u,b}\right)$.

Repeat Steps 2-7 until convergence is attained, i.e., $\left|m_{cr}\left(\lambda_{j+1}\right)-m_{cr}\left(\lambda_j\right)\right|/\left|m_{cr}\left(\lambda_j\right)\right|$ is less than a user-specified tolerance.

Note that combining Steps 4-7 yields

$$m_{cr}\left(\lambda_{j+1}\right)=\frac{C_{b,T}\left(\lambda_j\right)C_{p1}\sqrt{1+2\left[C_{h,a}m_{an}+C_{h,b}m_{cr}\left(\lambda_j\right)\right]}-m_a\left[z_{\max}\left(\lambda_j\right)\right]C_a m_{an}}{C_b m_b\left[z_{\max}\left(\lambda_j\right)\right]} \tag{5.25}$$

A flowchart of the proposed iterative procedure is provided in Fig. 5.6.

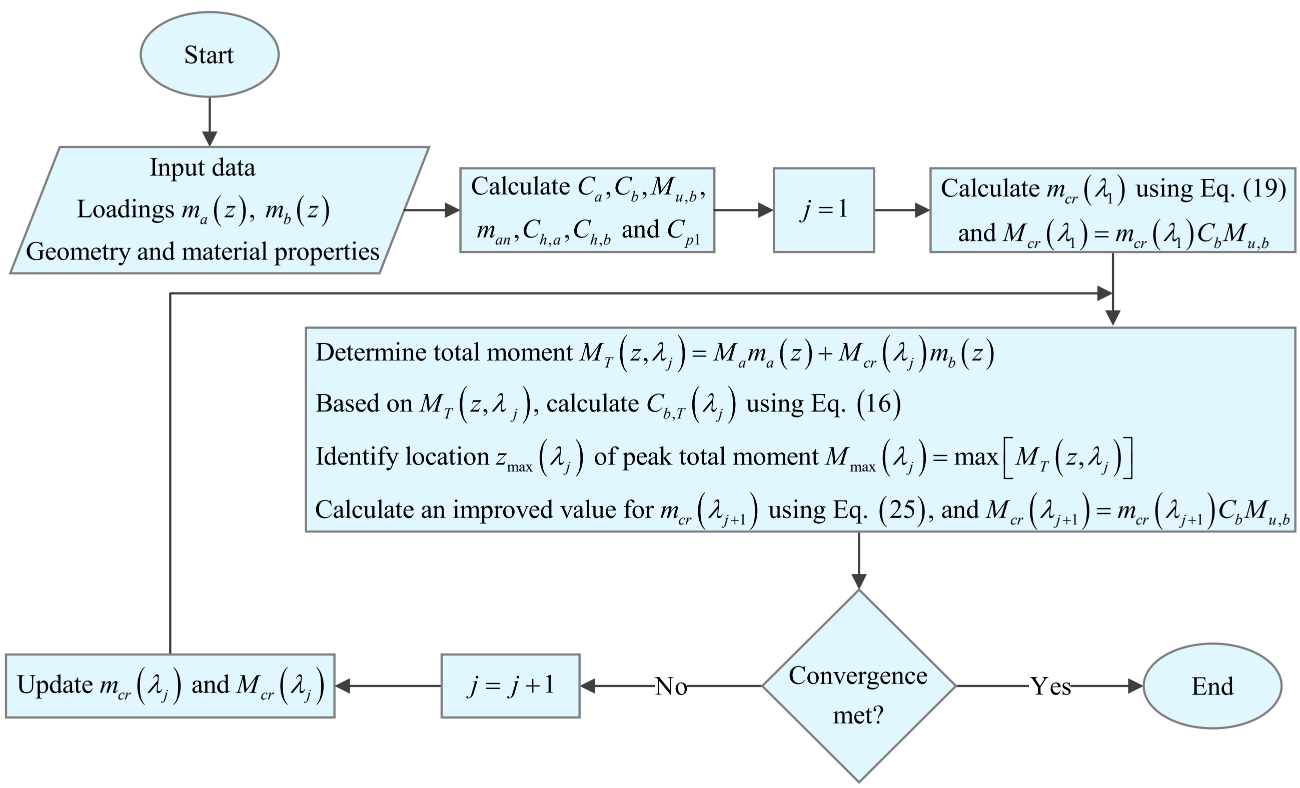

Fig. 5.6 Flowchart of proposed iterative procedure

The above procedures have been implemented as Python Apps that are freely accessible (LTB-Strengthen-UO 2023).

When both pre- and post-strengthening moment peaks coincide, one has $m_a\left(z_{\max}\right)=m_b\left(z_{\max}\right)=1.0$, and Eq. (5.24) reduces to $M_{\max}=M_a+M_{cr}$. Recalling the definitions $m_{an}=M_a\big/\left(C_a M_{u,b}\right)$, $m_{cr}=M_{cr}\big/\left(C_b M_{u,b}\right)$, $m_T=M_{\max}\big/\left(C_{b,T} M_{u,b}\right)$ and $m_T=m_{cr}+m_{an}$, one obtains $C_{b,T}=\left(C_a m_{an}+C_b m_{cr}\right)/\left(m_{cr}+m_{an}\right)$. From the new expression for $C_{b,T}$, by substituting into Eq. (5.25) and knowing that when the solution converges, $m_{cr}\left(\lambda_{j+1}\right)=m_{cr}\left(\lambda_j\right)=m_{cr}$, one recovers Eq. (5.19), signifying that the interaction equation for Case 1 is obtained as a special case of Case 2 solution.

5.8.3 Verification

To investigate the accuracy of the interaction equation based on total moments [Eq. (5.23)] and assess the validity of the proposed iterative process for nonsymmetric loadings, the reference beam (i.e., simply supported beam with W310×45 cross-section spanning 5m) is reconsidered and two sets of runs are performed: For Set 1, a point load applied at quarter span point (PLQ) is considered as a pre-strengthening load, and a triangular bending moment distribution with a moving peak value is considered as a post-strengthening load (Fig. 5.7). For Set 2, the pre-strengthening loads are taken to correspond to the triangular distributions with moving peaks (Fig. 5.7) and the post-strengthening load is taken as a PLQ. In loading cases 2-4 in Fig. 5.7, three load height scenarios were considered; shear centre, top flange loading, and bottom flange loading. Conversely, loading cases 1 and 5 involving point moments lend themselves to a single scenario compatible with shear centre loading.

Load case no.	Designation	Normalized location of peak moment z_i/L	Loading configuration	Bending moment distribution
1	LM	0.00		
2	PLQ	0.25		
3	PLM	0.50		
4	PL3Q	0.75		
5	RM	1.00		

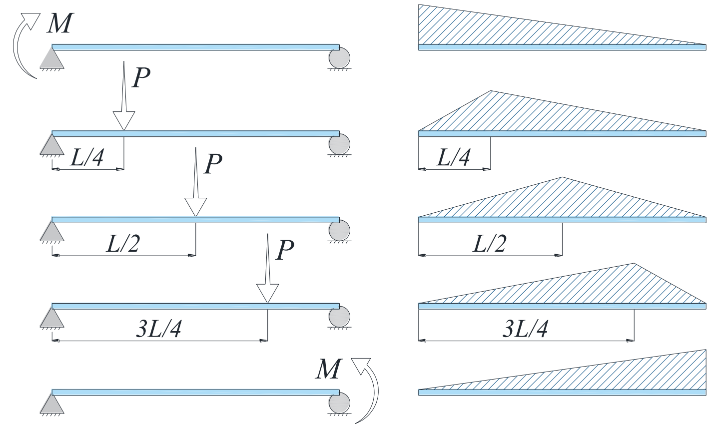

Fig. 5.7 Loading configurations and corresponding bending moment distributions for non-symmetric loadings

For both sets of runs, the normalized critical moment ratios m_{cr} are obtained using three methods: (EQ) Interaction equation for Case 1 [Eq. (5.19)], (IT) Iterative procedure based on Eq. (5.23), and (FEA) Results based on finite element analysis. Fig. 5.8 shows the predictions of all three methods for the shear centre, top flange and bottom flange loadings when PBD effects are omitted or included.

An identifier of the form L_1-L_2 is assigned to each set of runs, where L_1 represents the load height for both the pre- and post-strengthening loads (L_1=B for bottom flange loading, L_1=S for shear centre loading and L_1=T for top flange loading), and L_2 denotes the type of solution and takes the values EQ, IT, or FEA. For example, B-IT denotes that both pre- and post-strengthening loads are applied to the bottom flange, and the results are obtained from the proposed iterative procedure.

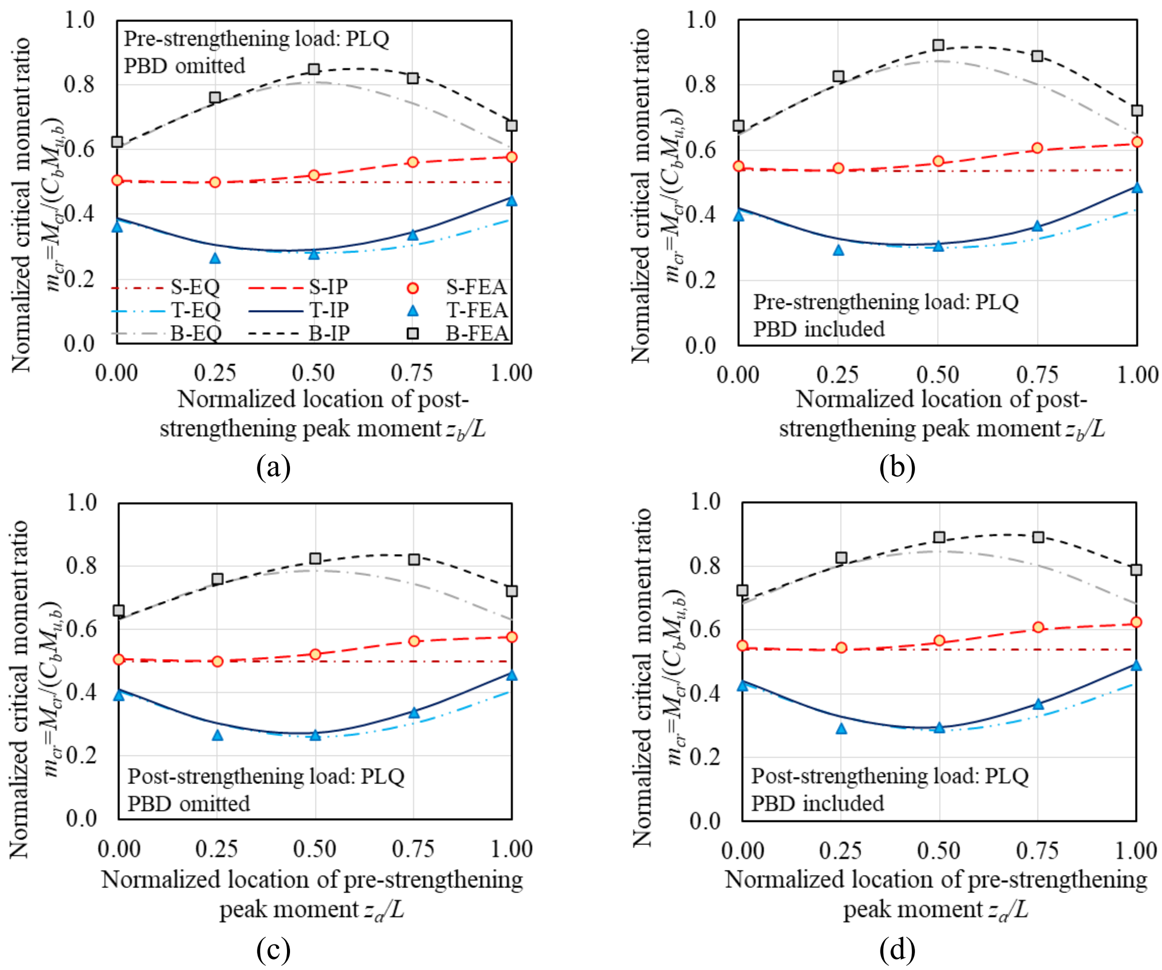

Fig. 5.8 Normalized critical moment ratio versus normalized location of (a) post-strengthening peak moment with PBD effects omitted, (b) post-strengthening peak moment with PBD effects included, (c) pre-strengthening peak moment with PBD effects omitted, and (d) pre-strengthening peak moment with PBD effects included

As Fig. 5.8 shows, when the location z_a of the peak moment due to pre-strengthening loads measured from the left support is close to that due to post-strengthening loads z_b, the critical moments obtained from both solutions EQ and IT are in close agreement with FEA results. However, as the distance between z_a and z_b increases, results obtained from EQ diverge from FEA results. In this case, the iterative process IT enables the solution to approach the FE prediction. On average, the ratio of IT to FEA predictions is 1.01 with a standard deviation of 0.039. The maximum difference between the predicted and FE results is 14.1% and corresponds to the case where both pre- and post-strengthening loads are PLQ applied to the top flange. As mentioned in the section "Load height factor", this difference is mainly due to the approximation involved in Eq. (5.10) which gives $\alpha_L = 8/3 = 2.67$ for PLQ. The FEA results for PLQ applied at the top flange give $\alpha_L = 3.27$. By adopting this value in computing m_{cr}, the 14.1% difference obtained between the predicted and FE results decreases to -0.109%.

5.9 Design examples

5.9.1 Example 1

A beam with a W310×52 cross-section $\left(d, b_f, t_w, t_f\right) = \left(318, 167, 7.6, 13.2\right) mm$ is made of A572 Gr. 50 steel ($F_y = 350 MPa$, $E = 2\times10^5 MPa$, $G = 77\times10^3 MPa$) is simply supported relative to transverse and lateral displacements and twist at both ends. Prior to strengthening, the beam is subjected to a UDL of $20 kN/m$ acting at the shear centre (i.e., $h_a = 0$). The beam is then strengthened with two cover plates $b_p \times t_p = 140\times10 mm$ and subsequently subjected to a post-strengthening PLM acting at the shear centre (i.e., $h_b = 0$). It is required to determine the maximum additional load that can be applied to the beam after strengthening where the span $L = 6.5m$ (Scenario *a*), and $L = 5.5m$ (Scenario *b*).

5.9.1.1 Example 1-Scenario *a* ($L = 6.5m$)

Cross-sectional properties for the unstrengthened cross-section based on centerline dimensions are $\left(I_x, I_y, J\right)_a = \left(1.20\times10^8, 1.03\times10^7, 3.01\times10^5\right) mm^4$ and $C_{w,a} = 2.38\times10^{11} mm^6$, for the strengthened section $\left(I_x, I_y, J\right)_b = \left(1.96\times10^8, 1.48\times10^7, 1.25\times10^6\right) mm^4$, $C_{w,b} = 3.73\times10^{11} mm^6$, the elastic section modulus $S_{x,b} = 1.16\times10^6 mm^3$, the plastic section modulus $Z_{x,b} = 1.29\times10^6 mm^3$, the radius of gyration about the *y*-axis $r_{y,b} = 39.7 mm$ and the distance h_0 between flange centroids is taken as $314.8mm$, and $I_{xP} = 1.17 \times 10^4 mm^4$ for each strengthening plate. The section meets the compactness requirements of ANSI/AISC360 (2022). The member span L exceeds $L_r = 1.95 E/(0.7F_y)\sqrt{\sqrt{I_{y,b}C_{w,b}}/S_{x,b}\left\{J_b/(S_{x,b}h_0) + \sqrt{[J_b/(S_{x,b}h_0)]^2 + 6.76(0.7F_y/E)^2}\right\}} = 6.46m$, and its flexural capacity is governed by elastic LTB. To capture the effects of pre-strengthening load, PBD and load height on the flexural capacity based on elastic LTB, the interaction equation $1/C_{p1}{}^2(m_{cr} + m_{an})^2 - 2(C_{h,a}m_{an} + C_{h,b}m_{cr}) \approx 1$ proposed in Eq. (5.19) is solved for the normalized critical moment ratio m_{cr}. The ingredients of the interaction equation are determined in the following steps.

1. Determine the pre-strengthening moment ratio

   The relevant calculations are $m_{an} = M_a/(C_a M_{u,b})$ in which $M_a = q_a L^2/8 = 105.6kNm$, $M_{u,b} = (\pi/L)\sqrt{EI_{y,b}GJ_b + (\pi E/L)^2 I_{y,b}C_{w,b}} = 280.8kNm$, and using Eq. (5.16)a, $C_a \approx C_{a-US} = 1.136$, which yield a pre-strengthening moment ratio $m_{an} = 0.331$.

2. Determine the load height factors

Given that $h_a = h_b = 0$, the load height coefficients $C_{h,a} = (\alpha_{L,a}C_a h_a EI_{y,b})/(M_{u,b}L^2) = 0$ and $C_{h,b} = (\alpha_{L,b}C_b h_b EI_{y,b})/(M_{u,b}L^2) = 0$.

3. Compute the pre-buckling deformation factor

   Here, we take advantage of the simplifications $C_{p2} \approx 0$ and $C_{p3} \approx 1.0$. The minor to major moment of inertia ratio is $n = I_{y,b}/I_{x,b} = 0.0758$ which gives a pre-buckling coefficient value $C_{p1} = 1/\sqrt{(1-n)\left[1 + (2C_b{}^2K_2 - 1)n\right]} = 1.043$.

From the above steps and knowing that $C_b \approx C_{b-US} = 1.316$ [Eq. (5.16)a], by substituting into Eq. (5.19) one recovers the critical moment ratios $m_{cr} = +0.712$ and $m_{cr} = -1.37$. The negative root is rejected considering that both pre- and post-strengthening loads are acting downwards. The positive root yields the sought nominal post-strengthening critical moment $M_{cr} = m_{cr} C_b M_{u,b} = 263.1 kNm$ based on an elastic critical moment mode of failure. The corresponding nominal midspan point load is $P_{cr} = 4M_{cr}/L = 161.9 kN$, which is 4.1% less than $P_{cr-FEA} = 168.9 kN$ as predicted by FEA. The difference is attributed primarily to the approximation involved in the ANSI/AISC360 (2022) moment gradient factor [Eq. (5.16)a]: By adopting the moment gradient factors $C_{a-FE} = 1.137$, $C_{b-FE} = 1.361$ as computed by FEA instead of $C_{a-US} = 1.136$, $C_{b-US} = 1.316$, the proposed procedure yields $P_{cr} = 167.5 kNm$, which is 0.8% less than P_{cr-FEA}.

5.9.1.2 Example 1-Scenario *b* ($L = 5.5m$)

According to ANSI/AISC360 (2022), the resistance of flexural members with compact sections is governed by inelastic LTB when the unbraced length L satisfies the condition $L_p \le L \le L_r$ where L_p is the laterally unbraced length below which LTB does not occur, given by Clause F2-5 as

$$L_p = 1.76 r_{y,b} \sqrt{E/F_y} \tag{5.26}$$

The nominal flexural capacity based on inelastic LTB M_{n-AISC} as given by Clause F2-2 is expressed by

$$M_{n-AISC} = C_b \left[M_p - \left(M_p - 0.7 F_y S_x \right) \frac{\left(L_b - L_p \right)}{\left(L_r - L_p \right)} \right] \le M_p, \qquad M_p = Z_{x,b} F_y \tag{5.27a-b}$$

in which M_p is the plastic moment for the strengthened section. The ANSI/AISC360 (2022) expression for coefficient C_b in Eq. (4.35)a accounts for moment gradient effects but omits the effects of load height, PBD and pre-strengthening loads. An alternative coefficient that captures moment gradient, load heights, PBD and pre-strengthening loads is obtained by normalizing the peak total elastic critical moment $M_{\max}$ as predicted by the present solution by the critical moment of the strengthened beam under uniform moments $M_{u,b}$ [i.e., $C = M_{\max} / M_{u,b}$]. It is proposed to use coefficient C thus computed, into Eq. (4.35) in lieu of C_b as computed by the ANSI/AISC360 (2022) expression.

The material and cross-sectional properties are identical to those of Scenario *a*. Recalling that $L_r = 6.46m$ and $L_p = 1.67m$, the unbraced length of the member falls within $L_p < L = 5.5m < L_r$ and ANSI/AISC360 (2022) predicts the resistance of member to be governed by inelastic LTB.

Given that the pre- and post-strengthening peak moments coincide at midspan, the peak total moment at the onset of elastic LTB is determined by summing the post-strengthening critical moment M_{cr} to the pre-strengthening peak moment M_a (i.e., $M_{\max} = M_{cr} + M_a$), and the sought factor is $C = \left(M_{cr} + M_a\right) / M_{u,b}$.

By taking similar steps to those in Scenario *a*, one obtains $C_a \approx 1.136$, $C_b \approx 1.316$, $M_a = q_a L^2 / 8 = 75.6kNm$, $M_{u,b} = \left(\pi / L\right) \sqrt{EI_{y,b} GJ_b + \left(\pi E / L\right)^2 I_{y,b} C_{w,b}} = 341.8kNm$, $m_{an} = M_a / \left(C_a M_{u,b}\right) = 0.195$, $C_{h,a} = C_{h,b} = 0$, $C_{p1} = 1.043$, $C_{p2} \approx 0$, $C_{p3} \approx 1.0$. The positive root for the post-strengthening critical moment ratio as obtained from Eq. (5.19) is $m_{cr} = 0.848$ and the corresponding critical moment is $M_{cr} = m_{cr} C_b M_{u,b} = 381.5kNm$, which is 3.6% less than the post-strengthening critical moment $M_{cr-FEA} = 395.7kNm$ as predicted by FEA and the sought coefficient is $C=\left(M_{cr}+M_{a}\right)/M_{u,b}=1.337$. In the present example, since loads are applied at the shear centre, coefficient C as computed by the above procedure is close to $C_{b}=1.316$, as expected. The small difference between both coefficients is attributed to PBD effects which are captured in the present solution but omitted in the ANSI/AISC360 (2022) equation.

The section plastic moment is $M_{p}=Z_{x,b}F_{y}=452.4kNm$. By replacing C_{b} with C in Eq. (4.35), the nominal flexural capacity based on inelastic LTB is found to be $M_{n-AISC}=424.8kNm$. Hence, the additional bending moment the beam can withstand after strengthening is $M_{n-AISC}-M_{a}=349.2kNm$ and the corresponding midspan point load is $4\left(M_{n-AISC}-M_{a}\right)/L=254kN$. For verification of the accuracy of inelastic LTB, one needs to perform a FEA that accounts for material and geometric nonlinearity, residual stresses, and initial out-of-straightness, and this is outside the scope of present study.

5.9.2 Example 2

Reconsider the beam in Example 1-Scenario *a* ($L=6.5m$) under a different loading history. Prior to strengthening, the beam is subjected to PLQ $=120kN$ acting at the shear centre (i.e., $h_{a}=0.0$) and after strengthening, a PL3Q is applied at the top plate (i.e., $h_{b}=-\left(d/2+t_{p}\right)=-169mm$). It is required to determine the maximum additional load that can be applied to the beam after strengthening.

The uniform critical moments $M_{u,a}$ and $M_{u,b}$ for the unstrengthened and strengthened beams are identical to those in Example 1. Also, as the section meets the compactness requirement and since $L=6.5m>L_{r}=6.46m$, the flexural capacity is governed by elastic LTB. As the location of pre-and post-strengthening peak moments do not coincide, the iterative procedure is adopted to determine m_{cr}.

<u>Step 1</u> As an initial guess for the iterative procedure, interaction equation (5.19) $1/C_{p1}^{2}\left(m_{cr}+m_{an}\right)^{2}-2\left(C_{h,a}m_{an}+C_{h,b}m_{cr}\right)\approx 1$ is solved for the normalized critical moment ratio m_{cr}. The ingredients of the equation are determined in the following steps.

1. <u>Determine the pre-strengthening moment ratio</u>

   Given $M_a = 3PL/16 = 146kNm$, $M_{u,b} = 281kNm$ and $C_a \approx C_{a-US} = 1.364$ the pre-strengthening moment ratio is computed as $m_{an} = M_a / \left(C_a M_{u,b}\right) = 0.382$.

2. <u>Determine load height factors</u>

   The ANSI/AISC360 (2022) moment gradient equation [Eq. (5.16)a] predicts $C_a = C_b \approx 1.364$. Coefficients $\alpha_{L,a}$ and $\alpha_{L,b}$ for the PLQ as pre-strengthening and PL3Q as post-strengthening loads determined from Eq. (5.10) are $\alpha_{L,a} = \alpha_{L,b} = 2.667$. Given $h_a = 0.0$ and $h_b = -169mm$, by substituting into Eq. (5.9), one recovers the load height coefficients $C_{h,a} = 0.0$ and $C_{h,b} = \left(\alpha_{L,b} C_b h_b EI_{y,b}\right) / \left(M_{u,b} L^2\right) = -0.154$.

3. <u>Compute the pre-buckling deformation factor</u>

   Here, we take advantage of the simplifications $C_{p2} \approx 0$ and $C_{p3} \approx 1.0$. The ratio of moments of inertia is $n = I_{y,b} / I_{x,b} = 0.0758$ which gives a pre-buckling coefficient value $C_{p1} = 1 / \sqrt{(1-n)\left[1+\left(2C_b^{2}K_2 - 1\right)n\right]} = 1.047$.

From Steps 1-3, by substituting into Eq. (5.19) one recovers the critical moment ratios $m_{cr} = +0.569$ and $m_{cr} = -1.67$. The negative root is rejected considering that both pre- and post-strengthening loads are acting downwards and the positive root is taken as an initial guess for the iterative procedure. The corresponding critical moment is $M_{cr}\left(\lambda_1\right) = m_{cr}\left(\lambda_1\right) C_b M_{u,b} = 218kNm$.

Step 2 For the pre-strengthening and post-strengthening loads, one has

$$m_a\left(z\right) = \begin{cases} 4z/L & z \le L/4 \\ 4\left(1 - z/L\right)/3 & z > L/4 \end{cases}, \qquad m_b\left(z\right) = \begin{cases} 4z/\left(3L\right) & z \le 3L/4 \\ 4\left(1 - z/L\right) & z > 3L/4 \end{cases}$$

and the total moment $M_T\left(z, \lambda_j\right) = M_a m_a\left(z\right) + M_{cr}\left(\lambda_j\right) m_b\left(z\right)$ at the onset of buckling is

$$M_T\left(z, \lambda_j\right) = \begin{cases} 4M_a z/L + 4M_{cr}\left(\lambda_j\right) z/\left(3L\right) & z \le L/4 \\ 4M_a\left(1 - z/L\right)/3 + 4M_{cr}\left(\lambda_j\right) z/\left(3L\right) & L/4 < z \le 3L/4 \\ 4M_a\left(1 - z/L\right)/3 + 4M_{cr}\left(\lambda_j\right)\left(1 - z/L\right) & z > 3L/4 \end{cases}$$

Step 3 Based on Eq. (5.16)a and the total moment expression $M_T\left(z, \lambda_j\right)$ obtained in Step 2, the moment gradient for the total moment is found to be $C_{b,T}\left(\lambda_1\right) = 1.077$.

Step 4 The peak total moment $M_{\max}\left(\lambda_j\right) = \max\left[M_T\left(z, \lambda_j\right)\right]$ occurs at three quarter span point (i.e., $z_{\max}\left(\lambda_1\right) = 3L/4$). The corresponding interpolation constants are $m_a\left(3L/4\right) = 1/3$ and $m_b\left(3L/4\right) = 1.0$.

Step 5 From $C_{p1} = 1.047$, $C_{h,a} = 0.0$, $C_{h,b} = -0.154$, $m_{an} = 0.382$ and $m_{cr}\left(\lambda_1\right) = 0.569$, by substituting into Eq. (5.23), one obtains $m_T\left(\lambda_1\right) = C_{p1}\sqrt{1 + 2\left[C_{h,a} m_{an} + C_{h,b} m_{cr}\left(\lambda_1\right)\right]} = 0.951$.

Step 6 From $m_T\left(\lambda_1\right) = 0.951$, $C_{b,T}\left(\lambda_1\right) = 1.077$ and $M_{u,b} = 281kNm$, the peak total moment is found to be $M_{\max}\left(\lambda_1\right) = m_T\left(\lambda_1\right) C_{b,T}\left(\lambda_1\right) M_{u,b} = 288kNm$.

Step 7 From $M_{\max}\left(\lambda_1\right) = 288kNm$, $m_a\left(3L/4\right) = 1/3$, $m_b\left(3L/4\right) = 1.0$ and $M_a = 146kNm$, by substituting into Eq. (5.24), one obtains $M_{cr}\left(\lambda_2\right) = \left\{M_{\max}\left(\lambda_1\right) - m_a\left[z_{\max}\left(\lambda_1\right)\right] M_a\right\} / m_b\left[z_{\max}\left(\lambda_1\right)\right]$

$= 239kNm$. The corresponding normalized critical moment is $m_{cr}(\lambda_2) = M_{cr}(\lambda_2) / (C_b M_{u,b}) = 0.624$.

Since $|m_{cr}(\lambda_2) - m_{cr}(\lambda_1)| / |m_{cr}(\lambda_1)| = 0.096 > 0.001$, Steps 2 to 7 are repeated. Convergence is attained after three iterations at which point, one obtains $C_{b,T}(\lambda_3) = 1.095$ and $m_{cr}(\lambda_3) = 0.628$. The corresponding nominal post-strengthening critical moment is $M_{cr} = m_{cr} C_b M_{u,b} = 241kNm$ based on an elastic critical moment mode of failure. The corresponding midspan point load is $P_{cr} = 16M_{cr}/(3L) = 198kN$, which is 4.8% less than $P_{cr-FEA} = 208kN$ as predicted by FEA.

5.10 Summary, conclusions and recommendations

The present study formulated a simplified equation compared to FEA that captures the interaction between the pre-strengthening loads and post-strengthening LTB capacity, while incorporating the effects of moment gradient, pre-buckling deformation and load height for pre- and post-strengthening loads. The equation is applicable for cases in which the locations of the pre- and post-strengthening peak moments coincide. The validity of the interaction equation was then assessed against FEA predictions based on 396 parametric combinations covering a wide range of pre- and post-strengthening loading patterns and load heights, while evoking/suppressing PBD effects. The ratios of critical moments predicted by the proposed interaction equation to FEA predictions ranged from 0.957 to 1.12 with an average of 1.00 and a standard deviation of 0.013. An iterative procedure was also developed for more general loading cases in which the pre- and post-strengthening peak moments are offset. The validity of the iterative procedure was assessed against FEA predictions for 60 parametric combinations. The ratio of critical moments predicted by the iterative procedure to those of FEA predictions was found to range from 0.955 to 1.14 with an average of 1.01 and a standard deviation of 0.039. The steps of applying the proposed procedures in design situations were explained in two illustrative examples. The main findings of the study are:

1. The derived energy-based expression for moment gradient factor was found to lead to slightly unconservative predictions with a ratio of energy-based to FEA predictions averaging 1.04 and a standard deviation of 0.034. This value compares to an average ratio of standard to FEA predictions of 0.974 and a standard deviation of 0.044 when using the moment gradient expression of ANSI/AISC360 (2022) and an average value of 0.974 and standard deviation of 0.039 when using the moment gradient expression of CAN/CSA-S16 (2019), i.e., standards slightly err on the conservative side. The study thus recommended adopting standard-based moment gradient equations when applying the procedures developed herein to characterize the LTB strength of I-beams strengthened while under loading.
2. The 196 runs conducted to investigate the accuracy of energy-based load height factor derived showed that the ratio of critical moments predicted by using the load height factors derived to those based on FEA ranged from 0.957 to 1.12 with an average value of 0.998 and a standard deviation of 0.015.
3. The 140 FEA runs conducted to investigate the accuracy of PBD coefficients have shown the energy-based to FEA critical moment ratio ranged between 0.986 and 1.05 with an average of 1.00 and a standard deviation of 0.0084, suggesting that the proposed PBD coefficients are accurate.
4. Accounting for PBD effects was shown to increase the critical moments predicted by 7.13% on average. However, the beneficial effect of considering PBD effects was found to increase up to 21.6% for loading cases involving high pre-strengthening load levels.
5. The interaction equation derived was found to characterize the effect of PBD effects by three coefficients, of which only one was deemed influential. A simplified interaction equation was thus

proposed based on a single PBD coefficient. Comparisons between the results of 109 parametric combinations confirmed that the ratio of critical moments predicted by the simplified interaction equation to those based on the original interaction equation range from 0.952 to 1.0 with an average of 0.987 and a standard deviation of 0.0075, i.e., the introduced simplification consistently errs slightly on the conservative side.

The following recommendations for future studies are made:

1. The procedures for quantifying the critical moments developed in the present research can be integrated with optimization techniques to quantify the required cover plate geometries for a given beam to withstand specified additional loading.

2. The applicability of the procedure proposed in Example 1 to estimate the inelastic LTB resistance by integrating the procedure for obtaining the elastic critical moment proposed in the present study with the present provisions ANSI/AISC360 (2022) (originally intended for unstrengthened beams) need to be assessed/verified through comparisons with inelastic FEAs that incorporate the effects of material and geometric nonlinearity, residual stresses, and initial out-of-straightness.

5.11 Appendix 5.A: Recovering Interaction Equation for Case 1 (Peak moments Coinciding)

From Eqs. (5.4) and (5.5), by substituting into the variational expression defined in Eq. (5.1), performing integrations and recalling the definitions $m_{an} = M_a / \left(C_a M_{u,b} \right)$, $m_{cr} = M_{cr} / \left(C_b M_{u,b} \right)$, $M_{u,b}$, $C_{h,a}$, $C_{h,b}$, α, n and m as given in Eqs. (5.3)and (5.7)-(5.12), one obtains

$$\bar{\bar{\Pi}} = \bar{A}^2 \frac{\pi^4 EI_{y,b}}{4L^3} - \bar{A}\bar{B}\frac{\pi^2 M_{u,b}}{2L}\left[(1-n)m_{cr} + \left(1-\alpha\frac{n}{m}\right)m_{an}\right] + \bar{B}^2\frac{LM_{u,b}^{\ 2}}{4EI_{y,b}}\left(1+2C_{h,b}m_{cr}+2C_{h,a}m_{an}\right)$$
$$+\bar{B}^2\frac{LM_{u,b}^{\ 2}}{4EI_{y,b}}\left\{\left[(1-n)^2-\frac{1}{C_{p1}^{\ 2}}\right]m_{cr}^{\ 2} + \left[C_{p2}+\left(1-\alpha\frac{n}{m}\right)^2-\left(\frac{C_{p3}}{C_{p1}}\right)^2\right]m_{an}^{\ 2} - 2\left[\frac{C_{p3}}{C_{p1}^{\ 2}}-\left(1-\alpha\frac{n}{m}\right)(1-n)\right]m_{an}m_{cr}\right\}$$

(5.28)

At the stability limit, the second variation of the total potential energy ceases to be positive definite. This requires the first variation of $\bar{\bar{\Pi}}$ to vanish, and the condition of neutral stability is given by the Trefftz criterion $\delta\bar{\bar{\Pi}} = \left(\partial\bar{\bar{\Pi}}/\partial\bar{A}\right)\delta\bar{A} + \left(\partial\bar{\bar{\Pi}}/\partial\bar{B}\right)\delta\bar{B} = 0$. By evoking the stationary conditions $\partial\bar{\bar{\Pi}}/\partial\bar{A} = \partial\bar{\bar{\Pi}}/\partial\bar{B} = 0$, and putting the resulting equations in a matrix form, one obtains

$$\begin{bmatrix} \dfrac{\pi^2 EI_{y,b}}{L^2 M_{u,b}} & -\left[(1-n)m_{cr} + \left(1-\alpha\dfrac{n}{m}\right)m_{an}\right] \\ Symm. & \begin{aligned} &\dfrac{L^2 M_{u,b}}{\pi^2 EI_{y,b}}\left\{1+2m_{cr}C_{h,b}+2m_{an}C_{h,a}+\left[C_{p2}+\left(1-\alpha\dfrac{n}{m}\right)^2-\left(\dfrac{C_{p3}}{C_{p1}}\right)^2\right]m_{an}^{\ 2}\right. \\ &\left.+\left((1-n)^2-\dfrac{1}{C_{p1}^{\ 2}}\right)m_{cr}^{\ 2}-2\left[\dfrac{C_{p3}}{C_{p1}^{\ 2}}-\left(1-\alpha\dfrac{n}{m}\right)(1-n)\right]m_{cr}m_{an}\right\}\end{aligned} \end{bmatrix}\begin{Bmatrix}\bar{A}\\ \bar{B}\end{Bmatrix} = \begin{Bmatrix}0\\0\end{Bmatrix} \quad (5.29)$$

The non-trivial solution of Eq. (5.29) is obtained by setting to zero the determinant of the matrix of coefficients, which yields the interaction equation given in Eq. (5.6).

5.12 Appendix 5.B: Recovering Interaction Equation for Case 2 (Peak moments Non-coinciding)

From Eqs. (5.4)a-b, by substituting into Eq. (5.20), performing integrations and recalling the definitions $C_{b,T}(\lambda)$ and $M_{\max}(\lambda)$ as given in Eqs. (5.21)b-c, one obtains

$$\bar{\bar{\Pi}} = \bar{A}^2\frac{EI_{y,b}\pi^4}{4L^3} + \bar{B}^2\frac{LM_{u,b}^{\ 2}}{4EI_{y,b}} - \bar{A}\bar{B}\frac{\pi^2 M_{\max}(\lambda)}{2LC_{b,T}(\lambda)} \quad (5.30)$$

Evoking the critical state and putting the resulting equations in a matrix form yields

$$\begin{bmatrix} \dfrac{\pi^2 EI_{y,b}}{L^2} & -\dfrac{M_{\max}(\lambda)}{C_{b,T}(\lambda)} \\ -\dfrac{M_{\max}(\lambda)}{C_{b,T}(\lambda)} & \dfrac{L^2 M_{u,b}{}^2}{\pi^2 EI_{y,b}} \end{bmatrix} \begin{Bmatrix} \bar{A} \\ \bar{B} \end{Bmatrix} = \begin{Bmatrix} 0 \\ 0 \end{Bmatrix} \tag{5.31}$$

By setting to zero the determinant of the matrix of coefficients and solving for $M_{\max}(\lambda)$, one recovers $M_{\max}(\lambda) = \pm C_{b,T}(\lambda) M_{u,b}$, of which the positive root is adopted in Eq. (5.21)a.

5.13 References

Andrade, A. and D. Camotim (2004). "Lateral-torsional buckling of prismatic and tapered thin-walled open beams: assessing the influence of pre-buckling deflections." Steel and Composite Structures **4**(4): 281-301.

ANSI/AISC360 (2016). "Specification for structural steel buildings (ANSI/AISC 360-16)." American Institute of Steel Construction, Chicago-Illinois.

ANSI/AISC360 (2022). "Specification for structural steel buildings (ANSI/AISC 360-22)." American Institute of Steel Construction, Chicago-Illinois.

AS-4100 (2020). "Steel structures. Sydney, Australia."

Bazant, Z. and L. Cedolin (2010). Stability of structures: elastic, inelastic, fracture and damage theories, World Scientific.

Bresser, D., G. Ravenshorst and P. Hoogenboom (2020). "General formulation of equivalent moment factor for elastic lateral torsional buckling of slender rectangular sections and I-sections." Engineering Structures **207**: 110230.

CAN/CSA-S16 (2019). "CSA S16: 19, Design of Steel Structures, Canada." Canadian Standards Association.

Hsu, W. T., D. M. Lue and Y. F. Chen (2012). "Design aid for moment strength of built-up crane runway girders." International Journal of Steel Structures **12**(3): 403-417.

Hsu, W. T., D. M. Lue and B. T. Hsiao (2009). "Numerical approach for torsion properties of built-up runway girders." Journal of Applied Science and Engineering **12**(4): 381-389.

Iranpour, A. and M. Mohareb (2022). Elastic Lateral Torsional Buckling Resistance of Beams Strengthened with Cover Plates under Pre-Existing Loads. CSCE 2022 Annual Conference, Structural Specialty, Whistler, British Columbia, Canada, Canadian Society for Civil Engineering (CSCE).

Iranpour, A. and M. Mohareb (2023). "Elastic Lateral Torsional Buckling of I-Beams Strengthened While under Loading." Journal of Structural Engineering **149**(1): 04022206.

Kitipornchai, S., C. M. Wang and N. S. Trahair (1986). "Buckling of monosymmetric I-beams under moment gradient." Journal of Structural Engineering **112**(4): 781-799.

Liu, Y. and L. Gannon (2009a). "Experimental behavior and strength of steel beams strengthened while under load." Journal of Constructional Steel Research **65**(6): 1346-1354.

Liu, Y. and L. Gannon (2009b). "Finite element study of steel beams reinforced while under load." Engineering Structures **31**(11): 2630-2642.

MacCrimmon, R. (2009). Guide for the Design of Crane-Supporting Steel Structures. Markham, ON, CA, Canadian Institute of Steel Construction.

Machado, S. P. and V. H. Cortínez (2005). "Lateral buckling of thin-walled composite bisymmetric beams with prebuckling and shear deformation." Engineering Structures **27**(8): 1185-1196.

Mohri, F. and M. Potier-Ferry (2006). "Effects of load height application and pre-buckling deflections on lateral buckling of thin-walled beams." Steel and composite structures **6**(5): 401.

Pezeshky, P. and M. Mohareb (2018). "Distortional lateral torsional buckling of beam-columns including pre-buckling deformation effects." Computers & Structures **209**: 93-116.

Pezeshky, P., A. Sahraei, F. Rong, S. Sasibut and M. Mohareb (2020). "Generalization of the Vlasov theory for lateral torsional buckling analysis of built-up monosymmetric assemblies." Engineering Structures **221**: 111055.

Pham, P. V., M. Mohareb and A. Fam (2017). "Elastic Analysis of Steel Beams Strengthened with GFRP Plates Including Preexisting Loading Effects." Journal of Structural Engineering **143**(12): 04017163.

Pi, Y. L. and N. Trahair (1992b). "Prebuckling deflections and lateral buckling. II: applications." Journal of Structural Engineering **118**(11): 2967-2985.

Reichenbach, M. C., Y. Liu, T. A. Helwig and M. D. Engelhardt (2020). "Lateral-Torsional Buckling of Singly Symmetric I-Girders with Stepped Flanges." Journal of Structural Engineering **146**(10): 04020203.

Roberts, T. and Z. Azizian (1983). "Instability of thin walled bars." Journal of Engineering Mechanics **109**(3): 781-794.

Sahraei, A., P. Pezeshky, M. Mohareb and G. Doudak (2018). "Simplified expressions for elastic lateral torsional buckling of wooden beams." Engineering Structures **174**: 229-241.

Slein, R., R. J. Sherman and D. W. White (2022). "Manual Estimation of Elastic Lateral Torsional Buckling Resistance of I-Section Members with Cross-Section Transitions." Journal of Bridge Engineering **27**(10): 04022099.

Trahair, N. S. and S. T. Woolcock (1973). "Effect of major axis curvature on I-beam stability." Journal of the Engineering Mechanics Division **99**(1): 85-98.

Vacharajittiphan, P., S. Woolcock and N. S. Trahair (1974). "Effect of in-plane deformation on lateral buckling." Journal of Structural Mechanics **3**(1): 29-60.

Wang, Y.-q., L. Zong, R.-x. Zhu, X.-y. Liu and Y.-j. Shi (2015). "Behavior of I-section steel beam welding reinforced while under load." Journal of Constructional Steel Research **106**: 278-288.

5.14 Notation

The following symbols are used in this paper:

b_f : Flange width of for unstrengthened section;

b_p : Cover plate width;

C : Coefficient accounting for moment gradient, load height, PBD and pre-strengthening load effects;

C_a , C_b : Moment gradient factors for the pre- and post-strengthening loads;

C_{a-E} , C_{a-US} , C_{a-CA} , C_{a-AS} : Energy-based, ANSI/AISC360 (2022), CAN/CSA-S16 (2019), and AS-4100 (2020) moment gradient factors for the pre-strengthening loads;

C_{b-E} , C_{b-US} , C_{b-CA} , C_{b-AS} : Energy-based, ANSI/AISC360 (2022), CAN/CSA-S16 (2019), and AS-4100 (2020) moment gradient factor for the post-strengthening loads;

C_{b-FEA} : Moment gradient factor predicted by FEA (in the absence of PBD, load height and pre-strengthening load effects);

$C_{h,a}$, $C_{h,b}$ = Load height factors for the pre- and post-strengthening loads;

C_{p1} = Pre-buckling coefficient based on post-strengthening moment distribution;

C_{p2} - C_{p3} = Pre-buckling coefficients capturing interaction between pre- and post-strengthening loads;

$C_{b,T}(\lambda)$: Moment gradient factor due to the total bending moments, in terms of post-strengthening load multiplier λ ;

$C_{b,T-E}(\lambda)$: Energy-based moment gradient factor based on total bending moments;

$C_{w,a}$, $C_{w,b}$ = Warping constants of the unstrengthened and strengthened cross-sections;

d = Overall depth of the unstrengthened section;

E = Young modulus taken as $E = 2\times10^5 MPa$;

F_y = Yield stress taken as $350MPa$;

G = Shear modulus taken as $77\times10^3 MPa$;

h, h_0 = Distance between flange centroids of unstrengthened section (i.e., $h = d - t_F$) and the strengthened section $h_0 \approx h + t_P$;

h_a, h_b = Pre- and post-strengthening load heights (positive when gravity loads act below shear center);

I_{xP} = Moment of inertia about x-axis for each strengthening cover plate;

$I_{x,a}$, $I_{y,a}$ = Moment of inertia about x-axis and y-axis for unstrengthened cross-section;

$I_{x,b}$, $I_{y,b}$ = Moment of inertia about x-axis and y-axis for strengthened cross-section;

i = Cross-section and load identifier ($i = a$ for pre-strengthened $i = b$ for post-strengthened);

J_a, J_b = Saint Venant torsional constants of unstrengthened and strengthened cross-sections;

K_1, K_2, K_3 = Factors capturing pre-strengthening moment distribution, post-strengthening moment distribution, and interaction between pre- and post-strengthening moment distributions;

L = Beam span (taken equal to the unbraced length in all problems investigated in the study);

L_p = ANSI/AISC360 (2022) laterally unbraced length below which LTB does not occur;

L_r = ANSI/AISC360 (2022) threshold unbraced length delineating inelastic LTB from elastic LTB;

M_a, M_b = Pre- and post-strengthening peak moments;

$\tilde{M}_a(z)$, $\tilde{M}_b(z)$ = Pre- and post-strengthening moment functions;

$M_{cr,a}$ = Critical moment of unstrengthened beam based on pre-strengthening load pattern $M_{cr,a} = C_a M_{u,a}$;

M_{cr} = Post-strengthening critical moment $M_{cr} = \lambda M_b$ carried by the beam in addition to the pre-strengthening moment;

$M_{cr-FEA-np}$ = FEA-predicted critical moment in the absence of PBD, load height and pre-strengthening load effects;

M_{cr-FEA} = FEA-predicted critical moment;

$M_{\max}(\lambda)$ = Peak value of total moment $M_{\max}(\lambda) = \max\left[M_T(z,\lambda)\right]$;

M_{n-AISC} = Nominal flexural capacity based on inelastic LTB as estimated by ANSI/AISC360 (2022);

M_p = Plastic flexural resistance of strengthened section $M_p = Z_{x,b} F_y$;

$M_{u,a}$, $M_{u,b}$ = Critical moments of unstrengthened and strengthened beams under uniform moments;

$M_T(z,\lambda)$ = Total bending moment function $M_T(z,\lambda) = \tilde{M}_a(z) + \lambda \tilde{M}_b(z)$;

$M_{1,a}$, $M_{2,a}$, $M_{3,a}$, $M_{\max,a}$ = Absolute values of bending moments at quarter point, midspan, three quarter point, and peak moment within the unbraced length corresponding to pre-strengthening loads;

$M_{1,b}$, $M_{2,b}$, $M_{3,b}$, $M_{\max,b}$ = Absolute values of bending moments at quarter point, midspan, three quarter point, and peak moment within the unbraced length corresponding to post-strengthening loads;

m = Ratio of major moment of inertia of the unstrengthened section to that of the strengthened section;

$m_a(z)$, $m_b(z)$ = Normalized pre- and post-strengthening moment functions [$m_a(z)=\tilde{M}_a(z)/M_a$ and $m_b(z)=\tilde{M}_b(z)/M_b$];

m_{an}, m_{cr}, m_T = Normalized pre-strengthening moment, post-strengthening critical moment, and total moment ratios [$m_{an}=M_a/(C_a M_{u,b})$, $m_{cr}=M_{cr}/(C_b M_{u,b})$ and $m_T=M_{\max}/(C_{b,T} M_{u,b})$];

n = Ratio of minor to major moments of inertia of the strengthened section;

P_a, P_b = Pre- and post-strengthening point loads acting at $z=z_0$ along the span;

P_{cr}, P_{cr-FEA} = Additional post-strengthening point load inducing elastic LTB as estimated by present solution and FEA;

$q_a(z)$, $q_b(z)$ = Pre- and post-strengthening loads;

q_t = Temporary loads applied to straight cover plates to bring them into perfect contact with curved flanges of the curved beam;

R_p = Ratio of critical moment while accounting for PBD to that based on omitting PBD effect;

R_s = Ratio of approximate critical moment (based on $C_{p2}\approx 0.0$ and $C_{p3}\approx 1.0$) to the critical moments based on retaining C_{p2} and C_{p3}.

$r_{y,b}$ = Radius of gyration about y-axis of strengthened cross-section;

$S_{x,b}$ = Elastic section modulus about x-axis of strengthened cross-section;

t_f = Flange thickness of unstrengthened section;

t_p = Cover plate thickness;

t_w = Web thickness;

$U(z)$ = Lateral displacement of shear center axis;

V_a, V_b = Transverse deflection of unstrengthened beam under pre-strengthening loads, and that of strengthened beam under post-strengthening loads;

$V_g(z)$ = Gap between the straight cover plates and the bent unstrengthened beam;

$V_p(\lambda, z)$ = Total pre-buckling transverse deflections at onset of buckling $V_p = V_a + V_r + \lambda V_b$;

$V_r(z)$ = Transverse deflection of unstrengthened system after removal of loads temporarily applied to the strengthening plates;

x, y, z = Coordinates along the lateral, transverse and longitudinal directions;

$Z_{x,b}$ = Plastic section modulus about x-axis for strengthened section;

$\tilde{z}$ = Normalized location of applied point load (or two point loads) $\tilde{z} = z_0/L$;

z_a, z_b = Longitudinal coordinates of pre- and post-strengthening peak moments;

$z_{\max}$ = Longitudinal coordinate of peak total moment;

z_0 = Longitudinal coordinate of applied point load (or two point loads);

α : Rebound coefficient;

$\alpha_{L,a}$, $\alpha_{L,b}$: Load configuration factor for the pre- and post-strengthening;

δ : First variation of argument function;

ϕ_b : Resistance factor for flexure;

λ : Load multiplier to be determined from buckling analysis;

Π : Total potential energy throughout buckling;

Π_L : Additional energy due to work done by the offset of pre- and post-strengthening loads from shear centre;

Π_P : Internal strain energy contribution capturing the pre-buckling deformation effect;

Π_U : Internal strain energy;

Π_V : Destabilizing energy due to work done by loads;

$\theta(z)$: Angle of twist;

Ω : Pre-strengthening moment fraction $\Omega = M_a / M_{cr,a}$;

$(\ )'$, $(\ )''$ = First and second derivative with respect to z ; and

$\overline{(\ )}$, $\overline{\overline{(\ )}}$ = First and second variations of the argument function.

Chapter 6: Variational Principle and Finite Element Formulation for Strengthened Monosymmetric Beams[1]

Abstract

The present study develops a variational principle and finite element (FE) formulation based on the kinematics of thin-walled beam theory to determine the elastic lateral torsional buckling capacity of singly symmetric beams strengthened with cover plate(s) while under loading. The formulation captures the effects of pre-strengthening load and pre-buckling curvature. Comparative analyses with shell models reveal that the proposed solutions reliably predict the post-strengthening critical moments when cross-section distortion is suppressed. Practical recommendations for suppressing distortion are provided. The FE model developed is then used to develop a systematic parametric study to assess the effects of load height, magnitude of pre-strengthening loads, flange dimensions, strengthening cover plate dimensions, beam unbraced length, loading patterns, and boundary conditions on the total elastic critical moment capacity. The study examines the loading conditions under which the magnitude of pre-strengthening loads significantly influences the predicted total critical moments.

Keywords: Lateral torsional buckling, Strengthening, I-beams, Cover plates, Moment gradient, Load height, Pre-buckling deformation, Pre-strengthening loads

6.1 Introduction

Strengthening techniques are crucial in extending the lifespan of existing structures expected to operate under load increases above original design loads. A common strengthening method for existing steel beams is to weld cover plate(s) to the flange(s). In practical situations, it is often

[1] This chapter has been submitted for review and possible publication in an international journal.

impractical to fully unload the beam before implementing the strengthening process. In such cases, the strengthening process needs to take place while the beam is loaded or partially loaded. Strengthening may be undertaken by welding cover plate(s) either to both flanges, or to a single flange, as may be the case when the top flange is inaccessible (e.g., covered by flooring), leaving only the bottom flange accessible for strengthening. In such circumstances, the accurate determination of the lateral torsional buckling (LTB) capacity of the strengthened system would require an elaborate finite element (FE) analysis that models the entire process of pre-strengthening load application, addition of strengthening plates, and post-strengthening load application up to the point of buckling.

Within this context, the current study develops a variational principle and FE formulation that characterizes the resistance of pre-loaded monosymmetric I-shaped beams that are strengthened with cover plates, and subsequently loaded until elastic LTB failure. The formulation captures the effects of pre-strengthening loads and pre-buckling deformation (PBD) induced by the beam strong-axis curvature prior to buckling.

6.2 Literature review

The classical differential equations governing the LTB capacity of monosymmetric I-shaped cross-sections were presented in Vlasov (1961), Trahair (1993), etc. Several researchers (e.g., Anderson and Trahair 1972, and Wang and Kitipornchai Wang and Kitipornchai 1986a) developed a direct solution of the governing differential equations for classical LTB. Other studies (e.g., Wang and Kitipornchai 1986a, Wang and Kitipornchai 1986b, Roberts and Benchiha 1987, Attard 1990, Mohri et al. 2003, Mohammadi et al. 2016) developed energy-based approximate LTB solutions based on the Vlasov theory.

Krajcinovic (1969), Barsoum and Gallagher (1970) and Papangelis et al. (1998) adapted the LTB solution of Vlasov (1961) into a FE context to characterize the elastic LTB capacity of monosymmetric beams with monolithic cross-sections.

The effect of shear deformation on the LTB strength of beams with monosymmetric sections was investigated by Erkmen and Mohareb (2008), Attard and Kim (2010), Erkmen (2014) and Sahraei et al. (2015).

FE solutions that capture the PBD effect on the elastic LTB strength of monosymmetric cross-sections were developed by Attard (1986), and Pi and Trahair (1992a, 1992b).

The above studies omitted the effect of cross-sectional distortion. Thin-walled beam formulations that capture distortional effects in the context of monosymmetric beams include the work of Bradford (1985, 1990), Ma and Hughes (1996), Hughes and Ma (1996), and Pezeshky and Mohareb (2018). Shell FE models investigations of distortional buckling for monosymmetric beams include the work of Helwig et al. (1997), Samanta and Kumar (2006), and Kumar and Samanta (2006). Using Generalized Beam Theory, Schardt (1994), Dinis et al. (2006), and Basaglia and Camotim (2013) investigated the distortional lateral buckling of beams with monosymmetric cross-sections.

A common theme in previous studies is that they focused on the LTB of monolithic beams. In this respect, the LTB of strengthened beams and built-up monosymmetric assemblies were investigated by MacCrimmon (2009), Hsu et al. (2009, 2012), and Pezeshky et al. (2020). Also, Reichenbach et al. (2020) studied the LTB behavior of monosymmetric non-prismatic beams. The above studies did not attempt to capture the effect of loads that may act on the member prior to strengthening. Also, present steel design standards (e.g., CAN/CSA-S16 2019, AS-4100 2020, ANSI/AISC360

2022) are not intended for beams that are strengthened while under load. In this respect, Liu and Gannon (2009a, 2009b) and Wang et al. (2015) experimentally and numerically investigated the LTB capacity of I-beams strengthened while under loading. The studies flagged a concern regarding the potential detrimental effect of pre-strengthening loads on the LTB capacity of strengthened beams.

In this regard, Iranpour and Mohareb (2022, 2023a, 2023b) developed a family of solutions that capture the effect of pre-strengthening loads on elastic LTB capacity of strengthened beams. The solutions developed were limited to beams with doubly symmetric cross-sections that are symmetrically strengthened with identical cover plates connected to both flanges, resulting in a doubly symmetric assembly. In practical situations, however, it is common that only one of the flanges is accessible for strengthening. Within this context, the present study extends past work to tackle the LTB strength of doubly symmetric beams that are unsymmetrically strengthened either with a single cover plate, or two unequal cover plates as well as monosymmetric beams strengthened with a single or two cover plates, while capturing the effects of pre-strengthening loads and PBD.

6.3 Statement of Problem

A prismatic beam with an open cross-section is subjected to transverse loads inducing strong axis bending and no axial loading. The loaded beam is strengthened with one or two cover plates welded to the flange(s) resulting in a strengthened system that is either monosymmetric or doubly symmetric. Additional loads are subsequently applied to the beam so that it buckles in a lateral torsional mode. It is required to determine the magnitude of additional loads that would buckle the strengthened system.

6.4 Assumptions

The assumptions of the formulation are similar to those for symmetrically strengthened beams in Iranpour and Mohareb (2023a), i.e.,

(a) Weld-induced deformations are negligible,

(b) Strains are small, and rotations are moderate,

(c) Pre-buckling response is linear,

(d) Materials are linearly elastic isotropic,

(e) The beam, strengthening plates, and resulting strengthened system follow the kinematics of the Vlasov beam, which omit cross-sectional distortions and shear strains at the middle surface, and those of the Kirchhoff plate theory, which assumes a line normal to the middle surface remains normal after deformation,

(f) The loads remain constant throughout buckling, such that the curvature in the *yz*-plane remains unchanged, i.e., the member buckles in an inextensional mode (e.g., Trahair 1993), and

(g) Before welding, the strengthening plates are assumed to slide relative to the beam flanges in a frictionless manner, and after welding, no relative slip occurs between the plates and the flanges, resulting in a strengthened section that is monolithic.

6.5 Strengthening and Loading Sequence

Fig. 6.1 depicts the strengthening-loading-deformation sequence and Table 6.1 summarizes the loads and corresponding displacements for each step. In Fig. 6.1 and Table 6.1, V denotes the transverse displacement along the *y*-axis, and U is the lateral displacement along the *x*-axis, both defined at the shear centre (SC), while θ is the angle of twist of the section about the longitudinal *z*-axis.

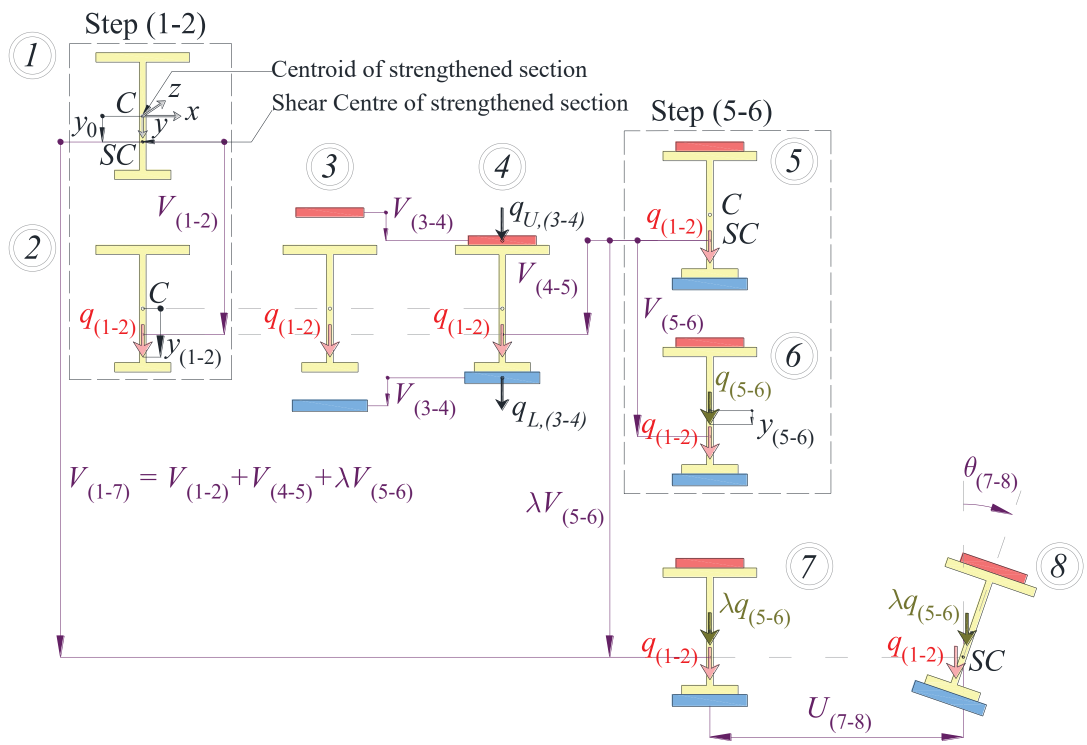

Fig. 6.1 Configurations of strengthening and loading history

Table 6.1 Loads and displacements for each component corresponding to each step

Description	Step	Element	New loads	Total Loads at the end of the step	$U(z)$	$V(z)$	$\theta(z)$
Pre-Buckling Steps (Before Strengthening)	1-2	Beam	$q_{(1-2)}$	$q_{(1-2)}$	0	$V_{(1-2)}$	0
	3-4	Upper Plate	$q_{U,(3-4)}$	$q_{U,(3-4)}$	0	$V_{(3-4)}$	0
		Beam	0	$q_{(1-2)}$	0	0	0
		Lower Plate	$q_{L,(3-4)}$	$q_{L,(3-4)}$	0	$V_{(3-4)}$	0
Pre-Buckling Steps (After Strengthening)	4-5	Non-composite system	$-q_{U,(3-4)} - q_{L,(3-4)}$	$q_{(1-2)}$	0	$V_{(4-5)}$	0
	5-6	Composite system	$q_{(5-6)}$	$q_{(1-2)} + q_{(5-6)}$	0	$V_{(5-6)}$	0
	5-7	Composite system	$\lambda q_{(5-6)}$	$q_{(1-2)} + \lambda q_{(5-6)}$	0	$\lambda V_{(5-6)}$	0
Buckling Step	7-8	Composite system	0	$q_{(1-2)} + \lambda q_{(5-6)}$	$U_{(7-8)}$	0	$\theta_{(7-8)}$

6.5.1 Pre-buckling steps

In going from Configurations 1 to 2 (denoted by Step 1-2), the unstrengthened beam (denoted by subscript *B*, Fig. 6.2a), is subjected to a load $q_{(1-2)}(z)$. This load is positioned at a distance $\left(y_{(1-2)} - y_0\right)$ from the shear centre, with positive values indicating a location below the shear centre.

Upon the application of the load $q_{(1-2)}(z)$, the beam undergoes a transverse deflection $V_{(1-2)}(z)$ to reach Configuration 2. Configuration 3 introduces two initially straight strengthening plates; an upper plate denoted by *U* and a lower plate denoted by *L* (Fig. 6.2a). The gaps $V_{(3-4)}(z)$ between the straight plates and the bent beam flanges along the span are closed through multiple clamps positioned along the span, to facilitate the welding operation. For the upper plate, for example, when the clamps are tightened, the plate undergoes a downward displacement while the beam experiences a slight upward displacement. This adjustment continues until the gap $V_{(3-4)}(z)$ between the plates and the beam is eliminated. Welding is subsequently performed and followed by the removal of the clamps resulting in a strengthened beam.

As a simplification, the process can be simulated in three steps: (1) applying temporary loads $q_{U,(3-4)}(z)$ and $q_{L,(3-4)}(z)$ to the plates until they come into contact with the curved flanges along the span, (2) holding together the strengthening plates against the beam flanges along the normal direction but enabling them to slide relative to one another along the tangential direction, and (3) removing the temporary loads, thus enabling the system to rebound while undergoing displacement $V_{(4-5)}(z)$. Welding is then performed at Configuration 5. Subsequent to weld solidification, the system functions as a monolithic entity. Additional post-strengthening reference loads $q_{(5-6)}$ are then applied at distance $\left(y_{(5-6)} - y_0\right)$ from the shear centre in Step 5-6. When subjected to such loads, the strengthened beam attains a new state of equilibrium at Configuration 6 by undergoing an additional transverse displacement $V_{(5-6)}$. During Step 6-7, the post-strengthening loads are assumed to increase to attain $\lambda q_{(5-6)}$ so that the system attains the state of onset of LTB (Configuration 7), in which λ is an unknown load multiplier to be determined from a buckling analysis. Under the linear pre-buckling response assumption, the transverse displacement proportionally increases to $\lambda V_{(5-6)}(z)$. Thus, at the onset of buckling (Configuration 7), the loads exerted on the system reach $q_{(1-2)} + \lambda q_{(5-6)}$, leading to a transverse displacement of $V_{(1-2)}(z) + V_{(4-5)}(z) + \lambda V_{(5-6)}(z)$.

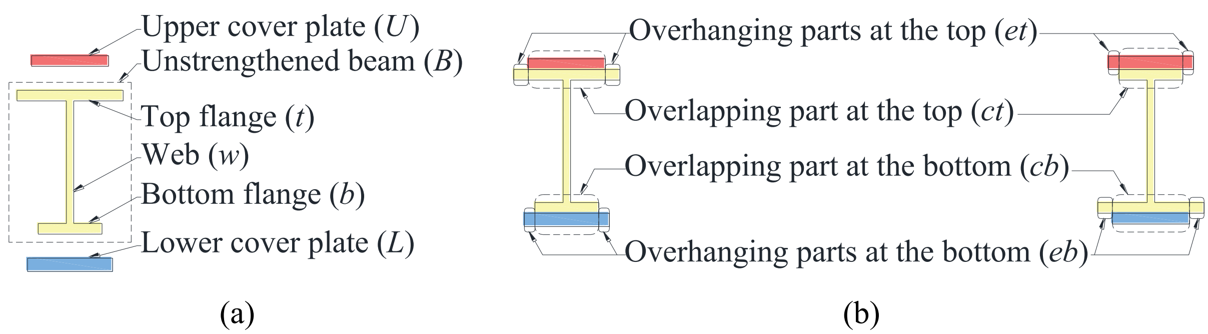

Fig. 6.2 Definitions and notation for (a) Unstrengthened beam; and (b) Strengthened system

6.5.2 Buckling step

In Step 7-8, the strengthened system undergoes LTB. Throughout buckling, the applied loads $q_{(1-2)} + \lambda q_{(5-6)}$ remain unchanged, and the shear centre axis of the strengthened system undergoes a lateral displacement $U_{(7-8)}(z)$ and an angle of twist $\theta_{(7-8)}(z)$. Additionally, a cross-section originally normal to the *z*-axis undergoes a rotation $U'_{(7-8)}(z)$ about the *y*-axis and a warping deformation $\theta'_{(7-8)}(z)$.

6.6 Displacement fields

Fig. 6.3 depicts the coordinate systems (x, y_B, z) for the beam, (x, y_U, z) and (x, y_L, z) for the upper and lower strengthening plates, and (x, y, z) for the whole strengthened system (Fig. 6.3c). The origin O_i for each component is taken to coincide with its own centroid ($i = B$, U, L respectively denote the unstrengthened beam, the upper plate, the lower plate and the absence of subscripts denotes the strengthened system).

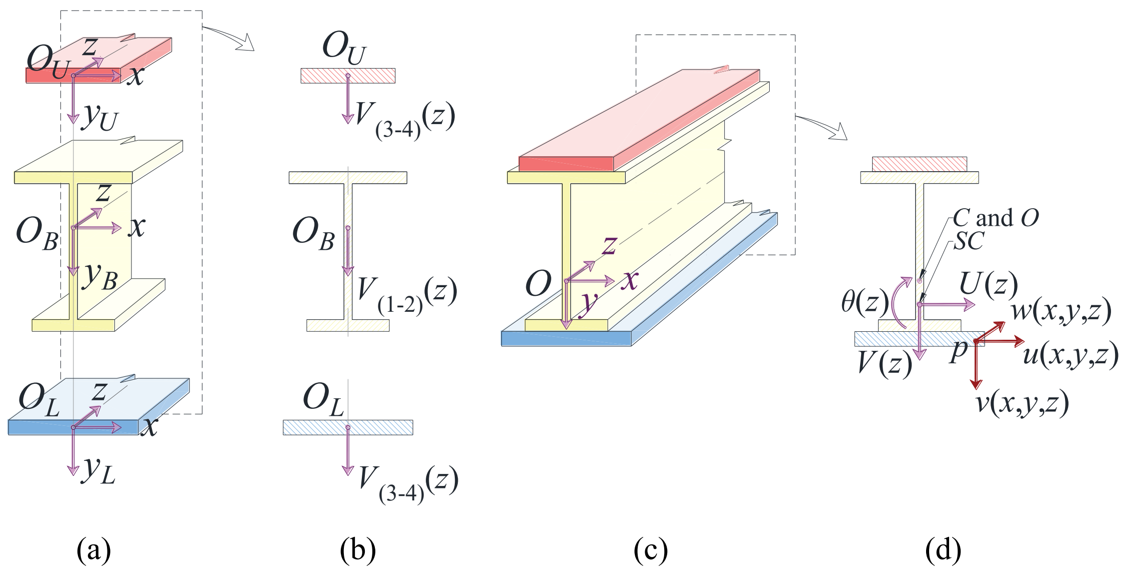

Fig. 6.3 (a) Coordinates of individual components (beam *B*, upper plate *U*, and lower plate *L*) prior to strengthening, (b) Displacements before strengthening, (c) Coordinates of strengthened system and (d) Displacements of strengthened system

Displacements u, v and w for a generic point $p(x, y, z)$ of the strengthened section are related to the displacements $U(z)$ and $V(z)$ of the shear centre axis, and angle of twist $\theta(z)$ as the sum of linear and nonlinear components (e.g., Pi et al. 1992, Pi and Trahair 1992a). In the absence of axial loading, the longitudinal displacement at the beam centroid must vanish throughout buckling, hence,

$$\begin{Bmatrix} u \\ v \\ w \end{Bmatrix} = \begin{Bmatrix} U-(y-y_0)\theta \\ V+x\theta \\ -xU'-yV'-\omega\theta' \end{Bmatrix} + \begin{Bmatrix} -\frac{1}{2}x\theta^2+\left[-\frac{1}{2}x\left(U'^2+U'V'\theta\right)-\frac{1}{2}(y-y_0)\left(U'V'+U'^2\theta\right)-\omega U'\theta'\right] \\ -\frac{1}{2}(y-y_0)\theta^2+\left[-\frac{1}{2}x\left(U'V'+V'^2\theta\right)-\frac{1}{2}(y-y_0)\left(V'^2-U'V'\theta\right)-\omega V'\theta'\right] \\ y\left(U'\theta+\frac{1}{2}V'\theta^2\right)-x\left(V'\theta-\frac{1}{2}U'\theta^2\right)+\frac{1}{2}\omega\theta'\left[V'^2+U'^2\right] \end{Bmatrix} \quad \text{(6.1)a-c}$$

in which the twist of the deformed cross-section axes has been approximated by θ' (Pi et al. 1992), ω is the sectorial coordinate (e.g., Vlasov 1961), and all primes denote differentiation with respect to z. Numerical investigations under the present study indicated that the terms enclosed in square brackets in Eq. (6.1) have a negligible contribution to the results.

6.7 Strain-displacement and stress-strain relations

From Eq. (6.1)a-c, by substituting into the longitudinal strain-displacement relationship $\varepsilon = w' + \left(u'^2+v'^2+w'^2\right)/2$, omitting the term $1/2\left(w'^2\right)$ relative to w' and also omitting the nonlinear strain-displacement contribution (e.g., Trahair 1993) to the shear strain, one obtains,

$$\begin{aligned} \varepsilon = \left(-xU''-yV''-\omega\theta''\right)+\frac{1}{2}\Big\{ & U'^2+V'^2+\left[x^2+(y-y_0)^2\right]\left(\theta'^2+\theta^2\theta'^2\right)+ \\ & -x\left(2V''\theta-U''\theta^2\right)+y\left(2U''\theta+V''\theta^2\right)+2y_0\theta'\left(\theta V'+U'\right)\Big\} \end{aligned} \quad \text{(6.2)a-b}$$

$$\gamma = -2n\theta'$$

in which n is the distance normal to section contour for the point of interest. Eqs. (6.2)a-b are generic and thus applicable for any of the deformed configurations in Fig. 6.1. In pre-buckling steps (1-2) to (5-7), the section undergoes only a transverse deflection V, and hence $U=\theta=0$ which leads to vanishing shear strains and stresses. The longitudinal normal strain is

$\varepsilon_{i,(m-n)} = -y_i V''_{(m-n)} + 0.5 V_i'^2 \approx -y_i V''_{(m-n)}$. Under the linearly elastic isotropic assumption [Assumption (d)], the stress induced within a pre-buckling step $m-n$, is

$$\sigma_{i,(m-n)} \approx -E y_i V''_{(m-n)} \qquad i = B, U, L \tag{6.3}$$

where y_i is the *y*-coordinate taken from the centroid of component i (Fig. 6.3). The expressions for normal and shear strains for all steps are summarized in Table 6.2. In all pre-buckling steps $m-n$, the moment-curvature relationship is obtained by integrating the moments of the stresses as obtained from Eq. (6.3) over the area A_i, i.e.,

$$M_{(m-n)}(z) = \int_{A_i} y_i \sigma_{i,(m-n)}(z)\, dA_i = -E I_{xx-i} V''_{(m-n)}(z), \qquad I_{xx-i} = \int_{A_i} y_i^2\, dA_i \qquad \text{(6.4)a-b}$$

in which $M_{(m-n)}(z)$ is the bending moment, I_{xx-i} is the moment of inertia about the *x*-axis. By equating the curvatures of the plates to those of beam, i.e., $V''_{(1-2)} = V''_{(3-4)}$, one obtains the total temporary bending moment $M_{(3-4)}$ needed to close the gap between the curved beam and the straight plates prior to welding, yielding

$$M_{(3-4)}(z) = \frac{I_{xx-U} + I_{xx-L}}{I_{xx-B}} M_{(1-2)}(z) \tag{6.5}$$

Table 6.2 Expressions for normal and shear strains of each component in each step

Type	Step	Component	Normal Strain	Shear Strain
Pre-Buckling Steps (Before Strengthening)	1-2	Beam	$\varepsilon_{B,(1-2)} = -y_B V''_{(1-2)}$	0
	3-4	Upper Plate	$\varepsilon_{U,(3-4)} = -y_U V''_{(1-2)}$	0
		Beam	0	0
		Lower Plate	$\varepsilon_{L,(3-4)} = -y_L V''_{(1-2)}$	0
Pre-Buckling Steps (After Strengthening)	4-5	Upper Plate	$\varepsilon_{U,(4-5)} = -y_U V''_{(4-5)}$	0
		Beam	$\varepsilon_{B,(4-5)} = -y_B V''_{(4-5)}$	0
		Lower Plate	$\varepsilon_{L,(4-5)} = -y_L V''_{(4-5)}$	0
	5-6	Composite system	$\varepsilon_{(5-6)} = -y V''_{(5-6)}$	0
	5-7	Composite system	$\lambda \varepsilon_{(5-6)}$	0
Buckling Step	7-8	Composite system	Eq. (6.11)a	$\gamma_{(7-8)} = -2n\theta'_{(7-8)}$

In Step 4-5, the temporary loads applied to the plates in the previous step are removed and the non-composite assembly undergoes an upward rebound deflection $V_{(4-5)}(z)$. The corresponding rebound curvature $V''_{(4-5)}$ is obtained by applying $-M_{(3-4)}(z)$ to the system. Given that $V''_{(1-2)} = V''_{(3-4)}$, one obtains

$$V''_{(4-5)}(z) = -\frac{I_{xx-U} + I_{xx-L}}{I_{xx-B} + I_{xx-U} + I_{xx-L}} V''_{(1-2)}(z) \tag{6.6}$$

The stresses $\sigma_{i,(4-5)} = -Ey_i V''_{(4-5)}$ corresponding to Step 4-5 are determined for the upper plate ($i = U$), the lower plate ($i = L$) and the unstrengthened beam ($i = B$). By summing $\sigma_{i,(4-5)}$ to the stresses $\sigma_{B,(1-2)} = -Ey_B V''_{(1-2)}$ corresponding to Step 1-2, and those of Step 3-4 ($\sigma_{U,(3-4)} = -Ey_U V''_{(1-2)}$ and $\sigma_{L,(3-4)} = -Ey_L V''_{(1-2)}$), and recalling that $V''_{(1-2)} = -M_{(1-2)}(z)/EI_{xx-B}$, the total normal stress $\sigma_{(1-5)}$ at Configuration 5 is found to be

$$\sigma_{(1-5)}(z) = -E\left(V''_{(1-2)} + V''_{(4-5)}\right)\begin{cases} y_U \\ y_B \\ y_L \end{cases} = \alpha \frac{M_{(1-2)}(z)}{I_{xx-B}} \begin{cases} y_U & -t_U/2 \le y_U \le t_U/2 \\ y_B & -d/2 \le y_B \le d/2 \\ y_L & -t_L/2 \le y_L \le t_L/2 \end{cases} \quad \text{(6.7)a-c}$$

in which t_U and t_L are the thicknesses of upper and lower plates, d is the overall depth of the unstrengthened beam and

$$\alpha = 1 - \frac{I_{xx-U} + I_{xx-L}}{I_{xx-B} + I_{xx-U} + I_{xx-L}} \quad (6.8)$$

Eqs. (6.7)a-c is rewritten based on a unified coordinate system with an origin located at the centroid of strengthened cross-section as

$$\sigma_{(1-5)}(z) = \alpha \frac{M_{(1-2)}}{I_{xx-B}} \begin{cases} y - y_{CU} & y_{CU} - t_U/2 \le y \le y_{CU} + t_U/2 \\ y - y_{CB} & y_{CU} + t_U/2 \le y \le y_{CL} - t_L/2 \\ y - y_{CL} & y_{CL} - t_L/2 \le y \le y_{CL} + t_L/2 \end{cases} \quad \text{(6.9)a-c}$$

in which y_{CB}, y_{CU} and y_{CL} are the centroid coordinates of unstrengthened beam, upper plate and lower plate measured from the centroid of the strengthened section.

From Eqs. (6.3) and (6.4)a, the additional stresses induced in Step 5-6 are

$$\sigma_{(5-6)}(z) = -EyV''_{(5-6)}(z) = \frac{M_{(5-6)}(z)}{I_{xx}} y \quad (6.10)$$

Throughout Step 5-7, the curvature increases linearly with the applied loads to $\lambda V''_{(5-6)}$ [Assumption (c)]. Hence, the corresponding stress is $\sigma_{(5-7)} = \lambda\sigma_{(5-6)} = \lambda M_{(5-6)}(z)\, y / I_{xx}$.

The additional strains $\varepsilon_{(7-8)}, \gamma_{(7-8)}$ induced throughout buckling Step 7-8 are obtained by deducting the total strains at the onset of buckling $\varepsilon_{(1-7)}, \gamma_{(1-7)}$ from the total strain at the buckled configuration $\varepsilon_{(1-8)}, \gamma_{(1-8)}$ yielding

$$\varepsilon_{(7-8)}=\left(-xU''_{(7-8)}-\omega\theta''_{(7-8)}\right)+\frac{1}{2}\left\{U'^{\,2}_{(7-8)}+\left[x^2+\left(y-y_0\right)^2\right]\left(\theta'^{\,2}_{(7-8)}+\theta^{2}_{(7-8)}\theta'^{\,2}_{(7-8)}\right)\right.$$
$$\left.-x\left(2V''_{(1-7)}\theta_{(7-8)}-U''_{(7-8)}\theta^{2}_{(7-8)}\right)+y\left(2U''_{(7-8)}\theta_{(7-8)}+V''_{(1-7)}\theta^{2}_{(7-8)}\right)+2y_0\theta'_{(7-8)}\left(\theta_{(7-8)}V'_{(1-7)}+U'_{(7-8)}\right)\right\}$$
$$\gamma_{(7-8)}=-2n\theta'_{(7-8)}$$

(6.11)a-b

6.8 Variational principles

The purpose of pre-buckling analyses is to determine the bending moment distributions $M_{(1-2)}\left(z\right)$ and $M_{(5-6)}\left(z\right)$, which are related to the transverse displacements $V_{(1-2)}\left(z\right)$ and $V_{(5-6)}\left(z\right)$ [Eq. (6.4) a]. The total potential energy $\Pi_{(1-2)}$ for Step 1-2 is given by

$$\Pi_{(1-2)}\left(V_{(1-2)},V''_{(1-2)}\right)=\frac{1}{2}\int_L\int_{A_B}\sigma_{B,(1-2)}\,\varepsilon_{B,(1-2)}dA_B\,dz-\int_L q_{(1-2)}\left(z\right)V_{(1-2)}\left(z\right)dz \tag{6.12}$$

in which A_B is the unstrengthened beam cross-sectional area. From the expressions of $\sigma_{B,(1-2)}$ and $\varepsilon_{B,(1-2)}$ in Eq. (6.3) and Table 6.2, by substituting into Eq. (6.12), recalling Eq. (6.4)b and setting to zero the first variation of the total potential energy, one obtains

$$\bar{\Pi}_{(1-2)}\left(V''_{(1-2)},\bar{V}_{(1-2)},\bar{V}''_{(1-2)}\right)=\int_L EI_{xx-B}V''_{(1-2)}\bar{V}''_{(1-2)}dz-\int_L q_{(1-2)}\left(z\right)\bar{V}_{(1-2)}\left(z\right)dz=0 \tag{6.13}$$

in which the overbar $\overline{(\ )}$ denotes the first variation of the argument function. The change in total potential energy $\Pi_{(5-6)}$ throughout Step 5-6 is given by

$$\begin{aligned}\Pi_{(5-6)}\left(V_{(5-6)},V''_{(5-6)}\right)=&\frac{1}{2}\int_L\int_A\sigma_{(5-6)}\,\varepsilon_{(5-6)}dA\,dz-\int_L q_{(5-6)}\left(z\right)V_{(5-6)}\left(z\right)dz\\&+\left[\int_L\int_A\sigma_{(1-5)}\,\varepsilon_{(5-6)}dA\,dz-\int_L q_{(1-2)}\left(z\right)V_{(5-6)}\left(z\right)dz\right]\end{aligned} \tag{6.14}$$

From the expressions of $\sigma_{(5-6)}$ in Eq. (6.3) and $\varepsilon_{(5-6)}$ in Table 6.2, by substituting into Eq. (6.14), setting to zero the variation of the total potential energy $\Pi_{(5-6)}$ and recalling that $\sigma_{(1-5)}$ remains constant throughout the variation, one recovers the equilibrium condition

$$\overline{\Pi}_{(5-6)}\left(V''_{(5-6)},\bar{V}_{(5-6)},\bar{V}''_{(5-6)}\right)=\int_L EI_{xx}V''_{(5-6)}\bar{V}''_{(5-6)}\,dz-\int_L q_{(5-6)}\left(z\right)\bar{V}_{(5-6)}\left(z\right)dz=0 \tag{6.15}$$

Equations (6.13) and (6.15) characterize the pre-buckling equilibrium configurations $V_{(1-2)}\left(z\right)$ and $V_{(5-6)}\left(z\right)$ and the corresponding bending moments.

For the buckling step, the total potential energy is given by

$$\begin{aligned}\Pi_{(7-8)}=&\frac{1}{2}\int_L\int_A\left[E\varepsilon_{(7-8)}{}^2+G\gamma_{(7-8)}{}^2\right]dAdz+\int_L\int_A\left[\left(\sigma_{(1-5)}+\lambda\sigma_{(5-6)}\right)\varepsilon_{(7-8)}\right]dAdz\\&+\frac{1}{2}\int_L\left[q_{(1-2)}\left(y_{(1-2)}-y_0\right)+\lambda q_{(5-6)}\left(y_{(5-6)}-y_0\right)\right]\theta_{(7-8)}\left(z\right)^2\,dz\end{aligned} \tag{6.16}$$

From the expressions for $\sigma_{(1-5)}$, $\sigma_{(5-6)}$, $\varepsilon_{(7-8)}$ and $\gamma_{(7-8)}$ in Eqs. (6.9)-(6.11), by substituting into Eq. (6.16), the total potential energy $\Pi_{(7-8)}$ is expressed in terms of the buckling displacements $U'_{(7-8)},U''_{(7-8)},\theta_{(7-8)},\theta'_{(7-8)}$ and $\theta''_{(7-8)}$ and pre-buckling curvature $V''_{(1-7)}$. Performing the area integrals, and noting the relationships

$$\begin{aligned}&\int_A y dA=\int_A \omega x dA=\int_A y_{Ci}\,dA=0\\&I_{xx}=\int_A y^2dA,\quad I_{yy}=\int_A x^2dA,\quad C_w=\int_A\omega^2dA,\quad J=\int_A 4n^2dA\\&I_{px}=\int_A y(x^2+y^2)dA=I_{px-B}+\sum_{i=U,L,B}\left[y_{Ci}\left(3I_{xx-i}+I_{yy-i}+A_iy_{Ci}{}^2\right)\right]\\&\tilde{I}_{px}=\sum_{i=U,L,B}\left[\int_{A_i}y_{Ci}\left(x^2+y^2\right)dA\right]=\sum_{i=U,L,B}\left[y_{Ci}\left(I_{yy-i}+I_{xx-i}+A_iy_{Ci}{}^2\right)\right]\end{aligned} \tag{6.17)a-i (}$$

and recalling that, at the neutral stability state (Configuration 7 in Fig. 6.1), the second variation of the total potential energy $\overline{\overline{\Pi}}_{(7-8)}$ must vanish throughout buckling, one obtains

$$\begin{aligned}
\bar{\bar{\Pi}}_{(7-8)} &= \frac{1}{2}\int_L \Big[EI_{yy}\overline{U''}_{(7-8)}(z)^2 + EC_w\overline{\theta''}_{(7-8)}(z)^2 + GJ\overline{\theta'}_{(7-8)}(z)^2 \Big] dz \\
&+ \int_L \Big[EI_{yy}V''_{(1-7)}(\lambda,z) + M_{(1-2)}(z) + \lambda M_{(5-6)}(z) \Big] \bar{\theta}_{(7-8)}(z)\overline{U''}_{(7-8)}(z)\,dz \\
&+ \frac{1}{2}\int_L \Big[EI_{yy}V''_{(1-7)}(\lambda,z) + M_{(1-2)}(z) + \lambda M_{(5-6)}(z) \Big] V''_{(1-7)}(\lambda,z)\bar{\theta}_{(7-8)}(z)^2\,dz \\
&+ \frac{1}{2}\int_L \Big[q_{(1-2)}\big(y_{(1-2)} - y_0\big) + \lambda q_{(5-6)}\big(y_{(5-6)} - y_0\big) \Big] \bar{\theta}_{(7-8)}(z)^2\,dz \\
&+ \frac{1}{2}\int_L \Big[\tilde{\beta} M_{(1-2)}(z) + \beta\lambda M_{(5-6)}(z) \Big] \bar{\theta}'^{\,2}_{(7-8)}\,dz = 0
\end{aligned} \tag{6.18}$$

in which pre-buckling curvature $V''_{(1-7)}$ is given by

$$V''_{(1-7)}(\lambda,z) = V''_{(1-2)}(z) + V''_{(4-5)}(z) + \lambda V''_{(5-6)}(z) = -\left(\frac{\alpha M_{(1-2)}(z)}{EI_{xx-B}} + \frac{\lambda M_{(5-6)}(z)}{EI_{xx}} \right) \tag{6.19}$$

and the monosymmetry parameters are

$$\beta = \frac{I_{px}}{I_{xx}} - 2y_0 \tag{6.20}$$

$$\tilde{\beta} = \alpha\frac{\left(I_{px} - \tilde{I}_{px}\right)}{I_{xx-B}} - 2y_0 \tag{6.21}$$

As a matter of notation, $\overline{\overline{(\ )}}$ denotes the second variation of the argument functions. The first bracketed term in Eq. (6.18) represents the additional internal strain energy stored during buckling, the expressions including $M_{(1-2)}(z)$ and $M_{(5-6)}(z)$ represent the work done by the loads, the terms including β and $\tilde{\beta}$ represent the effect of cross-section asymmetry while the expressions including $\left(y_{(1-2)} - y_0\right)$ and $\left(y_{(5-6)} - y_0\right)$ represent the effect of load heights.

6.8.1 Verification for Special Cases

By omitting the monosymmetric parameters β and $\tilde{\beta}$, the variational principle in Eq. (6.18) reduces to that of doubly symmetric beams in Iranpour and Mohareb (2023a). Furthermore, by omitting the terms involving $M_{(1-2)}$ and $q_{(1-2)}$ related to the effects of pre-strengthening loads and pre-buckling curvature $V''_{(1-7)}$ while retaining the monosymmetric parameter β, the variational principle reduces to that of LTB of monosymmetric assemblies discarding PBD effects as reported in Pezeshky et al. (2020).

6.9 Finite element formulation

6.9.1 Pre-buckling analyses

The two pre-buckling bending moments $M_{(1-2)}(z)$ and $M_{(5-6)}(z)$ appearing in Eq. (6.18) are determined from separate pre-buckling analyses based on the conventional two-node Euler Bernoulli element. Moments $M_{(1-2)}(z)$ correspond to the pre-strengthening loads $q_{(1-2)}$ acting on the unstrengthened beam with moment of inertia I_{xx-B} while moments $M_{(5-6)}(z)$ correspond to the post-strengthening/pre-buckling loads $q_{(5-6)}$ acting on the strengthened beam with moment of inertia I_{xx}. Each analysis yields end bending moments $M_{1(m-n)}$ and $M_{2(m-n)}$. Linear interpolation is then adopted over the element length L_e to recover the moment $M(z) = -M_{1(m-n)}(1 - z/L_e) + M_{2(m-n)}(z/L_e)$ at section z.

6.9.2 Buckling analysis

A two-node beam element with four buckling degrees of freedom per node (Fig. 6.4) is developed based on the variational principle in Eq. (6.18).

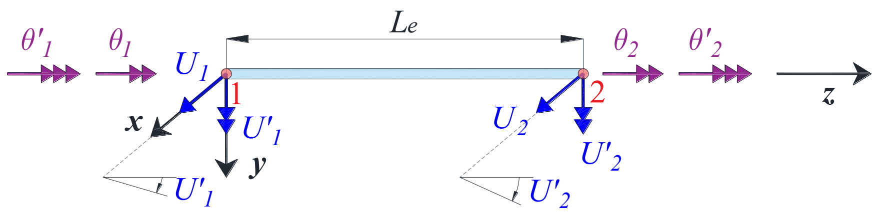

Fig. 6.4 Degrees of freedom of the buckling element

The first variation $\bar{U}(z)$ and $\bar{\theta}(z)$ of displacement functions are related to the vector of nodal degrees of freedom $\mathbf{d}^{\mathbf{T}} = \langle U_1 \quad U_1' \quad U_2 \quad U_2' \quad \theta_1 \quad \theta_1' \quad \theta_2 \quad \theta_2' \rangle$ through

$$\bar{U}(z) = \mathbf{H_U}^{\mathbf{T}}\bar{\mathbf{d}},\ \bar{\theta}(z) = \mathbf{H_\theta}^{\mathbf{T}}\bar{\mathbf{d}} \tag{6.22)a-b}$$

in which the vectors of shape functions are defined by

$$\begin{aligned} &\mathbf{H_U}^{\mathbf{T}} = \mathbf{H_U}^{\mathbf{T}}(z) = \langle H_1 \quad H_2 \quad H_3 \quad H_4 \quad 0 \quad 0 \quad 0 \quad 0 \rangle \\ &\mathbf{H_\theta}^{\mathbf{T}} = \mathbf{H_\theta}^{\mathbf{T}}(z) = \langle 0 \quad 0 \quad 0 \quad 0 \quad H_1 \quad H_2 \quad H_3 \quad H_4 \rangle \\ &\langle H_1,\, H_2,\, H_3,\, H_4 \rangle = \left\langle 1 - 3\zeta^2 + 2\zeta^3,\ L_e\zeta(1-\zeta)^2,\ 3\zeta^2 - 2\zeta^3,\ L_e\zeta^2(\zeta - 1) \right\rangle,\ \zeta = z/L_e \end{aligned} \tag{6.23)a-d}$$

From Eqs. (6.22)a-b, by substituting into the variational principle in Eq. (6.18) and evoking the stationarity conditions $\left(\partial\bar{\bar{\Pi}}/\partial\bar{\mathbf{d}}\right)\delta\bar{\mathbf{d}} = 0$, one obtains the quadratic eigenvalue problem

$$\left(\mathbf{k_E} + \lambda\mathbf{k_{G1}} + \lambda^2\mathbf{k_{G2}}\right)_{8\times8}\bar{\mathbf{d}}_{8\times1} = \mathbf{0}_{8\times1} \tag{6.24}$$

in which the elastic matrix $\mathbf{k_E} = \mathbf{k_{E\text{-}a}} + \mathbf{k_{E\text{-}b}} + \mathbf{k_{E\text{-}c}}$ consists of the conventional elastic matrix $\mathbf{k_{E\text{-}a}}$

$$\mathbf{k_{E\text{-}a}} = \int_{L_e}\left[EI_{yy}\mathbf{H_U''}\mathbf{H_U''}^{\mathbf{T}} + EC_w\mathbf{H_\theta''}\mathbf{H_\theta''}^{\mathbf{T}} + GJ\mathbf{H_\theta'}\mathbf{H_\theta'}^{\mathbf{T}}\right]dz \tag{6.25}$$

and $\mathbf{k_{E\text{-}b}}$ reflects the combined effects of pre-strengthening loads and their PBD effects, and is defined by

$$\mathbf{k_{E\text{-}b}} = \int_{L_e}\left[\frac{\alpha M_{(1-2)}(z)^2}{EI_{xx-B}}\left(\frac{\alpha I_{yy}}{I_{xx-B}} - 1\right)\mathbf{H_\theta}\mathbf{H_\theta}^{\mathbf{T}} - M_{(1-2)}(z)\frac{\alpha I_{yy}}{I_{xx-B}}\left(\mathbf{H_\theta}\mathbf{H_U''}^{\mathbf{T}} + \mathbf{H_U''}\mathbf{H_\theta}^{\mathbf{T}}\right)\right]dz \tag{6.26}$$

and $\mathbf{k}_{\mathbf{E\text{-}c}}$ represents the effect of pre-strengthening loads and is given by

$$\mathbf{k}_{\mathbf{E\text{-}c}} = \int_{L_e} M_{(1-2)}(z)\left(\mathbf{H}_{\boldsymbol{\theta}}\mathbf{H}_{\mathbf{U}}''^{\mathbf{T}} + \mathbf{H}_{\mathbf{U}}''\mathbf{H}_{\boldsymbol{\theta}}^{\mathbf{T}}\right) + q_{(1-2)}\left(y_{(1-2)} - y_0\right)\mathbf{H}_{\boldsymbol{\theta}}\mathbf{H}_{\boldsymbol{\theta}}^{\mathbf{T}} + \tilde{\beta}M_{(1-2)}(z)\mathbf{H}_{\boldsymbol{\theta}}'\mathbf{H}_{\boldsymbol{\theta}}'^{\mathbf{T}}\, dz \qquad (6.27)$$

Also, in Eq. (6.24), the geometric stiffness matrix $\mathbf{k}_{\mathbf{G1}} = \mathbf{k}_{\mathbf{G1\text{-}a}} + \mathbf{k}_{\mathbf{G1\text{-}b}} + \mathbf{k}_{\mathbf{G1\text{-}c}}$ consists of a destabilizing matrix due to the post-strengthening loads (akin to the conventional LTB destabilizing matrix for monosymmetric cross-sections)

$$\mathbf{k}_{\mathbf{G1\text{-}a}} = \int_{L_e} M_{(5-6)}(z)\left(\mathbf{H}_{\boldsymbol{\theta}}\mathbf{H}_{\mathbf{U}}''^{\mathbf{T}} + \mathbf{H}_{\mathbf{U}}''\mathbf{H}_{\boldsymbol{\theta}}^{\mathbf{T}}\right) + q_{(5-6)}\left(y_{(5-6)} - y_0\right)\mathbf{H}_{\boldsymbol{\theta}}\mathbf{H}_{\boldsymbol{\theta}}^{\mathbf{T}} + \beta M_{(5-6)}(z)\mathbf{H}_{\boldsymbol{\theta}}'\mathbf{H}_{\boldsymbol{\theta}}'^{\mathbf{T}}\, dz \qquad (6.28)$$

and $\mathbf{k}_{\mathbf{G1\text{-}b}}$ represents the PBD effects related to the post-strengthening loads and is given by

$$\mathbf{k}_{\mathbf{G1\text{-}b}} = -\int_{L_e} \frac{I_{yy}}{I_{xx}} M_{(5-6)}(z)\left(\mathbf{H}_{\boldsymbol{\theta}}\mathbf{H}_{\mathbf{U}}''^{\mathbf{T}} + \mathbf{H}_{\mathbf{U}}''\mathbf{H}_{\boldsymbol{\theta}}^{\mathbf{T}}\right) dz \qquad (6.29)$$

and $\mathbf{k}_{\mathbf{G1\text{-}c}}$ is an additional matrix that captures the interaction between the pre-strengthening loads and PBD effects associated with the pre-and post-strengthening loads, defined by

$$\mathbf{k}_{\mathbf{G1\text{-}c}} = \int_{L_e} \frac{M_{(1-2)}(z)M_{(5-6)}(z)}{EI_{xx-B}}\left(\frac{2\alpha I_{yy}}{I_{xx}} - \alpha - \frac{I_{xx-B}}{I_{xx}}\right)\mathbf{H}_{\boldsymbol{\theta}}\mathbf{H}_{\boldsymbol{\theta}}^{\mathbf{T}}\, dz \qquad (6.30)$$

In Eq. (6.24), $\mathbf{k}_{\mathbf{G2}}$ accounts for the effect of PBD due to post-strengthening loads and is defined by

$$\mathbf{k}_{\mathbf{G2}} = -\int_{L_e} \frac{M_{(5-6)}(z)^2}{EI_{xx}}\left(1 - \frac{I_{yy}}{I_{xx}}\right)\mathbf{H}_{\boldsymbol{\theta}}\mathbf{H}_{\boldsymbol{\theta}}^{\mathbf{T}} dz \qquad (6.31)$$

6.10 Verification

A $6m$ span monosymmetric beam is considered, in which the overall depth d of the section is $360mm$, web thickness $t_w = 6mm$, top flange width and thickness are $b_t = 100mm$ and $t_t = 10mm$, and bottom flange width and thickness are $b_b = 140mm$ and $t_b = 10mm$ as a reference case. The beam is simply supported relative to transverse and lateral displacements and relative to twist. Young modulus is taken as $E = 2\times10^5 MPa$ and the shear modulus is taken as $G = 77\times10^3 MPa$. Prior to strengthening, the reference beam is subjected to uniformly distributed transverse load (UDL) applied at the shear centre (of the strengthened section) that induces a peak moment corresponding to a specified fraction $\Omega = 80\%$ of the critical moment M_{cr-B} of the unstrengthened beam due to pre-strengthening loads as determined from the ANSI/AISC360 (2022) provisions

$$M_{cr-B} = C_B \frac{\pi^2 EI_{yy-B}}{L^2}\left[\frac{\beta_B}{2} + \sqrt{\left(\frac{\beta_B}{2}\right)^2 + \frac{C_{w-B}}{I_{yy-B}}\left(1+0.039\frac{J_B}{C_{w-B}}L^2\right)}\right]$$
$$C_B = \frac{12.5M_{\max-B}}{2.5M_{\max-B}+3M_{1-B}+4M_{2-B}+3M_{3-B}} \qquad (6.32)\text{a-b}$$

in which C_B is the moment gradient factor corresponding to the pre-strengthening loads and $M_{\max-B}$, M_{1-B}, M_{2-B} and M_{3-B} are the absolute values of peak moment, the quarter point, midspan, and third-quarter point moments of the unbraced length corresponding to the pre-strengthening loads. The beam is then strengthened by welding a cover plate $b_L \times t_L = 120mm\times15mm$ connected to the bottom flange. The strengthened beam is subsequently subjected to additional UDL applied at the shear centre of the strengthened section. According to ANSI/AISC360 (2022), the capacity of unstrengthened and strengthened beams would be based on an elastic LTB mode of failure in cases where either flanges are under compression based on assumed yield strength of 350MPa.

6.10.1 Description of present model

A mesh study indicated that convergence is attained in the present model when 8 to 12 elements are taken along the span, depending on the loading case. Thus, all runs were modeled using 12 elements. The location of shear centre y_0, warping constant C_w and Saint-Venant torsional constant J are computed by assuming full shear transfer at the plate-flange interface (in a manner consistent with the Abaqus models as will be described subsequently), i.e., the strengthened section was considered to act as a monolithic entity. In this case, y_0 is given by

$$y_0 = \frac{1}{I_{y,b}}\left[I_{yt}y_{Ct} + I_{yb}y_{Cb} + I_{yU}y_{CU} + I_{yL}y_{CL} + A_L A_b\left(b_b^{\,2} - b_L^{\,2}\right)/\left(8b_{mb}\right) + A_U A_t\left(b_U^{\,2} - b_t^{\,2}\right)/\left(8b_{mt}\right)\right] \tag{6.33}$$

in which y_{Ct}, y_{Cb}, y_{CU} and y_{CL} denote the coordinates of centroid of the top flange, bottom flange, upper plate, and lower plate (measured from the centroid of strengthened cross-section), the area of top flange $A_t = b_t t_t$, area of bottom flange $A_b = b_b t_b$, area of upper plate $A_U = b_U t_U$, area of lower plate $A_L = b_L t_L$, maximum width at the top $b_{mt} = \max\left(b_t, b_U\right)$, maximum width at the bottom $b_{mb} = \max\left(b_b, b_L\right)$, and *y*-axis moment of inertias for the top flange, bottom flange, upper plate and lower plate are given by

$$I_{yt} = \frac{t_t b_t^{\,3}}{12}, \qquad I_{yb} = \frac{t_b b_b^{\,3}}{12}, \qquad I_{yU} = \frac{t_U b_U^{\,3}}{12}, \qquad I_{yL} = \frac{t_L b_L^{\,3}}{12} \tag{6.34a-d}$$

By omitting the negligible effect of local warping, the global warping constant $C_w = \int_A \omega^2 dA$ is given by

$$C_w = \sum_{i=ct,cb,et \text{ and } eb} I_{yi}h_i^2 = I_{yct}h_{ct}^{\,2} + I_{ycb}h_{cb}^{\,2} + I_{yet}h_{et}^{\,2} + I_{yeb}h_{eb}^{\,2} \tag{6.35}$$

in which

$$I_{yct} = \frac{t_{ct}b_{ct}^{\,3}}{12}, \quad I_{ycb} = \frac{t_{cb}b_{cb}^{\,3}}{12}, \quad I_{yet} = \frac{t_{et}}{12}\left[\left(b_{vt} + b_{et}\right)^3 - b_{vt}^{\,3}\right], \quad I_{yeb} = \frac{t_{eb}}{12}\left[\left(b_{vb} + b_{eb}\right)^3 - b_{vb}^{\,3}\right]$$

$$h_{ct} = h_{et} + t_{vt}/2, \qquad h_{cb} = h_{eb} + t_{vb}/2, \qquad h_{et} = \begin{cases} h_t & b_U \le b_t \\ h_U & b_U > b_t \end{cases}, \; h_{eb} = \begin{cases} h_b & b_L \le b_b \\ h_L & b_L > b_b \end{cases} \tag{6.36a-h}$$

where h_t, h_b, h_U and h_L represent the absolute distance between shear centre of the strengthened section and the centroid of the top flange, bottom flange, upper plate and lower plate, and

$$b_{ct} = \min(b_U, b_t), \qquad b_{cb} = \min(b_L, b_b), \qquad t_{ct} = t_t + t_U, \qquad t_{cb} = t_b + t_L$$
$$b_{et} = |b_U - b_t|, \qquad b_{eb} = |b_L - b_b|, \qquad t_{et} = \begin{cases} t_t & b_U \le b_t \\ t_U & b_U > b_t \end{cases}, \quad t_{eb} = \begin{cases} t_b & b_L \le b_b \\ t_L & b_L > b_b \end{cases}$$
$$b_{vt} = \frac{b_{ct}}{2h_{et}}(2h_{ct} + t_{vt}), \quad b_{vb} = \frac{b_{cb}}{2h_{eb}}(2h_{cb} + t_{vb}), \quad t_{vt} = \begin{cases} t_U & b_U \le b_t \\ -t_t & b_U > b_t \end{cases}, \quad t_{vb} = \begin{cases} t_L & b_L \le b_b \\ -t_b & b_L > b_b \end{cases}$$

(6.37)a-l

The widths b_{ct}, b_{cb} and thicknesses t_{ct}, t_{cb} of the overlapping parts and those of the overhanging parts b_{et}, b_{eb}, and t_{et}, t_{eb} are shown on Fig. 6.5. The figure also depicts the absolute values of the distances h_{et} and h_{eb} between shear centre of the strengthened section and the centroid of overhanging parts at the top and bottom of the cross-section.

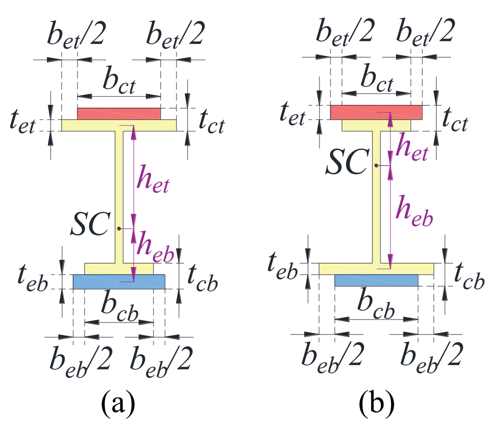

Fig. 6.5 Overlapping and overhanging dimensions for (a) $b_U < b_t$, $b_L > b_b$; and (b) $b_U > b_t$, $b_L < b_b$

The Saint Venant torsional constant J is given by

$$J = \sum_{i=w,ct,cb,et,eb} k_i b_i t_i^3 = k_w h t_w^3 + k_{ct} b_{ct} t_{ct}^3 + k_{cb} b_{cb} t_{cb}^3 + k_{et} b_{et} t_{et}^3 + k_{eb} b_{eb} t_{eb}^3$$
$$k_i = \frac{1}{3}\left[1 - \frac{192 t_i}{\pi^5 b_i} \sum_{k=1,3,5,\ldots}^{\infty} \frac{1}{k^5} \tanh\left(\frac{k\pi b_i}{2t_i}\right)\right] \approx \frac{1}{3}\left[1 - \frac{192 t_i}{\pi^5 b_i} \tanh\left(\frac{\pi b_i}{2t_i}\right)\right] \qquad (6.38)\text{a-b}$$

in which $i = w$ for the web, $i = ct$ for the overlapping width between the top flange and upper cover plate, $i = cb$ for the overlapping width between the bottom flange and lower cover plate, $i = et$ and eb for the overhanging width at the top and bottom of the cross-section (Fig. 6.2b), and $b_w = h$ is the distance between the flange centroids.

By omitting the shear transfer at the flange-plate interface, the plates would be considered as separate cross-sections from the I-beam. The predictive equations for y_0, J and C_w for the built-up section in this case are found to coincide with the solution of Pezeshky et al. (2020), i.e.,

$$
\begin{aligned}
y_0 &= \left(\sum_{i=t,b,U \text{ and } L} I_{yi} y_{Ci} \right) \Big/ I_{yy} = \left(I_{yt} y_{Ct} + I_{yb} y_{Cb} + I_{yU} y_{CU} + I_{yL} y_{CL} \right) \big/ I_{yy} \\
C_w &= \sum_{i=t,b,U \text{ and } L} I_{yi} h_i^2 = I_{yt} h_t^2 + I_{yb} h_b^2 + I_{yU} h_U^2 + I_{yL} h_L^2 \\
J &= \sum_{i=w,t,b,U \text{ and } L} b_i t_i^3 / 3 = \left(h t_w^3 + b_t t_t^3 + b_b t_b^3 + b_U t_U^3 + b_L t_L^3 \right) \big/ 3
\end{aligned}
\qquad (6.39)\text{a-c}
$$

in which subscripts $i = w, t, b, U$ and L denote the web, top and bottom flanges of unstrengthened cross-section, and upper and lower plates (Fig. 6.2a).

6.10.2 Description of Abaqus model

The S4 element in Abaqus was used to mesh the 3D FEA model. The S4 is a four-node shell element with six degrees of freedom per node. A mesh study indicated that convergence is attained when an element size of nearly 15mm is used throughout. The interaction between the plates and beam flanges was modelled using the *CONTACT PAIR keyword in Abaqus, with the FINITE SLIDING, TYPE=SURFACE TO SURFACE features. FINITE SLIDING is a general approach to model the relative motion between two surfaces forming a contact pair (SIMULIA 2020). In order to prevent penetration between both surfaces, a HARD contact pressure over-closure relationship was defined between both surfaces. The Abaqus analysis involves three loading steps;

(1) the unstrengthened beam was first subjected to pre-strengthening loads while the cover plates were concurrently bent to match the bent configuration of the beam, (2) A ROUGH friction model was activated at the interfaces between the cover plates and the flanges by using the *FRICTION, ROUGH keyword while suppressing the separation between the two surfaces after contact by using the *SURFACE BEHAVIOR, NO SEPARATION, PRESSURE-OVERCLOSURE=HARD keyword. The use of the above combination of features ensures surfaces to remain fully bonded together, with no separation nor tangential sliding, once they have been in contact, even when the contact pressure between them is tensile, and (3) The post-strengthening point load is then applied and a linearized eigenvalue buckling analysis is performed, to obtain the post-strengthening critical moment that would induce buckling of the strengthened beam.

6.10.3 Outline of verification study

The predictions of the present formulation are compared against those based on Abaqus shell model. The effect of PBD on the critical moments cannot be directly captured within the linearized eigenvalue buckling analysis solver in Abaqus. Hence the FEA verification was done in two stages; (1) suppressing PBD effects in the present formulation to match the Abaqus solution, and (2) including PBD effects in the present formulation and comparing the results against Abaqus predictions based on an iterative process devised within the Abaqus model to account for pre-buckling effects.

6.10.3.1 Verification against 3D FEA analysis-Suppressing PBD

The PBD effects were suppressed from the present model by omitting matrices $\mathbf{k}_{\mathbf{E\text{-}b}}$, $\mathbf{k}_{\mathbf{G1\text{-}b}}$, $\mathbf{k}_{\mathbf{G1\text{-}c}}$ and $\mathbf{k}_{\mathbf{G2}}$ in order to enable a direct comparison with shell model predictions. Four series of analyses were then conducted using the shell model; (a) 0-Stiffeners: without attempting to prevent web distortion, (b) 2-Stiffeners: providing transverse stiffeners at beam ends to suppress web distortion at these locations, (c) 3-Stiffeners: providing transverse stiffeners at beam ends and midspan, and (d) 5-Stiffeners: providing transverse stiffeners at beam ends, midspan and quarter spans. The effect of the stiffeners was modelled in Abaqus by enforcing kinematic constraints that couple the angles of twist for all nodes of a given cross-section. In this manner, the stiffened section is restrained from distorting in its own plane but kept free to warp.

For the reference beam, the critical moment due to uniformly distributed load (UDL) before strengthening as predicted by Eq. (6.32) is $38.4kNm$ (Column 10 in Table 6.3). A uniformly distributed pre-strengthening load that induces a peak moment of $0.8\times 38.4kNm = 30.7kNm$ is applied. After strengthening, additional UDL is applied to the beam, and the additional post-strengthening critical moment as predicted by the present model is found to be $87.8kNm$ (Column 11) while that based on the shell model is found to be significantly lower at $55.4kNm$ (Column 12). The difference is attributed to web distortion, which is omitted in the present model but captured in the shell model. Suppressing the distortion at the beam ends is found to significantly increase the critical moment to $74.5kNm$ (Column 13). Providing an additional transverse stiffener at midspan increased the predicted critical moment to $82.7kNm$ (Column 14). Further suppressing distortional effects by providing stiffeners at $0, L/4, L/2, 3L/4$ and L is found to marginally increase the post-strengthening critical moments predicted by the shell model to $85.3kNm$ (Column 15). The above sequence of transverse stiffener strengthening has increased the ratio of post-strengthening critical moments predicted by the shell model to that based on the present thin-walled Vlasov-type element from 0.63 (Column 16) when no stiffeners are provided to 0.97 (Column 19) when five stiffeners are provided, resulting in an increase in the critical moment of 54% (Column 20), i.e., it essentially forced the beam to behave as a Vlasov beam.

Table 6.3 Comparison of critical moments obtained from 3D FEA (Abaqus) and present FEA - Small flange in compression - pre-buckling deformation effects omitted

	Dimensions			Loading information					Critical moments (kNm)						Comparison				
Run Number (1)	L (m) (2)	b_U (mm) (3)	t_U (mm) (4)	Pre-strengthening load (5)	Pre-strengthening load height (6)	Pre-strengthening moment fraction Ω (7)	Post-strengthening load (8)	Post-strengthening load height (9)	For unstrengthened beam $M_{cr\text{-}B}$ (10)	Present study (11)	Shell (distortion allowed) (12)	Shell (distortion suppressed at ends) (13)	Shell (distortion suppressed at ends and midspan) (14)	Shell (distortion suppressed at ends, midspan and quarter points) (15)	(12)/(11) (16)	(13)/(11) (17)	(14)/(11) (18)	(15)/(11) (19)	Suppressing distortion effect (15)/(12) (20)
1	**6**	0	0	UDL	SC	0.8	UDL	SC	38.4	87.8	55.4	74.5	82.7	85.3	0.63	0.85	0.94	0.97	1.54
2	**8**	0	0	UDL	SC	0.8	UDL	SC	28.0	67.7	48.4	62.0	65.7	66.9	0.71	0.92	0.97	0.99	1.38
3	**10**	0	0	UDL	SC	0.8	UDL	SC	22.3	55.1	42.6	52.6	54.5	55.1	0.77	0.95	0.99	1.00	1.29
4	6	**60**	10	UDL	SC	0.8	UDL	SC	38.4	102.8	71.9	94.2	100.0	101.9	0.70	0.92	0.97	0.99	1.42
5	6	**120**	10	UDL	SC	0.8	UDL	SC	38.4	143.2	105.2	134.2	138.6	140.7	0.73	0.94	0.97	0.98	1.34
6	6	**180**	10	UDL	SC	0.8	UDL	SC	38.4	219.1	169.6	204.6	209.3	212.7	0.77	0.93	0.96	0.97	1.25
7	6	0	0	**PLM**	SC	0.8	UDL	SC	44.5	89.9	58.0	76.8	84.7	87.3	0.64	0.85	0.94	0.97	1.51
8	6	0	0	**PLQ**	SC	0.8	UDL	SC	46.1	91.1	58.4	77.7	85.9	88.5	0.64	0.85	0.94	0.97	1.51
9	6	0	0	UDL	SC	0.8	**PLM**	SC	38.4	108.0	69.3	92.2	101.6	104.9	0.64	0.85	0.94	0.97	1.51
10	6	0	0	UDL	SC	0.8	**PLQ**	SC	38.4	113.7	71.9	96.0	105.6	109.8	0.63	0.84	0.93	0.97	1.53
11	6	0	0	UDL	**TF**	0.8	UDL	SC	38.4	77.7	39.6	62.3	71.5	74.8	0.51	0.80	0.92	0.96	1.89
12	6	0	0	UDL	**BF**	0.8	UDL	SC	38.4	89.4	57.1	75.6	84.0	86.7	0.64	0.85	0.94	0.97	1.52
13	6	0	0	UDL	SC	0.8	UDL	**TF**	38.4	65.2	36.4	52.6	59.8	62.8	0.56	0.81	0.92	0.96	1.73
14	6	0	0	UDL	SC	0.8	UDL	**BF**	38.4	92.4	58.6	77.2	86.4	89.3	0.63	0.84	0.94	0.97	1.52
15	6	0	0	UDL	SC	**0.0**	UDL	SC	38.4	119.0	86.9	106.1	114.0	116.5	0.73	0.89	0.96	0.98	1.34
16	6	0	0	UDL	SC	**0.2**	UDL	SC	38.4	111.2	79.0	98.2	106.1	108.7	0.71	0.88	0.95	0.98	1.38
17	6	0	0	UDL	SC	**0.4**	UDL	SC	38.4	103.4	71.1	90.3	98.3	100.9	0.69	0.87	0.95	0.98	1.42
18	6	0	0	UDL	SC	**0.6**	UDL	SC	38.4	95.6	63.2	82.4	90.5	93.1	0.66	0.86	0.95	0.97	1.47
										Average:					0.67	0.87	0.95	0.98	1.47
										Standard deviation:					0.067	0.043	0.018	0.010	0.15

Table 6.4 Comparison of critical moments obtained from 3D FEA (Abaqus) and present FEA - Large flange in compression - pre-buckling deformation effects omitted

	Dimensions			Loading information					Critical moments (kNm)						Comparison				
Run Number (1)	L (m) (2)	b_L (mm) (3)	t_L (mm) (4)	Pre-strengthening load (5)	Pre-strengthening load height (6)	Pre-strengthening moment fraction Ω (7)	Post-strengthening load (8)	Post-strengthening load height (9)	For unstrengthened beam M_{cr-B} (10)	Present study (11)	Shell (distortion allowed) (12)	Shell (distortion suppressed at ends) (13)	Shell (distortion suppressed at ends and midspan) (14)	Shell (distortion suppressed at ends, midspan and quarter points) (15)	(12)/(11) (16)	(13)/(11) (17)	(14)/(11) (18)	(15)/(11) (19)	Suppressing distortion effect (15)/(12) (20)
1F	**6**	0	0	UDL	SC	0.8	UDL	SC	68.3	105.5	57.7	90.2	97.1	100.3	0.55	0.85	0.92	0.95	1.74
2F	**8**	0	0	UDL	SC	0.8	UDL	SC	44.8	77.9	50.2	71.9	74.7	76.3	0.64	0.92	0.96	0.98	1.52
3F	**10**	0	0	UDL	SC	0.8	UDL	SC	33.0	61.8	44.1	59.4	60.7	61.5	0.71	0.96	0.98	0.99	1.39
4F	6	**60**	10	UDL	SC	0.8	UDL	SC	68.3	119.4	74.3	107.4	112.9	115.5	0.62	0.90	0.95	0.97	1.55
5F	6	**120**	10	UDL	SC	0.8	UDL	SC	68.3	145.2	95.6	130.7	136.9	139.6	0.66	0.90	0.94	0.96	1.46
6F	6	**180**	10	UDL	SC	0.8	UDL	SC	68.3	180.7	124.2	164.8	172.3	174.7	0.69	0.91	0.95	0.97	1.41
7F	6	0	0	**PLM**	SC	0.8	UDL	SC	79.1	106.0	58.5	90.7	98.7	101.4	0.55	0.86	0.93	0.96	1.73
8F	6	0	0	**PLQ**	SC	0.8	UDL	SC	82.0	111.8	62.8	96.1	102.5	106.6	0.56	0.86	0.92	0.95	1.70
9F	6	0	0	UDL	SC	0.8	**PLM**	SC	68.3	123.3	68.0	105.4	116.0	118.7	0.55	0.85	0.94	0.96	1.74
10F	6	0	0	UDL	SC	0.8	**PLQ**	SC	68.3	139.0	75.9	117.8	125.0	132.1	0.55	0.85	0.90	0.95	1.74
11F	6	0	0	UDL	**TF**	0.8	UDL	SC	68.3	102.7	54.1	88.0	94.6	97.6	0.53	0.86	0.92	0.95	1.80
12F	6	0	0	UDL	**BF**	0.8	UDL	SC	68.3	122.4	80.8	109.8	115.2	117.6	0.66	0.90	0.94	0.96	1.45
13F	6	0	0	UDL	SC	0.8	UDL	**TF**	68.3	100.2	54.1	86.7	92.8	95.5	0.54	0.87	0.93	0.95	1.77
14F	6	0	0	UDL	SC	0.8	UDL	**BF**	68.3	147.4	95.5	134.1	139.6	141.6	0.65	0.91	0.95	0.96	1.48
15F	6	0	0	UDL	SC	**0.0**	UDL	SC	68.3	159.5	111.8	144.5	151.0	154.0	0.70	0.91	0.95	0.97	1.38
16F	6	0	0	UDL	SC	**0.2**	UDL	SC	68.3	146.0	98.3	130.9	137.5	140.6	0.67	0.90	0.94	0.96	1.43
17F	6	0	0	UDL	SC	**0.4**	UDL	SC	68.3	132.5	84.7	117.3	124.0	127.1	0.64	0.89	0.94	0.96	1.50
18F	6	0	0	UDL	SC	**0.6**	UDL	SC	68.3	119.0	71.2	103.7	110.5	113.7	0.60	0.87	0.93	0.96	1.60
										Average:					0.61	0.89	0.94	0.96	1.58
										Standard deviation:					0.061	0.030	0.018	0.011	0.14

An additional 17 cases were investigated by varying the beam span, the width of the cover plate connected to the smaller flange, load configurations and heights before and after strengthening, and the magnitude of the pre-strengthening moment. Table 6.3 provides the input parameters for each case and the post-strengthening critical moments predicted by the present and shell models when the small flange is under compression. The ratios of post-strengthening critical moments predicted by the shell model without stiffeners to those based on the present model (Column 16) average 0.67 with a standard deviation of 0.067. Comparatively, when five stiffeners are provided, the ratios of post-strengthening critical moments predicted by shell model to those based on the present model (Column 19) average 0.98 with a standard deviation of 0.010. The comparison shows that (a) suppressing distortional effects increased the post-strengthening critical moment capacity by 47% on average and hence it is a desirable/recommended strengthening practice, and (b) the present model provides close predictions of the post-strengthening critical moments compared to shell model predictions for beams equipped with details suppressing web distortion. All cases in Table 6.3 are re-analyzed while subjecting the larger flanges to compression. The input parameters and critical moment predictions for these runs are provided in Table 6.4. In a manner similar to the runs in Table 3, when five stiffeners are provided, the ratios of post-strengthening critical moments predicted by shell model to those based on the present model (Column 19 in Table 6.4) average 0.96 with a standard deviation of 0.011.

6.10.3.2 Verification against 3D FEA analysis-Including PBD

As the linearized eigenvalue buckling analysis in Abaqus cannot directly account for PBD effects on the critical moment, the iterative procedure in Pezeshky and Mohareb (2018) and Iranpour and Mohareb (2023a) was employed to determine the elastic critical moment, including pre-buckling effect, in multiple steps using Abaqus. In this procedure, (1) a linearized eigenvalue analysis is first conducted to obtain the critical load. The linearized buckling analysis omits the pre-buckling curvature of the beam i.e., it assumes the beam at the onset of buckling to be perfectly straight as an approximation, (2) a static analysis is conducted under the critical load obtained in the previous step to obtain the pre-buckling deflected shape of the beam, (3) a new buckling model is built for the curved beam configuration as obtained in Step (2) and a new linearized eigenvalue analysis is conducted to account for the sagging beam configuration. Steps (2) and (3) are repeated until convergence is achieved.

Out of the 18 runs listed in Table 6.3, only eight were examined (runs 1, 3, 6, 9, 11, 13, 15 and 17) using the iterative procedure. Cross-sectional distortion was suppressed by providing five stiffeners at $L=0, L/4, L/2, 3L/4$ and L. Table 6.5 summarizes the values of post-strengthening critical moments based on the present model (Column 15) and those obtained from the iterative shell model (Column 16) when PBD are included. The ratios (Column 19) of both solutions averaged 0.97 with a standard deviation of 0.011, suggesting the accuracy of the present model in capturing PBD effects. Table 6.5 also summarizes the values of post-strengthening critical moments without PBD effects (Columns 17 and 18). On average, the present model and the iterative Abaqus procedure show that PBD effects increase the predicted post-strengthening critical moments by 2-3%. The runs investigated in Table 6.5 were reevaluated in Table 6.6 while subjecting the large flange to compression. A comparison of the average of ratios in Column (20) or (21) of Table 6.5 with those of Table 6.6 suggests that PBD effects have a slightly higher degree of importance when the large flange is in compression. The effect of PBD increases slightly with the magnitude of pre-strengthening loads, as demonstrated by comparing the ratios of runs 1 and 17. The other input parameters investigated in Table 6.5 and Table 6.6 appear to have little to no influence on the PBD effects.

Table 6.5 Comparison of critical moments obtained from 3D FEA (Abaqus) and present FEA - Small flange in compression - Distortion suppressed by five stiffeners at $L=0,\ L/4,\ L/2,\ 3L/4$ and L

	Dimensions			Loading information					Critical moments (kNm)					Comparison		
Run number (1)	L (m) (2)	b_U (mm) (5)	t_U (mm) (6)	Pre-strengthening load (9)	Pre-strengthening load height [$y_{(1-2)}$-y_0] (10)	Ω (11)	Post-strengthening load (12)	Post-strengthening load height [$y_{(5-6)}$-y_0] (13)	$M_{cr\text{-}B}$ (14)	Present study (PBD included) (15)	Shell (PBD included) (16)	Present study (PBD omitted) (17)	Shell (PBD omitted) (18)	Column(16) / Column(15) (19)	Column(15) / Column(17) (20)	Column(16) / Column(18) (21)
1	**6**	0	0	UDL	SC	0.8	UDL	SC	38.4	90.1	87.3	87.8	85.3	0.97	1.03	1.02
3	**10**	0	0	UDL	SC	0.8	UDL	SC	22.3	56.6	56.4	55.1	55.1	1.00	1.03	1.02
6	6	**180**	10	UDL	SC	0.8	UDL	SC	38.4	226.2	219.1	219.1	212.7	0.97	1.03	1.03
9	6	0	0	**PLM**	SC	0.8	UDL	SC	44.5	92.1	89.3	89.9	87.3	0.97	1.03	1.02
11	6	0	0	UDL	SC	0.8	**PLM**	SC	38.4	110.9	107.4	108.0	104.9	0.97	1.03	1.02
13	6	0	0	UDL	**TF**	0.8	UDL	SC	38.4	79.7	76.6	77.7	74.8	0.96	1.03	1.02
15	6	0	0	UDL	SC	0.8	UDL	**TF**	38.4	66.5	63.9	65.2	62.8	0.96	1.02	1.02
17	6	0	0	UDL	SC	**0.0**	UDL	SC	38.4	121.1	118.3	119.0	116.5	0.98	1.02	1.02
										Average:				0.97	1.03	1.02
										Standard deviation:				0.011	0.004	0.004

Table 6.6 Comparison of critical moments obtained from 3D FEA (Abaqus) and present FEA - Large flange in compression - Distortion suppressed by five stiffeners at $L=0$, $L/4$, $L/2$, $3L/4$ and L

	Dimensions			Loading information					Critical moments (kNm)					Comparison		
Run number (1)	L (m) (2)	b_L (mm) (7)	t_L (mm) (8)	Pre-strengthening load (9)	Pre-strengthening load height [$y_{(1-2)}$-y_0] (10)	Ω (11)	Post-strengthening load (12)	Post-strengthening load height [$y_{(5-6)}$-y_0] (13)	M_{cr-B} (14)	Present study (PBD included) (15)	Shell (PBD included) (16)	Present study (PBD omitted) (17)	Shell (PBD omitted) (18)	Column(16) / Column(15) (19)	Column(15) / Column(17) (20)	Column(16) / Column(18) (21)
1F	**6**	0	0	UDL	SC	0.8	UDL	SC	68.3	109.8	103.9	105.5	100.3	0.95	1.04	1.04
3F	**10**	0	0	UDL	SC	0.8	UDL	SC	33.0	64.0	63.5	61.8	61.5	0.99	1.04	1.03
6F	6	**180**	10	UDL	SC	0.8	UDL	SC	68.3	187.9	180.9	180.7	174.7	0.96	1.04	1.04
9F	6	0	0	**PLM**	SC	0.8	UDL	SC	79.1	110.3	105.1	106.0	101.4	0.95	1.04	1.04
11F	6	0	0	UDL	SC	0.8	**PLM**	SC	68.3	128.2	123.1	123.3	118.7	0.96	1.04	1.04
13F	6	0	0	UDL	**TF**	0.8	UDL	SC	68.3	106.9	101.2	102.7	97.6	0.95	1.04	1.04
15F	6	0	0	UDL	SC	0.8	UDL	**TF**	68.3	104.2	98.9	100.2	95.5	0.95	1.04	1.04
17F	6	0	0	UDL	SC	0	UDL	SC	68.3	163.2	157.2	159.5	154.0	0.96	1.02	1.02
										Average:				0.96	1.04	1.03
										Standard deviation:				0.014	0.006	0.005

6.11 Additional Observations Related to Distortional Effects

The following observations relate to runs provided in Table 6.3 and Table 6.4.

- Runs 1-3 suggest that distortional effects decrease with the span.
- A comparison of the entries in Column 16 for runs 1,4,5,6 shows that when monosymmetric sections approach those of doubly symmetric cross-sections, the corresponding moment ratios suggest that distortional effects tend to reduce (irrespective of which flange is in compression). The more pronounced distortional effect in beams with

monosymmetric cross-sections emphasizes the importance of providing web transverse stiffeners in such cases.

- Runs 1, 7-10, suggest that cross-sectional distortion is insensitive to the loading type.
- Runs 1, 11-14 indicate that the ratio of post-strengthening load predicted by shell analysis to that based on the present thin-walled beam element (Column 19 in Table 6.3 and Table 6.4) increases when either the pre- or post-strengthening loads are applied at the bottom flange (when compared to the top flange loading scenario).
- The entries of Column 16 (for the case of no stiffeners) for runs 1, 15-18, suggest that increasing the magnitude of pre-strengthening loads increases distortion. For example, a comparison of the entries for runs 1 and 15 in Table 6.3 shows that a decrease in the pre-strengthening load level from $\Omega = 0.8$ to zero, increased the ratio of distortional to non-distortional critical moment from 0.63 to 0.73 (Column 16 in Table 6.3) when the small flange is in compression. This difference corresponds to a 16% increase in ratios. Also, an identical decrease in load level when the large flange is in compression reduced the level of distortion and increased the ratio of distortional to non-distortional critical moments from 0.55 to 0.70, (Column 16 in Table 6.4), a 27% increase in ratio. The above results suggest that providing web transverse stiffeners to suppress distortion is more important when a) the level of pre-existing loads is higher, and b) when the larger flange is under compression.

6.12 Parametric study

In practice, designers may opt to determine the capacity of a strengthened beam under total loads without explicitly considering the effects of pre-strengthening loading. A concern arises as to whether the existing loads prior to strengthening would affect the capacity of the strengthened beam. To address this concern, the ratio $M_t/M_{t,nPL}$ is introduced, in which $M_t = M_a + M_{cr}$ represents the total moments sustained by the strengthened beam while accounting for the influence of pre-strengthening loads and $M_{t,nPL} = M_{cr}$ is the LTB capacity of the beam in the absence of pre-strengthening loads. A moment ratio $M_t/M_{t,nPL}$ exceeding unity signifies that accounting for the effect pre-strengthening loads increases the predicted LTB capacity while a value below unity indicates that omitting the effect of pre-strengthening loads has a detrimental effect and overestimates the LTB capacity.

In this section, three reference cases are defined, and subsequently, the effect of various parameters on the moment ratio introduced is investigated by altering the geometry and loading properties for each reference case. The reference cases, along with the constants and variables, are defined below to provide a clear understanding of the analysis.

All three reference cases R1-R3 are based on the cross-section geometry defined in Section 6.10: R1 is under pre- and post-strengthening UDLs acting at the shear centre and simply supported end conditions, R2 has loadings identical to those of R1 while restraining all degrees of freedom at one end and simply supported conditions at the other end, and R3 has boundary conditions identical to those of R1, with a midspan pre-strengthening point load $P_{(1-2)}$ acting at the top flange and a midspan post-strengthening point load $P_{(5-6)}$ acting at the bottom flange.

For all runs, the top flange dimensions $b_t \times t_t = 100 \times 10mm$, web thickness $t_w = 6mm$ and overall depth of the unstrengthened cross-section $d = 360mm$ are kept constant. No strengthening plate was provided to the top flange.

The parameters varied are the span to depth ratio L/d, loading configurations (UDL, PLM and PLQ), load heights (SC, TF and BF), pre-strengthening load magnitude Ω, dimensions of the bottom flange and lower plate, corresponding to four dimensionless parameters; the bottom flange to top flange dimension ratios b_b/b_t and t_b/t_t, and lower plate to top flange dimension ratios b_L/b_t and t_L/t_t. The effects of the above parameters on the moment ratio $M_t/M_{t,nPL}$ while including the PBD effects are investigated and depicted in Fig. 6.6.

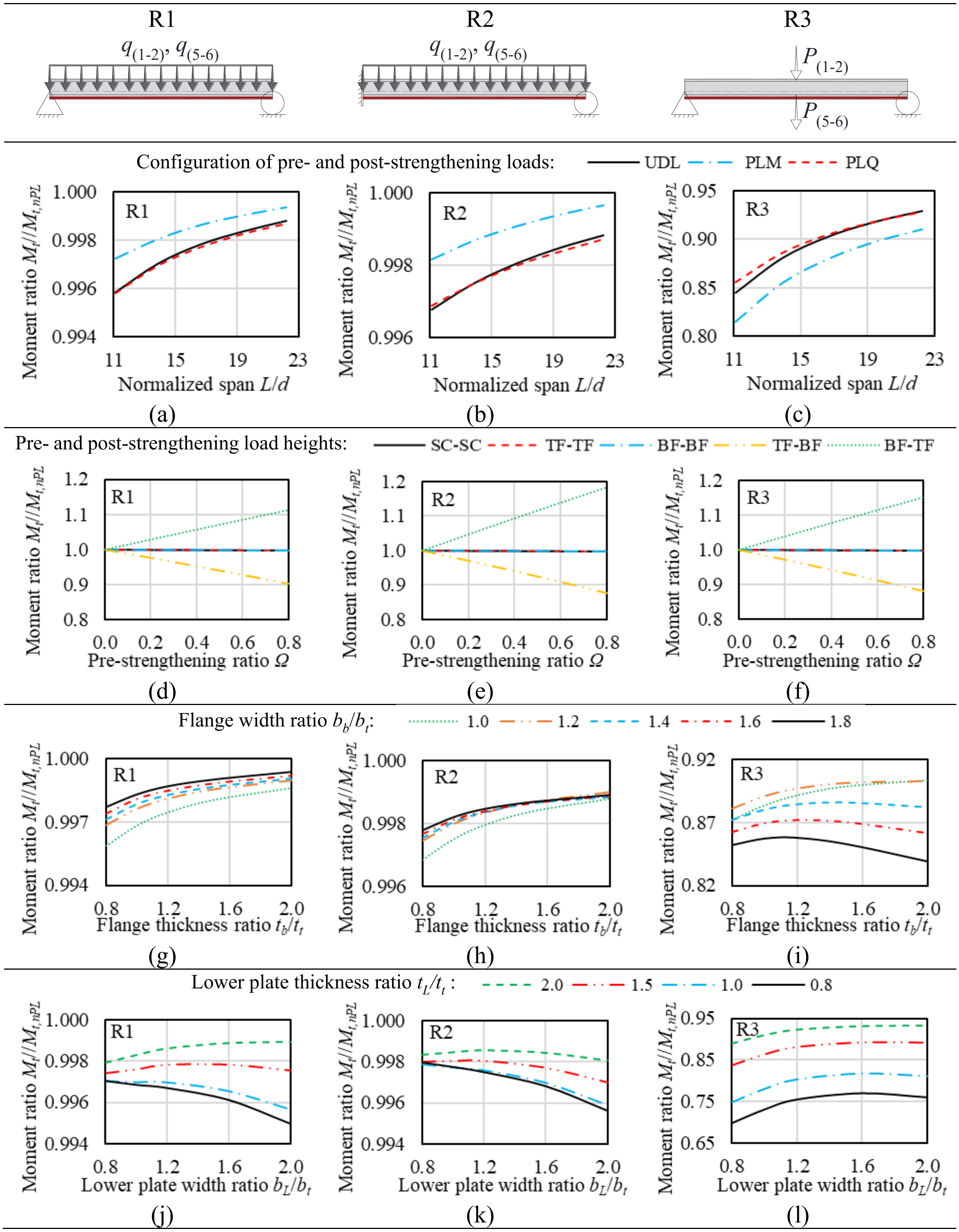

Fig. 6.6 Normalized moment ratio $M_t/M_{t,nPL}$ versus span-to-depth ratio L/d for various loading configuration (a-c) , pre-strengthening moment ratio Ω and Pre- and post-strengthening load heights (d-f), flange width and thickness ratios (g-i) , and lower plate width and thickness ratios (j-l)

6.12.1 Effects of loading configurations and span

For each of R1-R3, three loading configurations (UDL, PLM, and PLQ) were investigated with five spans per loading configuration ranging from 4 to 8 meters. For the beam depth $d = 360mm$, the corresponding span-to-depth ratios are 11.1, 13.9, 16.7, 19.4 and 22.2.

Fig. 6.6a-c shows that the moment ratio $M_t / M_{t,nPL}$ is nearly unity for R1 and R2 and consistently below unity for R3. Thus, for R3, omitting the pre-strengthening load effect, would over-predict the moment capacity $M_{t,nPL}$ relative to M_t. The moment ratio $M_t / M_{t,nPL}$ is observed to increase with the span-to-depth L/d, i.e., the difference between the predicted moment capacity $M_{t,nPL}$ relative to the capacity M_t increases as the span-to-depth L/d reduces, flagging the necessity to account for the pre-strengthening effects for relatively low spans. Also, for R3, the difference between $M_{t,nPL}$ and M_t is observed to be more pronounced for PLM when compared to UDL and PLQ.

6.12.2 Effects of load heights and pre-strengthening load magnitude

Five loading height combinations for pre- and post- strengthening loads were investigated. An identifier in the form XX-YY is assigned to each combination, in which XX and YY respectively denote the load height for the pre- and post-strengthening loads. Each of XX and YY take one of the values SC (for shear centre loading), TF (for top flange loading), or BF (for bottom flange loading). For example, TF-BF indicates top flange pre-strengthening loading followed by bottom flange post-strengthening loading. Furthermore, the magnitude of the pre-strengthening load is varied to correspond to a moment fraction Ω ranging from 0.0 to 0.8.

Fig. 6.6d-f show that when both the pre- and post-strengthening loads are acting at the same heights, the ratio $M_t / M_{t,nPL}$ nearly equal to one. However, when the loads are positioned at different heights, the ratio $M_t/M_{t,nPL}$ deviates from unity (upwards for BF-TF and downwards for TF-BF). In such cases the deviation of $M_t/M_{t,nPL}$ from unity increases with the magnitude of pre-strengthening load.

When the pre-strengthening load is applied at the bottom flange and the post-strengthening load is applied at the top flange (i.e., BF-TF), the moment ratio $M_t/M_{t,nPL}$ surpasses unity since pre-strengthening loads applied at the bottom flange have a stabilizing effect on the critical moment when determining M_t that is not captured when determining $M_{t,nPL}$. The findings in Fig. 6.6(e) shows that this stabilizing effect results in capacity increases of up to 18%.

Conversely, in the TF-BF load height scenario, the pre-strengthening load applied at the top flange is associated with a destabilizing effect on the critical moment capacity. Consequently, omitting this destabilizing effect when computing $M_{t,nPL}$, by considering all loads to act at the bottom flange, would result in overestimating the capacity, causing the moment ratio to fall below unity. Fig. 6.6(f) shows that this destabilizing effect of pre-strengthening loads acting at the top flange can reduce the predicted capacity by up to 12%.

6.12.3 Effects of bottom flange geometry

The effect of bottom flange geometry on the critical moment ratio $M_t/M_{t,nPL}$ is investigated by varying the bottom flange width from 100 to 180mm and its thickness from 8 to 20mm, leading to 25 runs in total, with b_b/b_t ratios ranging from 1.0 to 1.8 and t_b/t_t ranging from 0.8 to 2.0. In R1 and R2, where both pre- and post-strengthening loads are applied at the shear center, it is observed that, in most cases, the moment ratio $M_t/M_{t,nPL}$ increases with the bottom flange size [Fig. 6.6(g) and (h)].

However, for R3, no clear trend is observed between the moment ratio $M_t/M_{t,nPL}$ and the normalized bottom flange dimensions b_b/b_t and t_b/t_t [Fig. 6.6(i)]. The most unfavorable scenario encountered corresponds to the case ($b_b/b_t = 1.8$, $t_b/t_t = 2.0$) and resulted in a moment ratio $M_t/M_{t,nPL} = 0.84$.

6.12.4 Effects of lower strengthening plate geometry

The effect of lower plate geometry on the critical moment ratio $M_t/M_{t,nPL}$ was investigated by varying its width from 80 to 200mm and its thickness from 8 to 20mm, resulting in a total of 20 runs, with b_L/b_t and t_L/t_t ratios ranging from 0.8 to 2.0.

Fig. 6.6(j)-(l) reveal that the critical moment ratio $M_t/M_{t,nPL}$ increases with the lower plate thickness. For R3, the most unfavorable result corresponded to the smallest investigated plate dimensions ($b_L/b_t = t_L/t_t = 0.8$), resulting in a moment ratio $M_t/M_{t,nPL} = 0.70$.

6.13 Summary and conclusion

The present study developed a variational principle and finite element (FE) formulation to determine the elastic LTB capacity of singly symmetric assemblies. The formulation captures the pre-strengthening load and PBD effects. Comparative analyses with shell models reveal that the proposed model accurately predicts the post-strengthening critical moments when web distortion is effectively suppressed by transverse stiffeners. In this respect, providing transverse stiffeners was shown to be an effective means of suppressing web distortion. The most effective locations for providing transverse stiffeners include beam ends which was found to increase the LTB capacity by 32% on average in the cases considered. Providing additional transverse stiffeners at midspan increased the LTB capacity by an additional 9% on average. Furthermore, providing additional transverse stiffeners at quarter-span sections was found to increase the LTB capacity by an additional 3% on average.

A parametric study was conducted based on the FE model developed, to investigate the effect of various parameters on ratio $M_t/M_{t,nPL}$ of the predicted total moment capacity for the strengthened beam while accounting for the pre-strengthening load effect to that based on omitting the pre-strengthening load effect. Factors investigated include load heights, magnitude of pre-strengthening load, geometry of lower strengthening plate, beam span, geometry of the bottom flange, loading configurations, and boundary conditions.

The load height was found to be the most influencial parameter among the ones investigated. When the loads applied before and after strengthening are positioned at the same height, the critical moment ratio $M_t/M_{t,nPL}$ tends to remain close to unity, suggesting that omitting the pre-strengthening load effect can still yield good critical moment predictions. Conversely, when the pre- and post-strengthening load heights differ, the pre-strengthening load effect was found to be significant, leading potentially to inaccurate critical moment predictions. The most unfavorable result corresponded to the smallest investigated plate dimensions, resulting in a moment ratio $M_t/M_{t,nPL} = 0.70$, indicating that omitting pre-strengthening load effects overestimates the critical moment by 43%.

6.14 Appendix 6.A: Monosymmetry moment of inertia I_{px}

The process of deriving a simple expression for the monosymmetry moment of inertia I_{px} using the parallel axis theorem is presented in this appendix. Fig. 6.7 depicts an arbitrary element with its centroid positioned at a distance y_{C-EL} from the reference point along the *y*-direction. However, in the *x*-direction, the centroid of the element coincides with the reference point, resulting in zero distance between them.

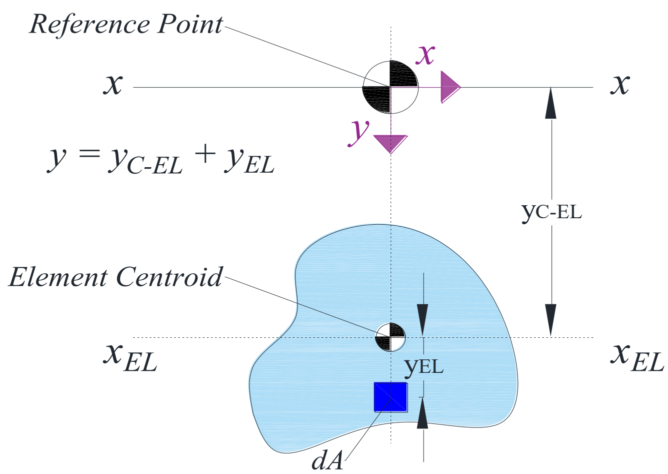

Fig. 6.7 Arbitrary element for deriving expression for I_{px}

Monosymmetry moment of inertia I_{px-EL} for the arbitrary element shown in Fig. 6.7 about its own centroid is expressed by

$$I_{px-EL} = \int_A y_{EL}\left(x^2 + y_{EL}{}^2\right) dA \tag{6.40}$$

From $y = y_{C-EL} + y_{EL}$, by substituting in Eq. (6.40) and simplifying the resulting expression, the monosymmetry moment of inertia I_{px} about the reference point can be obtained as

$$I_{px} = \int_A y\left[x^2 + y^2\right] dA = I_{px-EL} + y_{C-EL}\left(3I_{xx-EL} + I_{yy-EL} + A_{EL}y_{C-EL}{}^2\right) \tag{6.41}$$

6.15 References

Anderson, J. M. and N. S. Trahair (1972). "Stability of monosymmetric beams and cantilevers." Journal of the structural division **98**(1): 269-286.

ANSI/AISC360 (2022). "Specification for structural steel buildings (ANSI/AISC 360-22)." American Institute of Steel Construction, Chicago-Illinois.

AS-4100 (2020). "Steel structures. Sydney, Australia."

Attard, M. M. (1986). "Lateral buckling analysis of beams by the FEM." Computers & structures **23**(2): 217-231.

Attard, M. M. (1990). "General non-dimensional equation for lateral buckling." Thin-Walled Structures **9**(1-4): 417-435.

Attard, M. M. and M.-Y. Kim (2010). "Lateral buckling of beams with shear deformations–A hyperelastic formulation." International Journal of Solids and Structures **47**(20): 2825-2840.

Barsoum, R. S. and R. H. Gallagher (1970). "Finite element analysis of torsional and torsional–flexural stability problems." International J. for Numerical Methods in Engineering **2**(3): 335-352.

Basaglia, C. and D. Camotim (2013). "Enhanced generalised beam theory buckling formulation to handle transverse load application effects." International Journal of Solids and Structures **50**(3-4): 531-547.

Bradford, M. A. (1985). "Distortional buckling of monosymmetric I-beams." Journal of Constructional Steel Research **5**(2): 123-136.

Bradford, M. A. (1990). "Stability of monosymmetric beam-columns with thin webs." Journal of Constructional Steel Research **15**(4): 323-339.

CAN/CSA-S16 (2019). "CSA S16: 19, Design of Steel Structures, Canada." Canadian Standards Association.

Dinis, P. B., D. Camotim and N. Silvestre (2006). "GBT formulation to analyse the buckling behaviour of thin-walled members with arbitrarily 'branched'open cross-sections." Thin-Walled Structures **44**(1): 20-38.

Erkmen, R. and M. Mohareb (2008). "Buckling analysis of thin-walled open members—a finite element formulation." Thin-walled structures **46**(6): 618-636.

Erkmen, R. E. (2014). "Shear deformable hybrid finite-element formulation for buckling analysis of thin-walled members." Finite Elements in Analysis and Design **82**: 32-45.

Helwig, T. A., K. H. Frank and J. A. Yura (1997). "Lateral-torsional buckling of singly symmetric I-beams." Journal of Structural Engineering **123**(9): 1172-1179.

Hsu, W. T., D. M. Lue and Y. F. Chen (2012). "Design aid for moment strength of built-up crane runway girders." International Journal of Steel Structures **12**(3): 403-417.

Hsu, W. T., D. M. Lue and B. T. Hsiao (2009). "Numerical approach for torsion properties of built-up runway girders." Journal of Applied Science and Engineering **12**(4): 381-389.

Hughes, O. and M. Ma (1996). "Lateral distortional buckling of monosymmetric beams under point load." Journal of engineering mechanics **122**(10): 1022-1029.

Iranpour, A. and M. Mohareb (2022). Elastic Lateral Torsional Buckling Resistance of Beams Strengthened with Cover Plates under Pre-Existing Loads. CSCE 2022 Annual Conference, Structural Specialty, Whistler, British Columbia, Canada, Canadian Society for Civil Engineering (CSCE).

Iranpour, A. and M. Mohareb (2023a). "Elastic Lateral Torsional Buckling of I-Beams Strengthened While under Loading." Journal of Structural Engineering **149**(1): 04022206.

Iranpour, A. and M. Mohareb (2023b). "Design Expressions for Elastic Lateral Torsional Buckling Capacity of I-Beams Strengthened While under Loading." Journal of Structural Engineering **149**(7): 04023078.

Krajcinovic, D. (1969). "A consistent discrete elements technique for thinwalled assemblages." International Journal of Solids and Structures **5**(7): 639-662.

Kumar, A. and A. Samanta (2006). "Distortional buckling in monosymmetric I-beams: Reverse-curvature bending." Thin-walled structures **44**(7): 721-725.

Liu, Y. and L. Gannon (2009a). "Experimental behavior and strength of steel beams strengthened while under load." Journal of Constructional Steel Research **65**(6): 1346-1354.

Liu, Y. and L. Gannon (2009b). "Finite element study of steel beams reinforced while under load." Engineering Structures **31**(11): 2630-2642.

Ma, M. and O. Hughes (1996). "Lateral distortional buckling of monosymmetric I-beams under distributed vertical load." Thin-Walled Structures **26**(2): 123-145.

MacCrimmon, R. (2009). Guide for the Design of Crane-Supporting Steel Structures. Markham, ON, CA, Canadian Institute of Steel Construction.

Mohammadi, E., S. S. Hosseini and M. S. Rohanimanesh (2016). "Elastic lateral-torsional buckling strength and torsional bracing stiffness requirement for monosymmetric I-beams." Thin-Walled Structures **104**: 116-125.

Mohri, F., A. Brouki and J. Roth (2003). "Theoretical and numerical stability analyses of unrestrained, mono-symmetric thin-walled beams." Journal of Constructional Steel Research **59**(1): 63-90.

Papangelis, J., N. Trahair and G. Hancock (1998). "Elastic flexural–torsional buckling of structures by computer." Computers & structures **68**(1-3): 125-137.

Pezeshky, P. and M. Mohareb (2018). "Distortional lateral torsional buckling of beam-columns including pre-buckling deformation effects." Computers & Structures **209**: 93-116.

Pezeshky, P., A. Sahraei, F. Rong, S. Sasibut and M. Mohareb (2020). "Generalization of the Vlasov theory for lateral torsional buckling analysis of built-up monosymmetric assemblies." Engineering Structures **221**: 111055.

Pi, Y. L. and N. Trahair (1992a). "Prebuckling deflections and lateral buckling. I: theory." Journal of structural engineering **118**(11): 2949-2966.

Pi, Y. L. and N. Trahair (1992b). "Prebuckling deflections and lateral buckling. II: applications." Journal of Structural Engineering **118**(11): 2967-2985.

Pi, Y. L., N. Trahair and S. Rajasekaran (1992). "Energy equation for beam lateral buckling." Journal of structural engineering **118**(6): 1462-1479.

Reichenbach, M. C., Y. Liu, T. A. Helwig and M. D. Engelhardt (2020). "Lateral-Torsional Buckling of Singly Symmetric I-Girders with Stepped Flanges." Journal of Structural Engineering **146**(10): 04020203.

Roberts, T. and M. Benchiha (1987). "Lateral instability of monosymmetric beams with initial curvature." Thin-walled structures **5**(2): 111-123.

Sahraei, A., L. Wu and M. Mohareb (2015). "Finite element formulation for lateral torsional buckling analysis of shear deformable mono-symmetric thin-walled members." Thin-Walled Structures **89**: 212-226.

Samanta, A. and A. Kumar (2006). "Distortional buckling in monosymmetric I-beams." Thin-walled structures **44**(1): 51-56.

Schardt, R. (1994). "Lateral torsional and distortional buckling of channel-and hat-sections." Journal of Constructional Steel Research **31**(2-3): 243-265.

SIMULIA (2020). Abaqus/CAE user’s manual, Dassault Systemes.

Trahair, N. (1993). Flexural-torsional buckling of structures, CRC press.

Vlasov, V. (1961). Thin-Walled Elastic Beams. Jerusalem, Israel, Israel Program for Scientific Translations.

Wang, C. and S. Kitipornchai (1986a). "On stability of monosymmetric cantilevers." Engineering Structures **8**(3): 169-180.

Wang, C. M. and S. Kitipornchai (1986b). "Buckling capacities of monosymmetric I-beams." Journal of Structural Engineering **112**(11): 2373-2391.

Wang, Y.-q., L. Zong, R.-x. Zhu, X.-y. Liu and Y.-j. Shi (2015). "Behavior of I-section steel beam welding reinforced while under load." Journal of Constructional Steel Research **106**: 278-288.

6.16 Nomenclature

Boldface Letters:

$\mathbf{d}$	Vector of nodal degrees of freedom
$\mathbf{H_U}$, $\mathbf{H_\theta}$	Vector of shape function for lateral displacement and angle of twist
$\mathbf{k_E}$	Elastic stiffness matrix
$\mathbf{k_{G1}}$	Geometric stiffness matrix accounting for PBD and pre- and post-strengthening loads
$\mathbf{k_{G2}}$	Geometric stiffness matrix accounting for PBD effects due to post-strengthening loads

Latin Letters:

A_B, A_t, A_b, A_U and A_L	Cross-sectional areas of unstrengthened beam, top flange, bottom flange, upper plate, and lower plate
b_b, b_t, b_U and b_L	Width of bottom flange of unstrengthened cross-section, top flange of unstrengthened cross-section, upper plate, and lower plate
b_{ct}, b_{cb}, b_{et} and b_{eb}	Overlapping and overhanging widths shown on Fig. 6.5
b_{mt}, b_{mb}	Larger of flange and cover plate widths at top and bottom of cross-section [i.e., $b_{mt} = \max(b_t, b_U)$ and $b_{mb} = \max(b_b, b_L)$]
b_w	Distance between flange centroids of unstrengthened beam $b_w = h$
C_{w-B}, C_w	Warping constants of unstrengthened and strengthened cross-sections
C_B	Moment gradient factor corresponding to pre-strengthening loads
d	Overall depth of unstrengthened cross-section
E	Young modulus taken as $2\times10^5 MPa$
G	Shear modulus taken as $77\times10^3 MPa$
H_1, H_2, H_3 and H_4	Elements of shape function vector
h	Centre to centre web height of unstrengthened cross-section $h = d - (t_t + t_b)/2$
h_{ct}, h_{cb}	Absolute distance between shear centre of strengthened cross-section and centroid of overlapping part at top and bottom of cross-section

h_{et} , h_{eb}	Absolute distance between shear centre of strengthened cross-section and centroid of overhanging parts at top and bottom of cross-section (Fig. 6.5)
h_t , h_b , h_U and h_L	Absolute distances between shear centre of strengthened cross-section and centroid of top flange, bottom flange, upper plate, and lower plate
I_{yct} , I_{ycb}	Y-axis moment of inertias for overlapping parts at top and bottom of cross-section
I_{yet} , I_{yeb}	Y-axis moment of inertias for overhanging widths at top and bottom of cross-section
I_{yt} , I_{yb} , I_{yU} and I_{yL}	Y-axis moment of inertias for top flange, bottom flange, upper plate and lower plate
I_{xx-B} , I_{yy-B}	Moment of inertia about x-axis and y-axis for unstrengthened cross-section
I_{xx} , I_{yy}	Moment of inertia about x-axis and y-axis for strengthened cross-section
I_{xx-U} , I_{xx-L}	Moment of inertia about x-axis for upper and lower strengthening cover plates
I_{px} , $\tilde{I}_{px}$	Monosymmetry moment of inertias for strengthened beam
I_{px-B}	Monosymmetry moment of inertia for unstrengthened beam
i	Component identifier (subscript i for all components can be found in Fig. 6.2. Note that no subscript i denotes strengthened system)
J_B , J	Saint Venant torsional constants of unstrengthened and strengthened cross-sections
L	Beam span (taken equal to unbraced length in all problems investigated in this study)
L_e	Element length
M_{1-B} , M_{2-B} , M_{3-B} and $M_{\max-B}$	Absolute values of bending moments at quarter point, midspan, three quarter point, and peak moment within unbraced length corresponding to pre-strengthening loads
M_a	Pre-strengthening peak moment

M_{cr}	Post-strengthening critical moment carried by beam in addition to pre-strengthening moment
M_{cr-B}	Critical moment of unstrengthened beam based on pre-strengthening load pattern
$M_{(m-n)}$	Bending moment distribution function in going from Configuration *m* to *n*
$M_{1(m-n)}$, $M_{2(m-n)}$	Bending moments at end of each element
M_t	Total moments sustained by strengthened beam (up to the point of LTB) while accounting for influence of pre-strengthening loads
$M_{t,nPL}$	LTB capacity of beam in the absence of pre-strengthening loads
n	Distance normal to section contour
O_i	Origin of component i taken to coincide with its own centroid (Fig. 6.3)
$q_{(1-2)}$	Load applied on unstrengthened beam in Step 1-2
$q_{U,(3-4)}$, $q_{L,(3-4)}$	Load applied on upper and lower strengthening plates in Step 3-4
$q_{(5-6)}$	Additional post-strengthening reference loads applied on strengthened beam in Step 5-6
t_b, t_t, t_w, t_U and t_L	Thickness of bottom flange, top flange, web, upper and lower cover plates. (Fig. 6.2a summarizes definition of subscripts).
t_{ct}, t_{cb}, t_{et} and t_{eb}	Thickness of various components as shown on Fig. 6.5.
U, V	Lateral displacement along *x*-axis, and transverse displacement along *y*-axis (Fig. 6.3d)
U', V'	Rotations about *y*- and *x*-axis
V''	Curvature in *yz*-plane
$V_{(m-n)}$	Transverse deflection in going from Configuration *m* to *n* (Fig. 6.1)
u, v and w	Displacements of a generic point on strengthened cross-section along x, y, z directions (Fig. 6.3d)
x, y and z	Coordinates along lateral, transverse and longitudinal directions of strengthened cross-section (Fig. 6.3c)

y_B, y_U and y_L	Transverse coordinates for unstrengthened cross-section, upper strengthening plate, and lower strengthening plate relative to each component centroid (Fig. 6.3a)
y_0	Coordinate of strengthened cross-section shear centre measured from centroid of strengthened cross-section
$y_{(1-2)}$, $y_{(5-6)}$	Load height of pre- and post-strengthening loads below centroid of strengthened cross-section (Fig. 6.1)
y_{Ct}, y_{Cb}, y_{CB}, y_{CU} and y_{CL}	Centroidal coordinates for top flange, bottom flange, unstrengthened beam, upper and lower cover plates, measured from centroid of strengthened cross-section

Greek Letters:

α	Rebound coefficient
β, $\tilde{\beta}$	Monosymmetry parameters for strengthened cross-section
β_B	Monosymmetry parameter for unstrengthened cross-section
γ	Shear strain
ε, σ	Longitudinal strain and stress
θ, θ'	Angle of twist of strengthened cross-section about longitudinal *z*-axis (Fig. 6.3d), and warping deformation
λ	Buckling load multiplier to be determined from buckling analysis
$\Pi_{(m-n)}$	Total potential energy in going from Configuration *m* to *n*
Ω	Pre-strengthening moment fraction $\Omega = M_a / M_{cr,a}$
ω	Sectorial coordinate
$(\ )'$, $(\ )''$	First and second derivative with respect to z
$\overline{(\ )}$, $\overline{\overline{(\ )}}$	First and second variations of argument function

Chapter 7: Summary, Conclusions and Recommendations

7.1 Summary

The present thesis developed a series of solutions, ranging from the elaborate and accurate to the simplified but approximate, aiming to investigate the effects of pre-strengthening loads on the elastic Lateral Torsional Buckling (LTB) capacity of I-beams strengthened with cover plate(s) while under loading. The proposed solutions carefully simulate the entire history of loading and strengthening, including the application of pre-existing loads on the beam, applying clamping forces to bring into contact the initially straight steel cover plates with the bent configuration of the loaded beam, modelling the rebound effect arising after clamping force removal, the contact at the interfaces between cover plates and flanges induced by welding, and the application of post-strengthening loads up to the point of elastic LTB initiation for the strengthened system. The study contributed to the existing body of knowledge in four aspects: three contributions pertaining to doubly symmetric beams that are symmetrically strengthened using identical cover plates, while the fourth contribution pertains to the strengthening of monosymmetric beams or doubly symmetric beams with unsymmetric strengthening scheme.

7.1.1 Doubly symmetric strengthened beams

The behaviour of doubly symmetric beams strengthened symmetrically by identical cover plates while under load was investigated through three studies.

In the first contribution (Chapter 3), a shell-based finite element (FE) study was developed to analyze the effect of various geometric and loading parameters on the LTB capacity of beams strengthened while under load. A simplified design equation was then proposed to quantify the post-strengthening critical moment capacity. The predictions of the equation were found in reasonable agreement with FE predictions for the specific cases where (1) pre- and post-strengthening loads have similar distributions, (2) loads are applied to the shear centre of strengthened cross-section, (3) the entire beam span is strengthened with cover plates, and (4) beams are simply supported relative to weak axis rotation and twist.

To overcome the limitations of the first contribution, the second contribution (Chapter 4) formulated a variational principle to quantify the elastic LTB capacity of steel I-beams that are partially or fully strengthened by cover plates. The variational principle is subsequently used to develop a FE formulation, which was validated through comparisons with predictions of other numeric simulation techniques as well as experimental results by others. The FE formulation was subsequently used to conduct a parametric study to characterize the gain in elastic critical moment capacity attained by cover plate strengthening while investigating the influence of various geometric and loading condition parameters.

Although the FE formulation developed in the second contribution was shown to yield accurate predictions, it may be impractical to use in a design environment. To overcome this limitation, the third contribution (Chapter 5) exploited the variational principle developed in Chapter 4 to develop an approximate energy-based design-oriented interaction equation to quantify the LTB strength of doubly symmetric beams that are symmetrically strengthened. The solution captures the effect of loads acting on the beam before strengthening, the beneficial effects resulting from PBD, pre- and post-strengthening load heights, as well as moment gradient effects. Comparison against FE predictions suggested the accuracy of the predicted LTB capacity for cases where pre- and post-strengthening load distributions are similar. An iterative procedure was also developed for more general loading cases with differing pre- and post-strengthening loading patterns. The potential use of the equations developed in practical design applications was illustrated through design examples.

7.1.2 Monosymmetric strengthened beams

The fourth contribution expanded the variational formulation developed in Chapter 4 to beams with monosymmetric cross-sections and/or symmetric beams with unsymmetric cover plate geometries. The modified variational principle was used to develop a thin-walled beam FE formulation to predict the non-distortional LTB capacity of monosymmetric strengthened beams. Comparative analyses with shell models confirm the validity of the proposed solutions. The effects of various design parameters on the total elastic critical moment capacity were evaluated in a systematic parametric study.

7.2 Conclusions

The following conclusions related to the LTB capacity of strengthened beams arose from the study.

7.2.1 Doubly symmetric beams

1. Providing cover plates is an effective means of increasing the LTB resistance of existing steel beams.
2. For cases where the cover plate width is less than that of the flange, strengthening the end portions of the beam was found to be more effective than strengthening its mid-span portion. Conversely, for cases where the strengthening plates are wider than flanges, midspan strengthening can be more effective.
3. The PBD effect is most pronounced for midspan strengthening. For the numerical examples on midspan strengthening investigated in Chapter 4, omitting the PBD effect was found to underestimate the post-strengthening critical moment by 15%. In comparison, for full

strengthening, the omission of PBD effect underestimates the post-strengthening critical moment only by 7.4%.

4. Results in Chapter 5 also showed that, for full strengthening, accounting for PBD effects increases the critical moments predicted by 7.1% on average. However, the beneficial effect of considering PBD effects increases up to 21.6% for loading cases involving high pre-strengthening load levels.
5. In partial strengthening scenarios, the gain in post-strengthening critical moment achieved increases with the normalized plate length L_p/L, and decreases with the normalized plate width b_p/b_f (for the end and intermediate strengthening scenarios), the normalized plate thickness t_p/t_f (for partial strengthening scenarios) and with the section aspect ratio h/b_f
6. Web distortion can significantly reduce the elastic critical moment capacity. While distortional effects tend to have a minor to moderate effect on the elastic LTB resistance of unstrengthened beams, the present study has shown that distortion effects gain significance in the context of beams strengthened with cover plates. It is thus important to minimize web distortion in strengthened beams by providing transverse stiffeners at key locations along the beam span. The most effective locations for transverse stiffeners in simply supported beams include beam ends. Stiffeners at locations of cover plate ends were also shown to be very effective in end strengthening scenarios.
7. For the geometries considered in the present study, suppressing distortional effects at beam ends and at midspan of a simply supported beam with transverse stiffeners was found to increase the post-strengthening critical moment capacity by 17% on average and hence is a desirable/recommended strengthening practice when cover plates are provided.

8. The energy-based expression for the moment gradient factor established in Chapter 5 was found to slightly overestimate the critical moment predictions compared to finite element solutions. On the other hand, steel design standards [e.g., ANSI/AISC360 (2022) and CAN/CSA-S16 (2019)] slightly underestimate the critical moments. Thus, the study suggested utilizing standard-based moment gradient equations when employing the procedures developed in Chapter 5 to estimate the elastic LTB capacity of I-beams strengthened while under loading.
9. To account for the effects of pre- and post-strengthening load height and PBD effects, separate energy-based coefficients were developed in Chapter 5. When compared to FE results, the equations yielded accurate results across a diverse array of design scenarios.

7.2.2 Monosymmetric beams

1. The effect of accounting for pre-strengthening load effect was shown to become most pronounced in loading cases involving loading that is offset from the shear centre. When the loads applied before and after strengthening are positioned at different heights relative to the shear centre, neglecting the pre-strengthening load effect leads potentially to inaccurate critical moment predictions. Among the cases considered, the most unfavorable results corresponded to the smallest plate geometries, in which omitting pre-strengthening load effects overestimated the critical moment by as much as 43%.
2. The distortional effects are more pronounced in beams with monosymmetric cross-sections in comparison to those with doubly symmetric cross-sections. This observation emphasizes the importance of providing web transverse stiffeners in scenarios involving monosymmetric cross-sections.

3. Providing web transverse stiffeners to suppress distortion becomes more important when (a) the level of pre-strengthening load is higher, and (b) when the larger flange is under compression.
4. The most effective locations for providing transverse stiffeners for simply supported beams include beam ends which was found to increase the LTB capacity by 32% on average in the cases considered. Providing additional transverse stiffeners at midspan increased the LTB capacity by an additional 9.0% on average. Providing additional transverse stiffeners at quarter-span sections was found to marginally increase the LTB capacity by an additional 3.0% on average.

7.3 Recommendations for future research

1. For a given beam required withstand specified additional loading, the procedures for quantifying the elastic critical moments developed in Chapter 5 can be integrated with optimization techniques to determine the optimum cover plate geometries.
2. The procedure proposed in Example 1 in Chapter 5 to estimate the inelastic LTB resistance of a strengthened beam (by integrating the procedure for obtaining the elastic critical moment proposed in the present study with present ANSI/AISC360 (2022) and CAN/CSA-S16 (2019) provisions, originally intended for unstrengthened beams), need to be assessed/verified through comparisons with inelastic FEAs that incorporate the effects of material and geometric nonlinearity, residual stresses, and initial out-of-straightness.
3. Utilizing the variational principle introduced in Chapter 6 and procedures akin to those adopted in Chapter 5, it is recommended to formulate energy-based design-oriented equations for quantifying the LTB capacity of monosymmetric strengthened beams.

4. The variational principle developed in Chapter 6 can be modified to analyze monosymmetric beams that are partially strengthened along their span. The formulation would also be applicable to doubly symmetric beams that are partially strengthened with cover plates with different sizes, resulting in an unsymmetric strengthened section.
5. For a monosymmetric beam partially strengthened along its span by cover plates, the shear center axis exhibits a jump at the location(s) of section changes along the span. When a point load is applied at the location of section change, the load height relative to the shear centre axis undergoes a similar jump. The tackling/modeling of load height effect in such cases, becomes an interesting problem of practical interest. It is thus recommended to extend the work to tackle this class of problems.
6. Developing simplified design equations to estimate the elastic LTB capacity of strengthened non-prismatic beams or the beams that are strengthened partially along their span can be advantageous in certain design situations.
7. In some design situations, end details may restrain the warping deformation and/or weak axis rotation. In such cases, it could be beneficial to modify the solutions in Chapter 5 to develop energy-based coefficients that account for such constraints.